

**A STUDY OF POST-CRACKING
BEHAVIOUR OF REINFORCED CONCRETE SLABS**

THESIS

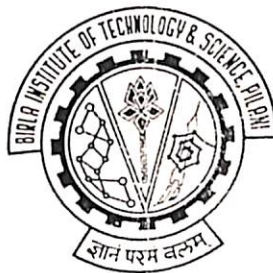
Submitted in partial fulfilment
of the requirements for the degree of
DOCTOR OF PHILOSOPHY

By

Paturu Neelakanteswara Rao

Under the Supervision of

Prof. H.S. Moondra



**BIRLA INSTITUTE OF TECHNOLOGY AND SCIENCE
PILANI (RAJASTHAN) INDIA**

1997

ACKNOWLEDGEMENTS

I wish to express deep sense of gratitude and sincere thanks to my thesis supervisor Prof. H.S. Moondra for his able guidance, encouragement and suggestions throughout the period of this research work.

I thank Dr. S. Venkateswaran, Director, B.I.T.S for giving me an opportunity to do research at the Institute. I also thank Dr. V.S. Rao, Dean, Practice School Division; Prof. K.E. Raman, Dean, Engg. Services Division; Dr. R.K. Patnaik, Dean, Instruction Division, and Dr. G.P. Avasthi, Dean, Faculty Division - I, for providing the necessary infrastructure and other facilities.

I also express my gratitude for the kind and affectionate enquiries about the work and the encouragement given by Dr. L.K. Maheshwari, Dean, R&C Division.

My sincere thanks to Dr. Rajiv Gupta, Group Leader, Civil Engineering and Dr. R.B. Kodali, Group Leader, Mechanical Engineering for providing necessary facilities to do the experimental work.

I wish to express my indebtedness to Dr. S.K. Ghosh, Associate Professor, BITS and Dr. G.C. Bajoria, Assistant Professor, S.G.I.T.S., Indore for their helpful discussions and cooperation.

Special thanks go to Mr. H.S. Kulhari who patiently typed many revisions of this thesis. I also wish to acknowledge Mr. Om Prakash for preparation of this thesis. I express my thanks to Mr. K.K.N. Sastry and Mr. K.N. Sharma, for their help in preparing drawings and graphs.

I would like to thank laboratory attendants Mr. Asha Ram, Mr. Suresh, Mr. Shivpal, Mr. Pramod, Mr. Soni, Mr. Satveer Singh, Mr. Mohan Lal, Mr. Rameswar and Mr. Manohar.

I would like to thank my students, Mr. B. Vasudev, Mr. B. Surendra Reddy, Mr. Y. Chandra Mohan and Mr. Ajit Singh for their timely help.

I would like to record my special affection and thanks to my wife Padmavathy, whose constant persuasion and moral support has been a source of inspiration to me. I also thank my son Sushanth for having cheerfully sacrificing the time that rightfully belonged to him.

Finally, I wish to acknowledge the support that I have received from colleagues, friends and to all the people who have helped me in the preparation of this thesis.

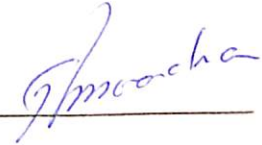
P.N. Rao

**BIRLA INSTITUTE OF TECHNOLOGY & SCIENCE
PILANI (RAJASTHAN)**

CERTIFICATE

This is to certify that the thesis entitled **A Study of Post – Cracking Behaviour of Reinforced Concrete Slabs** and submitted by **Paturu Neelakanteswara Rao** ID No. **89PHXF403** for award of Ph.D. Degree of the Institute, embodies original work done by him under my supervision.

Signature in full of
the Supervisor _____



Name in capital block
letters

H.S. MOONDRA

Date: *31/12/97*

Designation

Professor

LIST OF SYMBOLS

A

- a Length of the element along the x-direction.
 a_j Constant terms
 A_s Area of steel reinforcement per unit width
 A_{st1} Area of steel in shorter direction
 A_{st2} Area of steel in longer direction
 A_{sx} Area of tensile steel in the x-direction per unit width
 A_{sy} Area of tensile steel in the y-direction per unit width
 A'_{sx} Area of compression steel along the x-direction per unit width
 A'_{sy} Area of compression steel along the y-direction per unit width
 A_t Tributary surface area of steel reinforcement per unit width

B

- b Length of the element along the y-direction
[B] Strain-displacement matrix
 B_{nn} , Parameters related to normal displacements along crack
 B_{nt} , Parameters related to tangential displacements along crack
 B_{tt} Parameters related to shear displacements along crack

C

- C $\cos\theta$
CA Quantity of coarse aggregate
 C_d Depth of crack
CE Quantity of cement
[$c^{(e)}$] Matrix of curvatures at the centre of each element 'e'
 C_w Crack width
 C_1 Principal curvature correspond to maximum curvature
 C_2 Principal curvature correspond to minimum curvature
[c'] Curvatures along the axis of anisotropy.

D

- d Effective depth
[D] Material behaviour matrix
 d_b Diameter of steel bars
[D^c] Concrete material matrix
[D^s] Reinforcement material matrix

- [D^e] Elasticity matrix of an element 'e'
d_s Distance from extreme bottom fibre to centroid of the tensile steel
d'_s Distance from extreme top fiber to centroid of the compression steel
[D'] Material matrix along the axis of anisotropy.
[D(σ_{i-1})] Material behaviour matrix at (i-1) incremental step.

E

- e An element
E_a Modulus of aggregate interlock
E_b Modulus of bond
E_c Modulus of elasticity of concrete (lb/in²)
E_s Secant modulus
E_{st} Modulus of elasticity of steel
E_{stx}, E_{sty} Moduli of elasticity of steel in tension along the x and y directions
E'_{stx}, E'_{sty} Moduli of elasticity of steel in compression along the x and y directions
E_t Tangent modulus
E_{t1}, E_{t2}, E_{t3} Slopes of stress-strain curve in tension
E_{i(i=1,2)} Moduli of elasticity along the principal axes of orthotropy.

F

- FA Quantity of fine aggregate
f_c Uniaxial compression strength
f_r Modulus of rupture of concrete
f_{su} Ultimate tensile strength of steel
f_{sy} Yield strength of steel
f_x, f_y Components of tension steel forces in the direction of steel coordinates x and y per unit width
f_x, f_y Components of compression steel forces in the direction of steel coordinates x and y per unit width
F₁ Internal force along the principal curvature C₁
F₂ Internal force along the principal curvature C₂
f₁, f₂ Components of tension steel forces along the principal curvature per unit width
f₁, f₂ Components of compression steel forces along the principal curvature per unit width
f₁(s), f₂(s) Generalised functions in terms of parameter 'S'

G

- G Shear modulus
G_t Tangential shear modulus

g Proportion of load taken by the strip in the x-direction
 $(1-g)$ Proportion of load taken by the strip in the y-direction
 $g_1(s), g_2(s)$ Generalised functions in terms of 'S'

H

h Thickness of the slab

J

J_{ij} The coefficients of anisotropic constitutive matrix

K

$[K]$ Assembled global stiffness matrix
 k_a Shear stiffness of cracked concrete
 $[k^{(e)}]$ Stiffness matrix of an element 'e'
 kh Depth of neutral axis
 k_t Tangential bulk modulus

L

l_x Length of slab in x-direction
 l_y Length of slab in y-direction

M

m Number of steel bars
 $[M^{(e)}]$ Matrix of moments at the centre of each element 'e'
 M_n Bending moment in the normal direction
 M_{nt} Twisting moment
 M_t Bending moment in the tangential direction
 M_u Ultimate moment
 $M_{ulim.}$ Ultimate moment with respect to Limit State Method
 m_{un} Ultimate moment of resistance about a yield line
 m_{unt} Torsional moment along the yield line
 m_{ux} Ultimate moment in x-direction
 m_{uy} Ultimate moment in y-direction
 M_x Moment in x-direction
 m_x Bending moment in x-direction per unit length
 M_y Moment in y-direction
 m_y Bending moment in y-direction per unit length
 m_{xy} Twisting moment per unit length

$\Delta M_1, \Delta M_2$ & ΔM_{12} Incremental changes in moments along the axis of anisotropy.
[M'] Moments matrix along the axis of anisotropy
M_{1r}, M_{2r} Resisting moments along material axes

N

n Normal to the crack direction
N_i Shape functions (i = 1 to 16)
n_s Number of sampling points

P

p Percentage of steel
[P] Vector of nodal forces
{P_{ci}} Revised correction load vector
[p^(e)] Load vector of an element 'e'
{P_i} Load increment vector
{P_o} Initial load vector

Q

q Load per unit area
{Q^(e)} Nodal force vector of an element 'e' due to distributed load 'q'

R

R_E Modular ratio
R_f Stress ratio
R_o Strain ratio

S

S $\sin\theta$
s Spacing of cracks
SC Specific gravity of cement
s_p Spacing of reinforcement
SS Specific gravity of sand (Fine aggregate)
SA Specific gravity of coarse aggregate
S₁, S₂ Depth of tensile steel layers measured from neutral axis

T

- t Tangential to the crack direction
[T₁] Transformation matrix related to moments in x, y and n, t directions
[T₂] Transformation matrix related to curvatures in x,y and n,t directions

U

- u Nodal displacement in x-direction

V

- v Nodal displacement in y-direction
dv Elemental volume
V Volume of an element
V_a Interface shear stress transferred across crack

W

- W Unit weight of concrete in pounds per cubic foot
w Nodal displacement in z-direction (transverse displacement)
WA Quantity of water
w_i,w_j Weights for numerical integration
w_s Weight of the slab
W₁,W₂ Maximum and minimum collapse loads

X

- X Global x-coordinate

Y

- Y Global y-coordinate

Z

- Z₁,Z₂ Depths measured from neutral axes in compression zone
 \bar{Z}_1, \bar{Z}_2 Depths measured from neutral axes in tension zone

Special Characters

σ	Total stress
$\{\sigma\}$	Total stress vector
$\{\sigma^{(e)}\}$	Stress vector of an element 'e'
$\{\sigma_0\}$	Initial stress vector
$\{d\sigma\}$	Stress increment vectors
$\Delta\sigma_i$	Incremental stresses
$\Delta\sigma_{ci}$	Correct stress increment
σ_1	Maximum principal stress
σ_2	Minimum principal stress
$d\sigma_i$	Differential changes in principal stress
σ_s	Steel stress
$\{\sigma^c\}$	Concrete stress vector
$\{\sigma^s\}$	Reinforcement stress vector
σ_b	Bond stress
σ_{nt}	Tangential stress component along the crack
σ_{nn}	Normal stress component along the crack
$\{\sigma_i\}$	Stress vector at i^{th} incremental load
σ_p	Point of maximum stress
σ_t	Tensile strength of concrete
ε	Total strain
$\{\varepsilon^{(e)}\}$	Strains of an element 'e'
$\Delta\varepsilon_i$	Incremental strains
$\{\varepsilon\}$	Strain vectors
$\{d\varepsilon\}$	Strain increment vectors
$d\varepsilon_{iu}$	Change in equivalent uniaxial strain
ε_u	Ultimate strain of concrete
$\varepsilon_{t1}, \varepsilon_{t2} \ \& \ \varepsilon_{t3}$	Strain limits of concrete in tension
ε_{ys}	Yield strain of steel
ε_{sh}	Hardening strain of steel
ε_{su}	Ultimate strain of steel
ε_{ff}	Fracture strain
ε_s	Steel strain
ε_{cr}	Cracking strain of concrete
ε_t	Strain of concrete in tension zone
ε_x	Strain in x-direction
ε_y	Strain in y-direction
$\{\varepsilon_0\}$	Initial strain vector
$\{\varepsilon_i\}$	Strain at i^{th} incremental load
ε_{iu}	Total equivalent uniaxial strains ($i=1,2$)
ε_p	Peak strain of concrete in compression

ϵ_0	Initial strain
ϵ_{ti}	Uniaxial strain at the extreme top fibre of concrete section
ϵ_{bi}	Uniaxial strain at the extreme bottom fibre of concrete section
$\epsilon_{sx}, \epsilon_{sy}$	Steel strains along x,y coordinates
ϵ_1, ϵ_2	Principal strains
$\{\delta^{(e)}\}$	Nodal displacements of an element 'e'
δ_b	Bond slip
$d\delta_b$	Incremental bond slip
δ_s	Shear displacement along the crack
δ_t	Tangential displacement along the crack
δ_n	Normal displacement along the crack
$\{\delta_0\}$	Initial displacement vector (Null Vector)
δ_i	Displacement at i^{th} incremental load
$\Delta\delta_i$	Incremental displacements
α	Angle of steel orientation
η, ξ	Local coordinates
$\theta_x, \theta_y, \theta_{xy}$	Rotations of a point in bending
ν	Equivalent Poisson's ratio
ν_1	Poisson's ratio in the principal compression stress direction
ν_2	Poisson's ratio in the principal tension stress direction
ζ, ρ, λ	Stress variants in three dimensions
β	Shear retention factor
θ	Angle between global axis x and principal curvature C_i
α_1 to α_{16}	Parameters of transverse displacement functions
γ_{xy}	Shear strain
α_x, α_y	Coefficients of two way slabs
ϕ_j	Field variable
α_r	Ratio of principal stresses

ABSTRACT

Analytical procedures which can accurately determine internal stress and strain distributions in the concrete and reinforcing steel elements of reinforced concrete members are lacking for many cases. Among the most serious difficulties to the development of such analytical procedures is the non-homogeneous and nonlinear behaviour of concrete. The evaluation of stress and strain, deflection and cracking of reinforced concrete members by means of the finite element analysis is an approach currently receiving increasing attention as a possible method capable of greatly extending the scope of the problems that can be treated numerically. Finite element analysis of material nonlinearity is still under intensive research. One of the principal limitations in this area is the difficulty of adequately representing material properties. In other words, better techniques of computing material parameters and of utilizing experimental data must be devised. To represent the realistic behaviour of reinforced concrete incorporating material nonlinearity and stress-strain relationship, an appropriate finite element model has to be developed to get the load-deflection curve.

This thesis presents the modified stiffness method of finite element model to analyse the post-cracking behaviour of reinforced concrete slabs. In the analysis, the nonlinear variation of material properties, through the slab depth is taken into account by numerical integration. The steel reinforcement in the element is considered as uniformly distributed. The smeared crack approach with rotating strain based orthogonal cracks is applied in the analysis. For this an incremental orthotropic model has been used.

The softening phenomenon of concrete in compression and tension, bond between steel and concrete have been considered. In addition, the complex crack interface behaviour known as aggregate interlock is included in the analysis.

To examine the overall behaviour of the cracked element, combining all the above said factors, a software integrated finite element model is developed. Numerical results so obtained are in good agreement with the experimental results.

Table of Contents

	Page No.
Acknowledgements	i
Certificate	iii
List of Symbols	iv
Abstract	xi
1. INTRODUCTION	
1.1 Introduction	1
1.2 Motivation	4
1.3 Objectives of Thesis	5
1.4 Organisation of Thesis	6
2. LITERATURE REVIEW	
2.1 Introduction	9
2.2 Literature Review	10
2.3 Conclusions	31
3. FINITE ELEMENT ANALYSIS	
3.1 Introduction	33
3.2 Development of Finite Element Method	36
3.3 General Description of Finite Element Method	37
3.4 Selection of Plate bending Element	40
3.5 Nonlinear Material Behaviour	51
3.6 Material Characterization	54
3.7 Nonlinear solution Techniques	55

4. MODELING OF MATERIALS

4.1 Introduction	59
4.2 Behaviour of Concrete in Compression	61
4.2.1 Elasticity Based Models	62
4.2.1.1 Uniaxial behaviour	65
4.2.1.2 Biaxial behaviour	68
4.2.1.3 Triaxial behaviour	77
4.2.2 Plasticity Based Models	80
4.2.3 Plastic-Fracturing Models	81
4.2.4 Endochronic Models	81
4.2.5 Comparision of Models	82
4.2.6 Modeling of concrete in compression	83
4.3 Behaviour of Concrete in Tension	87
4.3.1 Tensile strength of concrete	88
4.3.2 Tension – softening	89
4.3.3 Modeling of concrete in Tension	93
4.4 Representation of Steel Reinforcement	95
4.4.1 Modeling of Steel Reinforcement	97
4.4.2 Constitutive Relationships for steel Reinforcement	100

5. POST-CRACKING BEHAVIOUR

5.1 Introduction	104
5.2 Cracking models	105
5.2.1 Discrete cracking models	106
5.2.2 Smearred cracking models	108
5.3 Tension-stiffening Effect	111
5.3.1 Bond – Slip phenomenon	115
5.3.2 Measurement of Bond-Slip	116
5.3.3 Bond Stress – Slip Relationships	118
5.4 Rough crack behaviour	123
5.4.1 Aggregate Interlock	127
5.4.2 Aggregate Interlock Stress-Strain Relationships	133

6. METHOD OF ANALYSIS

6.1 Introduction	138
6.2 Assumptions	139
6.3 Material Axes	139
6.4 Flexural Stiffness	140
6.4.1 Flexural Stiffness of concrete	145
6.4.2 Flexural Stiffness of steel	146
6.4.3 Effect of Bond	146
6.4.4 Effect of Aggregate Interlock	148
6.5 Transformation of flexural rigidity matrix	149
6.6 Solution procedure	152
6.6.1 Uncracked Element	153
6.6.2 Cracked Element	154

7. EXPERIMENTAL INVESTIGATION

7.1 Introduction	160
7.2 Test Specimens	160
7.3 Testing of Materials	161
7.3.1 Testing of Steel	161
7.4 Mix Design	164
7.5 Slab Design	168
7.6 Casting of Slabs	169
7.7 Testing of Slabs	170
7.8 Behaviour of Slabs	173

8. RESULTS

178

9. CONCLUSIONS

239

Appendix-A : Flowchart for Linear Analysis 245

Appendix-B : Slab Design 251

Appendix-C : Flowchart for Nonlinear Analysis 257

References 258

CHAPTER 1

INTRODUCTION

1.1 Introduction

The behaviour of reinforced concrete members in a structural system, specifically their response to loads and other actions, has been the subject of intensive investigation since the beginning of the present century. The study is still under progress because of its highly complex material behaviour. It has been the constant endeavor of structural engineers to improve their concepts of analysis and design so that an economical structure is obtained with safety and serviceability.

During the first half of this century, various methods of elastic analysis were developed in this direction to analyse beams, rigid frames, trusses, plates, shells, etc. for strength and stability. Consequently in the theory of elasticity three important assumptions have been made. These are:

- (a) The material is assumed to be isotropic and homogeneous,
- (b) The material is taken as linearly elastic, and
- (c) The stress at all points of an elastic body is taken ^{to be} within the elastic limit of the materials constituting the body.

These assumptions were made realistic for material such as steel subjected to relatively small loads. Accordingly, the actual performance of structural systems tallied with the theoretical predictions and great confidence was placed on these theories and their applications. However, the stress-strain relations are generally nonlinear for the various grades of concrete and accordingly the use of the elastic theory ~~leads to~~ concrete structures ^{leads} to an approximate solution.

Moreover, the orthodox method for designing concrete structures is based on suitable factor on the stress in each of materials constituting the structure and analysis is done with straight line theory in the case of reinforced concrete. In this elastic method the relationship between load and deflection or stress and strain is assumed to be linear upto the collapse of structure. But concrete and steel both cease to be fully elastic after a certain stage of loading. The inelastic behaviour of concrete starts right from very low stresses, while steel shows inelastic deformations after elastic limit has reached. So behaviour of ^{a concrete} structure cannot remain elastic at higher loads as the failure approaches. Consequently, ultimate load theory is used to evaluate the collapse load on structure which is the outcome of inelastic or plastic strains that occur in material before it fails. Yield line analysis is an ultimate load method, in that the load at which slab will fail is assessed, and is invaluable as a design technique for finding the solution for the behaviour of the slabs. In most of the cases, a structural member designed by ultimate load theory is too slender to be adopted. Also it may exhibit new problems like excessive

deflection, excessive crack width etc. at service condition.

As a remedial measure limit state analysis⁵ being used to control maximum deflection and maximum crack width. However, this analysis fails to incorporate nonlinear variation of materials and effects due to cracking of concrete. The finite element method which takes care of different elements of⁶ structure with different elastic properties^{5,6,7} is an approach currently receiving increasing attention as a possible method. In addition, in finite element method the requirement of homogeneity is relaxed, which is a restriction imposed by the theory of elasticity. As the structure is loaded progressively, the reinforcement at some points can yield, the concrete can get crushed locally at several points and cracking can be extensive. During the load increments, based on well established failure criteria the finite element method can progressively modify the structural properties of the various elements constituting the body, and trace the nonlinear load-deformation relationship till the failure or collapse load is identified.

The finite element method is very versatile to carryout nonlinear analysis of structural systems to any desired level of accuracy. The finite element method is clearly related to the power and versatility of modern digital computers. This new tool is ideally suited for computer simulation of complex structural behaviour. It is important to note that stresses, strains, deformations and displacements can all be predicted by this method at any point in a body even in the nonlinear stage, just as

the theory of elasticity can do the same at the elastic stage of behaviour.

Structures may exhibit nonlinear behaviour due to material nonlinearities or geometric nonlinearities. Geometric nonlinearities are associated only with certain special structural elements and systems in which the effect of displacements on internal forces must be considered in the analysis. Long columns, flexible arches and some thin shell structures are examples of such special cases. On the other hand, material nonlinearities occur in all reinforced concrete structures and should be considered in any accurate rational analysis. Only material nonlinearities in reinforced concrete will be considered hereafter.

1.2 Motivation

Subsequent studies were undertaken predominately to study overall behaviour of reinforced concrete slabs. The objectives of these studies were to determine the basic failure mechanisms for complex reinforced concrete slabs. The basic failure mechanism for a number of these structures were not well defined. Physical experiments to determine the sequence of crack formation and the locations of the failure modes were not easy to conduct. The scaling of these structures were demanding but expensive. The construction of physical models of the size to fit into the laboratories were very difficult. Some of the attempts to actually construct reduced models proved to be unsatisfactory. This prompted the use of numerical experiments. A number of these early studies using smeared crack model

within layered plate element produced reasonable values of nonlinear behaviour.

From this background active movements have appeared to rearrange the present status and look over the future prospects of rational analysis of reinforced concrete slabs.

1.3 Objectives of Thesis

1. Material nonlinearity of reinforced concrete should be considered for any accurate rational analysis, i.e., considering nonlinear stress-strain relations for concrete and steel.
2. Reinforced concrete members and structures are subject to tensile concrete cracking at relatively low loads. These cracks propagate gradually with increasing loads. They have a profound effect on local stresses and displacements, as well as overall behaviour and strength. In terms of a finite element analysis, progressive cracking means that the structure being analyzed experiences a continuous topology of cracking as the load is increased.
3. Progressive destruction of bond between concrete and reinforcement occurs as load is increased, permitting some longitudinal slip between the steel and the concrete. This starts almost with the initiation of flexural cracking at loads well

below service load, with local bond failure immediate adjacent to the cracks
The increase of slip with load is highly nonlinear.

4. Certain force transfer mechanisms in cracked concrete members, namely, interface shear transfer across cracks by aggregate interlock is difficult to incorporate into a general analytical model.
5. Representation of rational finite element model for incorporating constitutive relations of the above to reinforced concrete slab cracking and its overall behaviour.

1.4 Organisation of Thesis

Chapter 1 gives an introduction to material nonlinearity and thereby finite element analysis. The motivation and object of the present investigation has also been emphasised.

Chapter 2 deals with the literature review of earlier conventional design methods and classical elastic theory of plates used for slab analysis and their limitations. The development and limitations of yield line analysis and strip method are also described. In addition it discusses the versatility of finite element analysis of reinforced concrete members. The investigations of various authors and their limitations regarding nonlinear analysis of reinforced concrete slabs are also

incorporated here. The chapter concludes with further investigations required for post-cracking behaviour of reinforced concrete slabs.

The subject matter of Chapter 3 contains the finite element methodology and the selection of plate bending element for slab analysis. Nonlinear solution techniques are discussed to represent the non-linear material behaviour and the corresponding constitutive relations.

Chapter 4 explains the various models of reinforced concrete materials and the adopted models for nonlinear analysis of slabs and corresponding stress-strain relations.

The importance of tension-softening, tension-stiffening and rough crack behaviour has been explained in Chapter 5. The stress-strain relations for bond between steel reinforcement and concrete are derived. Aggregate interlock resulting from rough crack behaviour has been modeled and corresponding constitutive relations are developed for the analysis of slab.

The methodology of analysis and the solution procedure for reinforced concrete slabs have been described in Chapter 6. Flexural stiffness matrices developed for bond and aggregate interlock are also incorporated in the analysis here.

Chapter 7 presents the experimental investigation of simple supported rectangular slabs with and without central openings, when subjected to uniformly distributed load. Materials like cement, sand, coarse aggregate and steel bars were tested to get the required parameters. Concrete mix was designed according to Road Note method. A solid slab and five slabs with different size of central openings *were cast and tested to failure. Cracking of concrete, yielding of steel* reinforcement, crushing load and patterns of yield line were observed while testing of slabs. Slab deflections were measured at pre-specified points along the predicted yield line.

Slabs are modeled for proposed finite element analysis and the numerical results are compared with experimental load-deflection curves. The effects of bond and aggregate interlock are analysed in Chapter 8.

Conclusions are drawn in Chapter 9 based on the comparisons of experimental and proposed analysis results. By incorporating tension-stiffening effect due to bond between steel and concrete, it is found that the results are improved and giving more closer approximation towards exact values. The aggregate interlock effect is almost negligible. The tension stiffening model is observed effective from cracking of concrete to yielding of steel reinforcement.

CHAPTER 2

LITERATURE REVIEW

2.1 Introduction

Slabs are the most widely used structural elements of modern structural complexes and the reinforced concrete slab is the most useful discovery for supporting lateral loads (perpendicular to the horizontal plane) in buildings. A reinforced concrete slab is a broad, flat plate, usually horizontal, with top and bottom surfaces parallel or nearly so. It may be supported either by reinforced concrete beams (usually monolithic construction), by masonry or reinforced concrete walls, by structural steel members, directly by columns, or continuously by the ground. Slabs may be viewed as thin or moderately thick plates that transmit loads to the supporting walls or beams and sometimes directly to the columns by flexure, shear and torsion. It is difficult to decide whether the slab is a structural element, component or structural system in itself. Slabs are viewed here as structural elements.

Slabs may be visualised as intersecting, closely spaced, grid beams and hence they are seen to be highly indeterminate. Slabs, being highly indeterminate, are difficult to analyse by elastic theories. Since slabs are sensitive to support restraints and fixities, rigorous elastic solutions are not available for many practical

important boundary conditions. Their structural behaviour in the elastic, inelastic and ultimate stages is complicated. The deflection and cracking of slabs are important since they affect the performance of slabs and the comfort of the occupants. Still adequate information on these aspects have not been acquired. Since large volume of concrete go into slabs, the slightest reduction in the design depth will lead to considerable economy. The study of behaviour of slabs is indeed a challenge, particularly when precise technical information is not readily available and an intuitive feel is still the basis for the design of slabs. The presentation of the performance of slabs will be made in a graded manner, from the simple to complex.

2.2 Literature Review

Research on various types of slabs has been in progress since 1920. Earlier, construction of flat slabs and flat plates were popular because of simplicity, structural elegance and economy. An attempt has been made to understand theoretical basis and structural behaviour of flat slab by Westergaard and Slater[1]. A semi-empirical direct design method and an approximate elastic analysis known as the equivalent (building) frame method were developed on the basis of satisfying the conditions of equilibrium and geometrical compatibility. In either case the slab panel is divided into column strips and middle strips for design purpose. The equivalent (building) frame analysis for the design of buildings was first introduced by Stasio[2]. Analysis of two-way reinforced concrete slabs by the coefficient method was introduced in the United States by Rogers[3]. Distribution factors for

moments were developed based on three-dimensional elastic analysis and experimental results[4,5,6]. Rice[7] and Zweig[8] have represented various design aids and simplifications for the direct design method of flat slabs. According to ACI Code[9], special attention must be given for providing the proper resistance to shear as well as to moment, when designing by the direct method. An excellent review of this historical development has been given by Park and Gamble[10].

During this period the beam and slab construction (called the two-way slab system) was being established on a sound theoretical basis using classical theory of plates. When two-way slabs are supported by columns, as in flat slabs and flat plates or when slab carry concentrated loads as in footings, shear near the column is of critical importance.

These elasticity-based methods have the following important limitations. Slab panels must be square or rectangular. They must be supported along two opposite sides (one-way slabs), two pairs of opposite sides (two-way edge supported slabs) or by a fairly regular way of columns (flat plates and related forms). Loads must be uniformly distributed, at least within the bounds of any single panel. In practice many slabs do not meet these restrictions for example, slabs with large openings, slabs supported on two or three edges only, slabs carrying concentrated loads and non rectangular slabs. Yield line analysis provides solution for such problems.

The plastic hinge was introduced as a location along a member in a continuous beam or frame at which, upon overloading, there would be large inelastic rotations at essentially a constant resisting moment. For slabs, the corresponding mechanism is the yield line. For the overloaded slab, the resisting moment per unit length measured along a yield line is constant as inelastic rotation occurs. The yield line serves as an axis of rotation for the slab segment. It discusses the yielding of the slab reinforcement at several critical sections and the eventual collapse of the slab under the conditions of ultimate load.

The yield line theory was innovated by Danish engineer, Ingerslev[11] and greatly extended by Johansen. Early publications were mainly in Danish, and it was not until Hogenstad's English language summary[12] of Johansen's work that the method received wide attention. Since that time, a number of important publications on the method have appeared[13-19]. One can find literally hundreds of publications on yield line theory and yet research is progressing in unexplored avenues and development of yield line theory.

The yield line is a line in the slab about which plastic rotations occur when the reinforcement bars are yielding. The ultimate moment ' m_{un} ' of resistance about a yield line has been assumed as

$$m_{un} = m_{ux} \cos^2 \alpha + m_{uy} \sin^2 \alpha \quad \dots (2.1)$$

where α is the angle of inclination and m_{ux} , m_{uy} are ultimate moments in x,y directions respectively. Similarly, the torsional moment m_{unt} along the yield line are

$$m_{unt} = (m_{ux} - m_{uy}) \sin\alpha\cos\alpha \quad \dots(2.2)$$

The failure occurs when the computed normal moment exceeds the ultimate moment of resistance, which is called the yield criterion.

$$m_x\cos^2\alpha+m_y\sin^2\alpha+m_{xy}\sin^2\alpha = m_{ux}\cos^2\alpha+m_{uy}\sin^2\alpha \quad \dots(2.3)$$

where m_x , m_y and m_{xy} are bending moments and twisting moment per unit length respectively.

It has been assumed that at the yield lines, no torsional moments exist since m_{ux} and m_{uy} are principal moments. The value of m_{unt} is generally neglected.

Often, the yield lines occur at directions that are not parallel to the reinforcement direction. Consider the case of a rectangular slab which has been reinforced orthotropically (that is, the reinforcements in the short span and long span directions are spaced differently). The cracks first develop perpendicular to the short span direction at the mid-region of the slab. As the load is further increased,

these cracks continue to grow and fork to join the corners and form failure mechanism.

In isotropically reinforced concrete slabs, usually in the case of square slabs (i.e., reinforcements in both the directions are same) $m_{ux} = m_{uy}$ condition exists.

Therefore,

$$m_{un} = m_{ux} (\cos^2 \alpha + \sin^2 \alpha) \quad \dots (2.4)$$

gives

$$m_{un} = m_{ux} = m_{uy} \quad \dots (2.5a)$$

$$\text{and } m_{unt} = 0 \quad \dots (2.5b)$$

Thus the ultimate moment of resistance in any direction of an isotropically reinforced slab is the same and torsional moments are zero. Hence all directions are principal directions by analogy with "principal stress directions". It is important to note that when the m_{ux} and m_{uy} values are not the same in two directions (orthotropically reinforced slabs), torsional moments are present along the yield lines, in addition to normal moments.

However, the recent research on cracking of concrete states that cracking criterion is strain based rather than stress conditions, i.e., principal curvatures are important in flexural problems than principal moments.

Yield line theory is an upper bound method. It will predict a collapse load that may be greater than the true collapse load. The actual capacity will be less than the predicted if the selected mechanism is not the controlling one or if the specific locations of yield lines are not exactly correct. Yield line theory never specifies the spacing of reinforcement, other than a uniform lateral spacing along the yield line. It is possible that the required rotation will exceed the available rotation capacity, in which case the slab will fail prematurely.

The yield line analysis focuses entirely on the flexural capacity of the slab. It is presumed that failure will not occur due to shear or torsion and that cracking and deflections at service load will not be excessive. The yield line analysis neglects any consideration of strain compatibility along the yield line and assumes that the displacements at the level of the steel during yielding, which are essentially perpendicular to the yield line, are sufficient to produce yielding in both sets of bars. Yield line analysis assumes that at the yield lines no shear and torsional moments exist.

The strip method was introduced by Hillerborg[20]. He included the practical design of slabs on columns and L-shaped slabs. Important contributions have been made by Kemp[21] and Wood and Armer[22]. Load tests of slabs designed by the strip method were carried out by Armer[23] and confirmed that the method produces safe and satisfactory designs.

In contrast to the yield line analysis, the strip method is a lower bound approach, based on satisfaction of equilibrium requirements everywhere in the slab[24]. While searching for a lower bound solution, one must find a solution to the governing equilibrium equation for slabs which is

$$\frac{\partial^2 m_x}{\partial x^2} + \frac{\partial^2 m_y}{\partial y^2} - \frac{2\partial^2 m_{xy}}{\partial x \partial y} = -q \quad \dots (2.6)$$

where 'q' is load per unit area on the slab. The basis for the simple strip method is that the torsional moment is chosen equal to zero, i.e., no load is assumed to be resisted by the twisting strength of the slab.

$$m_{xy} = 0$$

The equilibrium equation then reduces to

$$\frac{\partial^2 m_x}{\partial x^2} + \frac{\partial^2 m_y}{\partial y^2} = -q \quad \dots (2.7)$$

This equation can be split up into two parts, representing twistless beam strip action

$$\frac{\partial^2 m_x}{\partial x^2} = -gq \quad \dots (2.8a)$$

$$\frac{\partial^2 m_y}{\partial y^2} = -(1-g)q \quad \dots (2.8b)$$

where the proportion of load taken by the strips is g in the x-direction and $(1-g)$ in the y-direction.

Apparent discontinuity in torque or deflection may be disregarded, but a discontinuity in moment or shear is not permitted. Advanced research on strip method had been carried by number of investigators. Important publications pertaining to the design of slabs were made.

The strip method may be simple and safe in its final application, but the basis for the method is rather subtle. While searching for lower bound solution to the governing equilibrium equation for slabs, twisting moment m_{xy} being deliberately taken equal to zero. As in any flexural member, a load anywhere on a strip produces a shear along the entire strip. Zero shear lines are assumed while treating the strips as beams.

Neither the strip method nor the yield line approach provide any information regarding cracking or deflections at service load. Also there is need for evaluation of the stress conditions around the supports in relation to shear and torsion as well as flexure. Two-way slabs, even single-panel simply supported, require a three-dimensional approach for analysis. Such slabs are rarely statically determinate in their internal moments and shears.

Cracking of one-way slabs is very similar to cracking of beams. Significant work has been done by Gergely and Lutz[25] and Beeby[26] on the general topic of cracking in concrete and has been the basis for various code clauses[27].

Cracking of two-way slabs has become important since cracking patterns of an orthogonal nature or yield line patterns can predominate in a slab depending on the nature and magnitude of reinforcement in a slab. Significant contributions have been made by Desai and Kulkarni[28] in this direction.

The prediction and control of deflections of reinforced concrete structural elements has always been difficult due to cracking, shrinkage, creep and non-homogeneity of such elements. The problems become acute in the case of slabs, and in spite of significant research and development by Brason[29] and Park and Gamble[10], a consensus to the approach to the deflection of slabs has not been reached.

The most comprehensive studies of reinforced concrete slab deflections have been recorded by Jofriet[30] who studied elastic and post-cracking behaviours. Further work has been done by Desai and Kulakarni[31,32] to take into account the tensile membrane action in predicting crack width and deflection. Moy and Mayfield[33] made additional investigation regarding the arrangement of reinforcement in two-way slabs and its influence on cracking, deflection, and ultimate failure load.

It is unfortunate that having included 'cracking and deflections' as an important limit state, the IS Code has not provided adequate computational procedures on the crack widths and deflections of slabs.

The essential difficulties in estimating the slab deflections is the estimation of crack width and crack pattern, estimation of creep and shrinkage coefficients, and above all, the estimation of the flexural stiffness EI which is representative of the varying stiffness along the short and long directions.

Finite difference and finite element methods are extremely useful in this direction. The finite difference methods have been extensively used for the study of continuous plates[34,35] until the more versatile finite element method came into excessive use[36,37].

The first model of finite element method to reinforced concrete was developed by Ngo and Scordelis[38]. The discrete crack model with predefined crack patterns was developed to determine the principal stresses in the reinforced concrete and bond stresses. Simple beams were analysed in which the concrete and steel reinforcement were represented by two-dimensional triangular elements. Special bond link elements were used to connect the steel to the concrete.

Soon there after a second and basically different approach of smeared crack model was developed in the design of containment structure for a gas cooled nuclear reactor by Rashid[39]. This second approach looked at a problem in a more global sense.

Nilson[40] introduced nonlinear material properties and a nonlinear bond-slip relationship into the analysis and used an incremental loading technique to account for these nonlinearities. Improved quadrilateral plane stress finite elements were used. Cracking was accounted for by stopping the solution when an element indicated a tensile failure, and hence redefining a new cracked structure, which was again input into the computer and reloaded incrementally. The method was applied to concentric and eccentric reinforced tensile members, which were subjected to loads applied longitudinally through the reinforcing bars. Then the results were checked against experimental results.

The research by Cedolin and Dei Poli[41] on studies of reinforced concrete beams clarified many points regarding behaviour of concrete.

A number of additional papers have also appeared dealing with the finite element analysis of reinforced concrete systems made up of plane stress finite elements. The more important papers are of Valliappan and Doolan[42], Colville and Abbassi[43], Nam and Salman[44]. The solutions generally are similar except the use of finite elements or different constitutive relationships and failure criteria for the concrete.

The fracture energy based finite element model for reinforced concrete capable of following strain-softening process both in tension and compression is

presented by Gajer and Dux[35]. The performance of the model is demonstrated by comparing with experimental behaviour of panels and deep beams.

Yamaguchi and Chen[46] studied finite element method for reinforced concrete structures with regard to various important aspects such as constitutive modeling and tensile cracking.

One of the first applications of finite element method to elastic-fracture behaviour of reinforced concrete slabs is reported by Jofriet and McNiece[47]. Later a similar approach called 'modified EI' or 'modified stiffness' is presented by Bell and Elms[48]. Triangular and quadrilateral plate bending elements are used to study the behaviour of reinforced concrete slabs. The slab with a known distribution of reinforcing steel is divided into elements. For each element, the stiffness matrix is derived using a rigidity Matrix based on uncracked section geometry.

2210
The elements are then assembled into the total slab structure and boundary conditions are applied. A unit load is applied and scaled down until only one region cracks. This is governed by the maximum principal moment. The flexural rigidity after cracking is taken as product of reduced modulus of elasticity ($0.57 E_c$) and the moment of inertia of the cracked transformed section.

The effect of steel and crack orientation on the rigidity matrix relative to the element coordinates system are determined. The stiffness matrix then changed appropriately to the cracked region. The unit load is applied again and results scaled to the next crack observation. This procedure is repeated until the desired load level is reached. The analysis allowed cracking in two orthogonal directions if the minor principal moment in an element reached the cracking moment value. It is assumed that once a crack forms at right angles to a principal moment direction, its orientation is unaltered during any increase of load. The cracking in each element by using changing orthotropic flexural rigidities attempts to account for tension stiffening.

Post yield behaviour is not included in the analysis. This approach is restricted by the limitations due to assumptions of a macroscopic equivalent moment - Curvature relationship. This method does not evaluate progressive cracking through the thickness of slab.

In layered finite element approach the slab element is assumed to be a number of parallel layers of material. Each concrete layer is assumed to be in a state of plane stress with properties defined through biaxial stress-strain relations and failure criteria. Reinforcing steel is introduced as a layer of material with orthotropic properties consistent with the amount and placement of steel. This approach is based on idealized stress-strain relations for concrete and steel together

with some assumptions regarding compatibility of deformation between the two constituent materials.

Hand et al[49] applied layered finite element approach to analyse reinforced concrete plates and shells. The steel is considered as an elastic-plastic material. The concrete is considered as an isotropic bilinear elastic-perfectly plastic material with a limited tensile strength. A 20 degree of freedom rectangular doubly curved shallow shell layered finite element is used. The material properties varies through the thickness of slab or shell as loading progresses. It produces a coupling in the constitutive relations between mid-surfaces strains and curvatures and thus between in-plane and normal displacements. The implication of this coupling is that even for plate bending problems, in-plane boundary conditions must be specified for a complete description of problem. The structural stiffness matrix is updated at the beginning of each load increment. The incremental variable elasticity technique is used to obtain the load-deflection curve.

The rough cracks are realized and the shear strength along the crack should be function of the crack width. Therefore, the need for shear retention factor to provide the torsional and shear stiffness for cracked concrete is demonstrated. A constant value of 40% was assumed for shear retention factor. Neglecting tension stiffening effect of the concrete between cracks is the major limitation. The analytical results are too small with respect to experimental values.

For concrete in tension, the important concept of tension stiffening to account for the participation of the concrete between cracks was first introduced by Scalon and Murray[50] in study of slabs. The study also included the time dependent effect of creep and shrinkage.

Wanchoo and May[51] developed a model for post-elastic bending behaviour of reinforced concrete slab. The variation of stress through the thickness is permitted by using a layered model. The analysis is restricted to small deformation theory and perfect shear bond is assumed between layers. Transverse shearing deformations are neglected. The concrete is modeled by an elastic-cracked behaviour in tension and elastic-plastic behaviour in compression. The reinforcing steel is modeled by a two-dimensional layer obeying Von Mises criterion and associated flow law.

When the maximum principal stress σ_1 reaches the uniaxial tensile strength of concrete, cracking is initiated in a direction perpendicular to this stress. As the cracking forms, stress transfer across the crack is reduced to zero, i.e. $\sigma_1 = 0$. The assumption is also made that there is no shear stress across the crack once it has formed. Abrupt drop in the principal stress σ_1 to zero rises the unbalanced stress in the model. To restore equilibrium, this unbalanced stress is distributed to the rest of the structure by an initial stress process. A rectangular element with 16 degrees of

freedom is adopted for analysis. The solution is in the nature of an upperbound on loads.

Lin and Scordelis[52] presented a nonlinear finite element analysis of reinforced concrete shells of general form. Some of the basic approaches adopted are similar to those of Hand's work[49]. A flat triangular element with 15 degrees of freedom, five at each corner node is used for the study. The steel is assumed to be elastic-plastic in both compression and tension. The concrete is assumed to be elastic-plastic in compression. The tension stiffening effect of the concrete between cracks, neglected in Hand's work[49] is included. Significant influence of this effect on the post-cracking load-deflection response of under reinforced concrete structures is observed. The concrete is considered to release its stress gradually after cracking. Therefore, the stress-strain curve for concrete in tension is considered to have an uncracked elastic portion and a cracked unloading portion.

Shear retention factor is assumed to account for dowel action and aggregate interlock. It is stated that inelasticity of the concrete is not by actual plastic flow, but by the cumulative effect of micro crack propagation. Incremental iteration procedure is used for the solution of nonlinear analysis.

Vebo and Ghali[53] presented an analytical method to derive the moment-curvature relationship for a slab element orthotropically reinforced and subjected to a general state of applied moment. The numerical procedure takes into

account the nonlinear behaviour of the materials and the effect of stiffening due to tensile stress in concrete between cracks. It is stated that, the effect of biaxial compression on the moment curvature relationship will be relatively small. Since the main characteristics of this relationship for under reinforced concrete sections depend mainly on the characteristics of the reinforcing steel. Therefore, uniaxial stress-strain relationship for concrete in compression is assumed. The elasto-plastic relationship is assumed for reinforcing steel. The bilinear descending relationship is considered for concrete in tension to include tension stiffening effect. Failure of the slab section is considered as the crushing of concrete at ultimate strain. No relative displacement (bond) is assumed to take place between the concrete and reinforcing steel. Poisson's ratio effects are neglected.

Bashur and Darwin[54] presented nonlinear model for reinforced concrete slabs that includes the nonlinear variation of material properties through the depth of slab. Reinforced concrete slabs are modeled as incrementally elastic, anisotropy plates. Concrete is modeled as a nonlinear material in compression and as a linear brittle material in tension. Steel is represented as a uniaxial material and idealized as an elastic-plastic material. The concept of equivalent uniaxial strain used to represent strain on the material axis. The moment-curvature equations are expressed in terms of "equivalent uniaxial curvature" which is analogous to equivalent uniaxial strain. Orthotropic material properties are used in the differential stress-strain relations.

A four node rectangular plate bending element with 16 degrees of freedom is used for the analysis. Material properties are calculated at the centre of each element. Loads are applied incrementally, and the solution is corrected using successive iterations (initial stress method). The analytical results are compared with experimental results of two beams and three slabs. Membrane stresses and strength variations due to biaxial stresses are not included. Since the effect of biaxial stresses on concrete stiffness and strength is insignificant in modeling the behaviour of reinforced concrete slabs under monotonic load. Tension stiffening effect and bond slip between steel and concrete are not included in the study. Also shear retention factor is not considered for analysis.

Gilbert and Warner[55] studied a layered discrete element method to investigate the behaviour of reinforced concrete slabs by taking into account the tension stiffening effect. The concrete is assumed to carry no stress normal to the crack but an additional stress will be carried at the steel level. This additional stress represents the total internal tensile force in fact carried by the concrete between the cracks, conveniently lumped at the level of the tensile reinforcement and oriented in the direction of the bar. After cracking the stress-strain relationship of steel is modified to account for this effect. The reinforcing steel is assumed to be elastic-plastic in both tension and compression with stiffness only in the bar directions. Concrete is assumed to be elastic-plastic in compression.

Shear retention factor is assumed as 0.6 to account for aggregate interlock and dowel action. A layered 16 degree of freedom rectangular plate bending element is selected for the study. Incremental iterative procedure (initial stress method) is applied for analysis. Comparisons of different tension stiffening models were made. Perfect shear bond is assumed to exist between adjacent layers and perfect bond between steel and concrete within the layer.

Cope and Rao[56-58] developed space element modelling in which a certain number of gauss points are used for integration through the thickness of the slab. Zarris[59] presented a theory regarding the stresses of reinforced concrete shear walls and slabs under service loads. Stresses are determined before and after cracking. The reinforcement provides forces and moments that compose tensors. These tensors, together with the corresponding concrete tensors, constitute the reinforced concrete tensors. After cracking, the force and moment tensors of reinforcement appear in their complete form, i.e., not only with the axial forces but also with the shear forces of steel bars. The existence of these shear forces is proved theoretically, and their magnitude is determined by the compatibility conditions of the strains at the crack. The angle of cracks, the steel stresses and the forces or moments of concrete between the cracks are obtained by equating the tensor of the internal forces or moments of plate with the tensor of reinforced concrete forces or moments respectively. Plates subjected to simple bending or pure torsion is analysed. It had been concluded that after cracking, the reinforcing bars

have shear stresses apart from the axial stresses. The relation between axial and shear stresses result from the compatibility conditions of strains at the crack. Aggregate interlock phenomenon is recognised but the effects are not considered in the analysis.

Lewiski and Wojewodzki[60] developed integrated finite element model for reinforced concrete slabs by simple numerical integration through the total thickness. The total strain description for the concrete under biaxial stresses is adopted. The concrete is assumed to be elastic-plastic and brittle cracking in tension. It is assumed that concrete carries no stress normal to cracks. The steel is assumed to be elastic-plastic in both compression and tension. The tension stiffening effect is taken into account on the assumptions that additional stress is carried by the steel reinforcement. The steel stiffness is increased due to bond between the bar and surrounding concrete. Stiffening factors having values between 0.25 to 1.0 are listed to increase the steel stiffness. Shear retention factor due to the aggregate interlock in rough cracks as well as to the dowel action is assumed equal to 0.4 for concrete cracked in one direction and 0.2 for concrete cracked in two directions. A 20 degree of freedom plane rectangular element is used having five degrees of freedom at each node.

Sathurappan et al[61] presented analysis for reinforced and pre-stressed concrete plates. A four node isoparametric quadrilateral plate shell element with

reinforcement as a discrete integral part of the element is used for the study. Five degrees of freedom at each node ($u, v, w, \theta_x, \theta_y$) is considered. The steel bars are assumed as elasto-plastic to have only axial stiffness. An elasto-plastic material model is used for the compressive behaviour of concrete. Yield function and associated flow rule has been used. In tension, concrete is assumed to behave as a linear elastic material and the smeared crack approach is used. Both material and geometric nonlinearities are considered. The position and the orientation of the reinforcement bar within an element is arbitrary in plan and parallel to the reference surface. Gaussian Integration is used in the thickness direction to evaluate concrete stiffness and internal loads equivalent to stresses in concrete. The contribution of each individual reinforcement bar to the stiffness of the element is evaluated as a line integral by using Gaussian integration.

Di and Cheung[62] developed^a laminated curved shell element and applied to the analysis of reinforced concrete plates and shell problems. The plate or shell is divided into several layers. Both geometrical and material nonlinearities are considered. The strain-hardening plastic approach is employed to model the compressive behaviour of the concrete. A dual criterion is considered for yielding and crushing in terms of stresses and strains, which is completed with a tension cut-off representation. Both the crack interface effects and dowel action are accounted for by using an average shear modulus. An incremental and iterative modified Newton-Raphson method is used for the nonlinear solution. An energy

criterion in terms of both forces and displacements is implemented for convergence. A full bond is assumed at the steel-concrete interface.

2.3 Conclusions:

Cracking criterion is strain based rather than stress conditions. That is principal curvatures are important in flexural problems than principal moments. The contribution of steel reinforcement towards flexural stiffness before cracking is neglected in earlier studies of finite element slab models of modified stiffness approach. All these models considered smeared crack approach with fixed direction of crack or along the principal moment direction. Tension - stiffening effect considered to account for the concrete between cracks in few models is in fact tension-softening which is property of plain concrete in tension. The real stiffening effect is due to bond-slip and bond-stress between concrete and steel reinforcement. None of the slab models considered this effect in the analysis.

The need for shear strength analysis of slab is strongly explained by Hand et al.[49] to account for aggregate interlock and dowel action. Also Zarri's theory of plates[59] in equilibrium and compatibility conditions emphasise the importance of shear friction and shear stresses. Di and Cheung[62] further emphasised on shear transfer across crack interface. The slab models discussed so far implemented these effects in terms of simple shear retention factor which may not adequately represent the behaviour of cracked concrete. The major difficulties in the nonlinear analysis

of reinforced concrete slabs arise in selecting appropriate finite element models, constitutive relations for elastic and inelastic response under combined stress states and failure criteria for the concrete representation of steel, bond and aggregate interlock.

Therefore, this prompts further investigation of slabs for the following aspects:

1. Contribution of steel in flexural stiffness matrix before cracking of concrete.
2. Cracking criterion based on principal curvatures or principal strains.
3. Tension-stiffening effect due to bond between steel reinforcement and concrete.
4. Aggregate interlock due to rough crack behaviour.

CHAPTER 3

FINITE ELEMENT ANALYSIS

3.1 Introduction

An analytical solution is a mathematical expression that gives the values of the desired unknown quantity at any location in a body, and as a consequence it is valid for an infinite number of locations in the body. Analytical solutions can be obtained only for certain simplified situations. It is not possible to obtain analytical mathematical solutions for many engineering problems. For problems involving complex material properties and boundary conditions, the engineer resorts to numerical methods that provide acceptable approximate solutions. In most of the numerical methods, the solutions yield approximate values of the unknown quantities only at a discrete number of points in the body. The process of selecting only a certain number of discrete points in the body can be termed discretization. One of the ways to discretize a body or a structure is to divide it into an equivalent system of smaller bodies or units. The assemblage of such units then represents the original body.

The best known earlier numerical method is Finite Difference. In the finite difference approximation of a differential equation, the derivatives in the equations are replaced by difference quotients which involve the values of the solution at discrete mesh points of the domain. The resulting discrete equations are solved,

after imposing the boundary conditions, for the values of the solution at the mesh points. Although the finite difference method is simple in concept, it suffers from several disadvantages. The most notable are the inaccuracy of the derivatives of the approximated solution, the difficulty in imposing the boundary conditions along nonstraight boundaries, the difficulty in accurately representing geometrically complex domains and the inability to employ non-uniform and non rectangular meshes.

In the variational solution of differential equations, the differential equation is put into an equivalent variational form. Then the approximate solution is assumed to be a combination ($\sum a_j \phi_j$) of given approximation functions ϕ_j . The parameters a_j are determined from the variation form. The variational method suffer from the disadvantage that the approximation functions for problems with arbitrary domains are difficult to construct.

The finite-element method overcomes the difficulty of the variational methods because it provides a systematic procedure for the derivation of the approximate functions. Finite element method is a numerical technique for approximating the governing differential equations for a continuous system with a set of algebraic equations relating a finite number of variables. The method is endowed with two basic features which account for its superiority over the competing methods. First, a geometrical complex domain of the problem is

represented as a collection of geometrically simple subdomains, called **finite elements**. Second, over each finite element the approximation functions are derived using the basic idea that any continuous function can be represented by a linear combination of algebraic polynomials. The approximation functions are derived using concepts from interpolation theory, and are therefore called **interpolation functions**. Thus, the finite element method can be interpreted as a piecewise application of the variational methods, in which the approximation functions are algebraic polynomials and the undetermined parameters represent the values of the solution at a finite number of pre-selected points, called nodes, on the boundary and in the interior of the element.

The finite element method has developed simultaneously with the increasing use of high-speed electronic digital computers and with the growing emphasis on numerical methods for engineering analysis. Although the method was originally developed for structural analysis, the general nature of the theory on which it is based has also made possible its successful application for solutions of problems in other fields of engineering.

Although the approach shares many of the features common to the previous numerical approximations, it possesses certain characteristics that take advantage of the special facilities offered by the high-speed computers. In particular, the method can be systematically programmed to accommodate complex and difficult problems

such as non homogeneous materials, non-linear stress-strain behaviour and complicated boundary conditions.

3.2 Development of Finite Element Method

The idea of representing a given domain as a collection of discrete elements is not novel with the finite element method. It was recorded that ancient mathematicians estimated the value of π by noting that the perimeter of a polygon inscribed a circle approximates the circumference of a circle. They predicted the value of π to accuracy of almost 40 significant digits by representing the circle as a polygon of a finitely large number of sides.

An approach similar to the finite element method, involving the use of piecewise continuous functions defined over triangular regions, was first suggested by Courant[63] in 1943 in the literature of applied mathematics.

The finite element method as known today has been presented in 1956 by Turner et al[64]. This paper presents the application of simple finite elements (pin-jointed bar and triangular plate with inplane loads) for the analysis of aircraft structure and is considered as one of the key contributions in the development of the finite element method. However, the term "finite element" was first used by Clough[65] in 1960. Since its inception, the literature on finite element applications has grown exponentially, and today there are numerous journals which are primarily

devoted to the application of finite element method. The book by Zienkiewicz[37] presents the broad interpretation of the method and its applicability to any general field problems.

3.3 General Description of Finite Element Method

The solution of a general continuum problem by the finite element method always follows an orderly step-by-step process. With reference to static structural problems, the step-by-step procedure can be stated as follows:

Step (i): Discretization of the Structure

The first step in the finite element method is divide the structure or solution region into subdivisions or elements. Hence, the structure that is being analyzed has to be modeled with suitable finite elements. The number, type, size and arrangement of the elements have to be decided.

Step (ii) Selection of a Proper Interpolation or Displacement Model

Since the displacement solution of a complex structure under any specified load conditions cannot be predicted exactly, assume some suitable solution within an element to approximate the unknown solution. The assumed solution must be simple from computational point of view, but it should satisfy certain convergence requirements. In general, the solution or the interpolation model is taken in the form of a polynomial.

Step (iii) Derivation of Element Stiffness Matrices and Load Vectors

From the assumed displacement model, the stiffness matrix $[k^{(e)}]$ and the load vector $[P^{(e)}]$, of element "e" are to be derived by using either equilibrium conditions or a suitable variational principle.

The element strains $\{\varepsilon^{(e)}\}$ and nodal displacements $\{\delta^{(e)}\}$ can be related by the [B] matrix

$$\{\varepsilon^{(e)}\} = [B] \{\delta^{(e)}\} \quad \dots(3.1)$$

The general stress-strain relation for an element is expressed as

$$\{\sigma^{(e)}\} = [D] \{\varepsilon^{(e)}\} \quad \dots(3.2)$$

in which [D] reflects any material behaviour of an element. Equilibrium between the external loads $[P^{(e)}]$ and stresses $\{\sigma^{(e)}\}$ is represented by the volume integral.

$$[P^{(e)}] = \int_v [B]^T \{\sigma^{(e)}\} dv \quad \dots(3.3)$$

substitution of equations (3.1) and (3.2) into equation (3.3) results in the well known stiffness relationship

$$[P^{(e)}] = [k^{(e)}] \{\delta^{(e)}\} \quad \dots(3.4)$$

in which the element stiffness matrix is given by

$$[k^{(e)}] = \int_v [B]^T [D][B]dv \quad \dots(3.5)$$

Step (iv): Assemblage of element equations to obtain the overall equilibrium equations

Since the structure is composed of several finite elements, the individual element stiffness matrices and load vectors are to be assembled in a suitable manner and the overall equilibrium equations have to be formulated as

$$[K]\{\delta\} = [P] \quad \dots(3.6)$$

Where $[K]$ is called the assembled stiffness matrix, $\{\delta\}$ is the vector of nodal displacements and $[P]$ is the vector of nodal forces for the complete structure.

Step (v): Solution for the Unknown Nodal Displacements

The overall equilibrium equations have to be modified to account for the boundary conditions of the problem. After the incorporation of the boundary conditions, the equilibrium equations are solved for unknown nodal displacements. For linear problems, the vector $\{\delta\}$ can be solved very easily. But for nonlinear problems, the solution has to be obtained in a sequence of steps, each step involving the modification of the stiffness matrix $[K]$ and/or the load vector $[P]$.

Step (vi): Computation of Element Strains and Stresses from the known nodal Displacements, if required. The element strains and stresses can be computed by using the necessary equations of solid or structural mechanics such as equations (3.1) and (3.2).

(The terminology used in the above six steps has to be modified to extend for field problems e.g., use the term continuum or domain in place of structure, field variable in place of displacement, characteristic matrix in place of stiffness matrix, and element resultants in place of element strains).

3.4 Selection of Plate Bending Element

One of the first tasks facing a potential practitioner of the finite element method is element selection. At this stage, one is confronted with the bewildering array of elements that has resulted from over forty years of research activity. An area for which this problem is particularly difficult is that of plate bending where the number of available elements is large and no one particular element has emerged as the so called "best" element.

Interest in plate bending elements came very early in the history of the finite element method. At the beginning of 1960, number of elements were proposed by researchers such as Melosh[36] and Clough and Tocher[66]. These elements, as with most others developed in that period, were of the displacement type.

By the middle of 1960s, the variational basis for finite element method has become better understood, and coupled with this, came the realization that inter element compatibility or conformity was an important property. Without it element convergence might not always be obtained.

The conformity requirement for plate problems proved to be particularly problematic in that inter element continuity is required for both the transverse displacement and the slope normal to the element boundary. Most early plate bending elements were of the non-conforming type.

The derivation of suitable triangular element proved to be considerably more difficult than rectangular elements. Clough and Tocher[66] discussed three of the early non-conforming triangular elements. One of these is an element which violates the constant strain requirement and does not converge. The second converges but is not geometrically isotropic and cannot be derived for certain shapes. The third does not pass the patch test and was found to converge to incorrect results. Therefore, satisfying the conformity requirement for triangular elements was found to be particularly difficult.

Conforming plate elements were not only difficult to obtain, but with the exception of the higher order elements, they were found to be too stiff. There was considerable scepticism about the need to meet the C^1 continuity requirement and

many researchers looked for alternate formulations. The subsequent research followed several different paths.

Success in achieving full conformity came easiest in the case of rectangular elements. Bogner et al.[67] developed 16 and 36 degree of freedom conforming rectangles that exhibited good convergence properties. It was necessary, however, to use second derivatives of displacement as degrees of freedom. It was explained later by Irons and Draper[68] that it is not possible to derive a conforming element using simple polynomials and only three geometric degrees of freedom.

A large number of plate bending elements have been developed and reported in the literature. A survey of these elements has been presented by Hrabok and Hruđey[69]. According to thin plate theory, the deformation is completely described by the transverse deflection of the middle surface of the plate (w) only. Thus, if a displacement model is assumed for w , the continuity of not only w , but also its derivatives have to be maintained between adjacent elements. The polynomial for w must be able to represent constant strain states. This means that the assumed displacement model must contain constant curvature states $\partial^2 w / \partial x^2$, $\partial^2 w / \partial y^2$ and constant twist $\partial^2 w / \partial x \partial y$. Also the polynomial for w should have geometric isotropy. Thus it becomes evident that it is much more difficult to choose a displacement model satisfying all these requirements.

The finite element used in this study is a four noded, rectangular plate bending element with sixteen degrees of freedom developed by Bogner et al.[67]. The displacement field is in terms of local coordinates ξ and η assumed as

$$\begin{aligned}
 w = & \alpha_1 + \alpha_2\xi + \alpha_3\eta + \alpha_4\xi^2 + \alpha_5\xi\eta + \alpha_6\eta^2 + \alpha_7\xi^3 + \alpha_8\xi^2\eta \\
 & + \alpha_9\xi\eta^2 + \alpha_{10}\eta^3 + \alpha_{11}\xi^3\eta + \alpha_{12}\xi\eta^3 + \alpha_{13}\xi^2\eta^2 \\
 & + \alpha_{14}\xi^3\eta^2 + \alpha_{15}\xi^2\eta^3 + \alpha_{16}\xi^3\eta^3 \quad \dots(3.7)
 \end{aligned}$$

It may be seen that the above equation is a 'complete polynomial' for the terms of the expression correspond to the product $(1 + \xi + \xi^2 + \xi^3)(1 + \eta + \eta^2 + \eta^3)$. This displacement function results in a cubic polynomial for the displacements and the slopes along the edges of the elements. It can be proved that the normal slope along any edge is completely defined, because of the choice of $\partial^2 w / \partial x \partial y$ as a degree of freedom at each node. Thus the element is fully compatible element. The nodal degree of freedom at each node is given by w , θ_x , θ_y and θ_{xy} . Where w is the transverse displacement and θ_x , θ_y and θ_{xy} are rotations respectively.

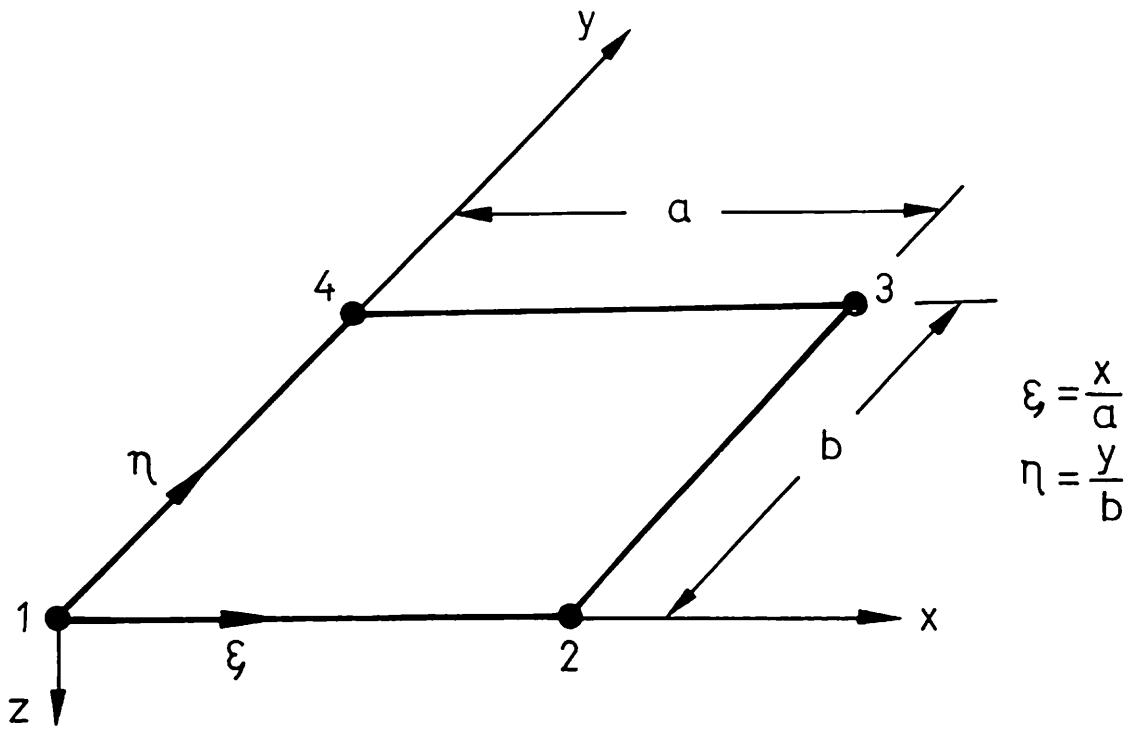


Fig.3.1a Rectangular plate bending element

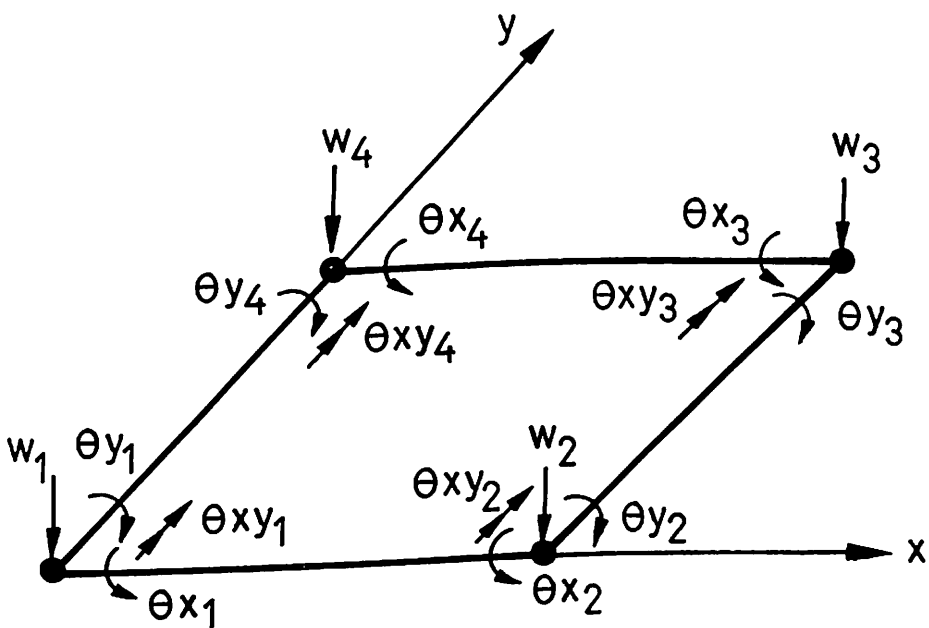


Fig.3.1b Nodal degrees of freedom $|\delta^{(e)}|_{16 \times 1}$

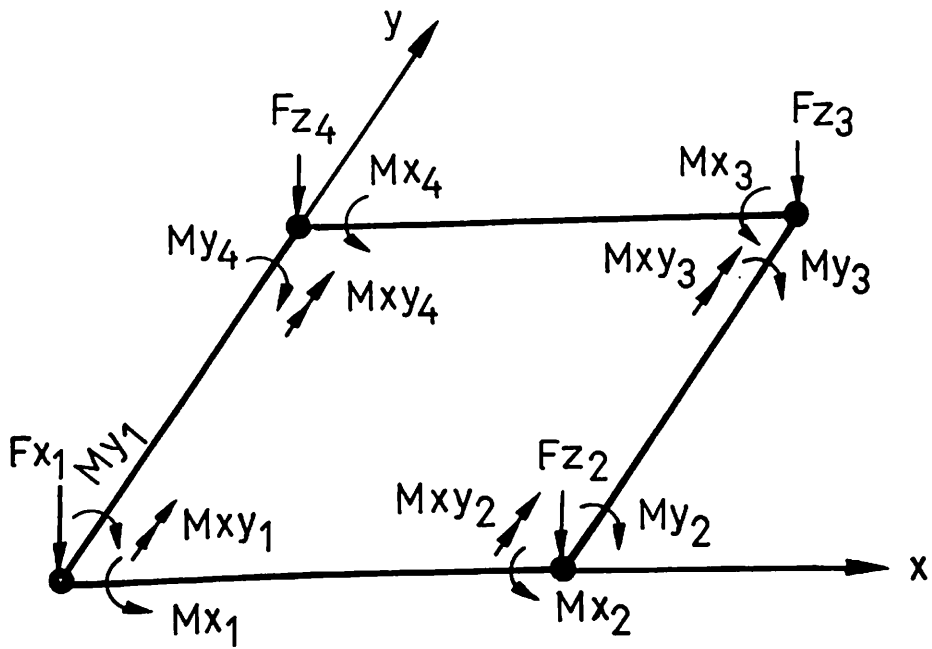


Fig.3.1c Element nodal forces $[P^{(e)}]_{16 \times 1}$

The interpolation functions are Cubic (Hermitian) polynomials which are listed below:

$$f_1(S) = 1-3S^2+2S^3$$

$$f_2(S) = 3S^2-2S^3$$

$$g_1(S) = S-2S^2+S^3$$

$$g_2(S) = S^3-S^2$$

The shape functions related to 16 degrees of freedom are written as below:

$$N_1 = f_1(\xi) f_1(\eta)$$

$$N_2 = a g_1(\xi) f_1(\eta)$$

$$N_3 = b f_1(\xi) g_1(\eta)$$

$$N_4 = ab g_1(\xi) g_1(\eta)$$

$$N_5 = f_2(\xi) f_1(\eta)$$

$$N_6 = a g_2(\xi) f_1(\eta)$$

$$N_7 = b f_2(\xi) g_1(\eta)$$

$$N_8 = ab g_2(\xi) g_1(\eta)$$

$$N_9 = f_2(\xi) f_2(\eta)$$

$$N_{10} = a g_2(\xi) f_2(\eta)$$

$$N_{11} = b f_2(\xi) g_2(\eta)$$

$$\begin{aligned}
N_{12} &= ab \, g_2(\xi) \, g_2(\eta) \\
N_{13} &= f_1(\xi) \, f_2(\eta) \\
N_{14} &= a \, g_1(\xi) \, f_2(\eta) \\
N_{15} &= b f_1(\xi) \, g_2(\eta) \\
N_{16} &= ab \, g_1(\xi) \, g_2(\eta) \qquad \dots(3.8)
\end{aligned}$$

where ξ and η are local coordinates.

If a distributed loading q is acting per unit area of an element in direction of w then the contribution of these forces to each of the nodes is

$$\begin{aligned}
\{ Q^{(e)} \} &= [N]^T q \, dx dy \\
&= q \sum_{i=1}^n \sum_{j=1}^n w_i w_j \begin{bmatrix} N_1 \\ N_2 \\ \vdots \\ N_{16} \end{bmatrix} \quad 16 \times 1 \qquad \dots(3.9)
\end{aligned}$$

Gauss quadrature with 4x4 sampling points is used to evaluate the above shape functions.

The strain-curvature relationship for plate is

$$\begin{Bmatrix} \epsilon_x \\ \epsilon_y \\ \gamma_{xy} \end{Bmatrix} = \begin{Bmatrix} \partial^2 w / \partial x^2 \\ \partial^2 w / \partial y^2 \\ 2\partial^2 w / \partial x \partial y \end{Bmatrix} \quad \dots(3.10)$$

The corresponding 'stresses' are infact the usual bending and twisting moments per unit lengths in x and y directions.

$$\{\sigma^{(e)}\} = \begin{Bmatrix} M_x \\ M_y \\ M_{xy} \end{Bmatrix} \quad \dots(3.11)$$

The [B] matrix will be determined in the form of shape function as

$$[B]_{3 \times 16} = \begin{Bmatrix} \partial^2 N_i / \partial \xi^2 \\ \partial^2 N_i / \partial \eta^2 \\ 2\partial^2 N_i / \partial \xi \partial \eta \end{Bmatrix} \quad \dots(3.12)$$

where N_i represents shape functions from N_1 to N_{16} .

The material behaviour matrix [D] is involved in the usual form.

$$[\sigma^{(e)}] = [M^{(e)}] = [D] (\{\epsilon\} - \{\epsilon_0\}) + [\sigma_0]$$

Where $\{ \epsilon_0 \}$ and $[\sigma_0]$ are initial strains and initial stresses correspondingly.

For an isotropic plate, the material behaviour matrix is

$$[D] = \frac{Eh^3}{12(1-\nu^2)} \begin{bmatrix} 1 & \nu & 0 \\ \nu & 1 & 0 \\ 0 & 0 & (1-\nu)/2 \end{bmatrix} \quad \dots(3.13)$$

Once the $[B]$ matrix and $[D]$ matrix are calculated, the element stiffness matrix can be computed using equation (3.4).

For each element the stiffness and load matrices are calculated. They are assembled to give global stiffness and load matrices. Then the boundary conditions are applied and unknown nodal displacements are calculated using Gauss-elimination method. These global nodal displacements are converted to element nodal displacements, to calculate curvatures $[C^{(e)}]$ and moments $[M^{(e)}]$ at the centre of each element.

$$[C^{(e)}] = [B] \{ \delta^{(e)} \} \quad \dots(3.14)$$

$$[M^{(e)}] = [D] [C^{(e)}] \quad \dots(3.15)$$

The principal curvatures corresponding to maximum and minimum curvatures are given by

$$C_i = \frac{C_x + C_y}{2} \pm \sqrt{\left(\frac{C_x - C_y}{2}\right)^2 + \left(\frac{C_{xy}}{2}\right)^2} \quad \text{for } i=1,2 \quad (3.16)$$

These fall in the principal planes of curvature whose directions are given by angle ' θ ' such that

$$\tan 2\theta = \frac{C_{xy}/2}{(C_x - C_y)/2} \quad (3.17)$$

Linear elastic analysis of slabs is performed using the developed software for linear elastic solutions. The solutions are based on classical plate theory assumptions[70]. The validity of the approximate, numerical treatment is therefore tested against plate theory solutions. For linear elastic analysis of structural problems the flow chart is given in Appendix – A. The convergence of selected plate bending element is seen from the obtained results (Appendix-A).

3.5 Nonlinear Material Behaviour

Application of the finite element method to problems involving materials that obey linear constitutive laws is straight forward, because the material parameters are constant. Only one application of the solution process is required to obtain results for a particular loading case.

The physical or material nonlinearity, encompasses problems in which the stresses are not linearly proportional to the strains, but in which only small displacements and small strains are considered. Displacements refer to the changes in overall geometry of the body, where as strains are related to internal deformations. The word "small" usually implies infinitesimal changes in the geometry of the body. Hence, the areas of the original, undeformed element can be used in computing stresses. Therefore, a separate solution process is required for nonlinear analysis.

The stiffness matrix for the nonlinear analysis is computed from the usual relationship,

$$[k^{(e)}] = \int_V [B]^T [D(\sigma)] [B] dv$$

The matrix $[D(\sigma)]$ is now variable and may need updating at each step of the procedure.

For nonlinear elastic behaviour the material parameters depend upon the state of stress or strain. An incremental approach often used for nonlinear analysis requires a separate solution process for each of the several increments of the load. Essentially the incremental technique approximates the behaviour as piecewise linear. In other words, during the application of each load increment, the material is considered to be linear and elastic, but different material properties are used for different increments. Hence, the principles developed for linear elastic behaviour become applicable in the range of each small increment.

Once the increments of displacements are obtained, the increments of the strains and stresses may be evaluated by using the proper strain-displacement equations and the current stress-strain law. For the small displacement, small strain case of nonlinear elasticity, for instance, the incremental forms of the strain-displacement equation, and the stress-strain equation are

$$\{\Delta \epsilon_i\} = [B] \{\Delta \delta_i\} \quad \dots(3.19)$$

$$\{\Delta \sigma_i\} = [D(\{\sigma_{i-1}\})] \{\Delta \epsilon_i\} \quad \dots(3.20)$$

For small displacements, the stresses and strains may be cumulatively added, so at the end of the i^{th} stage

$$\{\varepsilon_i\} = \{\varepsilon_o\} + \sum_{j=1}^i \{\Delta\varepsilon_j\} \quad \dots(3.21)$$

$$\{\sigma_i\} = \{\sigma_o\} + \sum_{j=1}^i \{\Delta\sigma_j\} \quad \dots(3.22)$$

where $\{\varepsilon_o\}$ and $\{\sigma_o\}$ are the initial strains and stresses at $\{\delta_o\}$, $\{P_o\}$. Usually $\{\delta_o\}$ and $\{P_o\}$ are null vectors because of undeformed state of the body. These values will be specified from the equilibrium state.

Once the current state, $(\{\sigma_i\}, \{\varepsilon_i\})$, is computed, enter the given constitutive law, such as a uniaxial test curve or an equivalent stress-strain curve, to compute the appropriate moduli.

In the piecewise, linear approximation, suitable elastic constants, such as E and ν for the isotropic case, may be obtained in one of two ways. The tangent modulus at any point A is defined as the slope of the stress-strain curve at point A.

$$E_t = \left. \frac{d\sigma}{d\varepsilon} \right|_A \quad \dots(3.23)$$

Alternatively, a secant modulus can also be defined in terms of the total stress and strain at a given stage such as

$$E_s = \frac{\sigma}{\varepsilon} \Big|_A \quad \dots(3.24)$$

A secant modulus computed between two points is known as chord modulus when neither of the points is the origin of the stress-strain curve.

3.6 Material Characterization

Usually the behaviour of real materials is highly complex and is influenced by factors such as the physical properties, the magnitude and nature of the loads, the temperature, the time, the rate of loading, and the previous history of the material. A constitutive relation is generally derived from field and/or laboratory experiments on the material. Ideally, these tests should simulate all significant factors and conditions existing in the actual body or prototype.

The results from any numerical or analytical technique are valid only to the extent that the constitutive model is accurate. Hence for realistic results from finite element analysis, it is imperative that the constitutive relations be carefully determined from proper tests.

In physically nonlinear problems the material properties vary. Therefore, an important aspect of analysis is a knowledge of the stress-strain curves or the constitutive laws.

$$\{\sigma\} = f(\{\sigma\}, \{\varepsilon\}) = [D(\{\sigma\})] \{\varepsilon\} \quad \dots(3.25)$$

There are two common procedures for incorporating a nonlinear stress-strain law into a finite element formulation for digital computation. The stress-strain law derived from a laboratory test can be used directly in a tabular or digital form. Several points on the curve are selected and are input in the form of number pairs denoting stress and strain at these points. The variable parameters such as E and are obtained from such curves by suitable interpolation. If the behaviour is represented by a single stress-strain curve, obtain strains by interpolation for a calculated state of stress. If the behaviour is represented by several curves, also interpolate between two curves for different values.

In the alternative procedure, the laboratory stress-strain curve is expressed in the form of a suitable mathematical function. This later procedure has been adopted for present study to analyse reinforced concrete slabs.

3.7 Nonlinear Solution Techniques

The solution of nonlinear problems by the finite element method is usually attempted by one of three basic techniques. Incremental or stepwise procedures, iterative or Newton methods, and step iterative or mixed procedures.

The principal advantage of the incremental procedure is its complete generality. It is applicable to nearly all types of nonlinear behaviour, with the possible exception of softening materials. Because of this generality, the stepwise procedure is the method often employed in finite element analysis. The other advantage of this technique is that it provides a relatively complete description of the load-deformation behaviour. Useful results are obtained at each of the intermediate states corresponding to any increment of load.

The incremental method is usually more time-consuming than the iterative technique. In addition, it is difficult to know in advance what increments of loads are necessary to obtain a good approximation to the exact solution.

The iterative method is easier to use and program than the incremental method. It is faster, provided we need to analyze only a few different loadings. It has been found useful in the case in which the materials have different elastic properties in tension and compression, the so-called bi-modular materials. Finally, the iterative procedure, combined with the secant stiffness approach, may prove successful for the analysis of bodies with work softening material properties, for which the incremental method fails.

The principal disadvantage of the iterative method is that there is no assurance that it will converge to the exact solution. Furthermore, the technique is

not applicable to materials with path dependent behaviour. A third limitation of the iterative procedure is that the displacements, stresses, and strains are determined for only the total load. Hence, no information concerning the behaviour at intermediate loads is obtained. Finally, the iterative method requires an initial estimate of a nonzero displacement vector in some situations.

The mixed method or step iteration combines the advantages of both the incremental and iterative procedures and tends to minimize the disadvantages of each. Therefore, step- iteration procedure is being utilized increasingly. The additional computational effort is justified by the fact that the iterative part of the procedure permits one to assess the quality of the approximate equilibrium at each stage.

A common solution procedure for elastic problems is the incremental method utilizing the tangent stiffness concept. The iterative technique is occasionally employed in conjunction with the secant stiffness approach. In either case, the solution procedure is straight forward if no unloading or hysteric elasticity occurs. If they do occur, the incremental method must be used and special modifications to the procedure may become necessary.

These special methods are basically mixed method in which the stiffness matrix is modified for each increment but is held for the iterations within the increment.

In initial stress method, the stress increment $\{\Delta\sigma_i\}$ will not generally be the correct stress necessary to equilibrate the loads $\{\Delta P_i\}$ because of the nonlinearity. If the correct stress increment is $\{\Delta\sigma_{ci}\}$, the difference between the computed and correct stress is treated as the "initial stress" and a revised correction load vector $\{\Delta P_{ci}\}$ is calculated from

$$\{\Delta P_{ci}\} = \int_{\mathcal{V}} [B]^T \{(\Delta\sigma_i) - (\Delta\sigma_{ci})\} dv. \quad \dots(3.26)$$

This process is repeated until convergence is obtained, usually in three or four iterations. However, it requires more computational time. The initial strain method reduces the computational time. Initial strain method is used in practice for locking materials in which the strain has importance over stress level. Iterations are continued till the convergence in strain occurs.

CHAPTER 4

MATERIAL MODELS

4.1 Introduction

The basic information required in any finite element calculations for reinforced concrete is the multi-dimensional stress-strain relations. These constitutive relations adequately describe the basic characteristics of reinforced concrete materials subjected to loading. The rapid advancement of computer technology made the use of a sophisticated constitutive law possible. Since then, the constitutive modeling of concrete has been an attractive subject of many researchers[71,72]. Various models thus proposed can be pursued quite well to study the behaviour of concrete upto failure. However, the simulation of post-cracking behaviour is still under development. The post-cracking behaviour of concrete cannot be neglected in the simulation study of the response of concrete structures to loads. Thus this subject has received a wide attention and is currently being studied very actively.

The response of reinforced concrete structures under static loading is shown in Figure 4.1. The load-displacement curve has three turning points. Within two points the relationship between displacement and loading is approximately linear. These points depend mainly on the properties of materials used i.e. concrete and

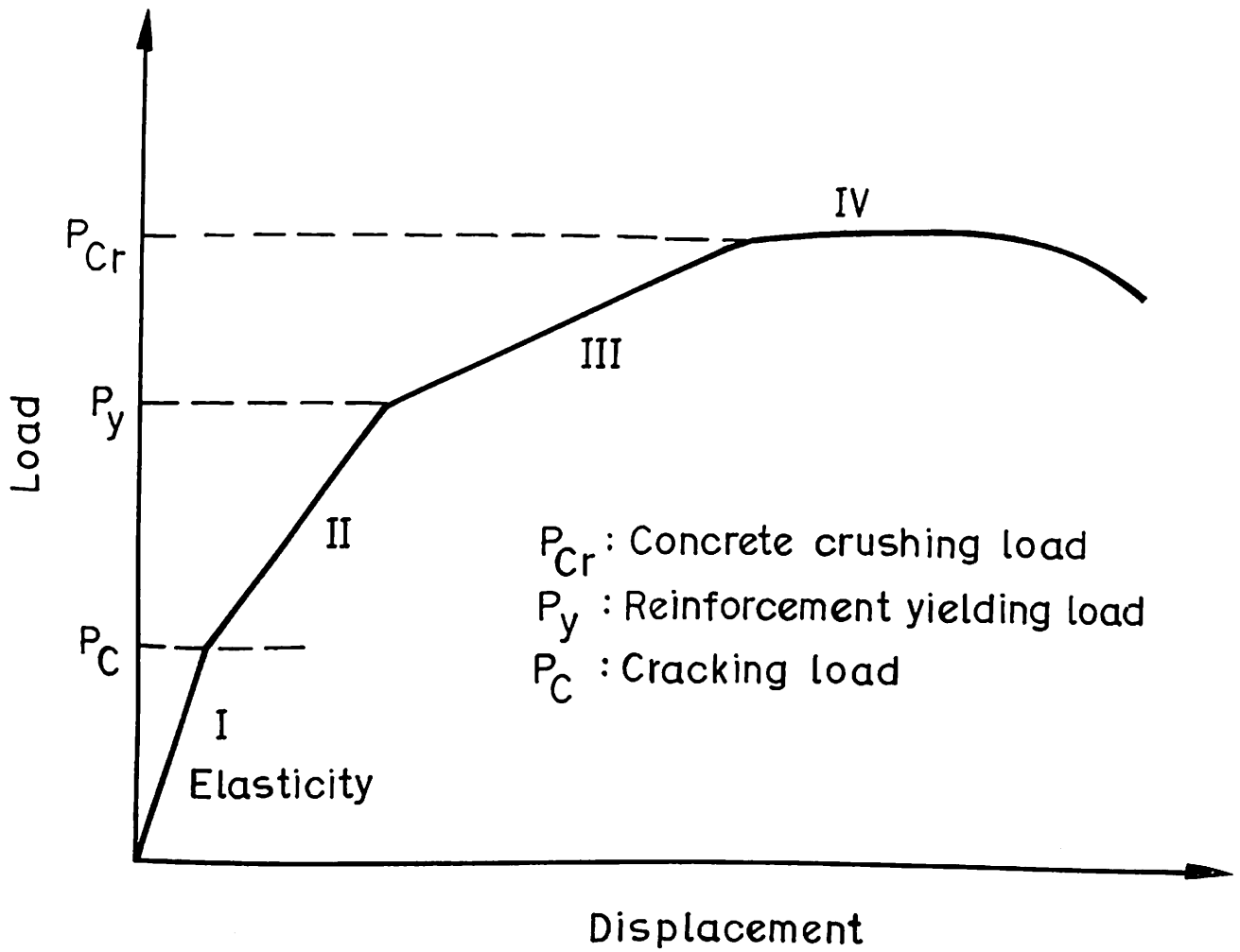


Fig.4.1 Behavior of Reinforced Concrete Structures. (62)

steel reinforcement. Therefore, the material models to be adopted should be able to represent these characteristics as close as possible.

To discuss the mathematical modeling of materials for non-linear reinforced concrete behaviour, three areas to be examined are:

- (a) The behaviour of concrete in compression,
- (b) The behaviour of concrete in tension and
- (c) The response of steel reinforcement.

4.2 BEHAVIOUR OF CONCRETE IN COMPRESSION

The earliest finite element models for reinforced concrete utilized linear representations for the concrete in compression. Non-linear behaviour in the form of cracking and compression softening were incorporated to improve the realism of the solution. Softening refers to any material response where the rate of change of incremental work is negative, in other words, where the slope of the stress-strain curve is negative. Over a period of time, the state-of-the-art progressed, and at present, many typical aspects of the experimental behaviour of plain concrete can adequately be represented.

The behaviour of concrete can be classified into three stages:

- (a) Linear elastic behaviour

- (b) Inelastic behaviour
- (c) Localized behaviour

These three stages are seen in a stress-strain relationship of plain concrete shown in Figure 4.2. The boundaries are not always obvious since it depends on strength of concrete. Hence, it is essential that all these three stages be embedded in the constitutive modeling to pursue a simulation of the complete behaviour.

4.2.1 Elasticity-based Models

A large number of elasticity-based constitutive models have been developed to represent the behaviour of concrete under general types of loading. The field of elasticity-based models is quite broad and can be broken down into sub-categories. Based on the form of the constitutive relations it can be modeled as incremental or total stress-strain models. Also based on the state of stress the concrete is modeled as uniaxial or biaxial or triaxial models.

The elasticity-based models have in common a Hook's^e formulation on either the total or the incremental stress-strain level. That is, the stress-strain behaviour can be expressed as either $\{\sigma\} = [D] \{\varepsilon\}$ or $\{d\sigma\} = [D] \{d\varepsilon\}$, where $[D]$ represents either the **secant** or **tangential** constitutive matrix; $\{\sigma\}$ and $\{\varepsilon\}$ are the stress and strain vectors; and $\{d\sigma\}$ and $\{d\varepsilon\}$ are the stress and strain increment vectors, respectively. The majority of the models are of the non-linear elastic type and are used primarily to represent concrete behaviour under monotonic or

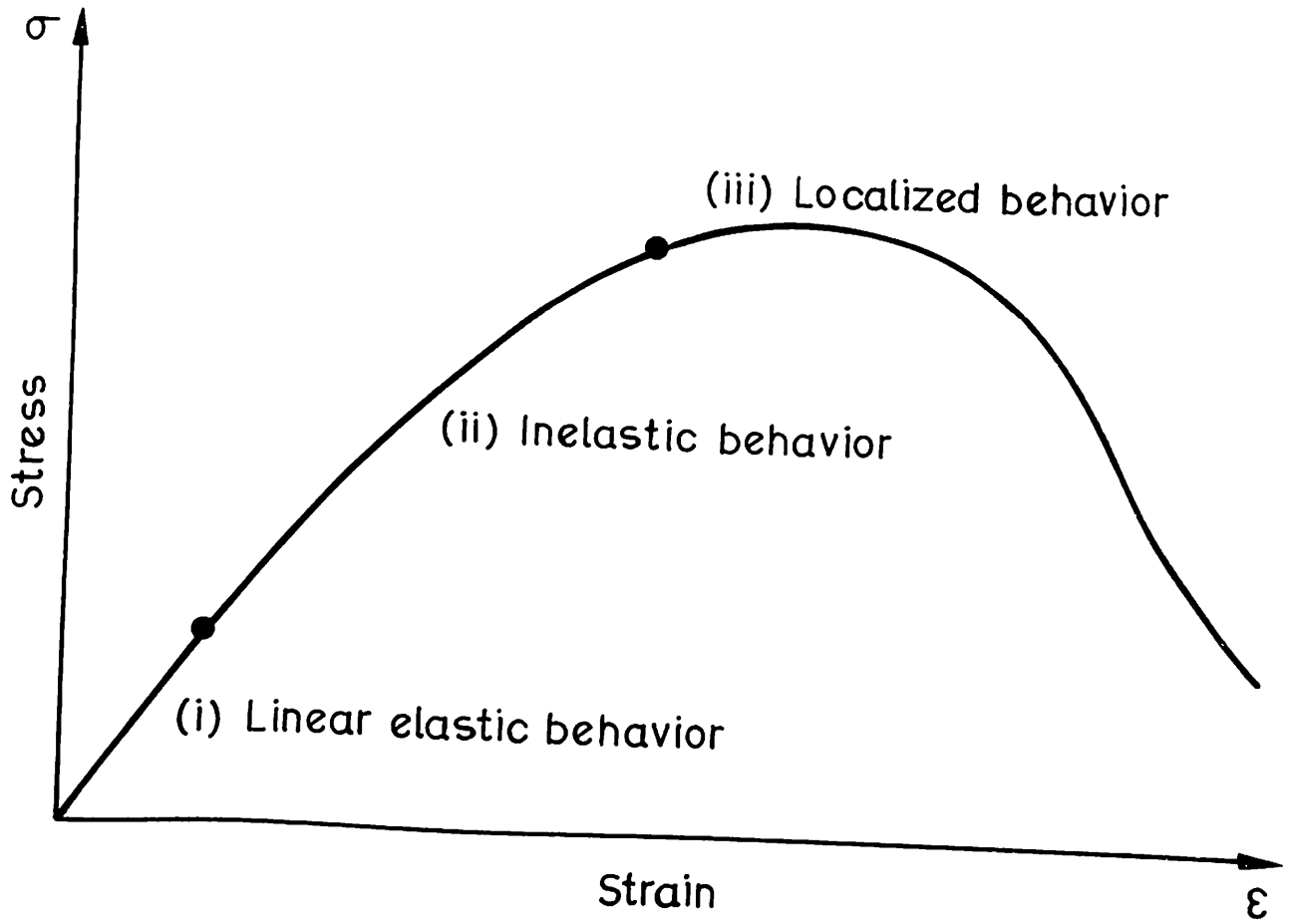


Fig.4.2 Typical stress-strain curve for concrete

proportional loading only. In general, two different approaches are employed in the formulation of the nonlinear elastic models for characterizing the degradation of concrete stiffness under loading. These are:

- (a) Finite (or total) material characterization in the form of secant stress-strain formulation.
- (b) Incremental (differential) material descriptions in the form of tangential stress-strain models.

In the total (secant) stress-strain models, the current state of stress $\{\sigma\}$ is determined as a function of the current state of strain $\{\epsilon\}$ or vice versa. The obvious limitation is that the behaviour is path-independent which is certainly not true for concrete in general. Thus, the range of application of such models is restricted primarily to monotonic or proportional loading regimes.

The incremental elasticity-based formulations belong to the class of constitutive relations known as hypoelastic. This type of formulation is often utilized to describe the behaviour of materials in which the state of stress depends on the current state of strain as well as on the stress path followed to reach that state. In a hypoelastic material model, the stress and strain increment tensors $\{d\sigma\}$ and $\{d\epsilon\}$ are linearly related through material response moduli that depend on stress $\{\sigma\}$ or strain $\{\epsilon\}$ or both. Due to their path-dependent behaviour

characteristic, incremental (hypoelastic) models provide more realistic descriptions of concrete behaviour under general loading conditions than the total stress-strain models. However, under general stress histories involving unloading and when a loading criterion is introduced to distinguish loading from unloading, both the above models fail to satisfy the continuity condition at or near neutral loading.

In the simplest approach of formulating hypoelastic models, the constitutive relations are restricted to be incrementally isotropic. The tangential stiffness matrix $[D]$ is then expressed in the same (isotropic) form as for the isotropic linear elastic models, with the tangential elastic moduli taken as functions of the stress or strain invariants. In an alternative approach, the incremental models have been constructed based on an assumed orthotropic form of the incremental stress-strain relations with the principal stress directions coinciding with the directions of orthotropy.

4.2.1.1 Uniaxial Behaviour

For a heterogeneous brittle material like concrete, cracking is a dominant factor for its behaviour. The development of microcrackings is closely related to the characteristics of stress-strain relation. In the uniaxial compression case, a comprehensive study has been made by Hsu et al [73], Shah and Chandra [74] and Krishnaswamy [75]. For about 30% of its uniaxial compressive strength (f_c) concrete behaves essentially as a linearly elastic material. However, it is known that

microscopic cracks or microcracks, begin forming at the mortar, coarse aggregate interface at stress as low as 30% of f_c . At about 70% of f_c microcracks begin to propagate through the mortar. The onset of mortar cracking occurs at the "discontinuity stress" and coincides with the increase in the Poisson's ratio of concrete. When subjected to increasing compressive strain, damage continues to accumulate and concrete enters the descending portion of its stress-strain curve.

Typical complete stress-strain curves for concrete under monotonic uniaxial compressive load are shown in Figure 4.3. The shape of the stress-strain curve is similar for low, normal and high strength concrete, with the high strength concrete exhibiting a slightly higher strain at the peak stress. On the descending portion of the stress-strain curve, high strength concrete tend to behave in a more brittle manner, with the stress dropping off more sharply than it does for concrete with lower strength. The initial modulus of elasticity of concrete (E_c) can be calculated with reasonable accuracy from the empirical equation

$$E_c = 33 W^{1.5} \sqrt{f'_c} \quad \dots(4.1)$$

For normal weight concrete,

$$E_c = 57000\sqrt{f'_c}$$

where

W is unit weight of concrete in pounds per cubic foot. E_c and f'_c are expressed in pounds per square inch.

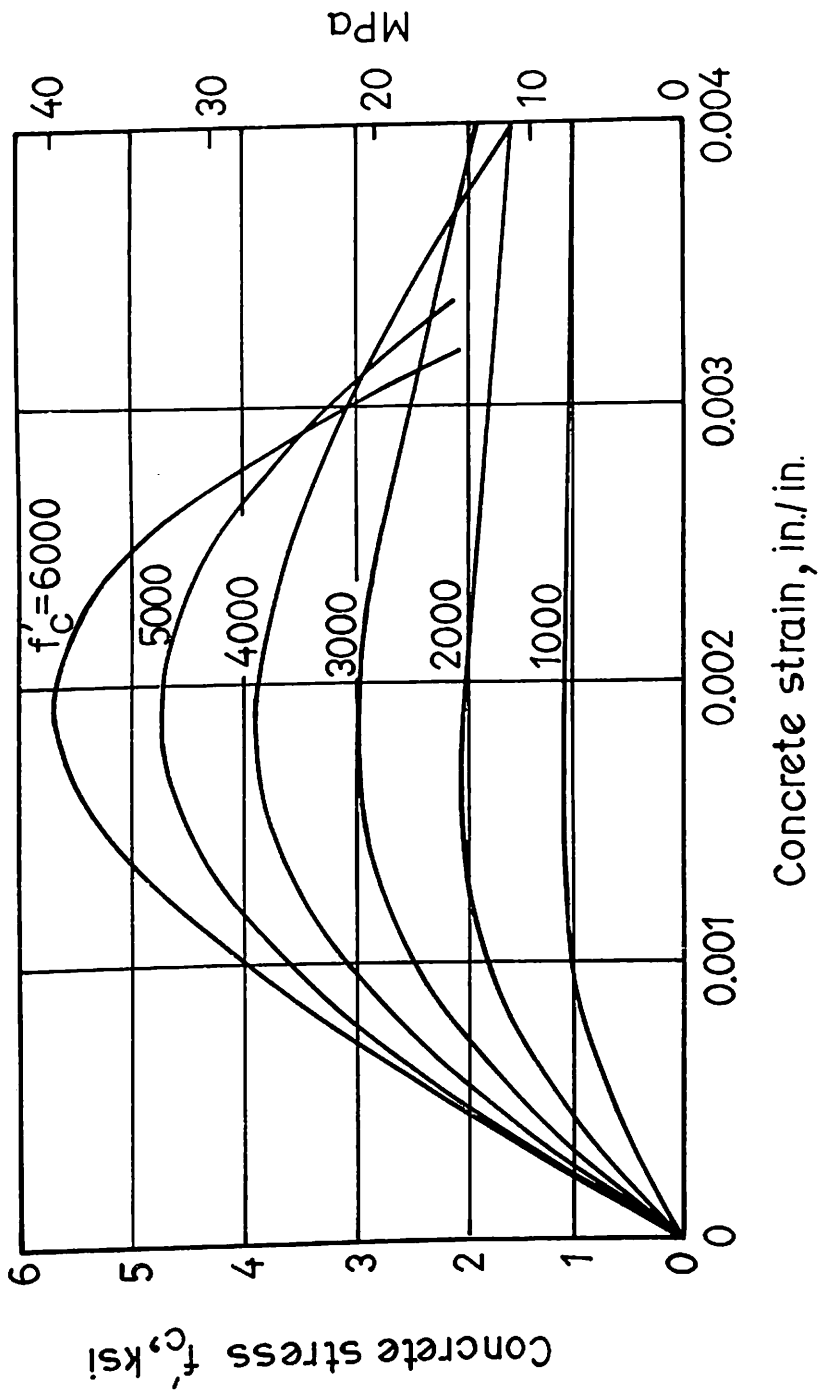


Fig.4.3 Typical concrete stress - strain curve for compression . (20)

The Poisson's ratio for concrete under uniaxial compressive stress ranges from about 0.15 to 0.22, with 0.19 or 0.20 being a representative value. Under uniaxial loading the ratio of lateral strain to principal compressive strain remains constant till 80% of f_c and later the apparent Poisson's ratio begins to increase, as may be evident from Kupfer et al [76] and Darwin and Pecknold [77].

A number of useful, special purpose material uniaxial models have been developed for use in modeling reinforced concrete structures in which the concrete can be represented as being in a state of uniaxial stress[78,79]. These representations fall under the general heading of fibre or filament models and have been successfully used for members under primarily flexural and/or axial load. For uniaxial models, there is not an important distinction between incremental and total stress-strain relations. Since the models are uniaxial, they are relatively simple to handle, even for complicated behaviour, because the stiffness and stress are functions of a single strain value.

4.2.1.2 Biaxial Behaviour

Figure 4.4 illustrates a typical biaxial strength envelope for concrete subjected to proportional biaxial loading. Under conditions of biaxial compression, concrete exhibits values of increased compressive strength upto about $1.25 f_c$ [76,80,81,82]. Under biaxial tension, concrete exhibits a constant, or perhaps a slightly increased, tensile strength, compared with values obtained under uniaxial loading[76].

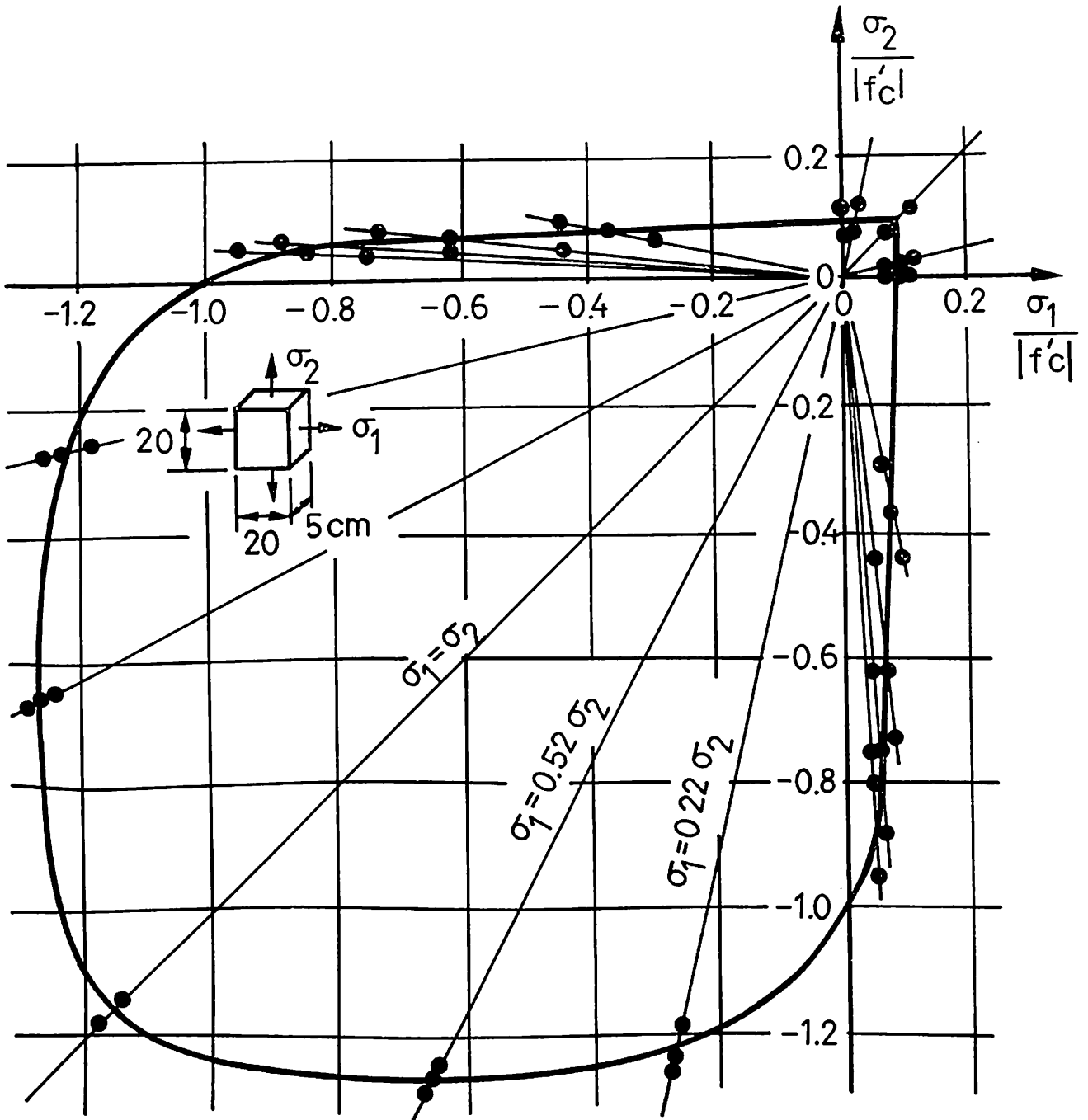


Fig.4.4 Biaxial strength of concrete. (76)

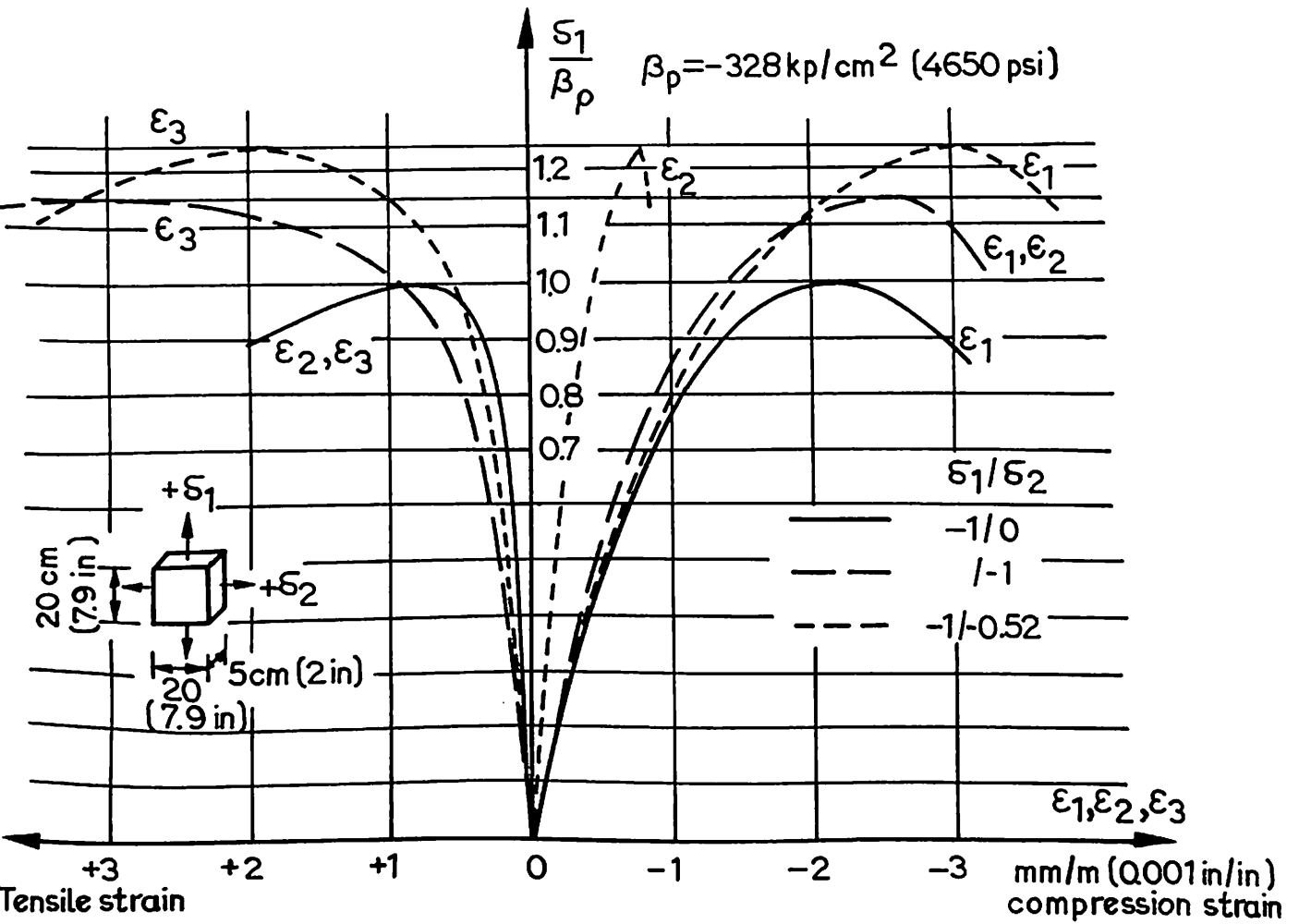


Fig.4.5 Stress strain relationships of concrete under biaxial compression. (76)

Under combinations of tension and compression, concrete exhibits a noticeably reduced strength. For biaxial compression, concrete exhibits an increased initial stiffness that may be attributed to the Poisson effect and an increased degree of ductility at the peak stress, which is an indication of the reduction in the degree of internal damage as compared to uniaxial loading as shown in Figure 4.5.

The maximum strength envelope seems to be largely independent of the loading path, although there is some indication that non-proportional loading produces a lower strength than proportional loading for light weight concrete. For proportional loading, the failure of concrete under various combinations of biaxial loading appears to be based on maximum tensile strain criteria[82].

Reinforced concrete structures can be adequately modeled by considering the concrete to be in a state of plane stress. The earliest and probably the most popular models have been of the biaxial type. Under the category of biaxial models, the most widely used representations are the isotropic total stress-strain models, the incremental isotropic and incremental orthotropic stress-strain descriptions.

In the earliest realistic finite element models of concrete, concrete has been represented as a linear isotropic material. Nonlinearity in the concrete was limited to cracking. In one case, the cracking was represented by a redefinition of the element topology after the concrete tensile strength had been attained[38]. While

this procedure is reasonably realistic, it is quite cumbersome to use in practice. The second procedure, in which the cracked concrete is treated as an orthotropic material, has proved to be more versatile[39,40]. The nonlinearity in these models was added by modifying the modulus of elasticity of the concrete as the stress in the concrete changed. None of these early models took into account the effect of biaxial stresses on the strength of concrete.

An isotropic total stress-strain model studied by Kupfer and Gerstle [83] based on monotonic tests of concrete under biaxial stress obtained a good match with experimental values of stress, but a poor match at high values of stress.

Another isotropic total stress-strain model for concrete under biaxial loading was developed by Romstad et al.[84]. Rather than utilizing continuous curves to represent the degradation of concrete, their model uses a number of damage regions, in which the material properties are altered to match the softening caused by increased stresses. Within each region the modulus of elasticity and Poisson's ratio are constant. The regions were developed in stress space and then transformed to strain space to avoid non-uniqueness of representation for the descending portion (softening) of the stress-strain curve.

Assuming the behaviour of concrete to be incrementally isotropic, Gerstle[85] has developed a tangential stress-strain model for concrete under

biaxial stresses. This formulation is based on the decoupling of the hydrostatic (volumetric) and deviatoric (shear) components of the response, which may be reasonable at low stress levels, but certainly not at high stress levels and particularly near failure. The constitutive relations are expressed in terms of tangential bulk and shear moduli (K_t and G_t), which are assumed to vary linearly as functions of the Octahedral normal and shear stresses respectively. The results of several biaxial test programs have been used to verify the effectiveness of the model, and for most of the cases considered, a good match with test data has been observed.

Parallel to the development of the isotropic biaxial models, a number of models were developed based on the observed behaviour characteristic of stress or strain induced anisotropy of concrete under biaxial stresses. Only a particular type of stress-induced anisotropy is, however, considered in these models since the concrete is represented as a biaxial orthotropic material, in which the moduli of elasticity along the principal axes of orthotropy, E_1 and E_2 , vary as a function of the state of stress and strain in each of the principal stress directions. Two representative models of this type are discussed below.

The model developed by Liu et.al. [80,81] controls the material properties based on total strains. The model originally developed for proportional loading express the principal stresses as closed form functions of the principal strains, the ratio of principal stresses and Poisson's ratio.

Referring to the principal axes of orthotropy (which are assumed to coincide with the current principal stress axes), the incremental constitutive equations take the following form:

$$\begin{bmatrix} d\sigma_1 \\ d\sigma_2 \\ d\tau_{12} \end{bmatrix} = \begin{bmatrix} \gamma E_1/E_2 & 1 & 0 \\ & \gamma & 0 \\ \text{Sym.} & & \frac{E_1+E_2}{E_1+E_2+2E_2\nu_1} \end{bmatrix} \begin{bmatrix} d\varepsilon_1 \\ d\varepsilon_2 \\ d\gamma_{12} \end{bmatrix} \quad \dots(4.2)$$

in which $\gamma = E_1/(E_1/E_2 - \nu_1^2)$, and $\nu_1 =$ Poisson's ratio associated with the principal compressive stress direction. The equations represent the shear modulus, G (lower right hand term in the constitutive matrix), such that the shear flexibility $1/G$ remains invariant with respect to the rotation of the coordinate axes. Minor errors in the stress obtained using E_i are corrected at each load step based on the total strains. A more serious objection is the requirement that principal stress axes coincide with principal strain axes, which does not hold for concrete under general loading. An incremental orthotropic model has been proposed by Darwin and Pecknold[77] based on the concept of **equivalent uniaxial strain**. The effects of biaxial stresses on internal damage in concrete are represented by equivalent uniaxial stress-strain curves for each of the principal stress axes. For a differential (incremental) change in principal stress ($d\sigma_i$) the change in equivalent uniaxial strain ($d\varepsilon_{iu}$), is $d\sigma_i/E_i$, or for finite changes, $\Delta\varepsilon_{iu} = \Delta\sigma_i/E_i$. The total equivalent uniaxial strains (accumulated in principal stress directions) are given by integration (or

summation) of $d\varepsilon_{iu}$ (or $\Delta\varepsilon_{iu}$) over the loading path; i.e., for $i = 1, 2$.

$$\varepsilon_{iu} = \int \frac{d\sigma_i}{E_i}$$

or

$$\varepsilon_{iu} = \sum_{\substack{\text{all load} \\ \text{increments}}} \frac{\Delta\sigma_i}{E_i} \quad \dots(4.3)$$

The equivalent uniaxial strains are not real strains, and do not transform under the rotation of axes, as do true strains. They are fictitious (except in a uniaxial test) and are only significant as a measure on which to base the variation of material properties.

Referring to the principal axes of orthotropy, the incremental constitutive relations are written as:

$$\begin{bmatrix} d\sigma_1 \\ d\sigma_2 \\ d\tau_{12} \end{bmatrix} = \frac{1}{(1-\nu^2)} \begin{bmatrix} E_1 & \nu\sqrt{E_1E_2} & 0 \\ & E_2 & 0 \\ \text{Sym.} & & \frac{1}{4}(E_1+E_2-2\nu\sqrt{E_1E_2}) \end{bmatrix} \begin{bmatrix} d\varepsilon_1 \\ d\varepsilon_2 \\ d\gamma_{12} \end{bmatrix} \quad \dots(4.4)$$

in which ν Poisson's ratio, and $d\varepsilon_1$, $d\varepsilon_2$ and $d\gamma_{12}$ are increments in the strain components in the current principal stress directions. In equation (4.4), the shear modulus, G , rather than $1/G$ as in equation (4.2), is invariant with respect to axes transformation.

The principal stress axes may rotate and do not, in general coincide with the principal strain directions. Potential weaknesses of the model may be the requirements that the equivalent uniaxial strains must be accumulated in the principal stress axes and, for monotonic loading, the values of the material parameters E_i are controlled by the principal stresses without regard to the rotation of the principal axes. For a proper objective formulation, the incremental constitutive relations for an (initially) isotropic concrete, such as equation (4.4) must be form invariant under any transformation of the coordinate axes. To achieve such invariant formulation for situations involving rotation of the principal stress directions, the equivalent uniaxial strain equation (4.3) might have scalars (not vectors or tensors) providing invariant measures of the strain history.

These aspects of the model have not appeared to affect its practical usefulness. The model is bound to be capable of modeling concrete behaviour under cyclic, as well as monotonic loads, and, to date, is the only elasticity-based model that provides this capability for conditions of plane stress. This model and its adoption have been applied to a wide variety of practical finite element problems.

Quite good agreement between the theoretical and available experimental test results has been obtained in several of the cases investigated.

4.2.1.3 Triaxial Behaviour

When subjected to triaxial loading, concrete appears to generate a fairly consistent failure surface, as that shown in figure 4.6, which is a function of the three principal stresses. Experimental studies have indicated that the three-dimensional failure surface for concrete can be defined in terms of the three stress variants ζ , ρ and λ that can be interpreted as the cylindrical geometric coordinates of the surface in the three-dimensional principal stress space. Some analyses indicate that failure under triaxial stress states may be represented by two stress invariants only i.e., the Octahedral normal and shear stresses, which are related to the invariants ζ and ρ . The most general formulation involves a third stress invariant ' θ ' to represent the complete three dimensional failure surface in stress space [86,87]. While some investigators find the failure surface to be independent of the loading path [88], others have found a significant dependence on the loading path [89]. Two of the most significant triaxial inelastic properties of concrete are the increase of volume due to large deviatoric strains, called inelastic dilatancy, and the large increase of ductility and strength caused by hydrostatic pressure.

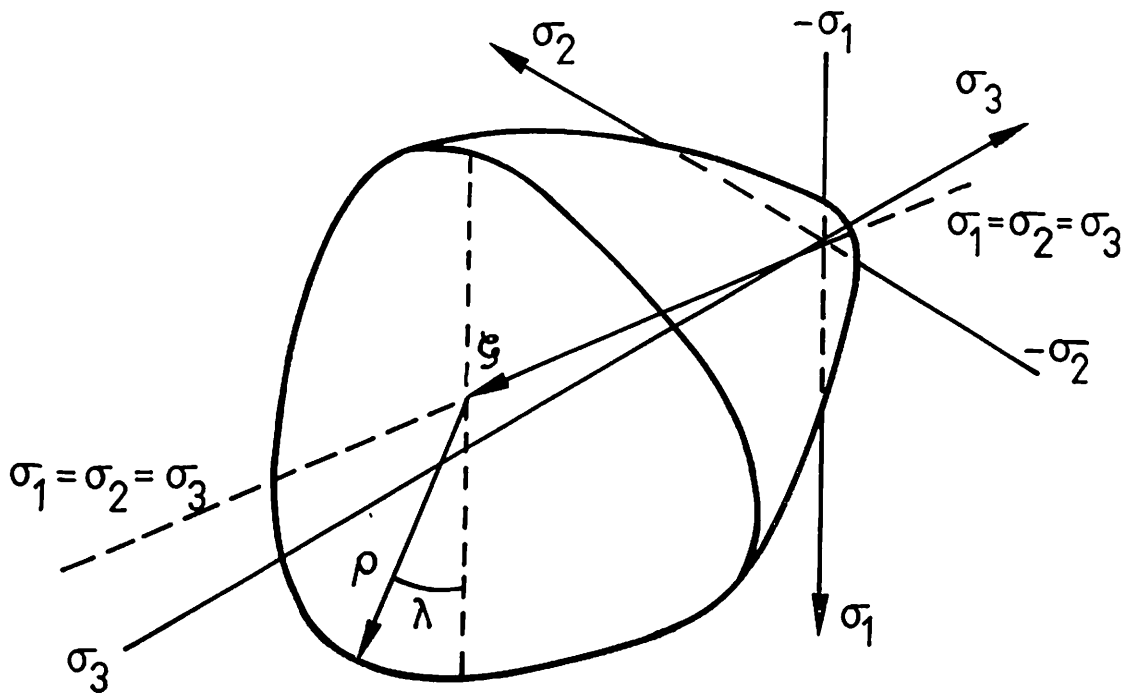


Fig.4.6 Triaxial strength surface in principal stress space. (86)

Bazant and Tsubaki [89] have recently developed, albeit at the cost of greater complexity, a total stress-strain model for triaxial compression with a broader range of applicability, which includes stress peaks, strain-softening, and inelastic dilatancy due to shear with its hydrostatic pressure sensitivity. The formulation is further extended by path-dependent terms which vanish for proportional loading. It results in the non-coincidence of the principal directions of stress and strain.

The majority of the triaxial models utilize isotropic total stress-strain material representations [90,91,92]. These models are designed to represent the behaviour of concrete under monotonic triaxial loading. The accuracy and sensitivity of the models range from those which are satisfactory for stresses up to about 70% of the ultimate load to those which are satisfactory right through failure.

Elwi and Murray [93] have developed an incremental orthotropic model for concrete under triaxial loading. Uniaxial strain approach is combined with the three-dimensional failure surface to represent concrete behaviour under three-dimensional axisymmetric loading.

Based on the classical hypoelastic formulation, Coon and Evans [94] have developed a first order (grade one) hypoelastic (incremental) model and applied it to describe concrete behaviour under the stress conditions in several tests (uniaxial and triaxial compression, and combined compression-torsion tests).

The triaxial elasticity based models have not been used widely because of the relative difficulty of three-dimensional finite element analysis compared to two dimensional analysis.

4.2.2 Plasticity-based Models

For typical stress-strain behaviour under compressive stresses, experimental results have indicated that the nonlinear deformations of concrete are basically inelastic, since upon unloading only a portion of the total can be recovered. Therefore, the stress-strain behaviour of concrete materials may be separated into recoverable and irrecoverable components. Attempts have been made to treat each component individually. The recoverable behaviour is treated within the framework of elasticity theory, while the irrecoverable part is based on theory of plasticity. Plasticity-based models have been used extensively to describe the behaviour of concrete [95-98]. In general, models based on the theory of plasticity describe concrete as an elastic-perfectly plastic material (perfect plasticity), or, to account for the hardening behaviour upto the ultimate strength, as an elastic-plastic-hardening material (strain-hardening plasticity).

The application of plasticity concept to concrete is criticised in that the inelastic behaviour predicted by a plasticity-based model is not accompanied by the degradation of elastic moduli, i.e. the decrease of the unloading stiffness. This degradation is sure to be observed in experiments. Also much more computational

efforts are required in finite element analysis since the stiffness matrix is no longer symmetric.

4.2.3 Plastic-Fracturing Models

In the plastic-fracturing theory the inelastic behaviour is attributed to two sources, plastic slip and micro cracking (or faulting). The former is formulated by the conventional plasticity concept while the latter is modelled by using the potential function in strain space. This second concept was initiated by Dougill [99]. Very good reproduction of the nonlinear multi-axial behaviour of concrete has been reported by Bazant and Kim [100]. However, much complexities in defining two loading functions are inevitable.

4.2.4 Endochronic Models

The endochronic theory was first applied to concrete by Bazant and Bhat [101]. The basic concept in this theory is that of intrinsic time, playing a similar role of effective plastic strain in the plasticity theory. The intrinsic time is the non-decreasing scalar variable representing the evolution of the measure of irreversible damage. This model can cover many phenomena like nonlinear behaviour, inelastic volume dilatancy, hydrostatic pressure sensitivity, etc. This can be achieved, however, only at the expense of greater complexity and increasing number of material parameters.

There is no basic difference between elasticity-based models and the plastic, plastic-fracturing and endochronic models. They all result in variable incremental material stiffness matrices (incremental "elasticity" matrices) applicable for certain ranges of loading directions. By "elasticity-based models", the tangential constitutive matrix is obtained or deduced directly by intuitive or approximate considerations that avoid the use of more sophisticated concepts such as loading functions, flow rules, intrinsic time, etc.

4.2.5 Comparison of Models

The strong point of most elasticity-based models is their conceptual simplicity in relation to other types of constitutive models. Most elasticity-based constitutive models do a reasonably good job of representing overall concrete behaviour, but a sizeable number do not give a close representation near ultimate stress. This drawback, however, has not seemed to cause major problems in the utilization of these models in finite element analysis. This apparent inconsistency is probably due to the fact that, even near the ultimate load, only a small portion of most structures is subjected to a high value of compressive stress, and the great majority of the nonlinear behaviour of the structure is controlled by cracking of concrete and yielding in reinforcing steel in tension. Current analysis procedures for two-dimensional reinforced concrete structures, such as plates and shells are essentially one-dimensional. A currently popular approach uses an equivalent uniaxial stress-strain relation for the biaxial stress-strain behaviour of concrete.

Hence various empirical stress-strain relations expressed in terms of their respective principal stress and strain values have been established from the curve-fitting of large amounts of biaxial test data. This approach is very appealing because of its broad data base and its conceptual simplicity. Multi-dimensional analyses are usually made by assuming the concrete behaviour to be incrementally elastic with variable moduli. However, it is not possible to describe accurately the three-dimensional stress-strain behaviour of concrete materials under general loading conditions in the framework of an incremental Hooke's law with variable moduli which are functions of the maximum stress and strain.

4.2.6 Modeling of Concrete in Compression

It is established that the presence of biaxial compression results in increased ultimate compressive strength, increased ductility and increased stiffness[76]. This increase depends upon the ratio of two applied stresses. The significance of these findings is that each fibre within the compression block and each direction at a point in the slab subjected to biaxial compression are governed by a different stress-strain relationship. The biaxial compressive effects may be included in the moment curvature computations if a numerical integration procedure is used in the computation of the section forces it is possible to include a different compressive stress-strain curve at each integration point. In the present approach, however, it would involve considerable additional computation effort to incorporate different compressive stress-strain curves. Besides, the effect of biaxial compression on the

moment-curvature relationship will be relatively small since the main characteristics of this relationship for under reinforced cross sections depend mainly on the characteristics of the reinforcing steel[53]. Therefore, no attempt is made to include the effect of biaxial compression.

The empirical stress-strain relationship for concrete in uniaxial compression proposed by Saenz[102] is generally accepted to model the nonlinear behaviour of concrete in compression zone of flexural members, and is therefore adopted here. The stress-strain relationship of concrete in compression is shown in Figure 4.7. The variables required to define the graph are peak strain ϵ_p and corresponding compressive strength of concrete f'_c , ultimate strain ϵ_u to describe the descending branch of the graph (softening of concrete in compression) and initial tangent modulus of concrete E_c as determined from uniaxial compression tests.

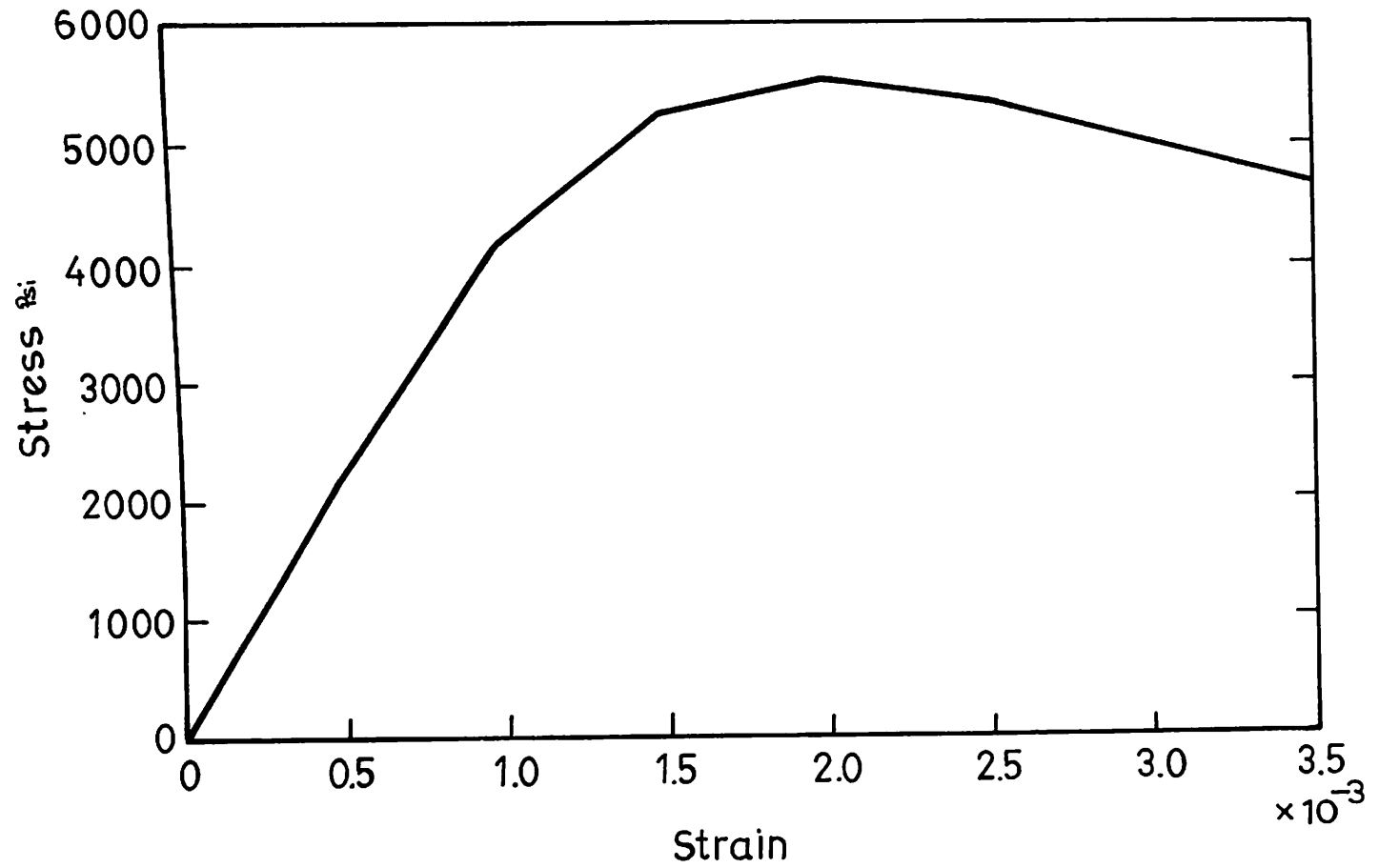


Fig.4.7 Concrete in compression

$$\{\sigma^c(\varepsilon)\} = \frac{\varepsilon}{A+B\varepsilon +C\varepsilon^2 +D\varepsilon^3} \quad \dots(4.5)$$

The conditions to be fulfilled are:

- for $\varepsilon = 0$ $\sigma = 0$ or point of origin
- for $\varepsilon = \varepsilon_p$ $\sigma = \sigma_p = f'_c$ or point of maximum stress
- for $\varepsilon = \varepsilon_f = \varepsilon_u$ $\sigma = \sigma_f = 0.85 f'_c$ or point of maximum strain
- for $\varepsilon = 0$ $d\sigma/d\varepsilon = E_c$ or value of initial elastic modulus.
- for $\varepsilon = \varepsilon_p$ $d\sigma/d\varepsilon = 0$ or maximum of the curve.

Fulfilling these conditions the value of the parameters are

$$A = \frac{1}{E_c}$$

$$B = \frac{(R_E+R-2)}{R_E\sigma_p}$$

$$C = \frac{-(2R-1)}{R_E\sigma_p \varepsilon_p}$$

$$D = \frac{R}{R_E\sigma_p \varepsilon_p^2}$$

Where

$$R = \frac{R_E(R_f - 1)}{(R_c - 1)^2} - \frac{1}{R_c} \text{ is the ratio relation}$$

$R_E = E_c/E_s$ is the modular ratio.

$E_s = \sigma_p / \epsilon_p$ is the secant modulus

$R_f = \sigma_p / \sigma_f$ is the stress ratio

$R_c = \epsilon_f / \epsilon_p$ is the strain ratio.

4.3 Behaviour of Concrete in Tension

The tensile weakness of concrete and the ensuing cracking that results therefrom, is a major factor contributing to the nonlinear behaviour of reinforced concrete elements. The tensile strength of concrete is receiving an increasing amount of attention since the loading capacity and durability of structures are being studied more thoroughly. Numerical methods require a comprehensive material behaviour i.e., complete stress deformation relation.

Tensile behaviour in concrete has been neglected until recently, since it usually does not significantly affect the ultimate strength of members. However, the effect of tensile stress in concrete must be taken into account when the load deflection characteristics of a member are needed, whether the member primarily carries tensile force or combined tensile and compressive stresses, as in flexural

problems, and when the ultimate strength is affected by the cracking history. In this case the effects of tension - softening or tension-stiffening become important and a realistic model should be used in the analysis.

4.3.1 Tensile Strength of Concrete

The magnitude of the tensile stress which causes the cracking to develop in roughly a direction perpendicular to the principal tensile stress is not a precisely defined quantity. There is significant scatter in test results. Further more, there are considerable experimental difficulties in conducting an experiment that produces the true tensile strength of the concrete. The direct tensile strength of concrete is difficult to measure and is normally taken as approximately $4\sqrt{f'_c}$. Many times, either the modulus of rupture or the split cylinder strength are used to approximate the tensile strength of concrete. The bending test of plain concrete beams establishes the modulus of rupture f_r . The numerical value of this strength is

$$f_r = 7.5\sqrt{f'_c} \quad \dots(4.6)$$

where f'_c in PSi.

The direct tension test such as that by Kupfer et al[76] yields results which are more direct measure of the tensile strength. The test results are slightly smaller than the split cylinder test values and smaller than those from the rupture test. These results are not as influenced by shrinkage, cracking, etc. as would be the

values established by the rupture test. The rupture test is, however, still the accepted method for the determination of the cracking moment in a beam because of the presence of the strain gradient. Of these values it would seem more appropriate to use the rupture values when a plane stress concrete element is being used to predict the behaviour of a member subjected primarily to flexure. However, when the problem is biaxial as with plates and shells, the values are normally quoted but adjusted in some manner to reflect more closely the modulus of rupture values.

4.3.2 Tension-Softening

The tension-softening phenomenon is associated with the crack-process zone development observed in plain concrete members after the tensile strength has been reached. Strain softening refers to any material response where the rate of change of incremental work is negative, in other words, where the slope of the stress-strain curve is negative.

On inspecting the stress-elongation diagram of a deformation-controlled uniaxial tensile test of concrete, few features can be distinguished from Fig. 4.8. The stress increases linearly with deformation upto about 60% of the maximum attainable stress, then the deformation increases more than proportionally with respect to the stress. The stress reaches the maximum, and finally a steep fall in stress occurs with increasing deformation until a certain deformation is reached

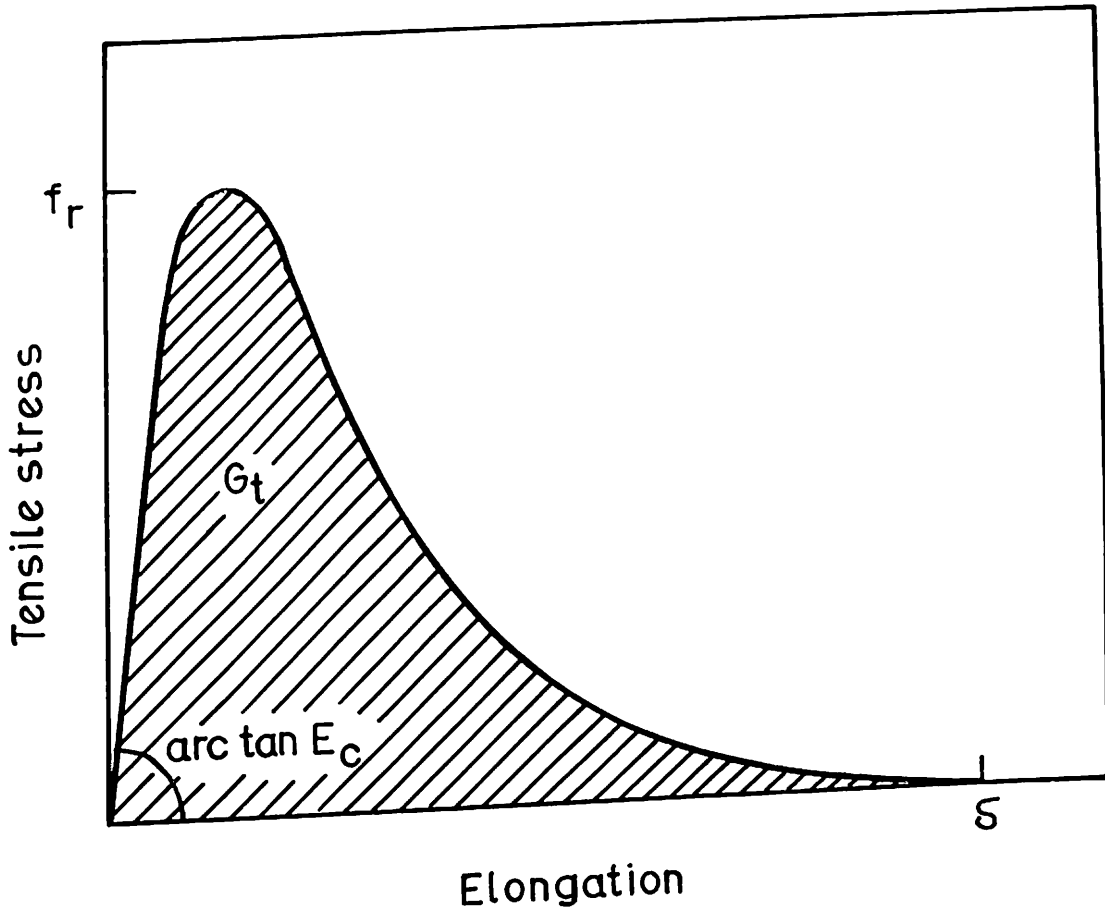


Fig.4.8 Relevant features of tensile behavior of concrete. (102)

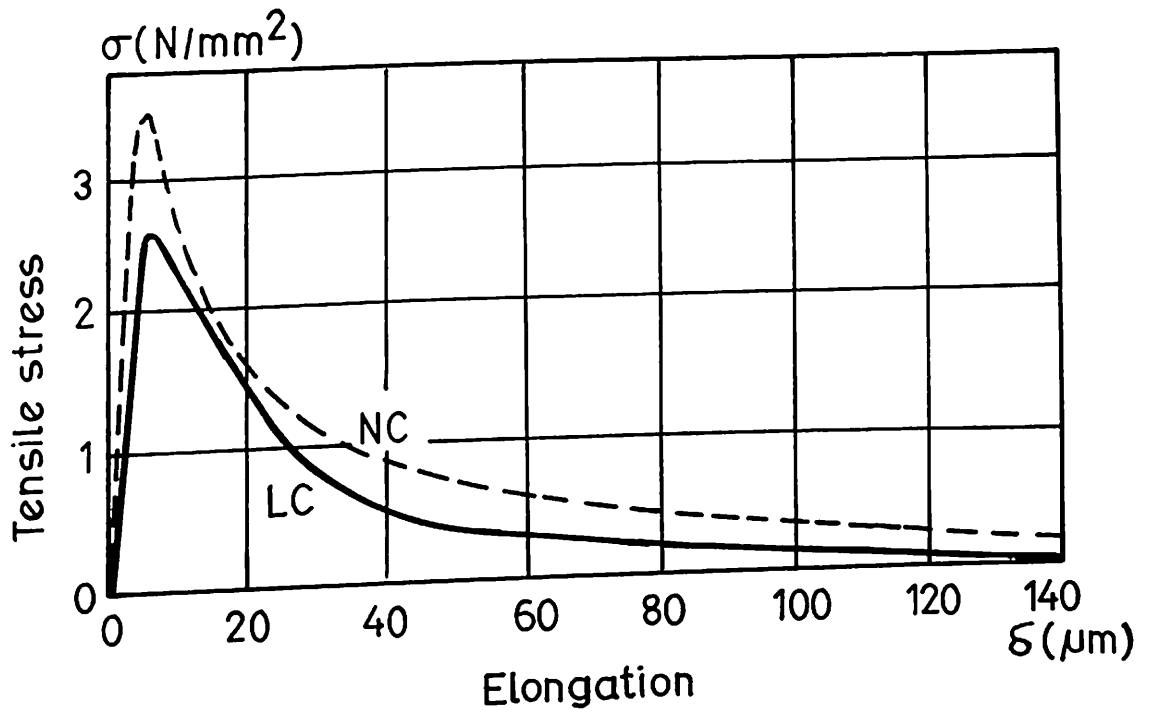


Fig.4.9 Typical results from uniaxial tests ;
 NC Normal concrete LC Lightweight concrete .
 (103)

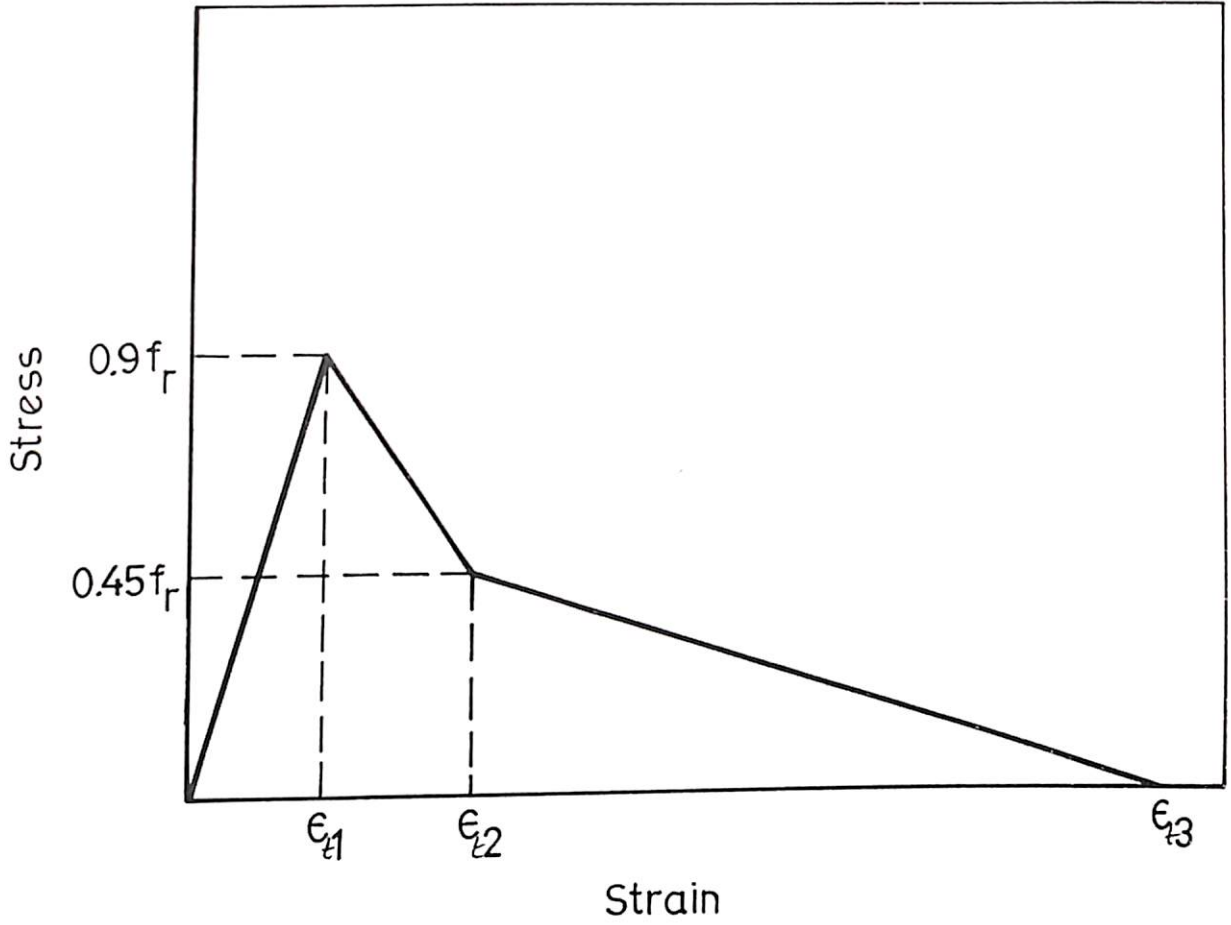


Fig.4.10 Model for concrete in Tension (53)

where the two parts of the specimen are separated. This behaviour means that after the tensile strength is reached, a large deformation can occur where stress transfer is still possible. Of course, it is not as pronounced as for an elastic-plastic material like steel, but it is certainly different from an elastic-brittle material. Concrete is a type of softening material. The softening takes place in a crack (or crack band) and is therefore a discrete phenomenon. The opposite term to 'strain hardening' would be 'strain softening' which is not unrestrictedly applicable to concrete.

Reinhardt et al [103] performed more than 100 deformation controlled uniaxial tensile tests. The aim of these tests was to provide an accurate description of the tensile behaviour of concrete, simple enough for application to numerical analysis. Fig. 4.9 shows two typical results, one for normal weight concrete and the other for light weight concrete.

4.3.3 Modeling of Concrete in Tension

The uniaxial stress-strain relationship developed by Vebo and Ghali [53], shown in Fig. 4.10, is adopted in this study. The ascending branch of the curve is linear upto $0.9 f_r$, where f_r is modulus of rupture with a slope of E_{t1} . The descending branch is a bilinear curve which has a slope E_{t2} and the second has a slope E_{t3} upto zero stress. The equation for stress for a concrete tensile strain ϵ_t has the following form

$$\begin{aligned}
\sigma_1 &= E_{11}\varepsilon_1 & \varepsilon_1 \leq \varepsilon_{11} \\
\sigma_1 &= 0.90 f_r + E_{12}(\varepsilon_1 - \varepsilon_{11}) & \varepsilon_{11} \leq \varepsilon_1 \leq \varepsilon_{12} \\
\sigma_1 &= 0.45 f_r + E_{13}(\varepsilon_1 - \varepsilon_{12}) & \varepsilon_{12} \leq \varepsilon_1 \leq \varepsilon_{13} \quad \dots(4.7a)
\end{aligned}$$

Where ε_{11} , ε_{12} and ε_{13} are three distinctive strains that define the curve levels. The values of the slopes for the three linear parts are

$$\begin{aligned}
E_{11} &= 0.75 E_c \\
E_{12} &= -0.5 E_c \\
E_{13} &= -0.05 E_c \quad \dots(4.7b)
\end{aligned}$$

Where E_c = modulus of elasticity of concrete in compression. The strain limits ε_{11} , ε_{12} and ε_{13} are defined as follows:

$$\begin{aligned}
\varepsilon_{11} &= \frac{1.2 f_r}{E_c} \\
\varepsilon_{12} &= \frac{2.1 f_r}{E_c} \\
\varepsilon_{13} &= \frac{11.1 f_r}{E_c} \quad \dots(4.7c)
\end{aligned}$$

4.4 Representation of Steel Reinforcement

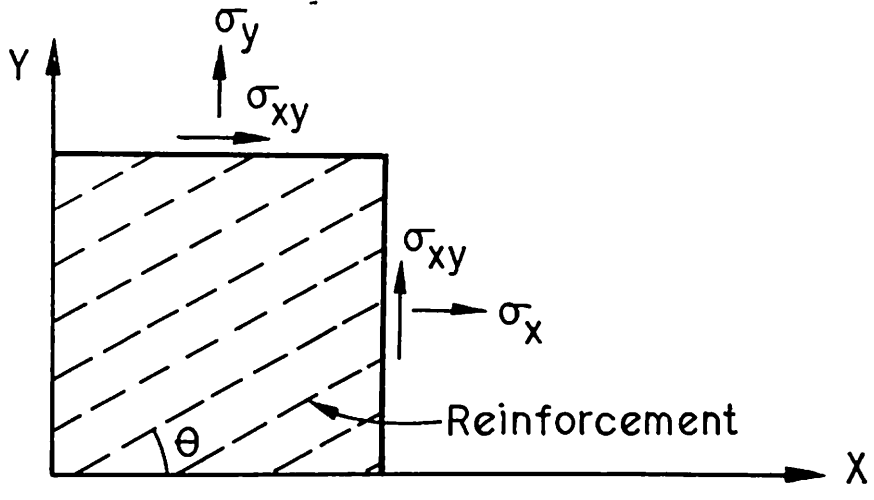
In developing a finite element model of a reinforced concrete member, the following alternatives can be used for representation of reinforcement.

- (a) distributed,
- (b) embedded and
- (c) discrete.

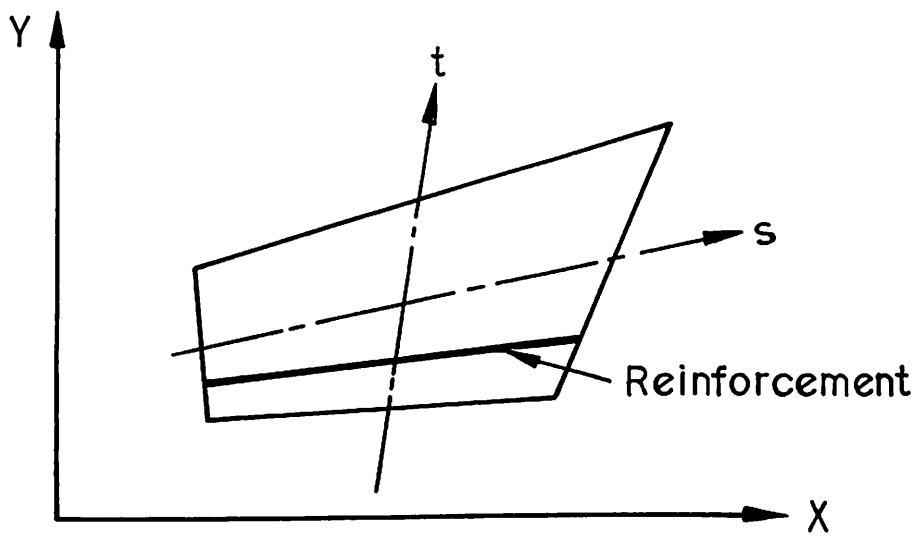
For a distributed representation, the steel is assumed to be distributed over the concrete element, with a particular orientation angle θ as shown in Fig. 4.11a. A composite concrete-reinforcement constitutive relation is used in this case. To derive such relation, perfect bond must be assumed between the concrete and steel.

An embedded representation as shown in Fig. 4.11b may be used in connection with higher order isoparametric concrete elements. The reinforcing bar is considered to be an axial member built into the isoparametric element such that its displacements are consistent with those of the element. Perfect bond has to be assumed.

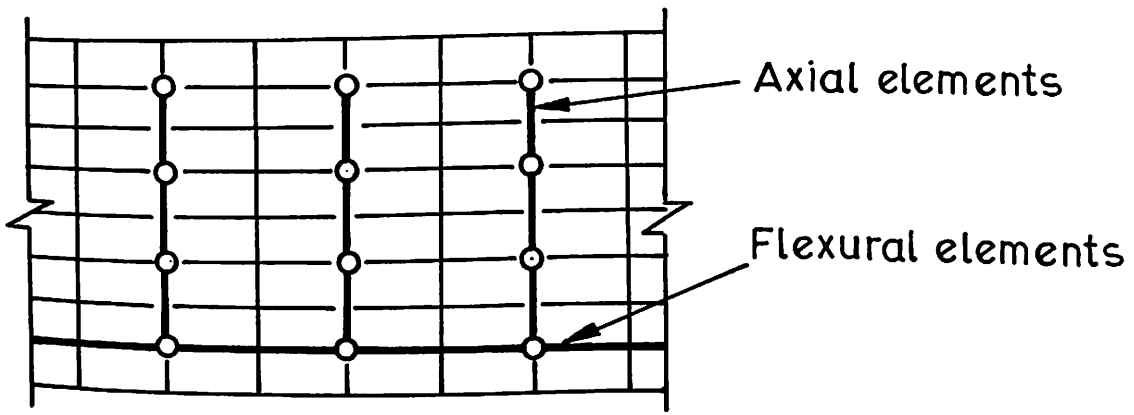
A discrete representation of the reinforcement using one-dimensional element as shown in Fig. 4.11c has been most widely used. Axial force members or bar links may be used and assumed to be pin connected with two degrees of freedom at the nodal points. Alternatively, beam elements may be used, assumed to



(a) Distributed



(b) Embedded



(c) Discrete

Fig.4.11 Alternate representations of steel.

be capable of resisting axial force, shear and bending. In this case, three degrees of freedom are assigned at each end. A significant advantage of the discrete representation, in addition to its simplicity, is that it can account for possible displacement of the reinforcement with respect to the surrounding concrete. A combination of representations may be used for particular types of problems. In beams, for which bending has a significant effect, discrete beam elements for the main steel might be employed. For slabs and shells, a distributed model might be used for the steel throughout the surface.

4.4.1 Modeling of Steel Reinforcement

Typical stress-strain curves for mild steel loaded monotonically in tension, are shown in Fig. 4.12a. The stress-strain curves for steel are characterized normally by the following features:

- i) An initial elastic region up to the yield strain, ϵ_{sy}
- ii) A yield plateau (i.e., a yield point beyond which the strain increases with little or no increase in stress) from ϵ_{sy} to the hardening strain, ϵ_{sh} ,
- iii) A strain hardening region from ϵ_{sh} to the ultimate strain, ϵ_{su} , to the fracture strain, ϵ_{ff} .

In addition to specifying a minimum required yield strength, f_{sy} , a minimum ultimate tensile strength, f_{su} , and a minimum fracture strain related to a gage length are also specified. Figure 4.12b shows the stress-strain curve for deformed bars.

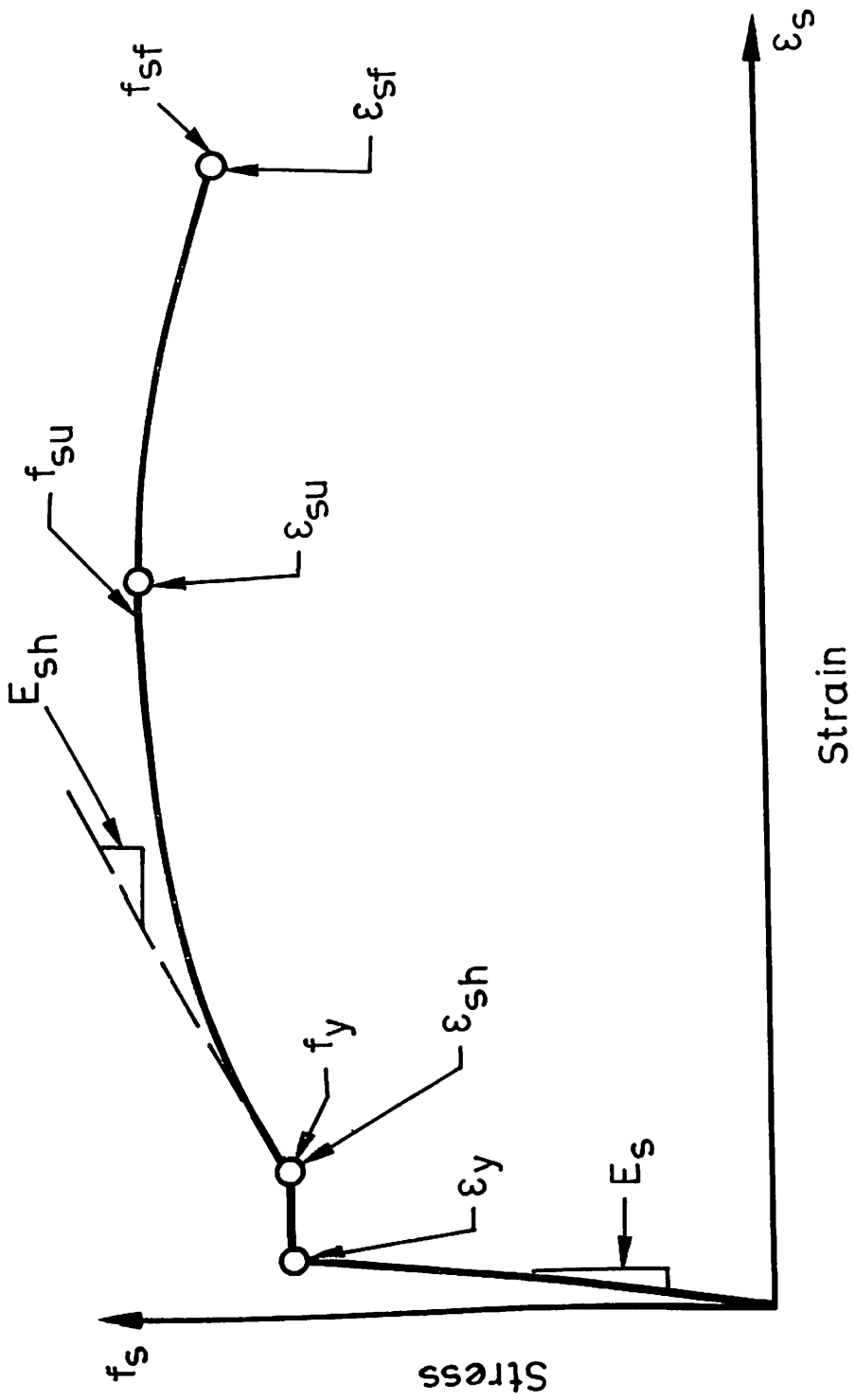


Fig. 4.12a Stress-strain curves for mild steel for $f_y=68$ ksi

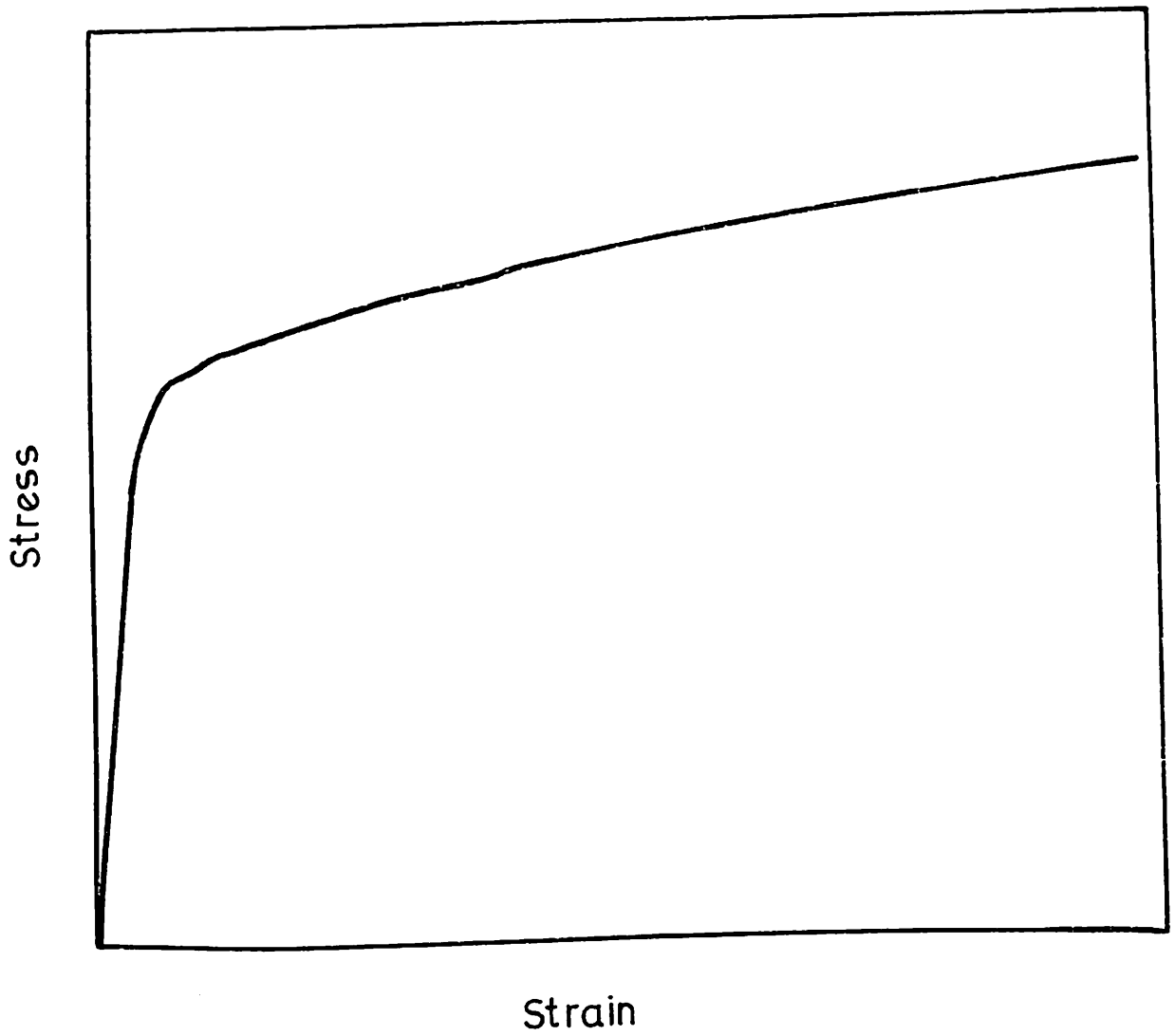


Fig.4.12 b Stress-strain curve for deformed reinforcement

The stress-strain curves for steel are assumed to be identical in tension and compression. For simplicity in design calculations, it is necessary to idealize the steel stress-strain curve. Three different idealizations shown in Fig. 4.13 have been used depending upon the accuracy required. For each idealization, it is necessary to determine experimentally the values of stress and strain at the onset of yield, strain hardening and the ultimate tensile strength. For present study the steel reinforcement is idealized as elastic-perfectly plastic both in compression and tension.

4.4.2 Constitutive Relationships for Steel Reinforcement

The degree of sophistication of the constitutive relationships for steel that is implemented into a finite element analysis depends to a large extent on the special purposes of the analysis. Generally, it is advantageous to use the simplest constitutive relationship that models the essential behaviour for the particular application. Since steel reinforcement elements in concrete construction are mostly one-dimensional, it is not necessary to introduce the complexities of multiaxial constitutive relationships. For applications to problems where the response is purely elastic, steel stress may be determined by the standard linear-elastic relationship

$$\{\sigma^s\} = E_{st} \epsilon_s \quad \text{for} \quad 0 \leq \epsilon_s \leq \epsilon_{sy} \quad \dots(4.8a)$$

$$\{\sigma^s\} = E_{st} \epsilon_{sy} \quad \text{for} \quad \epsilon_s \geq \epsilon_{sy} \quad \dots(4.8b)$$

in which ϵ_s is the total steel strain, and E_{st} is the modulus of elasticity of steel.

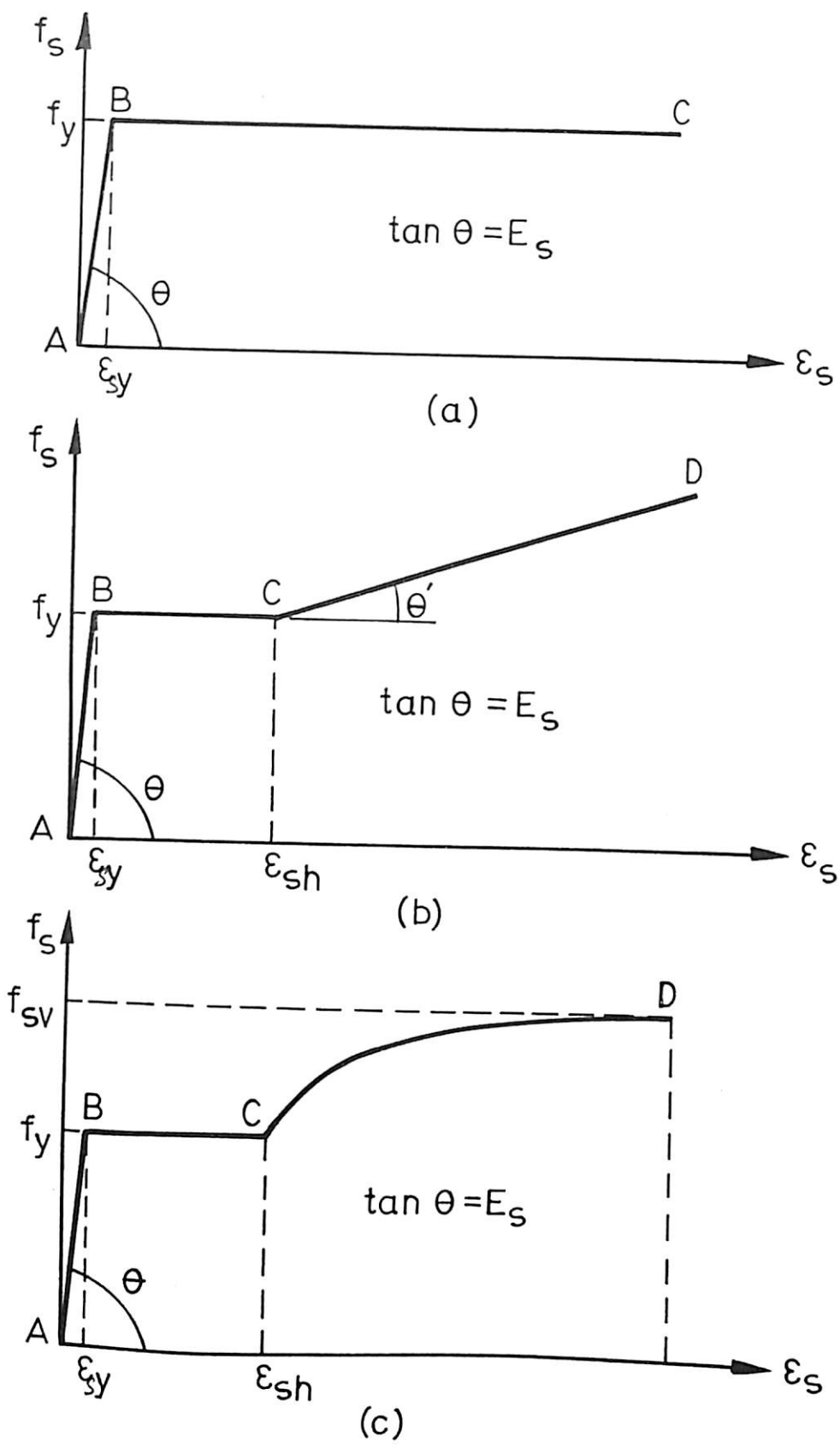


Fig.4.13 Idealizations for the stress strain curve for steel in tension or compression.
 a - Elastic perfectly plastic approximation
 b - Trilinear approximation
 c - Complete curve

For surface-type reinforced concrete structures such as plates and shells, it is often convenient to use the distributed representation of reinforcement, in conjunction with the assumption of a state of plane stress in the structure. The material stiffness of the composite concrete- steel element is obtained by superposition of the stiffness of the concrete and that of each set of reinforcing bars. A stress-strain relation for the element can be written in the form:

$$\{\sigma\} = [D] \{\varepsilon\} \quad \dots(4.9)$$

Where $\{\sigma\} = [\sigma_x \ \sigma_y \ \tau_{xy}]^T$ is the total stress vector, $[D]$ is the composite material stiffness matrix, and $\{\varepsilon\} = [\varepsilon_x \ \varepsilon_y \ \gamma_{xy}]^T$ is the strain vector. The strains are common for all component materials, while the total stress vector is the sum of the component stress vectors.

$$\{\sigma\} = \{\sigma^c\} + \{\sigma^s\} \quad \dots(4.10)$$

where $\{\sigma^c\}$ is the concrete stress vector and $\{\sigma^s\}$ is the reinforcement stress vector. Stresses $\{\sigma\}$, $\{\sigma^c\}$ and $\{\sigma^s\}$ act on a unit area of the composite cross section of the slab. The total stresses $\{\sigma\}$ do not represent real stresses but internal forces acting on a composite element.

These stresses can be found from the strains by

$$\{\sigma^c\} = [D^c] \{\varepsilon\} \quad \dots(4.11)$$

$$\{\sigma^s\} = [D^s] \{\varepsilon\} \quad \dots(4.12)$$

in which $[D^c]$ and $[D^s]$ are the concrete and reinforcement material matrices respectively. Substituting equations (4.11) and (4.12) in equation (4.10) and comparing equation (4.9) and (4.10), the composite material matrix can be formed by superposition of component material matrices as follows:

$$[D] = [D^c] + [D^s] \quad \dots(4.13)$$

The behaviour of concrete in compression represented by uniaxial stress – strain relation ship is considered for present study. The tension – softening phenomenon of concrete in tension adopted for present study is trilinear stress – strain relation. Steel is treated as elastic – perfectly plastic and distributed material.

CHAPTER 5

POST-CRACKING BEHAVIOUR

5.1 Introduction:

The tensile stress field which induces the cracking in concrete has major influence on the basic behaviour of the reinforced concrete member. Number of early studies to predict numerically the behaviour of reinforced concrete structures by finite element techniques focussed on the inclusion of the cracking behaviour in the mathematical model. As illustrated in a report by the ACI Committee [104], there are various approaches to model the post-cracking behaviour of reinforced concrete slabs in finite element analysis. Crack analysis of reinforced concrete structures is a subject that has been extensively studied and extensive experimental investigations have been carried out to understand the cracking mechanism.

The factors to be considered in the post-cracking behaviour of reinforced concrete slabs are tension - softening, tension-stiffening and aggregate interlock. The stiffness within the cracked element normal to the crack direction has allowed to decay to zero value over a finite strain interval rather than drop abruptly to zero value referred as tension-softening has been discussed in Chapter 4. Where as tension stiffening results from crack formation and bond slip between steel reinforcement and surrounding concrete. The resulting rough crack has an ability to transmit shear forces across the crack by aggregate interlock. All these factors

affects the service behaviour of reinforced concrete members by significantly increasing the bending stiffness in the post cracking range.

The aim of this chapter is to develop a rational method to define the post-cracking behaviour of reinforced concrete element. It is presented in three stages. First, models to represent cracking are discussed. Next the tension stiffening effect of reinforced concrete members is considered. Finally, the rough crack behaviour of cracked element is studied.

5.2 Cracking Models

This section is devoted to a discussion of the major categories of cracking models. Each model is composed of a suitable combination of three basic components, crack initiation, crack representation and a criterion for crack propagation. Most models rely on a strength criterion for crack initiation. There is, therefore, little difference between the various models in regard to this first component. Two methods of crack representation (discrete crack or smeared crack) and two approaches for crack propagation (strength or fracture toughness) are available.

Over the past 30 years a number of models have been developed to represent cracking in finite element analysis of a reinforced concrete member. The particular cracking model to be selected depends upon the purpose of the finite

element study and the nature of output desired from that study. If overall behaviour is desired, regardless to completely realistic crack patterns and local stresses, the so called "smeared" crack representation is probably the best choice. If detailed local behaviour is of interest, adaptations of the discrete cracking model are useful. For the special class of problems in which fracture mechanics is the appropriate tool, a specialized fracture model may prove to be necessary.

5.2.1 Discrete Cracking Models

The first finite element model of reinforced concrete to include the effect of cracking was developed by Ngo and Scordelis[38]. The cracks were modeled by the separation of nodal points. The crack location was successively redefined at the pre-selected locations. This model was designed to investigate local behaviour within reinforced concrete beams. The view point of the discrete cracking model is still macroscopic in principle, with the basic behaviour characteristics lumped in the elements. With the cracking passing along element boundaries, the use of simplex elements such as the constant strain triangular element is best suited to concept and application. However, these elements do not adapt to sharp strain gradients except with a fine mesh. The stresses in the vicinity of the crack tip are mesh dependent.

Nilson[40] modified this approach to allow the finite element model to generate the location of the cracks. Here cracking is based on the average stress in two adjacent elements. When the average stress exceeds the tensile strength of the

concrete (taken as the modulus of rupture) for these flexural dominant problems, the elements are disconnected at their common corners. For cracks at the exterior of the beam, the outside nodal points are separated. For cracks at the interior of the beam, both nodal points are separated.

Successive extensions of the crack are simulated by sequentially disconnecting single nodal points. The crack locations are restricted to the sides of the finite elements and are formed along the side of the element most nearly normal to the direction of the maximum principal stress. After each crack forms, the structure is unloaded, and the newly defined structure is reloaded. Compression zone behaviour is assumed to remain linear, thereby allowing path independence on reloading.

For problems that involve a few dominant cracks, it offers a more realistic representation of those cracks, i.e., a crack represents a strain discontinuity. This discontinuity is correctly represented by a discrete cracking model. Aggregate interlock can be represented with the discrete cracking representation. For those problems in which dowel forces are important, discrete cracking appears to be a natural tool.

The use of discrete cracking representations has received only limited acceptance due to the difficulty involved in providing for an economical redefinition

of the structural topology following the formation of a crack. In finite element analysis the trend has been to use higher order elements. These elements, particularly the isoparametric versions yield somewhat poor quality corner stress definitions which does not blend well with the edge cracking associated with the discrete crack concept.

With the changing of the topology in these models, the redefinition of the nodal points destroys the narrow band width in the structural stiffness matrix and greatly increases the computational effort required for the solution. The non-automatic method of defining cracks and the lack of generality in possible crack directions has made discrete cracking models unpopular.

The need for a cracking model that offers (a) automatic generation of cracks without the redefinition of the finite element topology and (b) complete generality in possible crack direction has led a vast majority of investigators to adopt the so called "Smeared" cracking model.

5.2.2 Smeared Cracking Models

The procedure, introduced by Rashid[39], represents cracked concrete as an orthotropic material. After cracking has occurred (usually defined when the principal tensile stress exceeds a tensile strength criterion for the material), the modulus of elasticity of the material is reduced to zero. In its earliest version, the

constitutive matrix was defined for plane stress, as follows:

$$\begin{bmatrix} d\sigma_1 \\ d\sigma_2 \\ d\tau_{12} \end{bmatrix} = \begin{bmatrix} 0 & 0 & 0 \\ 0 & E & 0 \\ 0 & 0 & 0 \end{bmatrix} \begin{bmatrix} d\varepsilon_1 \\ d\varepsilon_2 \\ d\gamma_{12} \end{bmatrix} \quad \dots(5.1)$$

The shear modulus was reduced to zero and the Poisson's ratio effect was neglected due to lack of interaction between the two orthogonal directions after cracking. Rather than representing a single crack, this procedure has the effect of representing many finely spaced (or smeared) cracks perpendicular to the principal stress direction.

The cracking model represented in equation (5.1), served a number of investigators adequately[105,106], but as it was applied to a wider range of problems, its use resulted in a number of numerical difficulties and in some cases a distortion in the crack patterns formed in the finite element models[49,52]. For this reason investigators[49,52,107] represented the shear modulus (G) usually with a retention factor, β as

$$\begin{bmatrix} d\sigma_1 \\ d\sigma_2 \\ d\tau_{12} \end{bmatrix} = \begin{bmatrix} 0 & 0 & 0 \\ 0 & E & 0 \\ 0 & 0 & \beta G \end{bmatrix} \begin{bmatrix} d\varepsilon_1 \\ d\varepsilon_2 \\ d\gamma_{12} \end{bmatrix} \quad \dots(5.2)$$

The use of a shear modulus, βG (with $0 \leq \beta \leq 1$) not only removes most of the numerical difficulties but also improves the realism of the cracking phenomenon generated during the finite element study. This shear factor may also be used as one way to suppress the real singularity that results when all the elements surrounding a particular node have cracked in the same direction. The other alternative would be to eliminate computation in the direction normal to the crack system. However, it is computationally very inconvenient to alter the equation solver to respond to the continual change in the number of equations being solved.

The particular value chosen for β (between 0 and 1) does not appear to be critical [108], but values greater than zero are necessary to prevent numerical difficulties. The presence of shear modulus is realistic since it represents the aggregate interlock that occurs across an open crack. However, the shear modulus in equation (5.2) more nearly represents a number of springs parallel to the crack, rather than the physical reality of a rough crack in concrete.

A number of variations on equation (5.2) are in use. Some investigators have retained the Poisson's effect in the modulus of elasticity parallel to the uncracked direction replacing E_c with $E_c/(1-\nu^2)$, and some constitutive equations are designed to automatically retain a shear modulus term that is a function of the stiffness in the remaining uncracked directions. In others, the shear modulus is taken as a function of the tensile strain perpendicular to the crack. In order to avoid

numerical problems the β factor cannot however be reduced to zero. Slabs are essentially plane stress problem, therefore smeared crack approach is used for the study.

The use of the orthotropic constitutive matrix equations (5.1) and (5.2) to represent cracked concrete may not be totally realistic. In the case of real crack, the surface itself is rough and any sliding parallel to the crack will have a tendency to generate some local stresses (or movement) normal to the crack to properly represent this behaviour, the off-diagonal terms in the constitutive matrices (relating shear strain with normal stress) should be non-zero. The relative magnitude of these off-diagonal terms would be expected to decrease with respect to increase of crack opening.

To improve the realism of the representation of the crack, rough crack behaviour and tension-stiffening effect are identified to describe the post-cracking behaviour of concrete.

5.3 Tension-Stiffening Effect

The tension-stiffening effect is a complex phenomenon in reinforced concrete members and is related to crack distribution and the tensile capacity of the intact concrete between the cracks. The tension-stiffening phenomenon can be

defined as the increase in stiffness in a reinforced concrete member due to the interaction between concrete and reinforcement, as illustrated in Fig. 5.1. As a member cracks, concrete between the cracks tends to rebound its original (unstressed) state but is restrained by the reinforcement, resulting in some tensile stresses in the concrete. This ability to restrain the unloading of concrete is a function of the bond between reinforcement and concrete. With perfect bond, no slip occurs between reinforcement and concrete, whereas with poor bond, relative displacement can occur. Good bond properties increase the stiffening effect. The tension stiffening decays as the load increases beyond the cracking load and proportionally is more significant for low reinforcement ratios than higher ones.

The tension stiffening effect has been represented using various methods. The first method of representing the stiffening effect is to increase the steel stiffness as illustrated in the modified stress-strain diagram in Fig. 5.2. The additional stress in the steel represents the total tensile force carried by both the steel and the concrete between the cracks. The added stress is lumped at the level of the steel and oriented in the same direction for reasons of convenience. In the other approach, the stress-strain relationship of reinforced concrete is constructed based

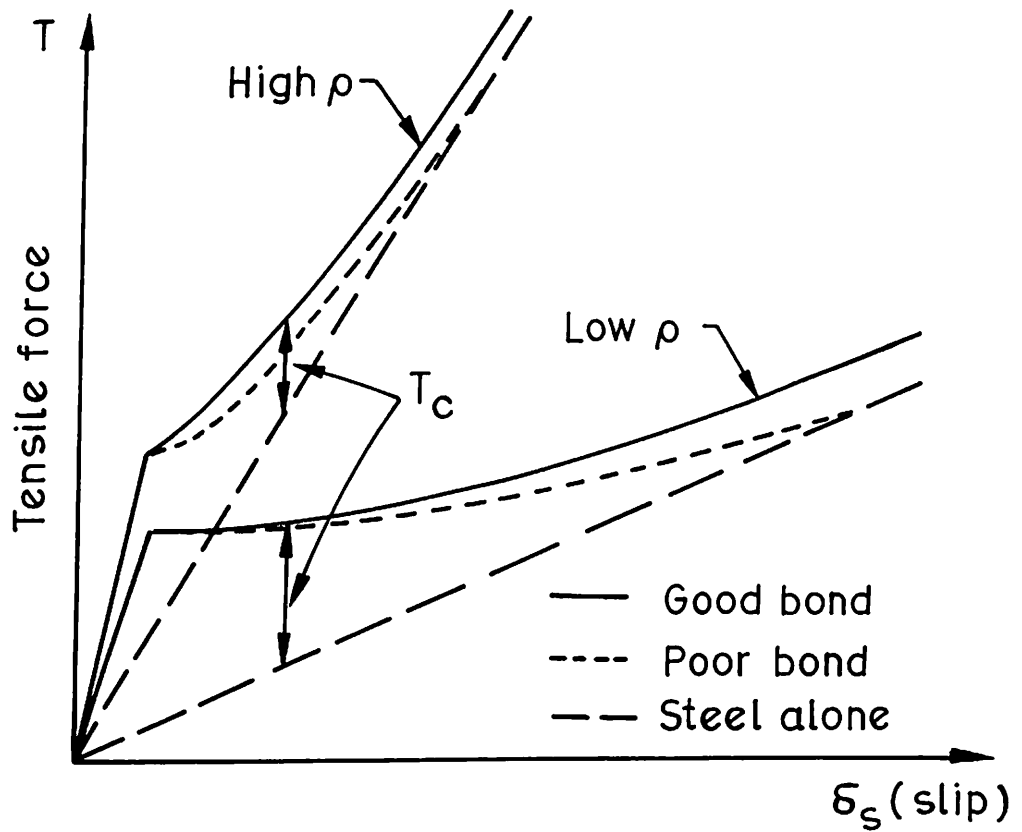


Fig.5.1 Tension - stiffening effect
 T_c - Tensile force carried by concrete
 ρ - Reinforcement ratio

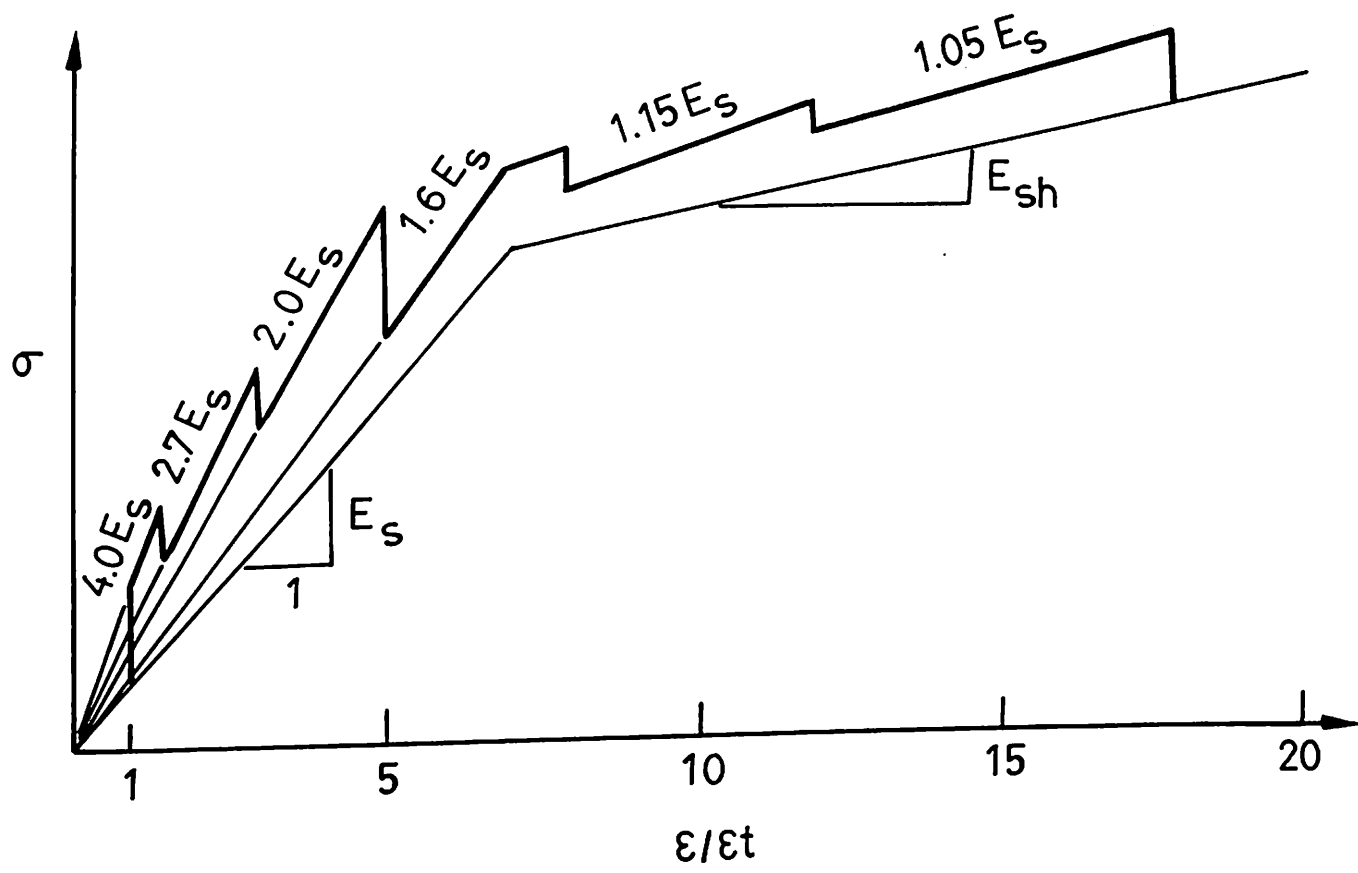


Fig.5.2 Modified stress-strain diagram for reinforcing steel.

on a bond stress distribution function or a bond-slip function. The tension stiffening effect can be more appropriately considered in this approach.

5.3.1 Bond-Slip phenomenon:

The bond between concrete and reinforcement is one of the most important conditions for the functioning of reinforced concrete. The load-carrying behaviour of reinforced concrete is influenced by the interaction between both of its components, plain concrete and steel reinforcement. The transfer of load between these two materials at the crack interface is called bond. The bearing mechanism of bond can be conceived as being comprised of three components: Chemical adhesion, friction and mechanical interlock between steel and concrete. Bond stresses in reinforced concrete member result from the change of the bar force along its length. Therefore, the effect of bond becomes evident in regions near cracks.

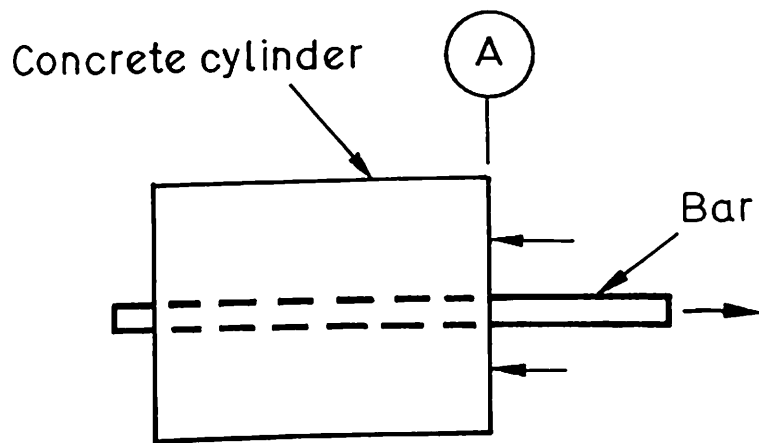
In the simplified analysis of reinforced concrete structures, complete compatibility between concrete and reinforcement is usually assumed, that means, perfect bond is presumed. But this assumption is only valid in those regions where no or only negligible stress transfer between the two components occurs. In regions of high stresses in the contact interfaces, near cracks, the bond stresses are related to relative displacements between concrete and reinforcement. The assumption of perfect bond in cracked zones would cause infinitely high strains to explain the

existence of finite crack width. In reality, there are different strains in the adjacent regions of the connections between concrete and reinforcement. As a result of this and of the crack propagation, relative displacements, which are usually called bond-slip, occur between these two components.

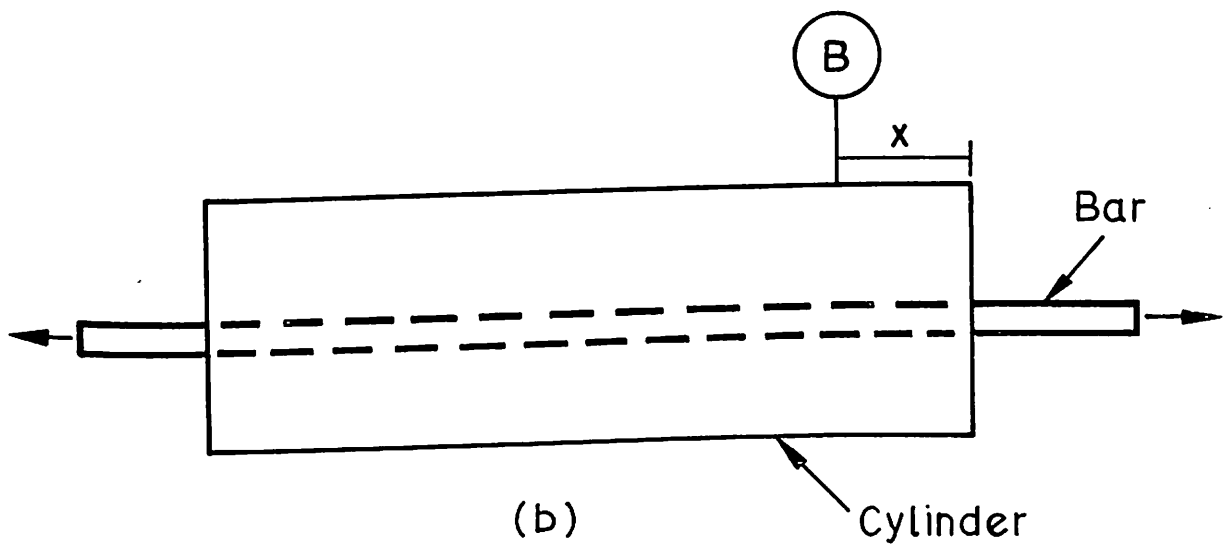
5.3.2 Measurement of Bond Slip

Bond force-displacement relations have been developed based on two type of tests; (a) anchorage tests, and (b) transfer tests. In an anchorage test such as the standard ASTM pullout test, Fig. 5.3a, force is applied to the projecting end of a bar embedded in a cylinder of concrete, and is progressively and totally transferred to the concrete. For a transfer test, Fig. 5.3b, self-equilibrating forces are applied to the two ends of a bar projecting from a concentrically-cast concrete block or cylinder. Tests of this second type are intended to simulate conditions in the tension zone of a concrete beam, between primary flexural cracks. For either type of test, bond stress may be calculated either as an average value or a local value, and slip may be determined externally or internally.

Local bond stress at an internal location on the interface may be found based on the change in steel stress per unit length along the bar, using steel strains measured at close intervals along the embedded bar by electrical resistance strain gages. These are placed in a hollow core formed by sawing the bar longitudinally in diametrical plane, milling a slot along the bar centre line of each cut surface, and



(a)



(b)

Fig.5.3 Bond tests

a -ASTM pullout test (anchorage test)

b -Symmetrical tension test (transfer test)

tack welding the bar together in its original configuration after fixing the gages in the grooves. The steel stress variation is easily obtained from these strains. Local bond stress is then calculated as the change in steel stress per unit length, divided by the bar perimeter.

Local bond slip is more difficult to determine. A practical method is to calculate the slip at specific locations along the interface, based on the difference between steel displacement and concrete displacement at each location. The steel displacement is found by numerical integration of steel strains, as given by the strain gages described above. To determine concrete displacement, special electrical resistance strain gages, cemented between two sheets of polyester resin having a roughened outer surface, are used. A number of such gages are embedded in the concrete a short distance from the steel-concrete interface, spaced along the interface, to obtain the concrete strain as a function of distance along the bar. These strains are integrated numerically to obtain the concrete displacement. Analysis based on stress-slip curves found in this way indicated that results are quite good.

5.3.3 Bond Stress-Slip Relationships

For use in finite element analysis it is necessary to develop a constitutive relationship between local bond stress and local bond slip at representative locations along the interface using either the pullout test or the concentric transfer type test.

Various formulations have been proposed to represent these experimental derived bond stress-slip. Nilson[40] evaluated the result of Breslar and Bertero[109] (using average slip values) in the form of a third order polynomial.

$$\sigma_b = 3.606 \times 10^6 \delta_b - 5.356 \times 10^9 \delta_b^2 + 1.986 \times 10^{12} \delta_b^3 \quad \dots(5.3)$$

in which σ_b is the bond stress in Psi and δ_b is the slip in inches.

Mirza and Houde[110] derived the following fourth order empirical bond stress-slip relationship from the results of tests on sixty two axially reinforced tension members and thirty two beam end specimens.

$$\sigma_b = 1.95 \times 10^6 \delta_b - 2.35 \times 10^9 \delta_b^2 + 1.39 \times 10^{12} \delta_b^3 - 0.33 \times 10^{15} \delta_b^4 \quad \dots(5.4)$$

The parameters studied included the total load level, the thickness of the concrete cover and the concrete strength. The bond stress at the steel-concrete interface reached the maximum value at an average of 12×10^{-4} inches as shown in Fig. 5.4.

The initial modulus of bond stress-slip relations is of the order of 2×10^6 Psi. Interface bond stiffness can be obtained by differentiation.

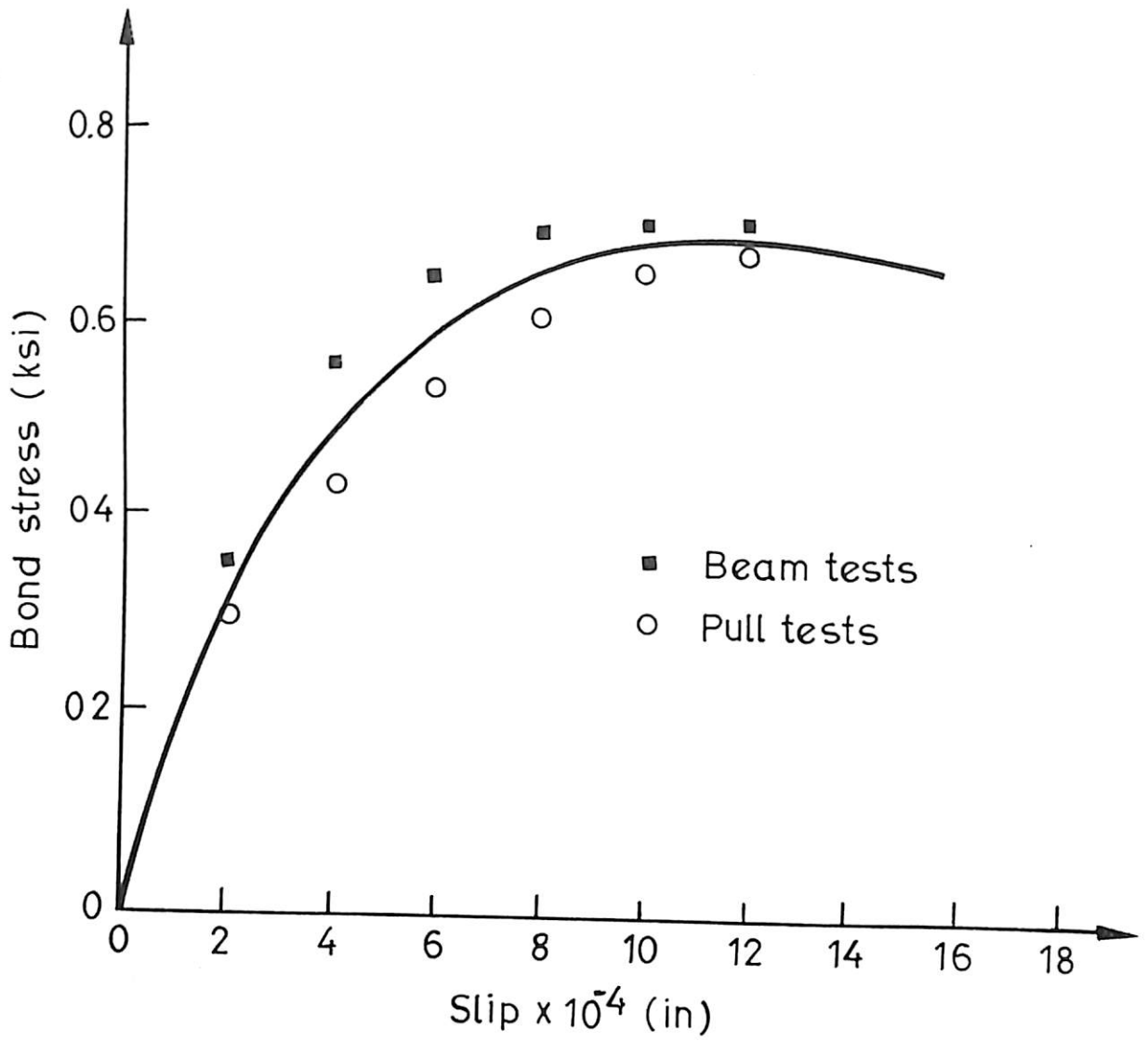


Fig.5.4 Unit bond stress Vs unit slip

Equation 5.4 is considered for present study because of its adaptability and accuracy. Then by differentiation with respect to slip δ_b , the incremental slip modulus (slope of the bond slip curve) is

$$\frac{d\sigma_b}{d\delta_b} = 1.95 \times 10^6 - 4.7 \times 10^9 \delta_b + 4.17 \times 10^{12} \delta_b^2 - 1.33 \times 10^{15} \delta_b^3 \quad \dots(5.5)$$

where $d\sigma_b/d\delta_b$ represents the slip stiffness in Psi per inch units.

To evaluate bond modulus, the following procedure is proposed to relate bond stress and bond strain.

The steel reinforcement tributary surface area per unit width is

$$A_t = \pi d_b \quad \dots(5.6)$$

where d_b represents the diameter of steel bar

If equation (5.5) is multiplied with tributary surface area, then bond modulus (E_b) will be

$$E_b = \frac{d\sigma_b}{d\delta_b} A_t \quad \dots(5.7)$$

The strains at bottom fibre of concrete, steel reinforcement level and crack width are shown in Fig. 5.5. The incremental slip $d\delta_b$ is derived as

$$d\delta_b = \int_0^l (\epsilon_s - \epsilon_{bi}) dx \quad \dots(5.8)$$

where l is length of steel reinforcement bar, ϵ_s is strain in steel reinforcement and ϵ_{bi} is strain of concrete in tension.

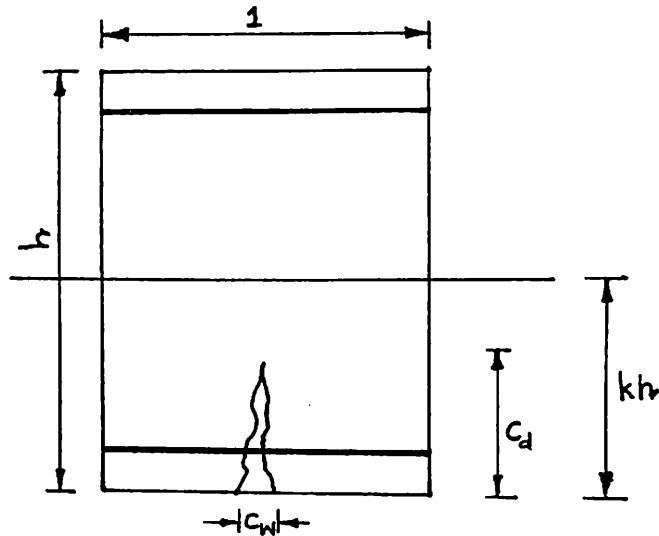


Figure 5.5 Flexural Crack Element

$$d\delta_b = (\epsilon_s - \epsilon_{bi}) l \quad \dots(5.9)$$

where l is equivalent to unit value.

This bond modulus is required for incorporating tension stiffening effect due to bond between steel reinforcement and surrounding concrete.

The above relation is valid with the following assumptions:

- (a) No crushing of concrete under the steel reinforcement.

- (b) No plastification of the steel reinforcement.
- (c) The influence of crack width on the free length of steel reinforcement is neglected.

Using the bond stress-slip relationship in non-linear finite element analysis program and an incremental load approach, the load-displacement response could be predicted with reasonable accuracy.

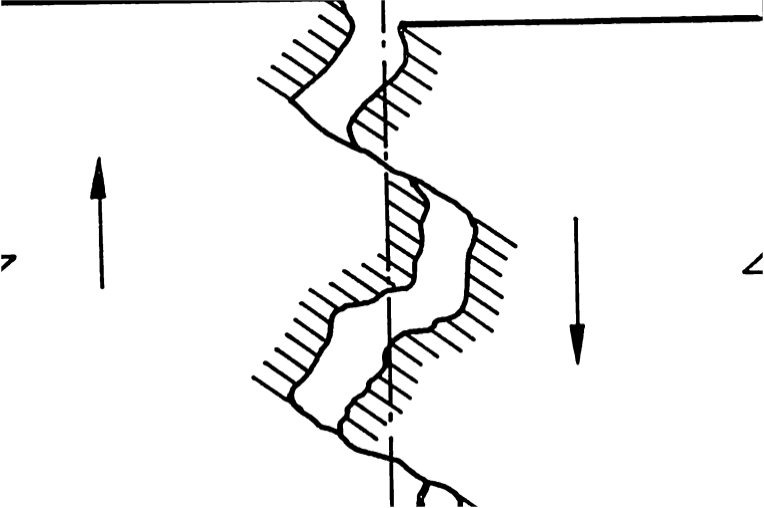
5.4 Rough Crack Behaviour

The shear transfer for cracked slab is incorporated by means of shear retention factor(β). Different values were used for shear retention factor in the analysis of reinforced concrete slabs in earlier studies. Hand et al[49], Lin and Scordelis[52] assumed to be 0.4, Suidan and Schnobrich[107] assumed that shear retention factor to be 0.5 and Gilbert and Warner[55] assumed this value to be 0.6. Lewinski et al[60], the cracked shear transfer coefficient is assumed to be a constant value equal to 0.4 for cracked concrete in one direction and 0.2 for cracked concrete in two directions.

The need for the shear retention factor, β is best described by Hand et al[49]. Without the shear retention factor, an unstable cracked configuration of slab was attained when the load was approximately one-fourth of the experimental ultimate. The cracked configuration at this load indicated that a series of cracks had

just reached the middle surface from the top, and a similar series of cracks had approached from the bottom. This effect is due to assuming no shear transfer across the crack.

If shear retention factor is not considered in the analysis would imply that cracked concrete behaves as a bundle of uniaxial fibres capable of sustaining only a tensile or compressive load parallel to the direction of the crack. With the introduction of the shear retention factor, a shear force can be transferred across the cracked planes. The surface of the crack that develop due to excess tensile stress in concrete are usually rough. The cracks follow generally irregular path not a plane surface as shown in Fig. 5.6a. Further this irregular path is disturbed as the crack pass around the coarse aggregate inclusions in the concrete. As these cracks are inclined to flexural reinforcement, then a certain amount of shear will be transferred. Thus the possibility of shear transfer by aggregate interlock and dowel actions arises. Shear strength along crack is a function of shear displacement and crackwidth. An idealized model of rough crack is shown in Fig. 5.6b. In assessing the mechanism of shear transfer, variables of importance include width of crack, size of aggregate, reinforcement ratio and bar size, and concrete strength. The mechanism of shear transfer just described has been termed as rough crack behaviour or interface shear transfer or shear friction theory.



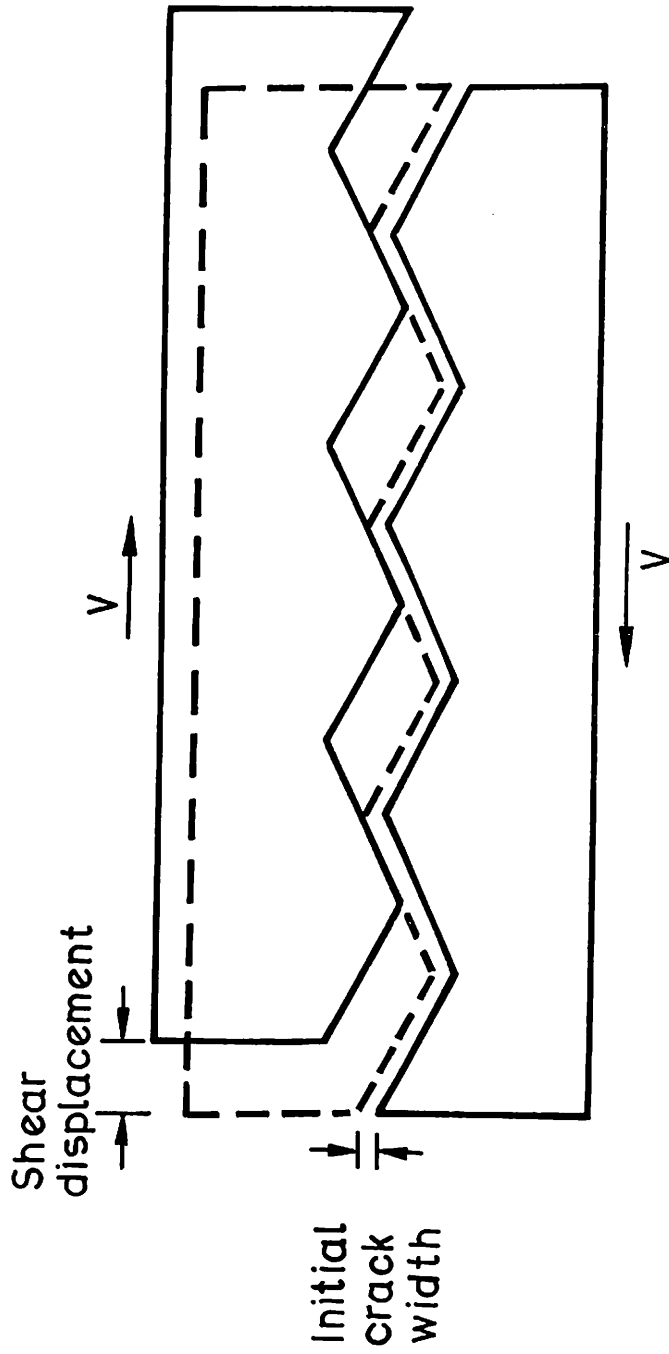


Fig.5.6b Idealized crack surface.

In the case of flexure, the maximum strain criterion is the basis for the computation of collapse loads. Such a simple criterion has not been feasible in the case of shear failure. Mohr's envelope, which is based on stresses, is perhaps the most satisfying for homogeneous bi-strength material such as plain concrete.

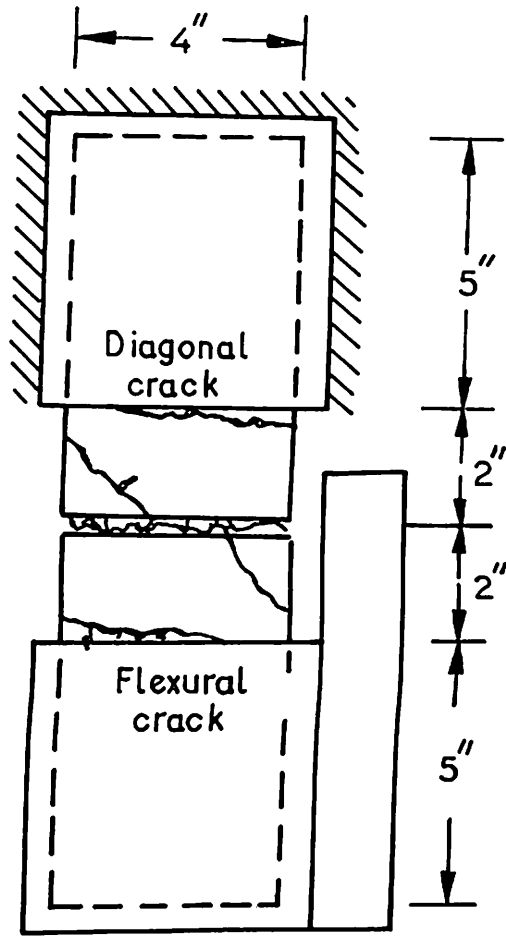
In a reinforced concrete member, flexure and shear combine to create a biaxial state of stress. The cracking load originating from flexure and shear is usually much smaller than would be expected from principal stress analysis and the tensile strength of concrete. This condition is largely due to the presence of shrinkage stresses, the redistribution of shear stresses between flexural cracks, and the local weakening of a cross section by transverse reinforcement.

5.4.1 Aggregate Interlock

The transfer of stresses through the crack faces, generally designated as aggregate interlock, has been the subject of several experiments from which empirical relationships have been proposed essentially in terms of resistance to shear displacement of concrete interfaces. Hardly any attention has been given to the coupling between normal and shear stress on the one hand, and crack opening and shear displacement on the other hand. An adequate simulation of aggregate interlock includes this wedging phenomenon[110, 111]. Therefore the simple shear retention factor usually adopted for a cracked element cannot take into the coupled nature of the phenomenon.

Experimental studies to determine the internal shear force distribution in reinforced concrete beams without considering interface shear mechanism over estimated severely the contribution of concrete in compression zone[112,113]. Taylor[114] conducted the first beam tests which considered the interface shear transfer forces and their influence on diagonal cracking. Concluded that interface shear transfer cannot be neglected when the internal force distribution of a cracked beam is analysed. The interface shear mechanism resisted between 33 to 50 percent of the total shear applied at the section. These beam tests, however, did not enable the researchers to determine fundamental load-displacement relationships for the interface shear transfer mechanism. Moreover, the beam specimens did not permit a systematic evaluation of the effect of several important parameters such as initial crack width, aggregate size, and the restraining effect permitted by the longitudinal reinforcement crossing the crack.

Fenwick and Pauley[115] performed the direct shear tests which permitted the transfer of pure shear stresses across the pre-cracked shear plane while the crack width was held at a constant value. The tests were designed to study the effect of initial crack width and concrete strength on the interface shear mechanism. The initial crack width at the shear plane varied between 0.0025 in. to 0.015 in., while the concrete cube strength, as measured by 4-in, concrete cubes, ranged between 2700 and 8120 Psi. Specimens of aggregate interlock tests always failed as a result of flexural or diagonal tension failure of the concrete as shown in Fig. 5.7.



Test arrangement

Fig.5.7 Aggregate interlock test

In no case the aggregate interlock action was observed of breakdown. These tests clearly indicated that the shear stiffness of the specimen increased with decreasing initial crack width, and increasing concrete strength.

From a regression analysis of the test results the fundamental shear stress displacement relationship for shear transfer across cracks by aggregate interlock action was determined for the type and proportions of aggregate used. This relationship expressed in terms of the inverse of the crack width and the square root of the compression strength of the concrete.

$$V_a = \left(\frac{467}{C} - 8410 \right) (0.0225 \sqrt{f'_c} - 0.409) (\delta_s - 0.0436C) \quad \dots(5.10)$$

where

V_a = interface shear stress transferred across crack (Psi)

C = initial crack width (in.)

f'_c = concrete compressive strength (Psi)

δ_s = shear displacement (in.)

White and Holley[116] conducted an investigation to determine the behaviour of the interface shear transfer mechanism on large pre-cracked specimens subjected to reverting shearing forces. Based on the test results, the accumulated maximum slip

is found to be a linear function of applied shear stress. Houde and Mirza[117] performed direct shear tests on pre-cracked concrete block specimens. After the concrete blocks were cracked along the shear plane and the initial crack width was set to a predetermined value, the specimens were sheared monotonically to failure. The test program evaluated the effect of the initial crack width, the concrete strength and the aggregate size. Within the range of the maximum aggregate size tested (3/8 - 3/4 in.), the influence of the maximum aggregate size was found to be negligible compared to the effect of crack width and the concrete strength. For the range of crack width tested (0.002 in. - 0.020 in), Houde and Mirza suggested the following shear displacement relation.

$$V_a = 57 (1/C)^{3/2} \quad \dots(5.11)$$

Pauley and Loeber[118] also studied the interface shear transfer using the direct shear specimens. The crack width was kept constant while the specimen was monotonically loaded to failure. No reinforcement crossed the crack. Upto an average shear stress of approximately 1000 Psi (6.9 N/mm²), a bilinear response was observed as shown in Fig. 5.8. No significant difference in the response of the specimens was noted when the investigators used different coarse aggregates, with 3/8 in. (9mm) and 3/4 in. (19 mm) nominal sizes. The following equation, obtained from a regression analysis of the experimental results, was proposed.

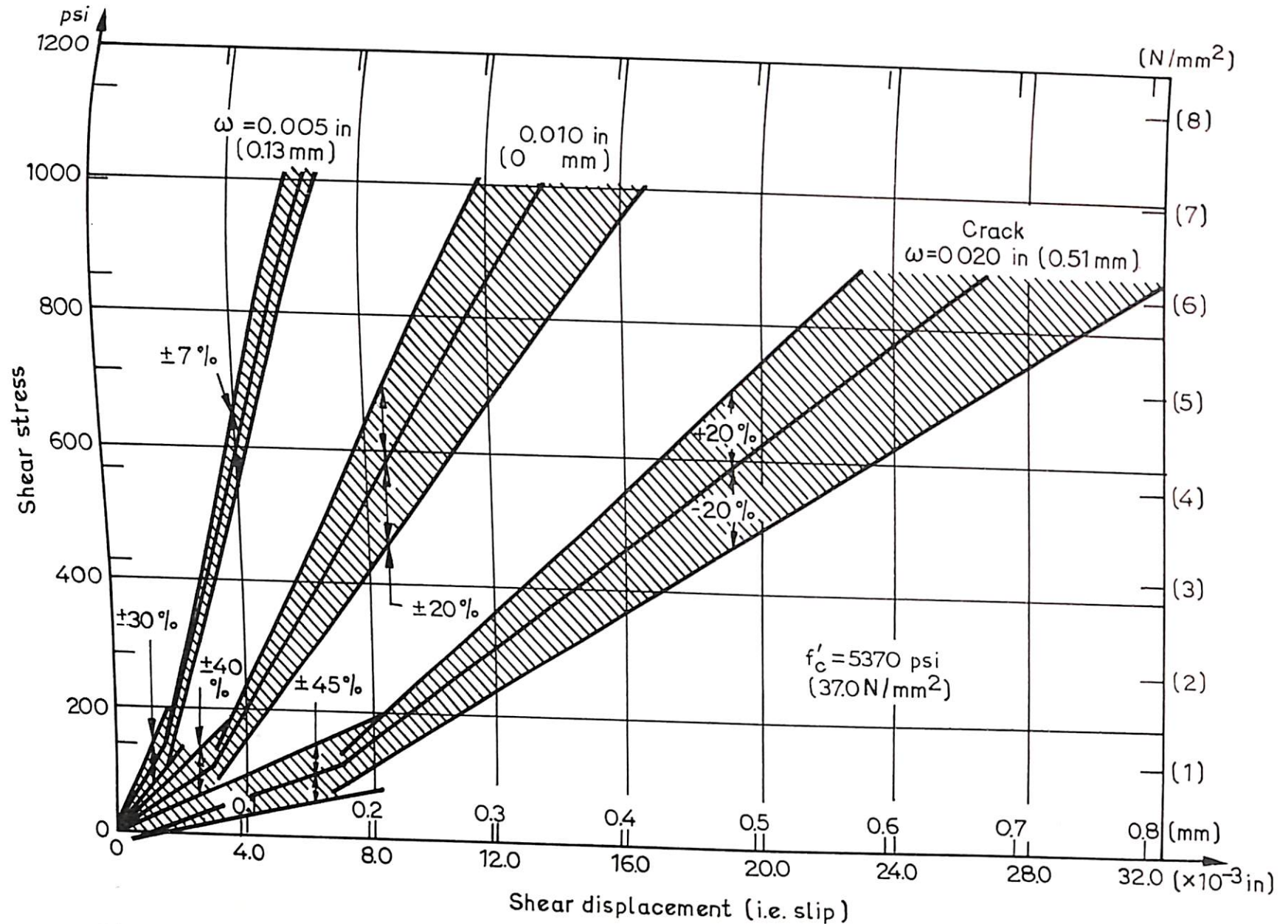


Fig.58 Typical mean shear stress shear displacement relationships for aggregate interlock mechanism

$$V_a = 73.0 + 50.9 \times 10^3 (\delta_s)^2 \quad \dots(5.12)$$

Observations clearly show that where beam action predominates shear transfer across the cracks by aggregate interlock action is of major importance. At the last load increment, at which measurements were made, aggregate interlock action resisted 73% of moment induced by the bond force.

5.4.2 Aggregate Interlock Stress-Strain Relationships

Cracked concrete can still transfer shear through aggregate interlock. Finite elements which do not allow the representation of shear are not suitable when post-cracking shear transfer is important.

Bazant and Gambarova[110], Frantzekakis and Theillout[111] have developed a stress-displacement constitutive relation for rough cracks. The material model developed for a reinforced concrete plate with a parallel set of continuous through cracks inclined to a system of reinforcing net of bars is shown in Fig. 5.9. The effect of cracks in concrete is described by a relation that involves δ_t , δ_n , σ_{nt} , σ_{nn} , i.e., the tangential and normal displacement and stress components on a crack.

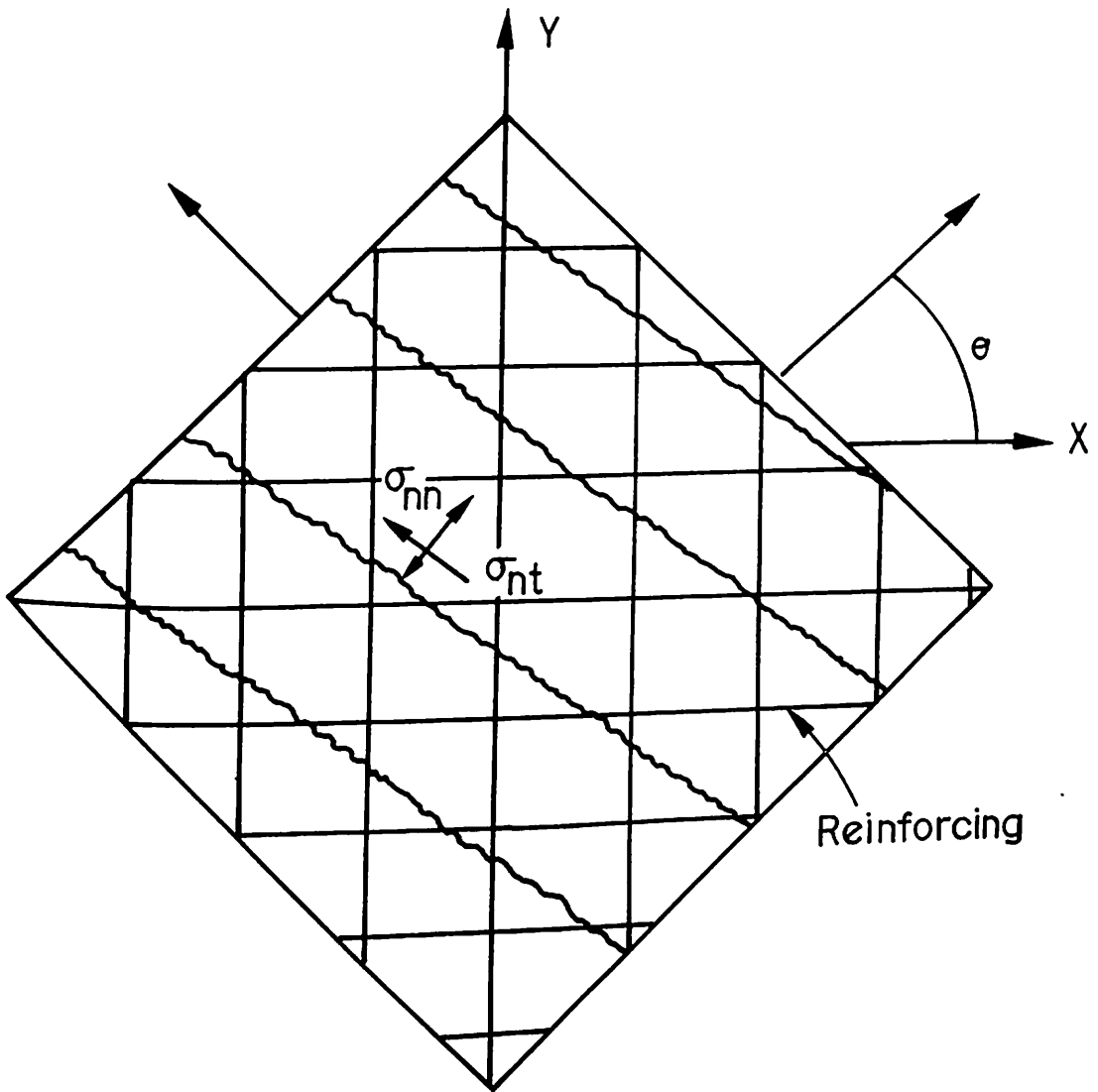


Fig. 5.9 Concrete plate considered by Bazant and Gambarova

As an average over large crack areas and many cracks, the relation between σ_{nn} , σ_{nt} , and δ_n , δ_t is considered to be a material property, similar to stress-strain relations, in the following form:

$$\begin{bmatrix} d\sigma_{nn} \\ d\sigma_{nt} \end{bmatrix} = \begin{bmatrix} B_{nn} & B_{nt} \\ B_{tn} & B_{tt} \end{bmatrix} \begin{bmatrix} d\delta_n \\ d\delta_t \end{bmatrix} \quad \dots(5.13)$$

This model is used for analysis of shear walls and beams. Moreover, it may be useful for layered approach. For present study this model may not be suitable. Therefore, a new approach has to be developed to incorporate aggregate interlock in the analysis of reinforced concrete slabs.

Equation (5.12) is adopted for present study to derive the simplified stress-strain relationship for aggregate interlock. The shear stiffness of cracked concrete (K_a) can be obtained by differentiating equation (5.12) with respect to shear displacement (δ_s), as

$$K_a = \frac{\partial V_a}{\partial \delta_s} = 101.8 \times 10^3 \delta_s \quad \dots(5.14)$$

in which K_a is expressed in Psi per inch and δ_s in inches. The shear displacement may be calculated as proposed by Frantezeskabis and Theillout[111] as

$$\delta_s = s C_i \quad \dots(5.15)$$

where s is spacing of cracks and C_i is principle curvatures.

Assuming cracks forms at 45° to the global axis, the spacing of crack for four node rectangular element as shown in Fig. 5.10 is expressed as

$$s = 0.5 \sqrt{a^2 + b^2} \quad \dots(5.16)$$

The important factor to be considered for aggregate interlock is crack width

C_w . This can be represented as

$$C_w = C_i C_d \quad \dots(5.17)$$

where C_i is principal curvature and C_d in depth of crack.

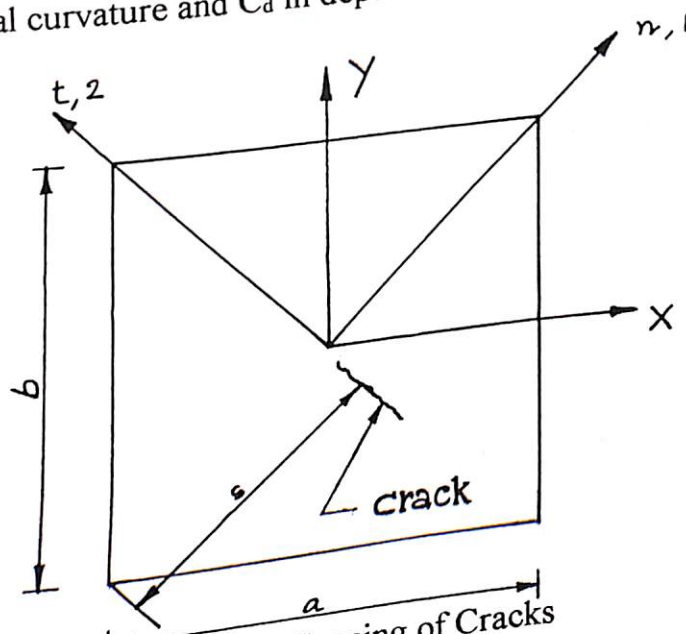


Figure 5.10 Spacing of Cracks

For simple calculations the crack width is assumed as constant value of 0.025 inches, since only one curve shown in Fig. 5.8 can be traced easily. Moreover, the aggregate interlock is effective only after the cracks crosses the steel reinforcement and yielding of steel reinforcement. At this stage the strains in concrete are more and therefore the crack width will be more.

The modulus of aggregate interlock can be obtained by multiplying shear stiffness with crack depth.

$$E_a = k_a.C_d$$

...(5.18)

where E_a is expressed in Psi.

Aggregate interlock resists the progress of cracking. Thus concrete strains will be reduced as loading progress because of friction between aggregate protrusions which resists the cracking of concrete. This value can be incorporated easily in flexural stiffness matrix of aggregate interlock to represent off diagonal terms.

The following assumptions are made for the above relation to be valid.

- (a) Dowel action of steel reinforcement is neglected.
- (b) Kinking of steel reinforcement at cracks is neglected.

CHAPTER 6

METHOD OF ANALYSIS

6.1 Introduction

In the analysis of reinforced concrete slabs, it is important to consider the effect of cracking of concrete on the slab load-deflection response. Cracking of certain regions reduces the overall flexural rigidity of the slab, causing an increase in deflection. Extensive cracking may well effect the serviceability of the structure and ultimate load. The basic prerequisite for the analysis is a suitable relation, usually in incremental form, between strain measures and stress resultants which adequately reflects cracking and crushing of concrete as loading progress. For flexural deformation, material property variation through the thickness must be taken into account.

For the nonlinear analysis of reinforced concrete slabs in the finite element method, both the modified stiffness and the layered approaches are widely used. The time required in finite element analysis is too great for layered approach. Therefore, it is not very efficient to use layered approach in the nonlinear analysis of slabs. A non-layered finite element model for reinforced concrete slabs that includes the nonlinear variation of material properties through the depths of slab is developed for the study. All parameters that influence the post-cracking behaviour of reinforced concrete slabs are taken into account to study the behaviour of slab

under progress of loading. These are softening phenomenon of concrete in tension and compression, the bond between steel reinforcement and concrete and the complex crack interface behaviour of concrete.

6.2 Assumptions

1. The lateral deformations are assumed small compared to the thickness of slab. No geometrical nonlinearity is considered for the analysis.
2. Long term loading, cyclic loading, membrane stresses and strength variation due to biaxial stresses are not included.
3. Time dependent effects such as creep, shrinkage, temperature, etc. are neglected in the analysis.
4. Kinking of steel reinforcement at crack is neglected.
5. Change of Poisson's ratio effects are neglected

6.3 Material Axes

Concrete slabs reinforced with uniformly and sufficiently densely distributed bars may be considered as homogeneous but anisotropic due to the reinforcement material. When the steel reinforcement is arranged in two orthogonal directions the compound material is orthotropic. The anisotropic properties of reinforced concrete slabs are primarily due to cracking of concrete and yielding of steel reinforcement. For reinforced concrete slabs, the crack directions do not necessarily coincide with the principal moments or with the reinforcing steel.

For present study, principal strain directions are considered to coincide with the crack directions. Therefore, principal curvatures are used to establish the material axes during the solution procedure.

Smearred cracks are assumed and only two cracks can form at a point. Cracks are assumed orthogonal and oriented in the direction of principal strains. This strain based rotating crack model represents more adequately the actual concrete behaviour. Therefore, progressive cracking and changes in the crack orientation are accounted for in the cracking model. The crack direction is determined as the direction of maximum principal curvature at the beginning of each load increment.

The orientation of the crack directions are shown in Figure 6.1, in terms of principal curvatures. Where θ is the angle between global axis X and principal curvature C_1 and α is the angle between global axes X and steel orientation x.

6.4 Flexural Stiffness:

The orthotropic concrete and the uniaxial steel representations are combined in the plate bending equations to form an anisotropic plate in which the material properties vary through the depth of the plate. The axis of anisotropy and the orthotropic axis of the concrete coincide with the crack directions along the principal curvatures. Incremental changes in moments are related to incremental

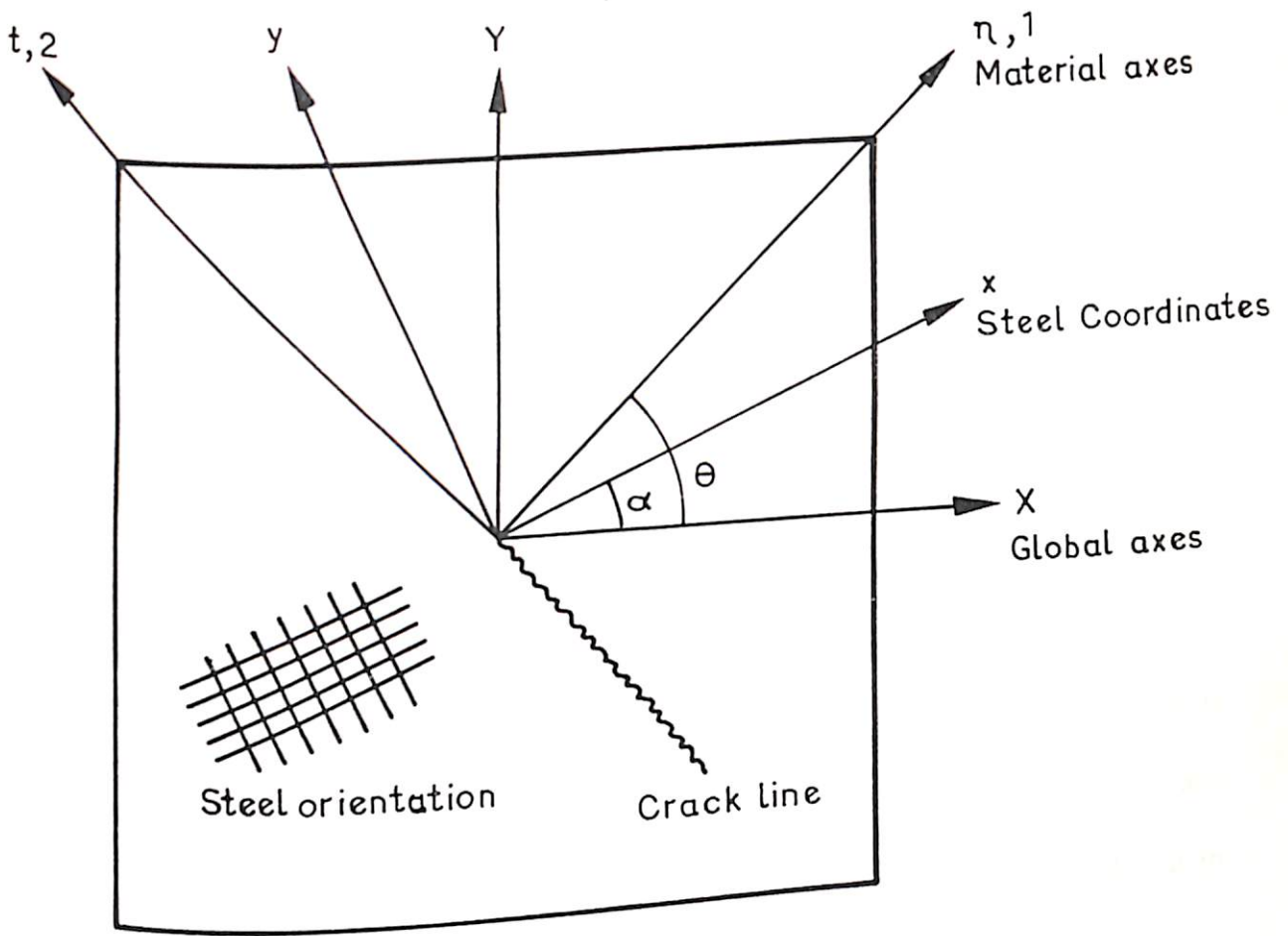


Fig.6.1 Material Axes of slab element

changes in curvatures on the axis of anisotropy as follows:

$$\begin{bmatrix} \Delta M_1 \\ \Delta M_2 \\ \Delta M_3 \end{bmatrix} = \begin{bmatrix} \int J_{11} Z_1^2 dZ & \int J_{12} Z_1 Z_2 dZ & \int J_{13} Z_1 Z_{12} dZ \\ \int J_{21} Z_1 Z_2 dZ & \int J_{22} Z_2^2 dZ & \int J_{23} Z_2 Z_{12} dZ \\ \int J_{13} Z_1 Z_{12} dZ & \int J_{23} Z_2 Z_{12} dZ & \int J_{33} Z_{12}^2 dZ \end{bmatrix} \begin{bmatrix} \Delta C_1 \\ \Delta C_2 \\ \Delta C_{12} \end{bmatrix}$$

or

$$\begin{bmatrix} \Delta M_1 \\ \Delta M_2 \\ \Delta M_{12} \end{bmatrix} = \begin{bmatrix} D_{11} & D_{12} & D_{13} \\ D_{21} & D_{22} & D_{23} \\ D_{31} & D_{32} & D_{33} \end{bmatrix} \begin{bmatrix} \Delta C_1 \\ \Delta C_2 \\ \Delta C_{12} \end{bmatrix} \quad \dots(6.1)$$

J_{ij} represent the coefficients of the anisotropic constitutive matrix and is functions of depth as well as location in the plate. Z_1, Z_2 ($Z_{12} = (Z_1+Z_2)/2$) are measured from the neutral axes in 1 and 2 directions respectively as shown in Fig. 6.2.

The flexural stiffness matrix of reinforced concrete slab may be expressed as the sum of separate contributions of materials. Also the flexural stiffness matrix due to post-cracking behaviour of tension-softening, tension-stiffening and aggregate interlock are proposed for the analysis.

Concrete in compression is modelled as an incrementally orthotropic

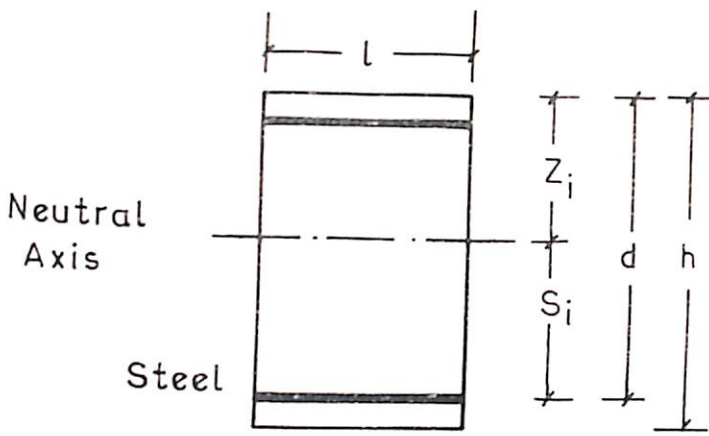


Fig.6.2 Cross section of slab per unit width

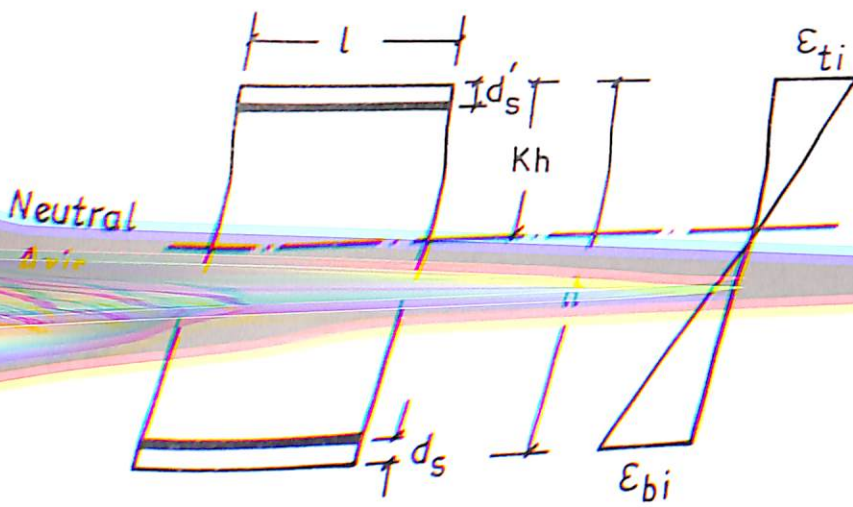


Fig.6.3 Cross section of slab in flexure

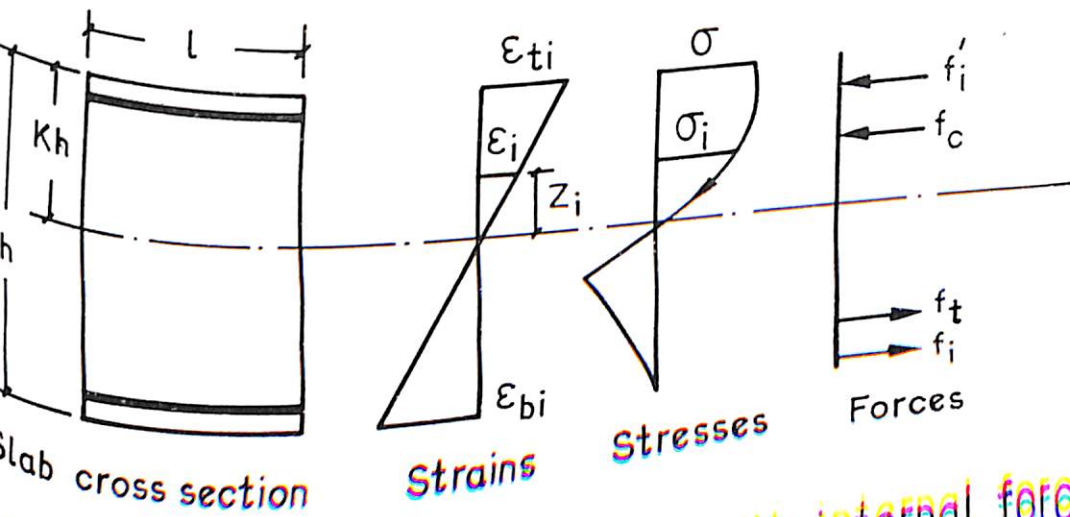


Fig.6.4 Cross section of slab with internal forces

material. It is represented using the differential stress-strain relations developed by Darwin and Pecknold [77].

$$\begin{bmatrix} d\sigma_1 \\ d\sigma_2 \\ d\tau_{12} \end{bmatrix} = \frac{1}{(1-\nu^2)} \begin{bmatrix} E_1 & \nu\sqrt{E_1E_2} & 0 \\ & E_2 & 0 \\ \text{Sym.} & & \frac{1}{4}(E_1+E_2-2\nu\sqrt{E_1E_2}) \end{bmatrix} \begin{bmatrix} d\varepsilon_1 \\ d\varepsilon_2 \\ d\gamma_{12} \end{bmatrix}$$

The tangent moduli E_1 , E_2 and the equivalent Poisson's ratio $\nu (= \sqrt{\nu_1\nu_2})$, are strain dependent.

In plate bending problems, the state of stress is essentially two dimensional. The strain in one direction is a function, not only of the stress in that direction but also of the stress in the orthogonal direction, due to the Poisson's effect. For the proposed nonlinear model it is convenient to analyze the two material directions independently. Keeping the track of the portion of the strain in each direction that controls the nonlinear behaviour of the concrete.

The principal curvature is used to represent this portion of the strain on the material axes.

$$C_i = \sum_{\text{All load increments}} \Delta C_i \quad \text{for } i = 1,2 \quad \dots(6.2)$$

in which ΔC_i is the incremental change in principal curvature.

6.4.1 Flexural Stiffness of Concrete:

$$D_{11}^c = \frac{1}{(1-\nu^2)} \int E_1 Z_1^2 dZ$$

$$D_{12}^c = \frac{\nu}{(1-\nu^2)} \int \sqrt{E_1 E_2} Z_1 Z_2 dZ$$

$$D_{13}^c = 0$$

$$D_{21}^c = D_{12}^c$$

$$D_{22}^c = \frac{1}{(1-\nu^2)} \int E_2 Z_2^2 dZ$$

$$D_{23}^c = 0$$

$$D_{31}^c = 0$$

$$D_{32}^c = 0$$

$$D_{12}^c = \frac{1}{4(1-\nu^2)} \int (E_1 + E_2 - 2\nu \sqrt{E_1 E_2}) Z_{12}^2 dZ \quad \dots(6.3)$$

in which E_1 and E_2 are tangent moduli along material axis. ν is the equivalent Poisson's ratio. Z_1 , Z_2 and $Z_{12} = 0.5 (Z_1 + Z_2)$ are depths measured from neutral axes in compression zone.

6.4.2 Flexural stiffness of Steel

$$D_{11}^s = (A_{sx}E_{sx}\cos^4\theta + A_{sy}E_{sy}\sin^4\theta)S_1$$

$$D_{12}^s = (A_{sx}E_{sx} + A_{sy}E_{sy})\sin^2\theta\cos^2\theta S_1S_2$$

$$D_{13}^s = (-A_{sx}E_{sx}\cos^2\theta + A_{sy}E_{sy}\sin^2\theta)\sin\theta\cos\theta S_1S_{12}$$

$$D_{22}^s = (A_{sx}E_{sx}\sin^4\theta + A_{sy}E_{sy}\cos^4\theta)S_2^2$$

$$D_{23}^s = (-A_{sx}E_{sx}\sin^2\theta + A_{sy}E_{sy}\cos^2\theta)\sin\theta\cos\theta S_2S_{12}$$

$$D_{33}^s = (A_{sx}E_{sx} + A_{sy}E_{sy})\sin^2\theta\cos^2\theta S_{12}^2$$

$$D_{ij}^s = D_{ji}^s \quad \dots(6.4)$$

in which A_{sx} , A_{sy} are areas per unit width of tensile steel in the X and Y (steel coordinates). E_{sx} and E_{sy} are the moduli of elasticity of steel in tension. S_1 , S_2 depth of tension steel layers measured from neutral axes and $S_{12} = (S_1 + S_2)/2$.

6.4.3 Effect of Bond

The contribution of bond between steel and concrete to flexural stiffness is

proposed as:

$$D_{11} = E_b A_s \cos^2 \theta S_1^2$$

$$D_{13} = E_b A_s \cos \theta \sin \theta S_1 S_{12}$$

$$D_{22} = E_b A_s \cos^2 \theta S_2^2$$

$$D_{23} = E_b A_s \cos \theta \sin \theta S_2 S_{12}$$

$$D_{33} = E_b A_s \sin^2 \theta S_{12}^2$$

$$D_{ij} = D_{ji} \quad \dots(6.5)$$

in which E_b is the moduli of bond, A_s is area of steel, S_1 , S_2 and S_{12} are depth of tension steel layers measured from neutral axes.

The longitudinal interaction between steel and concrete known as bond constitutive law is similar to the steel constitutive law. This modifies the steel stress-strain relationships. Therefore, bond effects are added to the steel flexural stiffness matrix in tension. This increases flexural stiffness in tension zone which incorporates the effect of tension stiffening effectively in the analysis of post-cracking behaviour of reinforced concrete slabs.

6.4.4 Effect of Aggregate Interlock:

The contribution of aggregate interlock towards flexural stiffness of slab is proposed as

$$D_{13}^a = \int E_a \bar{Z}_1 \bar{Z}_{12} dZ$$

$$D_{31}^a = D_{13}^a$$

$$D_{23}^a = \int E_a \bar{Z}_2 \bar{Z}_{12} dZ$$

$$D_{32}^a = D_{23}^a$$

$$D_{11}^a = D_{12}^a = D_{21}^a = D_{22}^a = D_{33}^a = 0. \quad \dots(6.6)$$

in which E_a is moduli of Aggregate interlock. \bar{Z}_1, \bar{Z}_2 are depths measured from neutral axes in tension Zone. $\bar{Z}_{12} = 0.5 (\bar{Z}_1 + \bar{Z}_2)$

Combining all these flexural stiffness matrices gives the total flexural stiffness along the material axes 1 and 2 in the following form

$$D_{ij}^{\text{total}} = D_{ij}^{\text{conc}} + D_{ij}^{\text{steel}} + D_{ij}^{\text{bond}} + D_{ij}^{\text{agg.}} \quad \dots(6.7)$$

6.5 Transformation of flexural rigidity matrix.

The stiffness matrix of an element is expressed by

$$[k^{(e)}] = \int_V [B]^T [D] [B] dV$$

in which $[D]$ is a 3x3 matrix of flexural plate rigidity properties with respect to the coordinate system X, Y of the element.

Dealing with a cracked region of a concrete slab the elastic properties are not the same in all directions. In case where the cracking direction coincides with either the X or Y directions, the problem is simply one of special orthotropy.

$$\begin{bmatrix} M_x \\ M_y \\ M_{xy} \end{bmatrix} = \begin{bmatrix} D_{11} & D_{12} & 0 \\ D_{21} & D_{22} & 0 \\ 0 & 0 & D_{12} \end{bmatrix} \begin{bmatrix} \partial^2 w / \partial x^2 \\ \partial^2 w / \partial y^2 \\ 2 \partial^2 w / \partial x \partial y \end{bmatrix} \quad \dots(6.8)$$

or $[M] = [D] [c]$.

In case where cracking direction does not coincide with either the X or Y direction the problem is one of the general orthotropy resulting in a fully populated D matrix. The terms of this matrix can no longer be derived directly from the material and sectional properties when viewed along the x and y direction.

For a cracked regions, the normal, n, to the cracking direction makes angle θ with the X axis. The n and t axes are now the principal axes of orthotropy with the moment curvature relationship given by

$$\begin{bmatrix} M_n \\ M_t \\ M_{nt} \end{bmatrix} = \begin{bmatrix} D_n & D_1 & 0 \\ D_1 & D_t & 0 \\ 0 & 0 & D_{nt} \end{bmatrix} \begin{bmatrix} \partial^2 w / \partial n^2 \\ \partial^2 w / \partial t^2 \\ 2 \partial^2 w / \partial n \partial t \end{bmatrix} \quad \dots(6.9)$$

in which M_n and M_t are the bending moments in the n and t directions; M_{nt} is the twisting moment; and w is the transverse displacement. The terms in the D matrix are calculated by replacing x with n and y with t.

The relationship in above equation may be rewritten in matrix algebra form as

$$[M'] = [D'] [c'] \quad \dots(6.10)$$

The moments M in the x and y directions are related to the moments M' in the n and t directions by the transformation

$$[M'] = \begin{bmatrix} C^2 & S^2 & -2CS \\ S^2 & C^2 & 2CS \\ CS & -CS & (C^2 - S^2) \end{bmatrix} [M]$$

in which C and S refer to $\text{Cos}\theta$ and $\text{Sin}\theta$ respectively. The above relationship may

be written in simple form as

$$[M'] = [T_1][M] \quad \dots(6.11)$$

Similarly for the curvatures

$$[c'] = \begin{bmatrix} C^2 & S^2 & -CS \\ S^2 & C^2 & CS \\ 2CS & -2CS & (C^2 - S^2) \end{bmatrix} [c]$$

$$\text{or } [c'] = [T_2][c] \quad \dots(6.12)$$

Substituting equations (6.11) and (6.12) into equation (6.10) gives

$$[T_1][M] = [D'] [T_2][c] \quad \dots(6.13)$$

In the X,Y coordinate system

$$[M] = [D][c]$$

is obtained, from which it follows that

$$[T_1][D][c] = [D'] [T_2][c] \quad \dots(6.14)$$

pre-multiplying both sides of equation with the square matrix $[T_1]^{-1}$ yields

$$[D][c] = [T_1]^{-1} [D'] [T_2][c] \quad \dots(6.15)$$

Again pre-multiplying both sides of equation with the square matrix $[D]^{-1}$ gives

$$[c] = [D]^{-1} [T_1]^{-1} [D'] [T_2][c] \quad \dots(6.16)$$

from which it follows that

$$[D]^{-1} [T_1]^{-1} [D'] [T_2] = [I] \quad \dots(6.17)$$

The inverse of $[T_1]$ is the transpose of $[T_2]$, thus the above equation becomes

$$[D] = [T_2]^T [D'] [T_2] \quad \dots(6.18)$$

Consequently a simple congruent transformation of $[D']$ gives the $[D]$ with respect to the X, Y coordinate system required in the analysis. It can now be incorporated directly in equation for the stiffness matrix.

6.6 Solution Procedure:

To obtain the load-deflection behaviour of slabs to failure, loads are applied incrementally. At first load increment the initial values of principal curvatures are assumed zero. That is the slab is treated as homogeneous, isotropic and ϕ linear-elastic material. At the end of first load increment the displacements are calculated using finite element analysis. Principal curvatures and angle of principal planes are calculated using equations (3.16) and (3.17) at the centre of each element. At each load increment, concrete strains at extreme fibres of unit width cross section as shown in Fig. 6.3 are calculated by usual relationship of strain-curvatures.

$$\begin{aligned} \epsilon_{ti} &= C_i k h \\ \epsilon_{bi} &= C_i (h-kh) \quad \text{for } i = 1,2 \end{aligned} \quad \dots(6.19)$$

where

h = depth of the slab

kh = depth of the neutral axis.

ϵ_{ti} = uniaxial strain at the extreme top fibre of concrete section

ϵ_{bi} = uniaxial strain at the extreme bottom fibre of concrete section

6.6.1 Uncracked Element:

If concrete strain value of an element in tension zone is less than the cracking strain of the concrete then the flexural stiffness matrix for an uncracked element will be treated as elastic as given below:

$$[D^{conc}] = \frac{E_c h^3}{12(1-\nu^2)} \begin{bmatrix} 1 & \nu & 0 \\ \nu & 1 & 0 \\ 0 & 0 & (1-\nu)/2 \end{bmatrix}$$

The angle of crack $\theta = 0$.

$$[D^{steel}] = \begin{bmatrix} A_{sx} E_{sx} S_1^2 & 0 & 0 \\ 0 & A_{sy} E_{sy} S_2^2 & 0 \\ 0 & 0 & 0 \end{bmatrix} \quad \dots(6.20)$$

6.6.2 Cracked Element

Where as for cracked element the flexural stiffness matrix will have the

contributions of tensile strength of concrete, bond between steel reinforcement and surrounding concrete and aggregate interlock as expressed in equation (6.7).

For cracked element the internal forces as shown in Fig. 6.4 are calculated on the material axes in terms of concrete stresses, uniaxial strains, principal curvatures and steel forces using the following equations which are similar to those used by Vebo and Ghali [53].

$$\begin{aligned}
 F_1 &= 1/c_1 \int_{\epsilon_{b1}}^{\epsilon_{t1}} \sigma_1(\epsilon) d\epsilon + f_1' - f_1 = 0 \\
 F_2 &= 1/c_2 \int_{\epsilon_{b2}}^{\epsilon_{t2}} \sigma_2(\epsilon) d\epsilon + f_2' - f_2 = 0 \quad \dots(6.21)
 \end{aligned}$$

in which ϵ = uniaxial strain at distance Z from the neutral axis. ϵ_{t1} , ϵ_{t2} are uniaxial strains at the extreme top fibre of section. ϵ_{b1} , ϵ_{b2} are uniaxial strains at bottom fibre of section. f_1 , f_2 are components of tension steel forces. f_1' , f_2' are components of compression steel forces per unit width.

In reinforced concrete slabs, the material axes in general do not coincide with steel reinforcement. Therefore, the steel forces must be transformed to the material axes.

$$\begin{aligned}
 f_1 &= f_x \cos^2 \theta + f_y \sin^2 \theta \\
 f_2 &= f_x \sin^2 \theta + f_y \cos^2 \theta \\
 f'_1 &= f'_x \cos^2 \theta + f'_y \sin^2 \theta \\
 f'_2 &= f'_x \sin^2 \theta + f'_y \cos^2 \theta \qquad \dots(6.22)
 \end{aligned}$$

in which f_x, f_y are components of tension steel forces per unit width in the direction of steel coordinates x and y respectively. f'_x and f'_y are components of steel forces in compression per unit width in the direction of steel coordinates x and y respectively. $\epsilon_{t1}, \epsilon_{t2}$

$$\begin{aligned}
 M_{1r} &= 1/c_1^2 \int_{\epsilon_{b1}}^{\epsilon_{t1}} \sigma_1(\epsilon) d\epsilon + f_1 (kh-d'_s) + f_1[(1-k)h-d_s]. \\
 M_{2r} &= 1/c_2^2 \int_{\epsilon_{b2}}^{\epsilon_{t2}} \sigma_2(\epsilon) d\epsilon + f_2 (kh-d'_s) + f_2[(1-k)h-d_s]. \qquad \dots(6.23)
 \end{aligned}$$

in which d_s and d'_s are distance from extreme fibres to the centroids of the tension and compression steel respectively. h is depth of slab, kh is depth of the neutral axis and M_{1r} and M_{2r} are the resisting moments along material axes respectively.

The unknown in the above equation is concrete strain at the extreme compressive fibre $\epsilon_c = \epsilon_{ti}$ or ϵ_{bi} , which together with the curvature establishes the location of neutral axis. The integrals are evaluated numerically using the three point Gaussian quadrature.

For an iteration, the components of steel forces f_1 and f_2 (f_1 and f_2) along the material axes which are functions of f_x and f_y (f_x and f_y) must be known. The values of steel forces are calculated using the following procedure.

The steel strains ϵ_{sx} and ϵ_{sy} at the steel level are related to by geometry to the ϵ_1 and ϵ_2 . That is transferred to the steel coordinates.

$$\begin{bmatrix} \epsilon_{sx} \\ \epsilon_{sy} \end{bmatrix} = \begin{bmatrix} C^2 & S^2 \\ S^2 & C^2 \end{bmatrix} \begin{bmatrix} \epsilon_1 \\ \epsilon_2 \end{bmatrix} \quad \dots(6.24)$$

Similarly, the curvatures in the two coordinates systems are related.

$$\begin{bmatrix} C_x \\ C_y \end{bmatrix} = \begin{bmatrix} C^2 & S^2 \\ S^2 & C^2 \end{bmatrix} \begin{bmatrix} C_1 \\ C_2 \end{bmatrix} \quad \dots(6.25)$$

The strains vary linearly with the depth of slab, the values of ϵ_x , ϵ_y and C_x , C_y are sufficient to define the strains in steel reinforcement.

$$\begin{aligned} \epsilon_{sx} &= C_x(h-d_s) \\ \epsilon_{sy} &= C_y(h-d_s) \\ \epsilon'_{sx} &= C_x(h-d'_s) \\ \epsilon'_{sy} &= C_y(h-d'_s) \end{aligned} \quad \dots(6.26)$$

The stresses in steel reinforcement are

$$\begin{aligned} \sigma_{sx} &= E_{sx} \epsilon_{sx} \\ \sigma_{sy} &= E_{sy} \epsilon_{sy} \\ \sigma'_{sx} &= E'_{sx} \epsilon'_{sx} \\ \sigma'_{sy} &= E'_{sy} \epsilon'_{sy} \end{aligned} \quad \dots(6.27)$$

and corresponding steel forces are

$$\begin{aligned} f_x &= A_{sx} \sigma_{sx} \\ f_y &= A_{sy} \sigma_{sy} \\ f'_x &= A'_{sx} \sigma_{sx} \\ f'_y &= A'_{sy} \sigma_{sx} \end{aligned} \quad \dots(6.28)$$

The steel forces are transformed back to the material axes to solve the equation. The most recent values of steel forces are calculated with aforementioned procedure at each iteration.

During each iteration the concrete strain at the extreme compressive fibre ϵ_c in the principal curvature directions is solved independently using Newton-Raphson technique.

$$\epsilon_{New} = \epsilon_{Old} - \frac{F}{\partial F} \dots (6.29)$$

till the change in strain is small. The convergence criterion for strains considered as change in strain ϵ_c is less than 10^{-7} .

These strains are used to calculate the updated steel forces. These updated steel forces are transferred back to the material axes which are again used to calculate the concrete strain in the extreme compressive fibre. The iterations are carried till convergence is obtained when the ratio of change in steel force in each direction to the original value is less than 1%. In most cases convergence is obtained in less than ten iterations, but more iterations are required when excessive strains occur in the concrete or steel reinforcement.

6.7 Failure Criterion

In order to terminate the computation of incremental iterative procedure, it is necessary to adopt a criterion representing failure of the slab. In normal reinforced cross section (under reinforced), failure will occur due to crushing of the concrete, when the concrete compressive strain reaches the ultimate strain. A limiting value for this strain 0.35%, therefore is adopted as the failure criterion. The related failure stress of concrete is $0.85 f_c$. The flow chart of software developed for nonlinear analysis of slabs is given in Appendix – C.

CHAPTER 7

EXPERIMENTAL INVESTIGATION

7.1 Introduction

Reinforced concrete slabs with and without openings supported on four edges and loaded transversely are usually seen in civil engineering structures. Transverse loads can be hydrostatic forces, point loads or uniform pressures. The objective of present experimental investigation is to provide a better understanding of the behaviour of rectangular slabs with and without openings. The behaviour of slender reinforced concrete slabs supported along four edges and loaded transversely is then studied through a limited parametric study.

Reinforced concrete slabs supported on four edges and subjected to transverse loads are encountered in many structural applications. However, few experimental data exist about their behaviour. The variable in the experimental investigation is the percentage area of central opening in the slab. Evaluation or analytical predictions of the test results are presented later.

7.2 Test Specimens

Six rectangular slabs were cast with side dimensions of 1000 mm by 750 mm with 60 mm overall depth and 40 mm as effective depth. The dimensions of slab were chosen keeping into consideration the available loading arrangements, dimension of the loading frame and the loading facilities.

7.3 Testing of Materials

The materials required for casting of slabs are ordinary Portland cement, sand, coarse aggregate and steel. These materials were tested before designing the concrete mix. The properties of the cement are presented in Table 7.1.

Table 7.1
Properties of Cement

SNo.	Parameter	Value
1.	Consistency	32%
2.	Initial Setting Time	36 min.
3.	Final Setting Time	4 hours
4.	Specific Gravity	3.146

The specific gravity of sand and coarse aggregate were found as 2.5 and 2.71 respectively.

7.3.1 Testing of Steel:

The reinforcing bars used were 6 mm diameter mild steel bars. More than 6 samples were tested. The gauge length was kept 8 inches. The extensometer was used to take the readings of extensions and readings were taken at 1 kN increments.

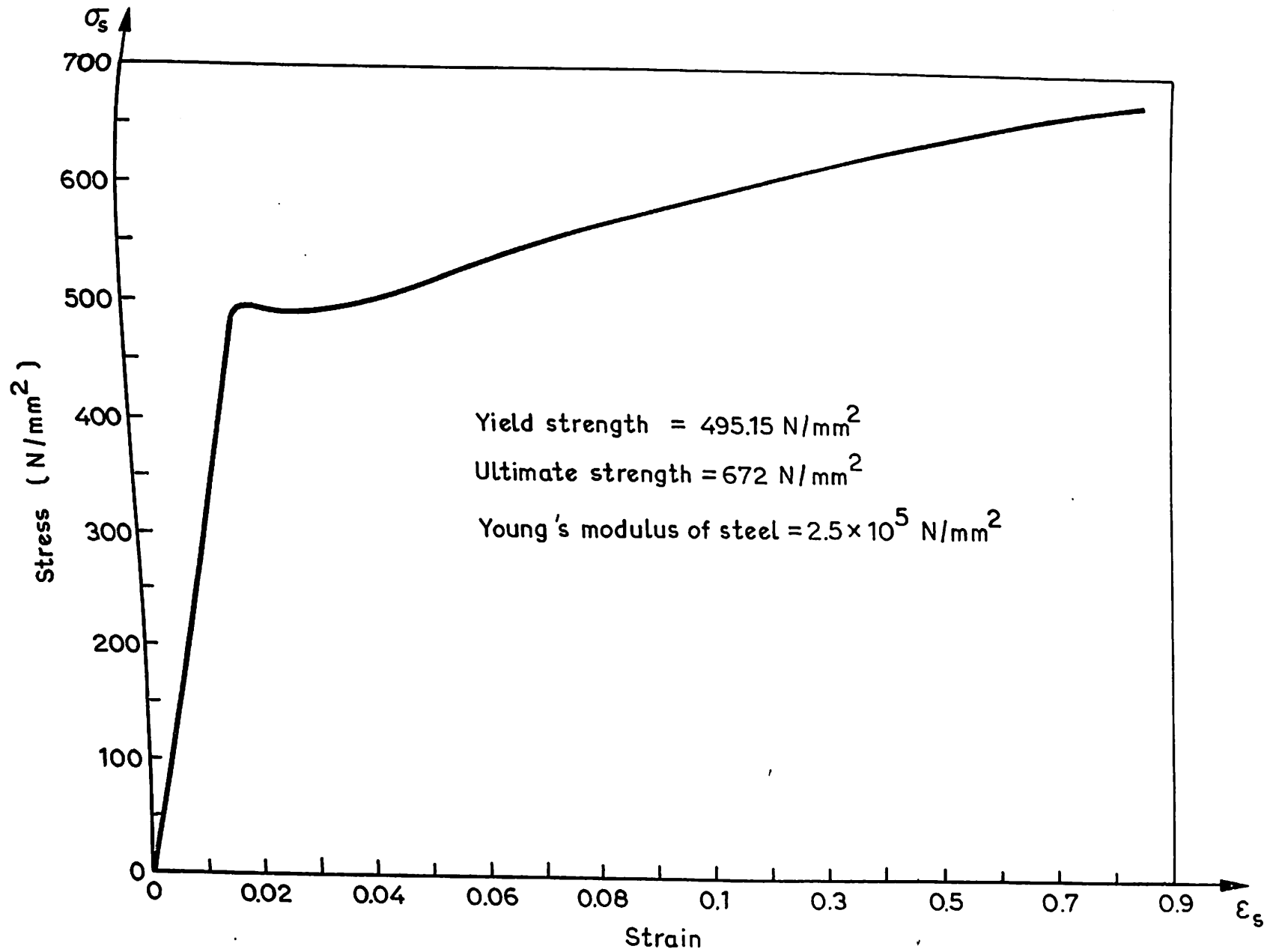


Fig.7.1 Stress -Strain Curve for Steel

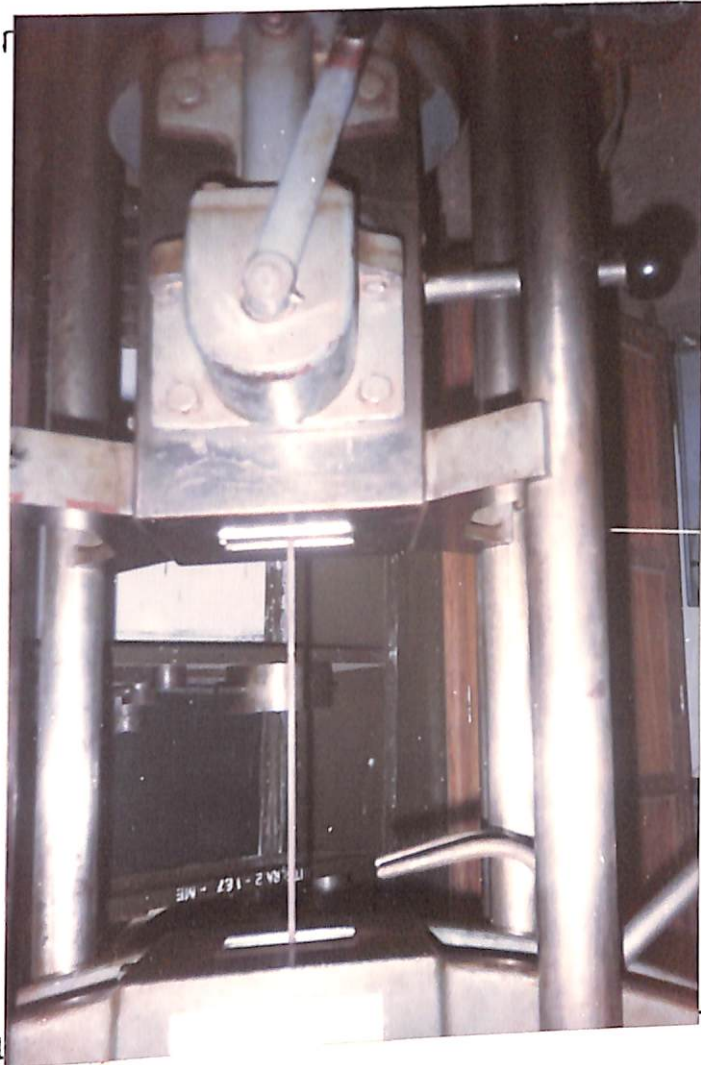


Fig. 7.2 Testing of Steel bar

The stress-strain curve for steel is shown in Fig. 7.1. The yield strength and modulus of elasticity of steel were calculated from Fig. 7.1 as 495.15 N/mm² and 2.5 x 10⁵ N/mm² respectively. The testing arrangement is shown in Fig. 7.2.

7.4 Mix Design:

The concrete was made with ordinary Portland cement, local available sand and coarse aggregate. The proportion of the cement, sand and coarse aggregate was designed according to Road-Note No. 4 method [119] for M₁₅ concrete mix.

The designed proportions obtained are given below:

$$\begin{aligned}
 \text{Aggregate cement ratio} &= 5.7 \\
 \text{Water cement ratio} &= 0.65 \\
 \text{Fine aggregate to coarse aggregate ratio} &= 0.5 \\
 \text{Cement: Fine aggregate : Coarse aggregate} &= 1:1.9:3.8
 \end{aligned}$$

For 1m³ of concrete, the quantity of cement required is calculated as below:

$$\frac{1}{1000} \left[\frac{WA}{SC} + \frac{CE}{SS} + \frac{FA}{SA} + \frac{CA}{SA} \right] = 1 - \text{Percentage of air voids} \quad \dots (7.1)$$

Where

WA is water,

CE is cement,

FA is fine aggregate,

CA is coarse aggregate,

SC is specific gravity of cement,

SS is specific gravity of sand, and

SA is specific gravity of aggregate.

Assuming 2% of air voids and substituting values in equation (7.1) gives

$$0.65CE + \frac{CE}{3.14} + \frac{1.9CE}{2.5} + \frac{3.8CE}{2.71} = 980$$

$$\Rightarrow CE = 313.03 \text{ Kg.}$$

Therefore, for 1m^3 of concrete the materials required are calculated as:

Cement	=	313.03 Kg.
Sand	=	594.75 Kg.
Coarse aggregate	=	1189.52 Kg.
Water	=	203.45 lts.

12 cubes of $150\text{mm} \times 150\text{mm} \times 150\text{mm}$ were made and kept for the curing in water. These cubes were tested for 3 days, 7 days and 28 days for compressive strength of concrete. The test results are given in Table 7.2.

Table 7.2.

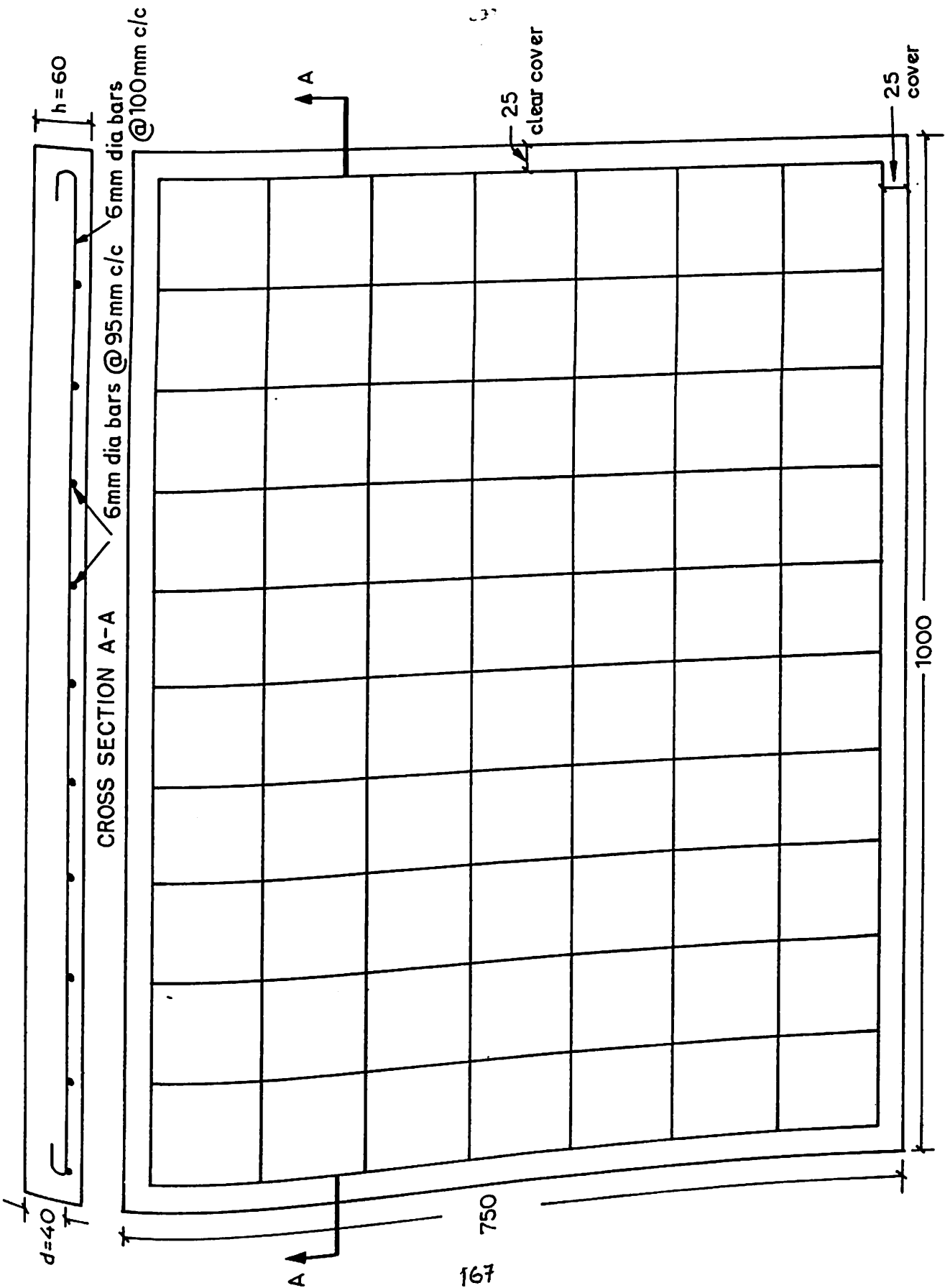
Compressive Strength of Concrete Cubes

SNo.	3 Days		7 Days		28 Days	
	Load (kN)	Strength (MPa)	Load (kN)	Strength (MPa)	Load (kN)	Strength (MPa)
1.	190	8.44	240	11.78	360	16.00
2.	170	7.56	230	11.33	300	13.33
3.	160	7.11	240	11.78	380	16.89
4.	160	7.11	280	12.78	355	15.78

7.5. Slab Design:

Dimensions of the slabs are fixed with respect to available size of loading frame and loading arrangements. The overall depth of slab and percentage of reinforcement were calculated meeting the requirement of deflection criteria and minimum spacing of steel reinforcement according to I.S. Code 456:1978 [120]. The design calculations are given in Appendix B.

Overall depth and effective depth were kept as 60 mm and 40 mm respectively. Keeping the spacing of steel reinforcement as 100 mm centre to centre, 11 and 8 number of 6 mm diameter bars were provided along long and short directions of slabs. Plan and cross sectional details of solid slab and slab with 5% central opening are shown in Fig. 7.3 and Fig. 7.4.



PLAN

PLAN

All dimensions are in mm

Fig.7.3 Plan and section details of solid slab

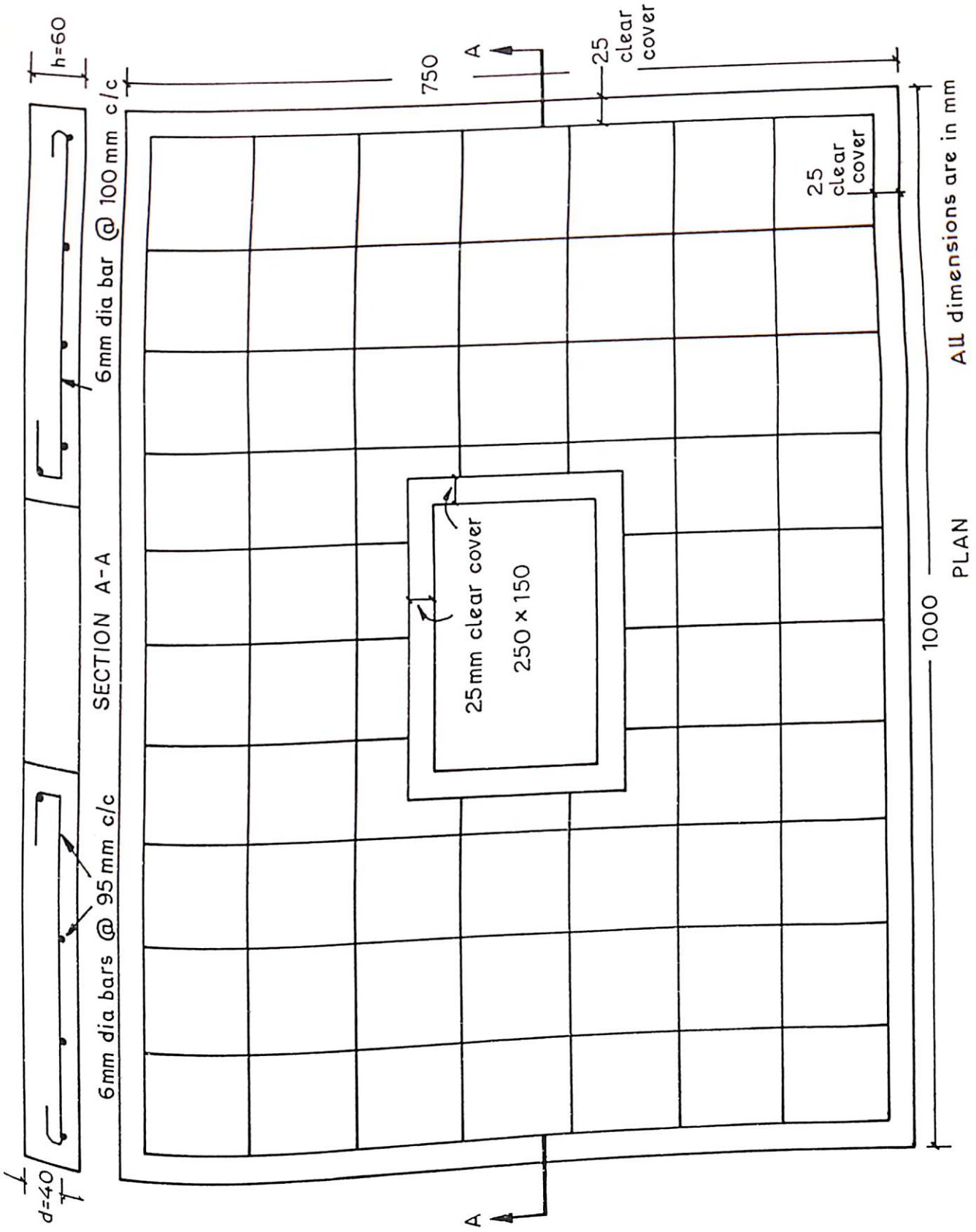


Fig.7.4 Plan and sectional details of slab with 5% central opening

7.6. Casting of Slabs

The slabs were cast in wooden form work. A clear cover of 20 mm was provided, placing cement mortar pallets of 20mm x 20mm x 20mm. The materials required for slabs were calculated with designed mix proportions as given in Table 7.3.

Table 7.3

Materials Requirements for Slabs

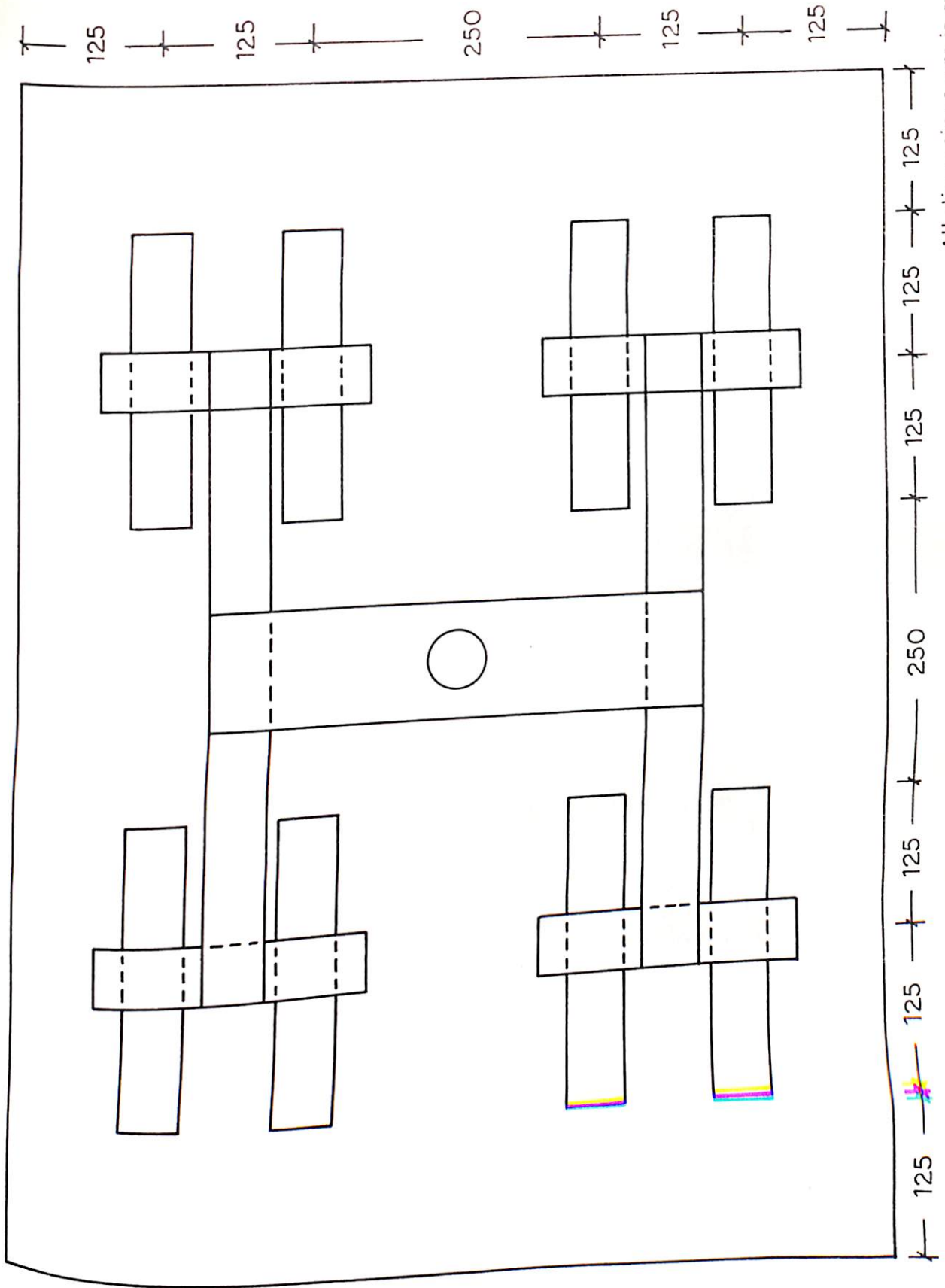
Slab No.	Cement Kg.	Fine Aggregate Kg.	Coarse Aggregate Kg.	Water Litres
1	18.21	34.60	69.20	11.84
2	18.07	34.33	68.67	11.75
3	17.78	33.78	67.56	11.56
4	17.50	33.25	66.50	11.38
5	17.22	32.72	65.44	11.19
6	16.94	32.19	64.38	11.01

The concrete was uniformly mixed by concrete mixer and placed in the wooden form work in two layers. Each layer was properly compacted. After 24 hours of casting, the form work was removed. Curing of slabs was done by placing jute gunny bags with sprinkling of water twice in a day. While casting the slabs,

three 150mm cubes of same material were also prepared and placed in water tank for curing after 24 hours.

7.7 Testing of Slabs

The slabs were tested on 500kN loading frame. The slabs were placed over a rectangular frame made of I-sections to provide simple supported boundary conditions. The uniformly distributed load was applied by symmetrical loading arrangement as shown in Fig. 7.5. Loads were applied on slab with hydraulic jack in small increments till the failure occurred. Fig. 7.6 shows the number of I-sections to transfer the load from hydraulic jack to the slab. It took about 45 minutes for failure from the time of critical loading. Six dial gauges were used to measure deflections at six different points of slabs. The deflections of slabs were recorded by dial gauges at 20 kN load increments.



All dimensions are in mm

Fig.7.5 Symmetrical loading arrangement on slab



Fig.7.6 Load Arrangement for testing a slab

7.8 Behaviour of Slabs

For solid slab, first crack appeared at the centre of slab at about 70 kN load. As the loading increased, cracks magnified and at the load of 150 kN cracks were sufficiently deep. Ultimately the cracks had gone to all four corners and failed due to crushing at 290 kN load.

For slab with 1% central opening the first crack appeared at 70 kN load and for the slab with 3% central opening the first crack appeared at 60 kN load respectively. For other slabs the first crack load was observed at about 50 kN load. These cracks magnified further and reached the four corners of slabs. Slabs were failed due to crushing of concrete.

Figures 7.7 to 7.12 shows the crack pattern of all six slabs. The observed ultimate load values are given in Table 7.4.

Table 7.4 Experimental Ultimate Load Values

Slab No.	% opening	Size of opening (mm x mm)	Cube strength (Mpa)	Initial crackload (kN)	Ultimate load (kN)
1.	-	-	15.41	70	290
2.	1.0	100x75	15.83	70	280
3.	3.0	150x150	15.91	60	270
4.	5.0	250x150	16.01	50	250
5.	7.0	250x210	16.24	50	240
6.	9.0	260x260	16.45	50	220



Fig.7.7 Crack pattern of Solid Slab



Fig.7.8 Crack pattern of Slab with 1% Central opening

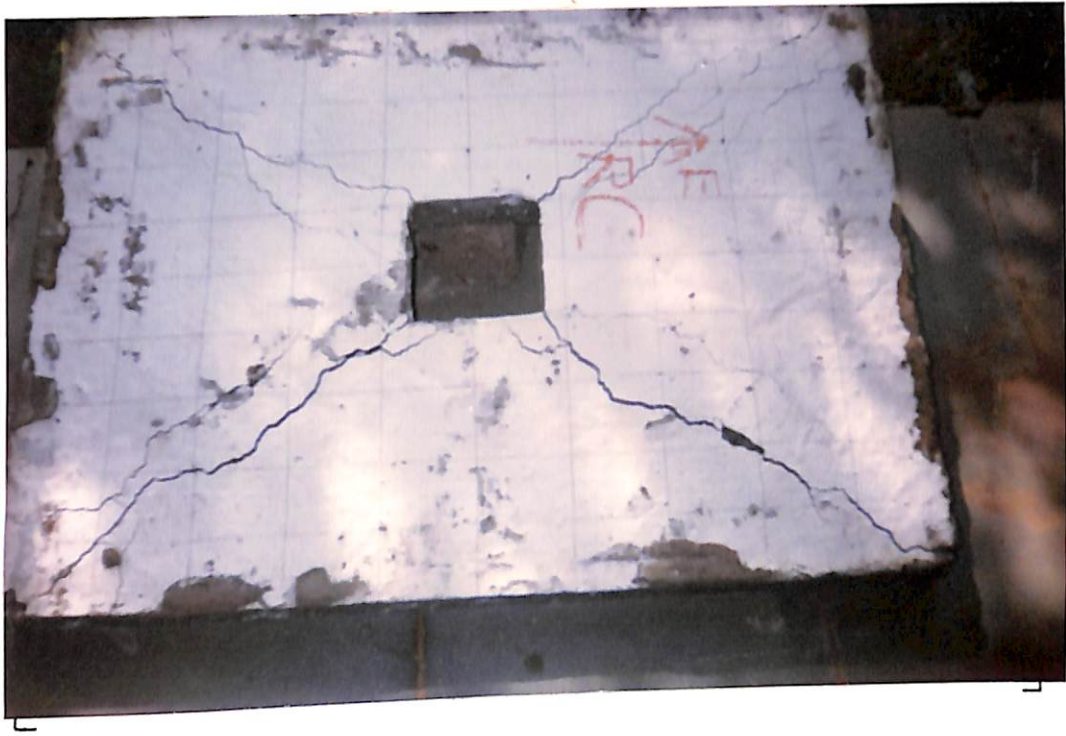


Fig.7.9 Crack pattern of Slab with 3% Central opening

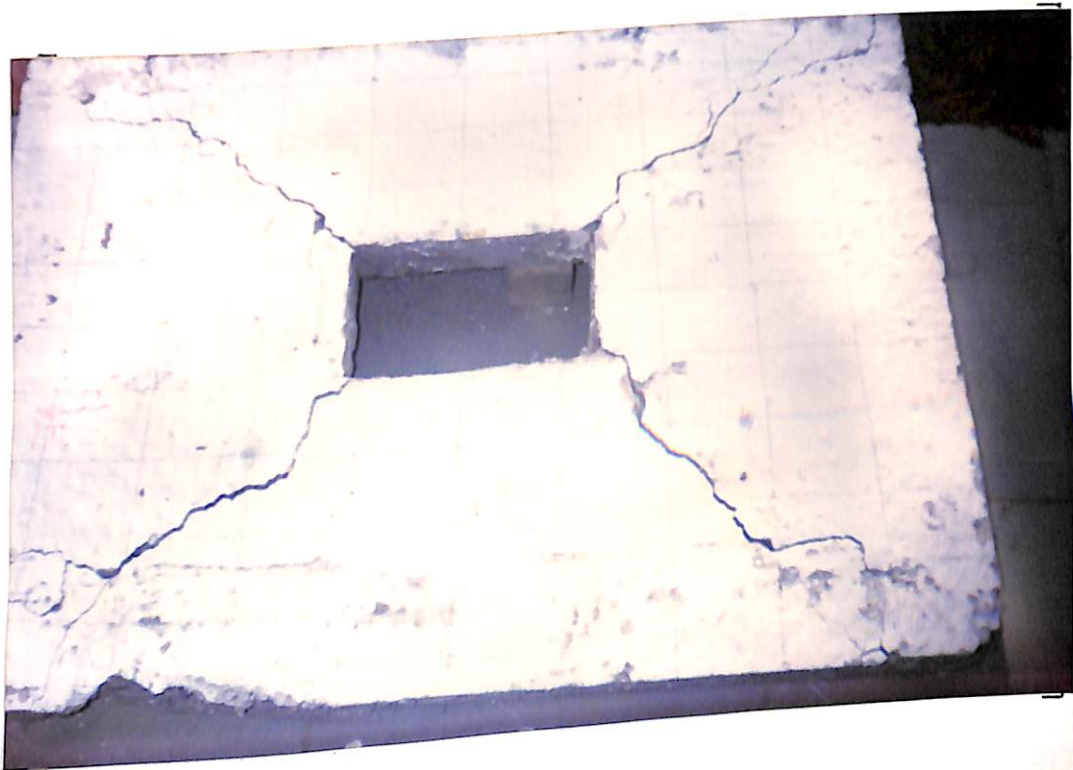


Fig.7.10 Crack pattern of Slab with 5% Central opening



Fig.7.11 Crack pattern of Slab with 7% Central opening



Fig.7.12 Crack pattern of Slab with 9% Central opening

CHAPTER 8

RESULTS

Six rectangular slabs with and without central openings were prepared and tested to failure as discussed in Chapter 7. These slabs were studied numerically by proposed nonlinear finite element analysis. The proposed analysis incorporated the effect of material nonlinearity by different appropriate models of concrete and steel reinforcement. Slabs were analysed for effects of tension-softening, tension-stiffening and aggregate interlock. Comparisons were made between the load deflection curves of experimental values and numerical results obtained by finite element analysis.

Initially, the nonlinear stress strain curve of concrete in compression, linear model of concrete in tension and elasto-plastic model of steel reinforcement are considered in the analysis and treated as first method of analysis. The second method of analysis includes the flexural stiffness of steel reinforcement before cracking of the concrete in material behaviour matrix. In third method of analysis, tension-softening phenomenon of concrete in tension is added to the previous analysis. Further, fourth method of analysis incorporates tension-stiffening effect due to bond-slip mechanism in the proposed analysis. Finally, aggregate interlock effect is added to the proposed analysis to predict the overall behaviour of slab. One quarter of the slabs has been considered for the analysis with respect to symmetry of

the slab and loading

Slab

The corner supported two-way slab, tested under a central point load by Mc Niece[47], is used to investigate the validity of developed models and proposed analysis for treating post- cracking behaviour of slab.

A plan of the slab is shown in Fig. 8.1, together with the material properties assumed in the analysis and the finite element mesh.

The slab was 36 in. (914 mm) square and 1.75 in. (44.5 mm) thick, with an isotropic mesh of 0.85% reinforcing steel at an effective depth of 1.31 in. (33.3 mm).

Deflections recorded during experimentation at node 2 in Fig. 8.1 are used to test the validity of the models developed here. In Fig. 8.2, comparisons are made between the experimental load deflection curve at node 2 of Mc Neices' slab and the numerical results obtained by using the various models.

The load deflection curves obtained by neglecting tension- softening phenomenon significantly under-estimates the slab stiffness in the post-cracking range. The tension-softening phenomenon fairly predicts the deflections recorded

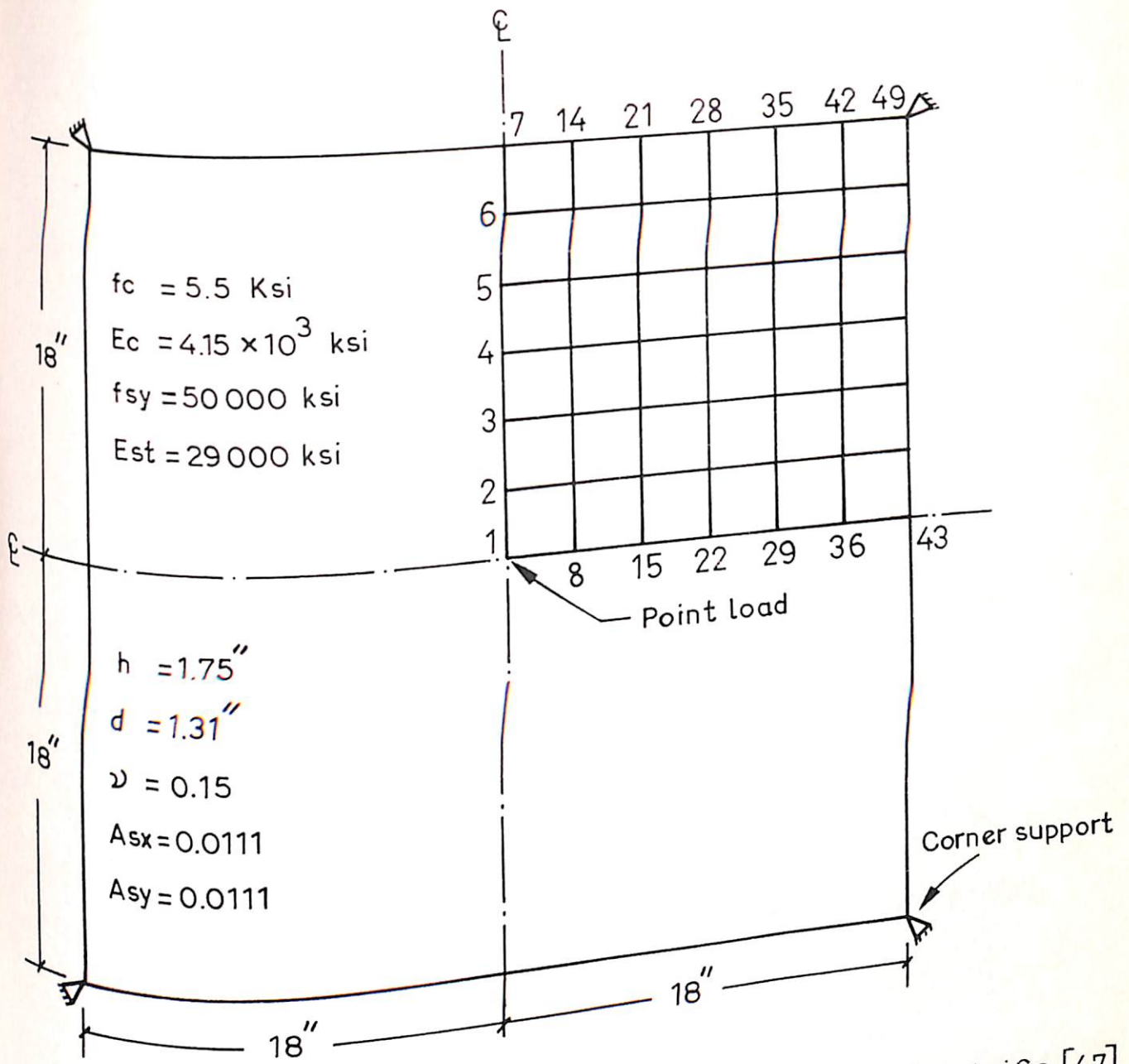


Fig.8.1 Corner supported Two-way slab Tested by Mc Neice [47]

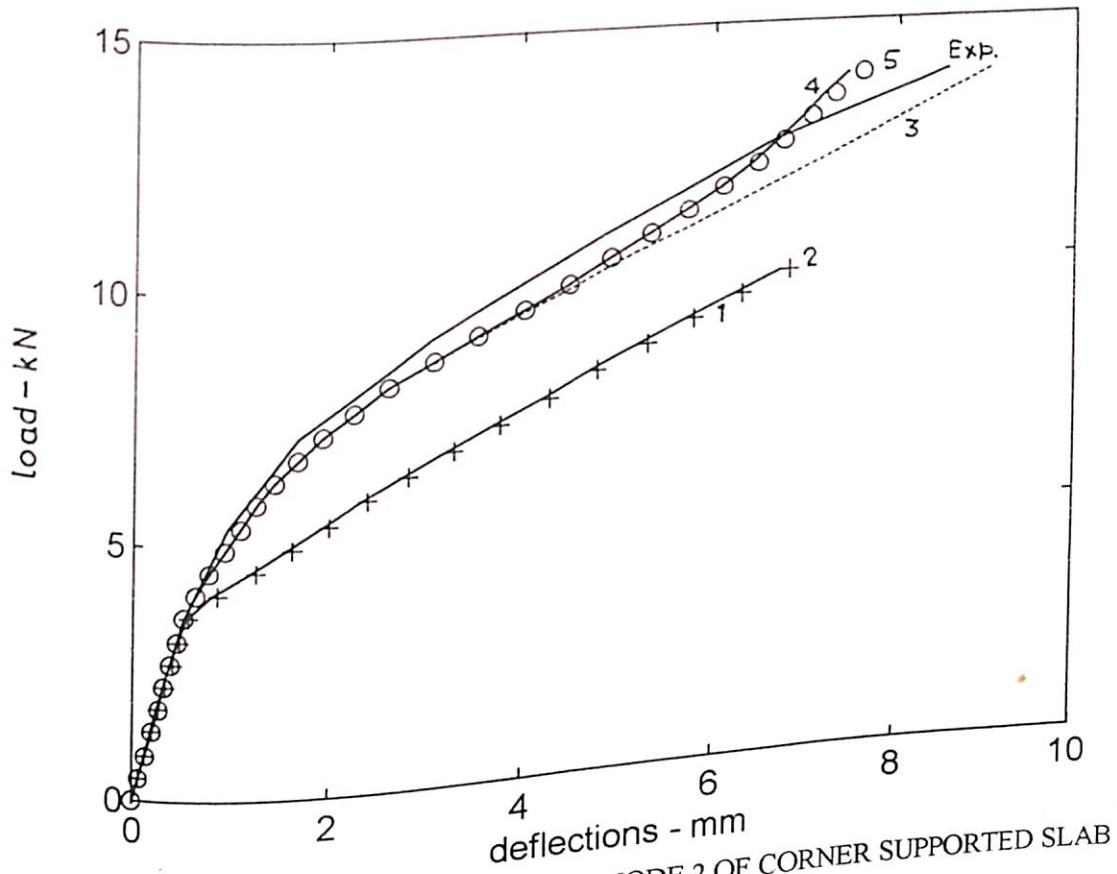


Fig. 8.2 LOAD-DEFLECTION CURVES AT NODE 2 OF CORNER SUPPORTED SLAB

- 1 Simple Nonlinear Analysis
- + 2 Effect of Initial Steel flexural stiffness
- 3 Tension-Softening Effect
- x 4 Bond Effect
- o 5 Aggregate Interlock Effect
- Exp. Experimental Curve

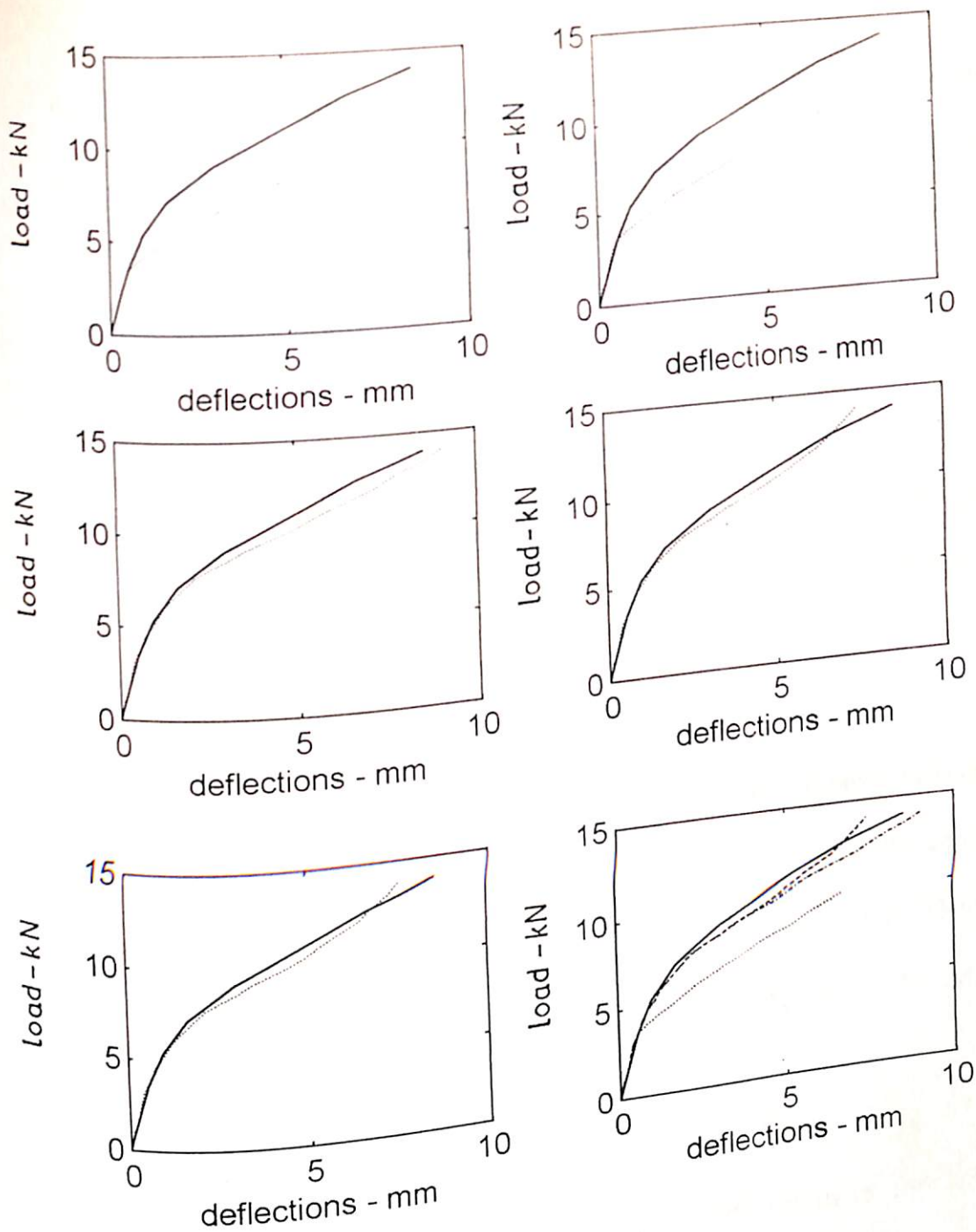


Fig. 8.2.1 LOAD-DEFLECTION CURVES AT NODE 2 OF SLAB WITH DIFFERENT METHODS OF ANALYSIS

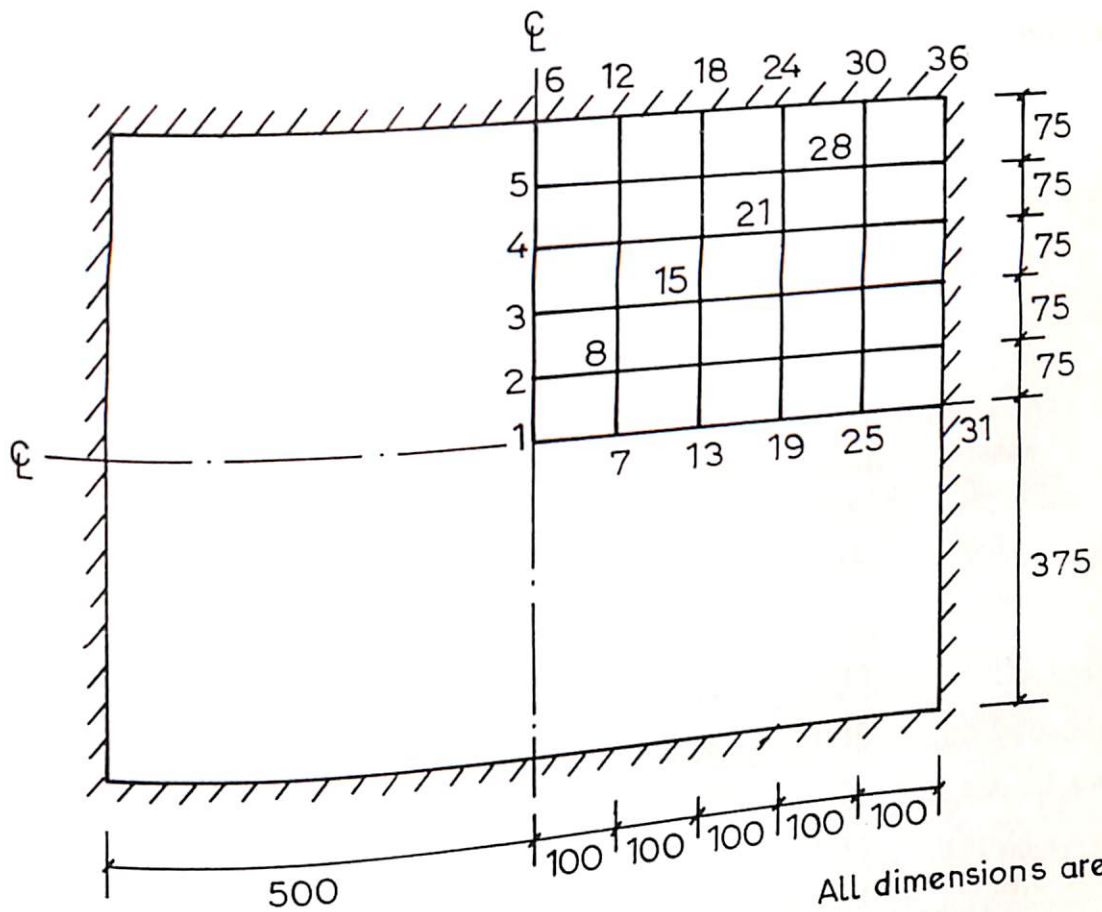
during the experimentation. The developed model of tension stiffening effect produced results in close agreement with the experimental curve as shown in Fig. 8.2. An overestimation of stiffness for the cracked slab is observed by incorporating aggregate interlock effect.

Slab 1:

A simple supported rectangular two-way slab tested under uniformly distributed load is investigated for the post-cracking behaviour. The slab is modeled as 5x5 rectangular mesh with uniform size of elements as shown in Fig. 8.3.

Initial cracks were observed at about 70 kN of progressive transverse load. Initial yielding of steel reinforcement was recorded at 150 kN of the applied load. Crushing load of 290 kN was observed during the experimentation. The recorded experimental values of deflections at node numbers 1, 8, 15, 21, 25 and 28 of Fig. 8.3 are presented in table 8.1.

The first method of nonlinear analysis under estimates the stiffness of cracked concrete. Therefore, the numerical results of deflections are too large. These values are 75 and 99 percent more than the recorded values for node 1 and node 28 at 220 kN. Second method of nonlinear analysis slightly increases the stiffness of slab. However, the deflections are still large, ranging from 70 to 95 per cent. The numerical ultimate load predicted by these two methods of analysis is too



All dimensions are in mm

$$f'_c = 15.41 \text{ N/mm}^2$$

$$E_c = 0.186 \text{ N/mm}^2$$

$$E_s = 2.5 \times 10^5 \text{ N/mm}^2$$

$$f_{sy} = 495.15 \text{ N/mm}^2$$

$$h = 60 \text{ mm}$$

$$d = 40 \text{ mm}$$

$$\rho = 0.15$$

$$A_{sx} = 0.31 \text{ mm}^2/\text{mm}$$

$$A_{sy} = 0.31 \text{ mm}^2/\text{mm}$$

Fig.8.3 Simple supported solid slab

less as given in Table 8.2. The analytical ultimate load is 75.86% of actual ultimate load and initial yielding of steel reinforcement is 73.33% of the recorded experimental value.

Table 8.1
Experimental deflections of Solid Slab

Load (KN)	Deflections (mm)					
	Node No.1	Node No.8	Node No.15	Node No.21	Node No.25	Node No.28
0	0.00	0.00	0.00	0.00	0.00	0.00
20	0.19	0.18	0.13	0.09	0.06	0.04
40	0.39	0.35	0.26	0.19	0.12	0.08
60	0.58	0.53	0.39	0.28	0.18	0.12
80	0.79	0.73	0.52	0.37	0.24	0.15
100	1.11	1.12	0.78	0.59	0.38	0.23
120	1.65	1.65	1.17	0.85	0.54	0.34
140	2.44	2.41	1.72	1.23	0.79	0.51
160	3.55	3.38	2.28	1.79	1.05	0.71
180	5.07	4.51	3.06	2.26	1.39	0.93
200	6.46	5.73	3.96	2.89	1.83	1.22
220	7.88	7.01	4.96	3.51	2.25	1.45
240	9.02	8.11	5.63	4.15	2.64	1.65
260	10.31	9.02	6.41	4.66	3.12	1.85
280	11.37	9.95	7.05	5.17	3.51	2.01
290	11.75	10.31	7.33	5.42	3.71	2.11

Table 8.2

Salient Results of Investigation

Method of analysis	Load value of initial crack (kN)	Load value of initial yielding of steel (kN)	Ultimate load (kN)
1	70	110	220
2	70	110	220
3	70	150	270
4	70	150	290
5	70	150	290
Exp.	70	150	290

Third method of analysis which incorporates tension-softening phenomenon, fairly predicts the experimental values. The slab stiffness of cracked concrete significantly increased due to this effect. The difference in recorded deflections and numerical results varies from 27 to 42.5 per cent for node 1 and node 28 at 270 kN. The model predicted the experimental value of initial yielding of steel reinforcement. However, the calculated ultimate load is 0.931 times less than the actual experimental load.

By adding the tension stiffening effect in proposed analysis, the slab stiffness of cracked concrete increased further and deflections are in close agreement with the experimental values. The numerical deflections are 1.58 and 4.7 per cent less than the measured deflections at node 1 and node 28 respectively.

The aggregate interlock slightly decreased the stiffness of cracked concrete further and difference in deflection values are observed as 1.8 and 4.6 per cent less than the recorded values of selected points. The point to point difference between the experimental and proposed analysis is clearly shown in figure 8.4 to 8.9. Figure 8.4.1 shows the difference between the experimental curve and proposed analytical results considering the effects of all models one after the other for central node of the slab. The maximum difference of 12.5 percent in deflections is observed immediately after the yielding of steel reinforcement for central node. The minimum difference of 1.58 per cent in deflections is observed at ultimate load for central node.

It is observed that the numerical value of initial crack load is well in agreement with the recorded value of experimentation. The concrete is failing in tension at 24.1 percent of ultimate load. Also the analytical yielding of steel reinforcement is coinciding with the observed value, which is about 51.7 per cent of ultimate load. From the load-deflection curves of Fig. 8.4 to 8.8, it is clearly evident that the tension-softening and tension-stiffening effects significantly increases the slab stiffness of the concrete and calculates the deflections nearer to experimental values.

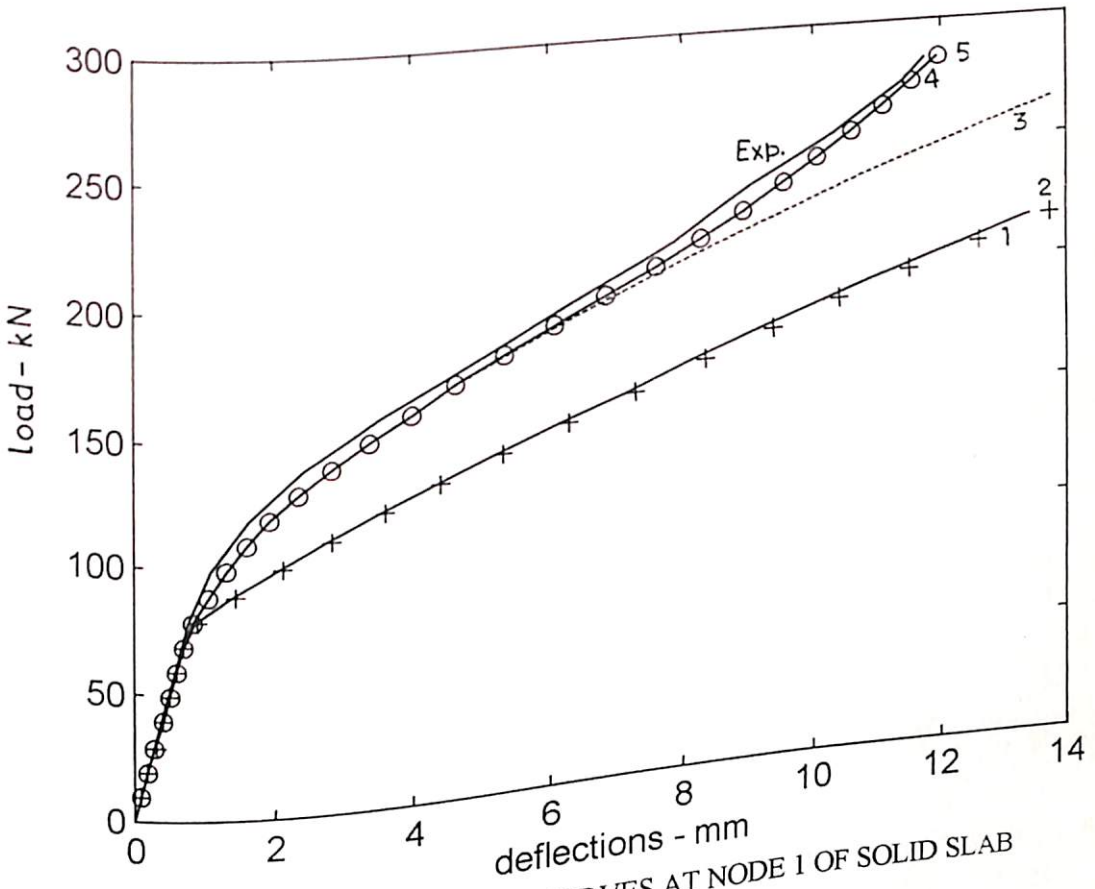


Fig. 8.4 LOAD-DEFLECTION CURVES AT NODE 1 OF SOLID SLAB

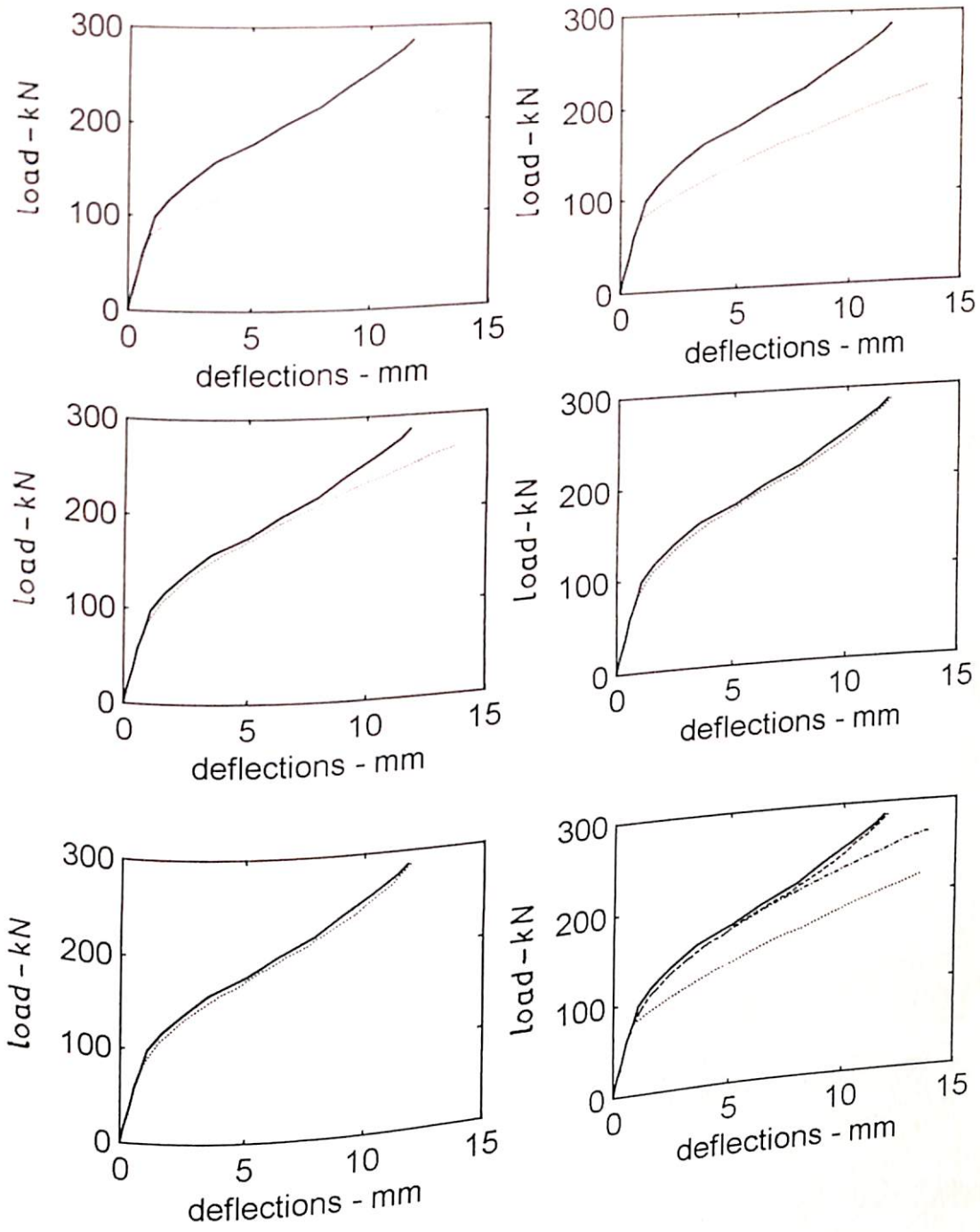


Fig. 8.4.1 LOAD-DEFLECTION CURVES AT NODE 1 OF SLAB WITH DIFFERENT METHODS OF ANALYSIS

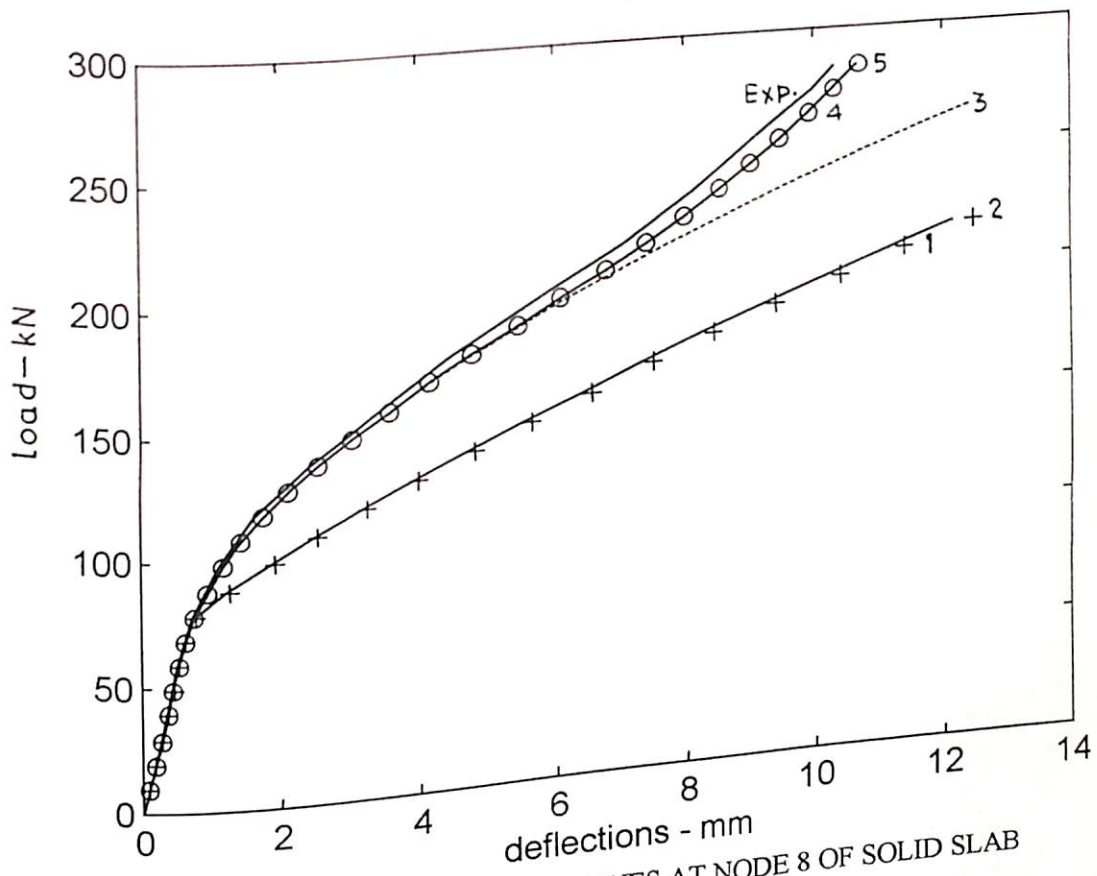


Fig. 8.5 LOAD-DEFLECTION CURVES AT NODE 8 OF SOLID SLAB

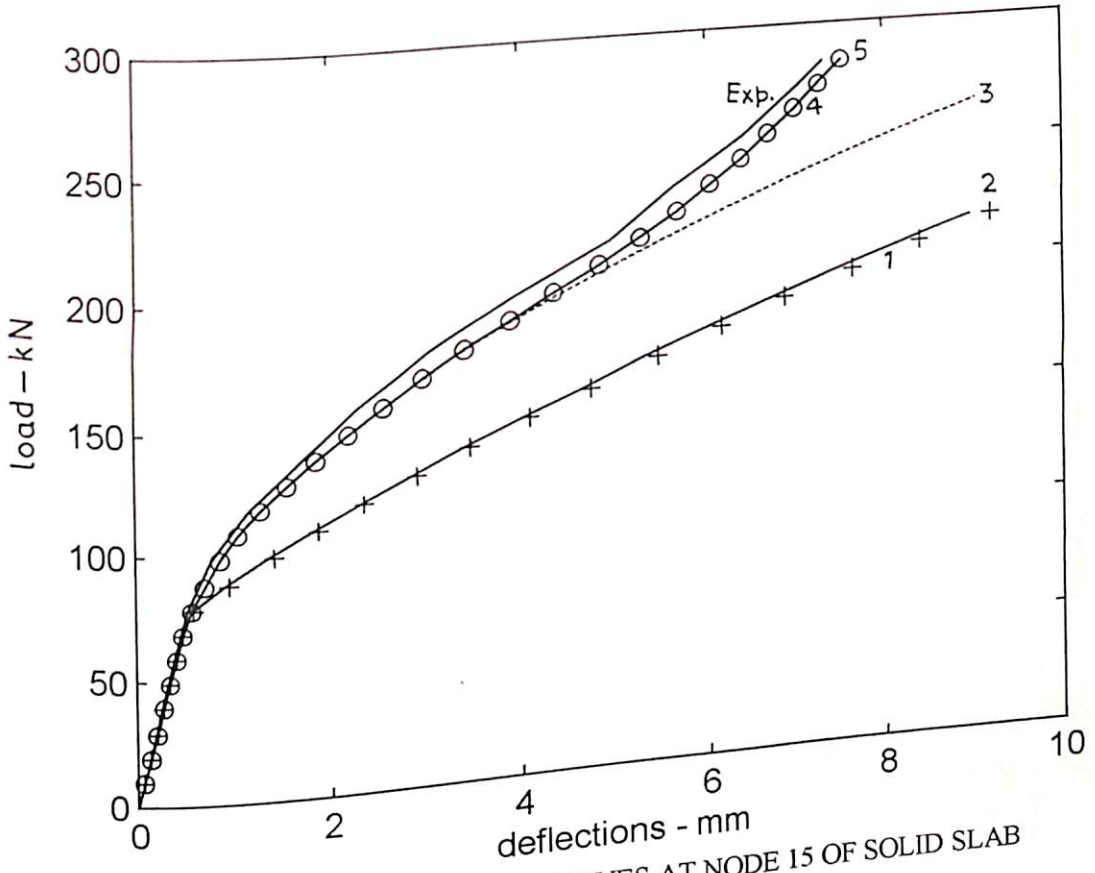


Fig. 8.6 LOAD-DEFLECTION CURVES AT NODE 15 OF SOLID SLAB

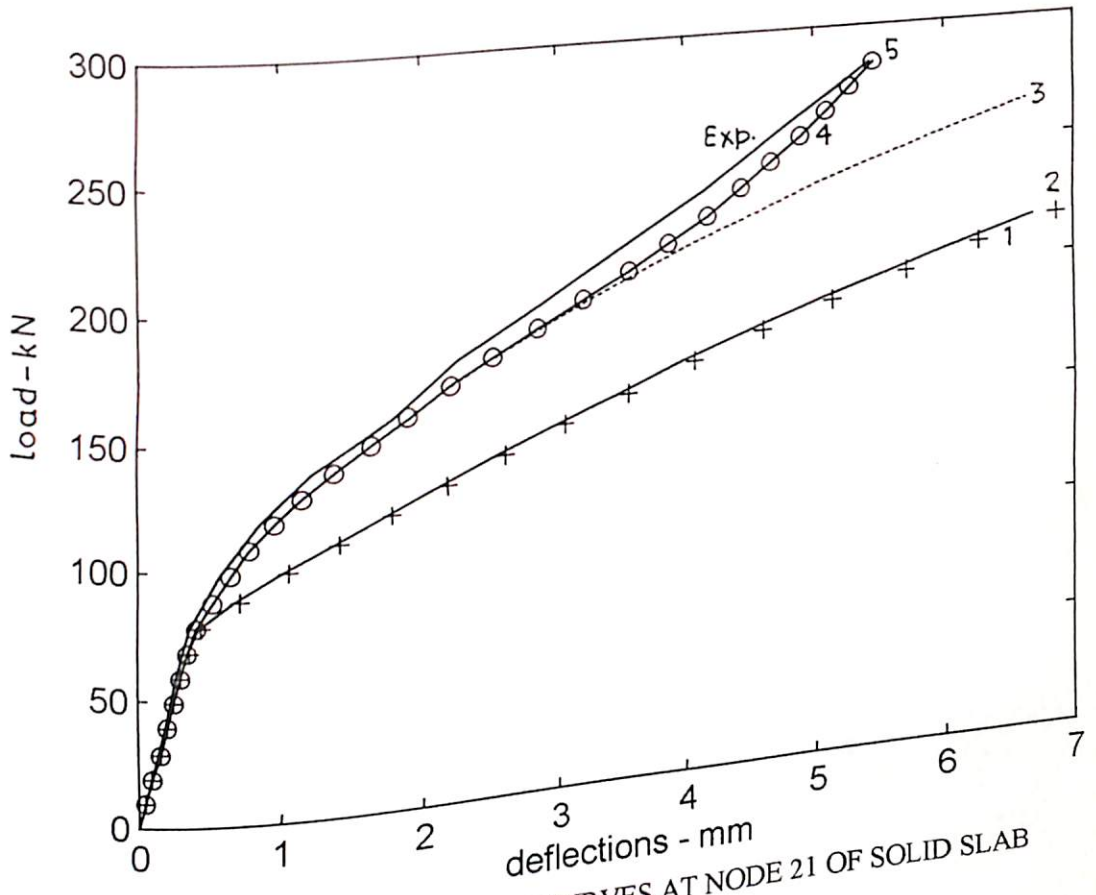


Fig. 8.7 LOAD-DEFLECTION CURVES AT NODE 21 OF SOLID SLAB

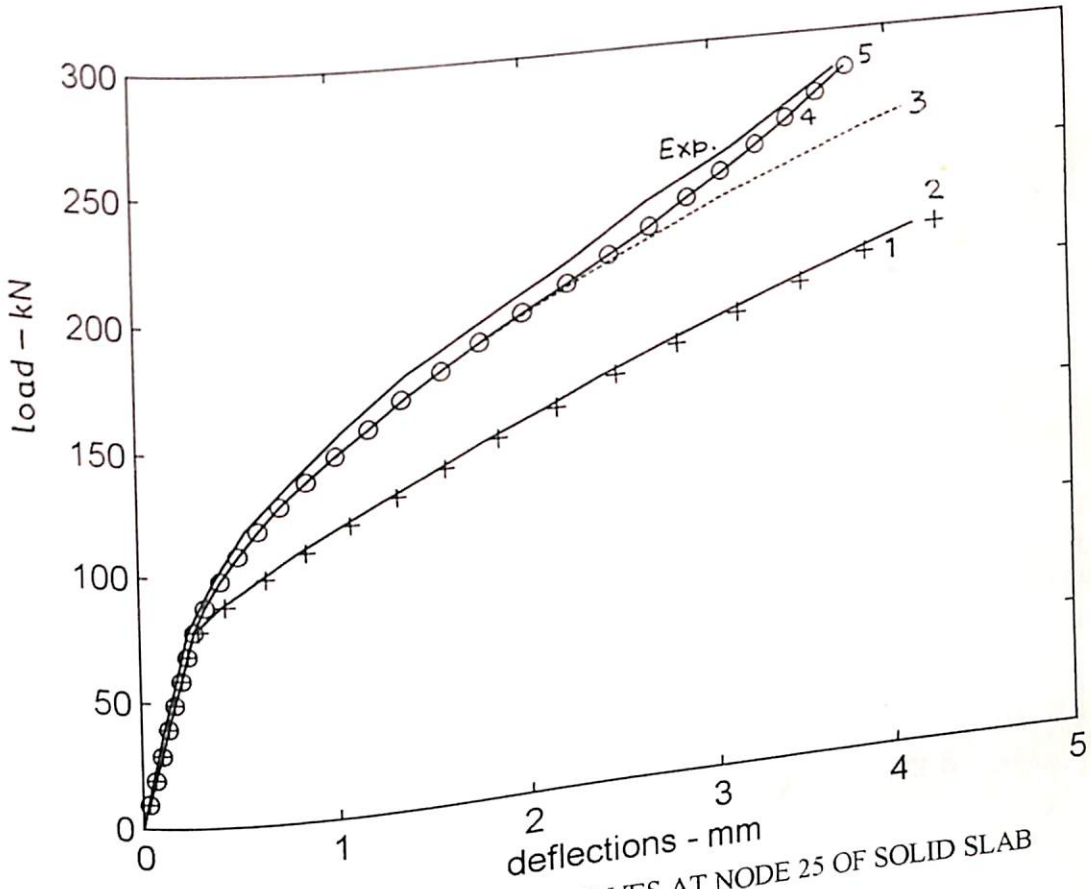


Fig. 8.8 LOAD-DEFLECTION CURVES AT NODE 25 OF SOLID SLAB

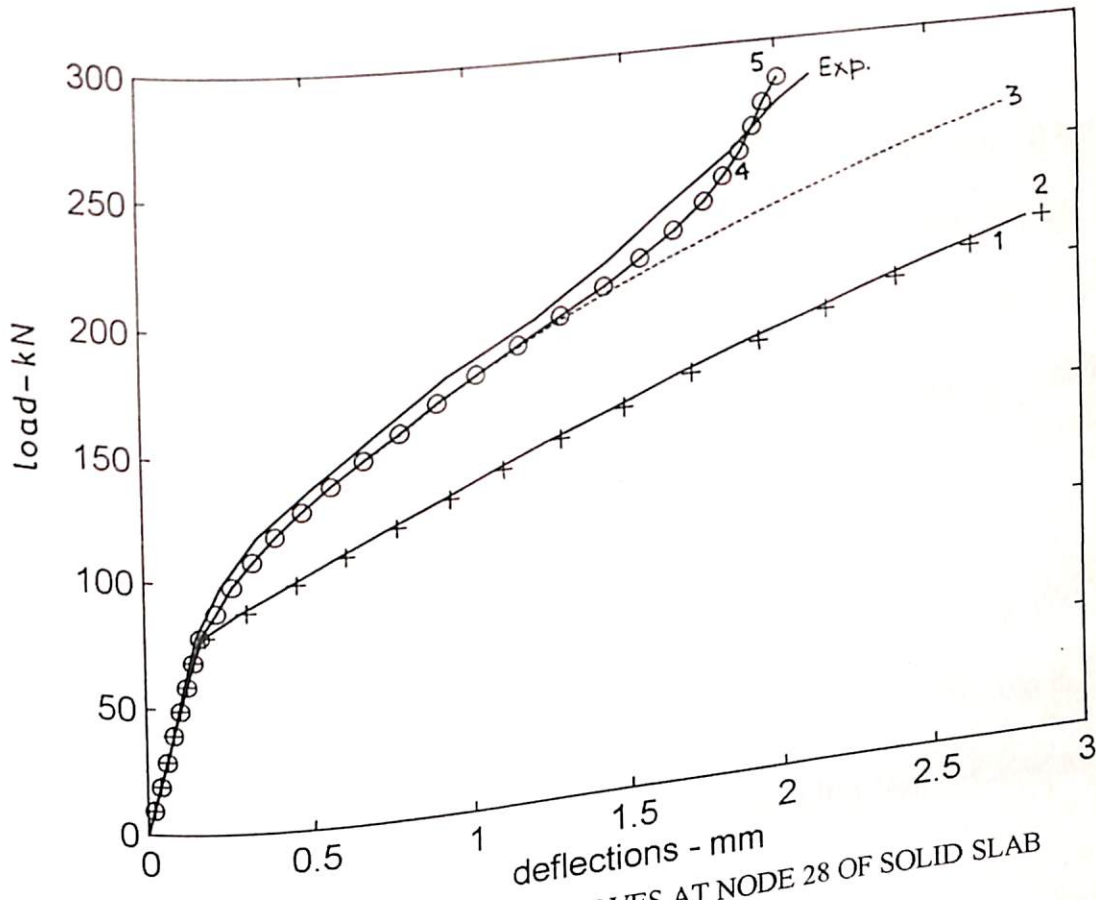


Fig. 8.9 LOAD-DEFLECTION CURVES AT NODE 28 OF SOLID SLAB

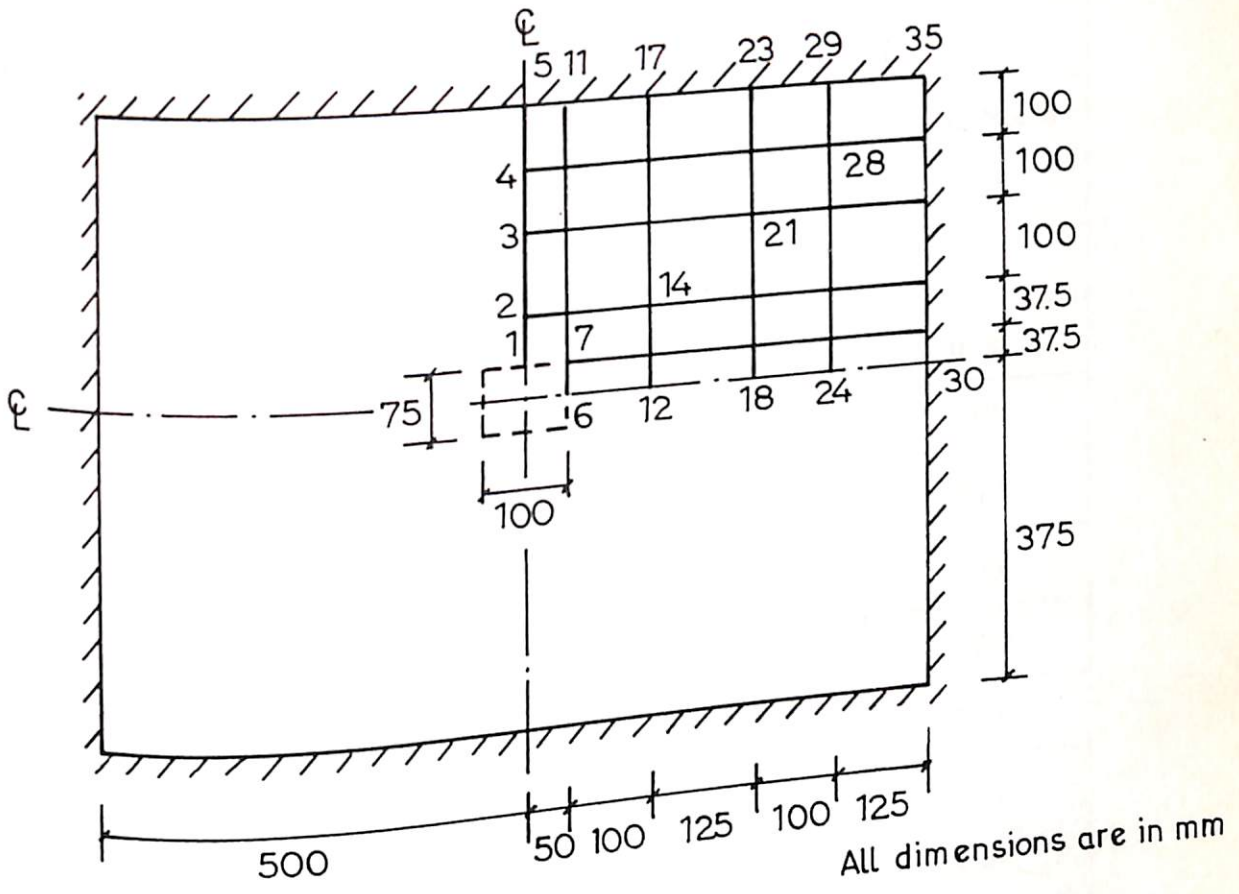
Slab 2:

A simple supported rectangular two-way slab with one percent central opening of size 100 mm x 75 mm tested under uniformly distributed load is analysed to know the behaviour of slab after cracking. The slab is modelled as shown in fig. 8.10 with 5x5 finite element mesh of different size of elements.

Initial cracks and yielding of steel reinforcement were observed at 70 kN and 150 kN load respectively. The slab crushed when the load has reached 280 kN. The measured experimental values of deflections at node number 7, 14, 21 and 28 of fig. 8.10 are presented in table 8.3. These points were pre-selected along the predicted yield lines of slab.

The initial value of crack load was observed as 25% of ultimate load. The steel was initially yielded at 53.57% of ultimate load. Comparing with solid slab, the ultimate load of slab is reduced by 10 kN, i.e. 0.965 times less than the ultimate load of solid slab.

The predicted values of initial cracking of concrete, yielding of steel reinforcement and crushing load of concrete by proposed analysis are presented in Table.8.4.



$$f'_c = 15.83 \text{ N/mm}^2$$

$$E_c = 0.188 \times 10^5 \text{ N/mm}^2$$

$$E_s = 2.5 \times 10^5 \text{ N/mm}^2$$

$$f_{sy} = 495.15 \text{ N/mm}^2$$

$$h = 60 \text{ mm}$$

$$d = 40 \text{ mm}$$

$$\rho = 0.15$$

$$A_{sx} = 0.31 \text{ mm}^2/\text{mm}$$

$$A_{sy} = 0.31 \text{ mm}^2/\text{mm}$$

Fig.8.10 Simple supported slab with 1% central opening

Table 8.3

Experimental Deflections of Slab with 1% Central opening

Load (kN)	Deflections (mm)			
	Node No.7	Node No.14	Node No.21	Node No.28
0	0.00	0.00	0.00	0.00
20	0.18	0.14	0.08	0.03
40	0.36	0.28	0.17	0.06
60	0.51	0.45	0.24	0.09
80	0.67	0.58	0.33	0.12
100	0.96	0.81	0.45	0.15
120	1.35	1.21	0.68	0.22
140	2.01	1.67	0.95	0.31
160	2.98	2.41	1.41	0.41
180	4.01	3.23	1.91	0.57
200	5.26	4.25	2.41	0.75
220	6.43	5.22	3.01	0.94
240	7.65	6.21	3.55	1.11
260	8.86	7.32	4.07	1.26
280	9.96	8.31	4.59	1.38

Table 8.4

Salient Results of Investigation

Method of analysis	Load value of initial crack (kN)	Load value of initial yielding of steel (kN)	Ultimate load (kN)
1	70	110	210
2	70	110	210
3	70	150	270
4	70	150	280
5	70	150	280
Exp.	70	150	280

First two methods of analysis predicted the ultimate load as 75% of experimental value. The numerical deflection value were found large, i.e. ranging from 83.6% to 102.5% of recorded values at this predicted ultimate load. The tension softening phenomenon which increases the slab stiffness, predicted the deflection values in the range of 21.89% to 24.9% for node numbers 7 to 28 at 270 kN load. Also it predicted the ultimate load very close to the actual experimental value, i.e., 96.43% of recorded value. The bond effect further reduced the difference in deflection values. The deflections found 1.38% to 3.63% times less than the observed values at pre-selected points of dial gauges. It is clearly observed that the bond effect is over estimating the slab stiffness. The aggregate interlock estimating the values 0.4% to 3.26% less than the recorded deflection values. Fig. 8.11 to 8.14

Table 8.4

Salient Results of Investigation

Method of analysis	Load value of initial crack (kN)	Load value of initial yielding of steel (kN)	Ultimate load (kN)
1	70	110	210
2	70	110	210
3	70	150	270
4	70	150	280
5	70	150	280
Exp.	70	150	280

First two methods of analysis predicted the ultimate load as 75% of experimental value. The numerical deflection value were found large, i.e. ranging from 83.6% to 102.5% of recorded values at this predicted ultimate load. The tension softening phenomenon which increases the slab stiffness, predicted the deflection values in the range of 21.89% to 24.9% for node numbers 7 to 28 at 270 kN load. Also it predicted the ultimate load very close to the actual experimental value, i.e., 96.43% of recorded value. The bond effect further reduced the difference in deflection values. The deflections found 1.38% to 3.63% times less than the observed values at pre-selected points of dial gauges. It is clearly observed that the bond effect is over estimating the slab stiffness. The aggregate interlock estimating the values 0.4% to 3.26% less than the recorded deflection values. Fig. 8.11 to 8.14

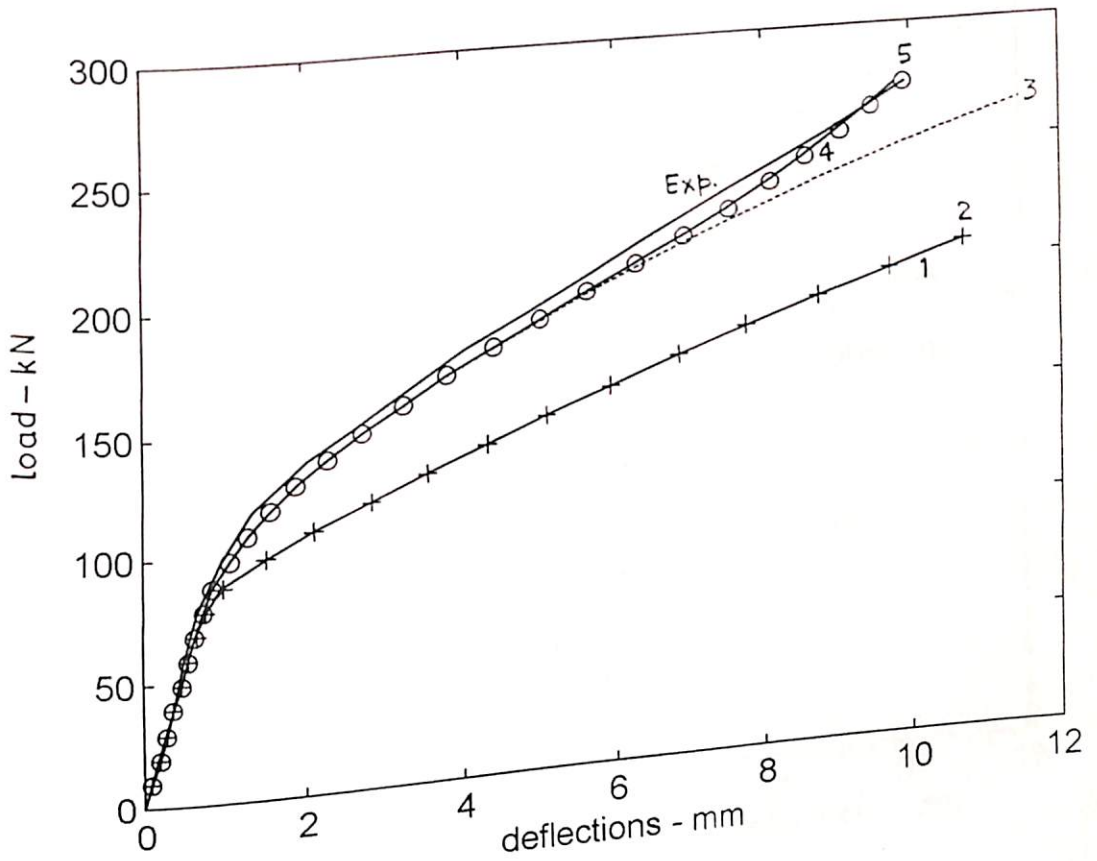


Fig. 8.11 LOAD-DEFLECTION CURVES AT NODE 7 OF SLAB WITH 1% CENTRAL OPENING

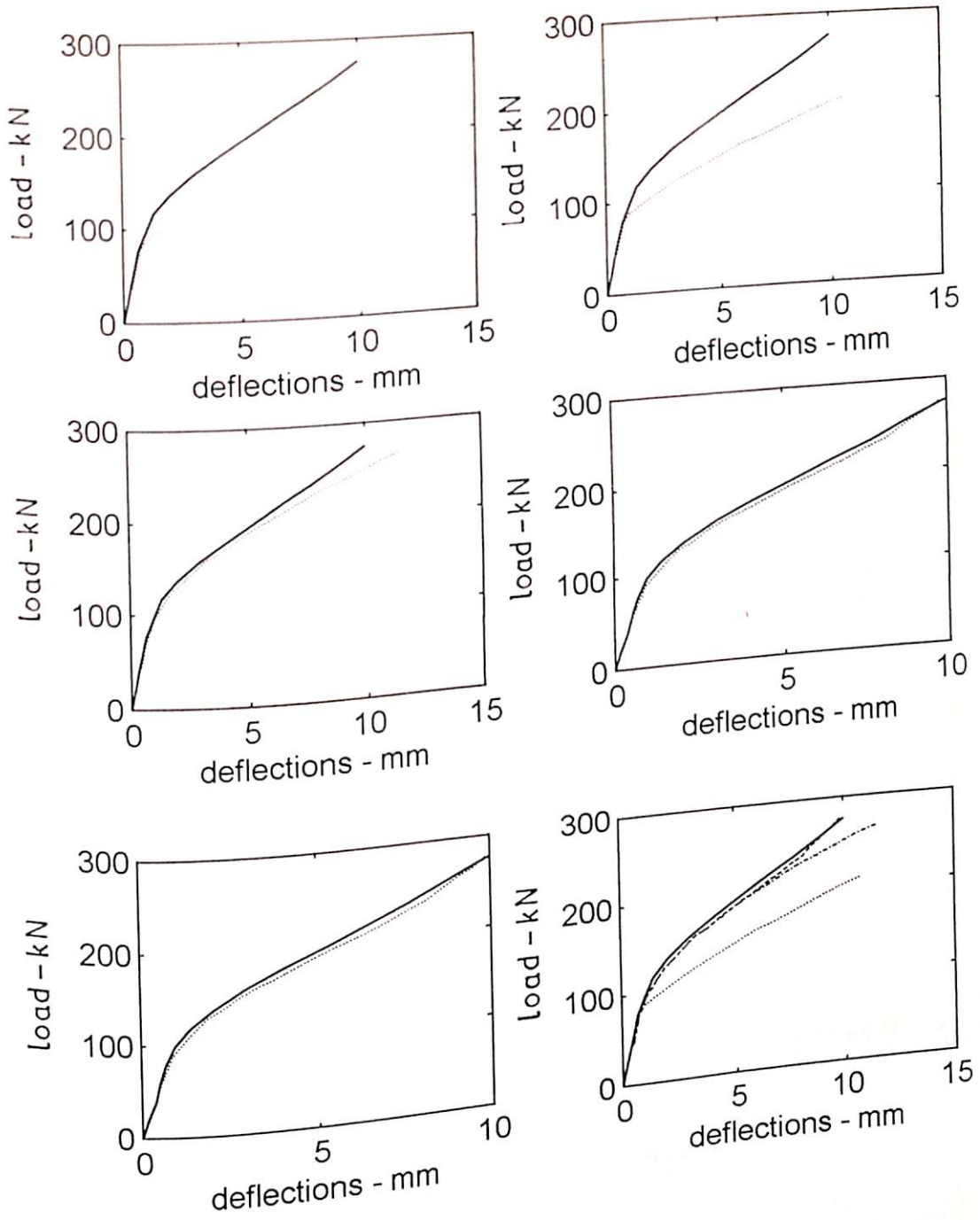


Fig. 8.11.1 LOAD-DEFLECTION CURVES AT NODE 7 OF SLAB WITH DIFFERENT METHODS OF ANALYSIS

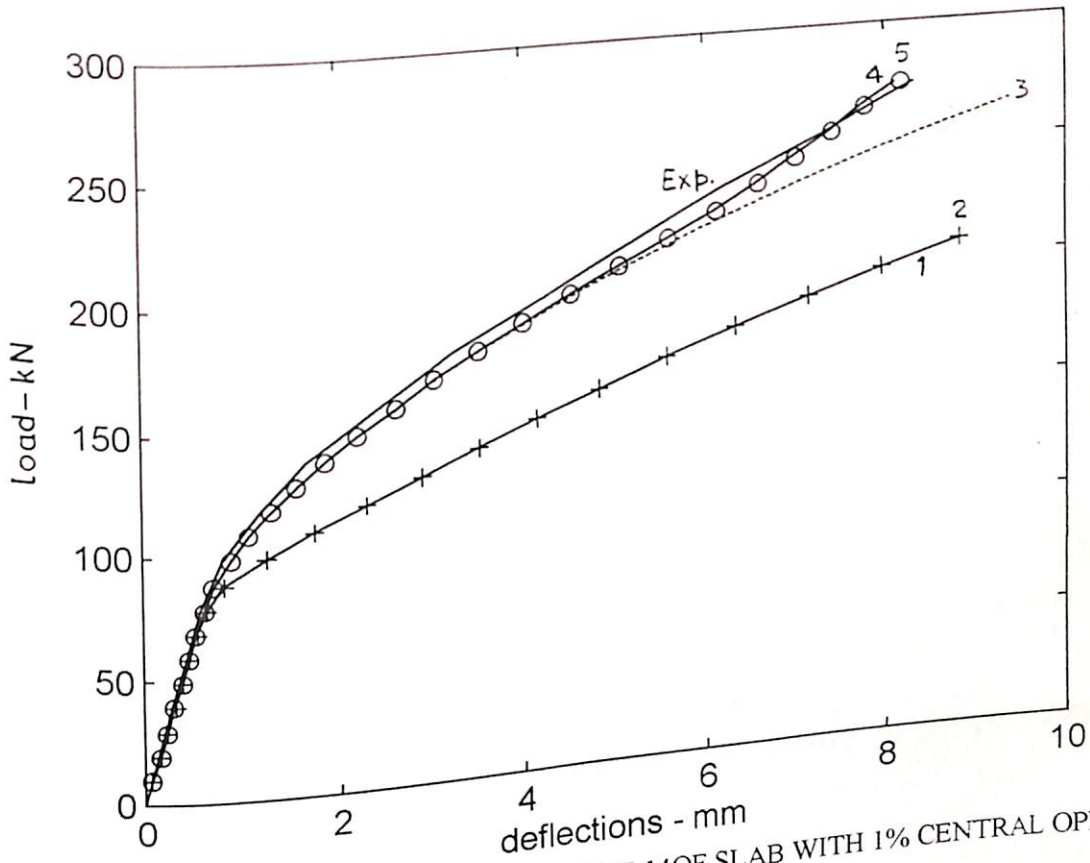


Fig. 8.12 LOAD-DEFLECTION CURVES AT NODE 14 OF SLAB WITH 1% CENTRAL OPENING

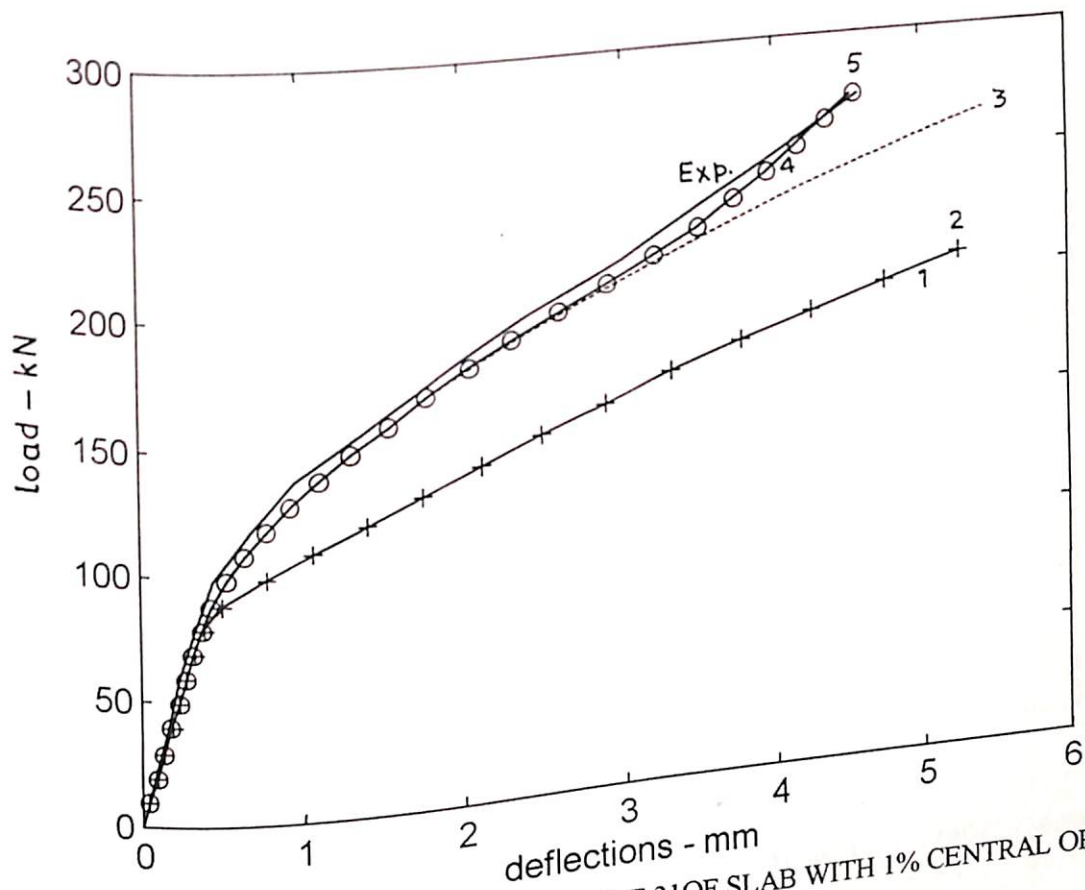


Fig. 8.13 LOAD-DEFLECTION CURVES AT NODE 21 OF SLAB WITH 1% CENTRAL OPENING

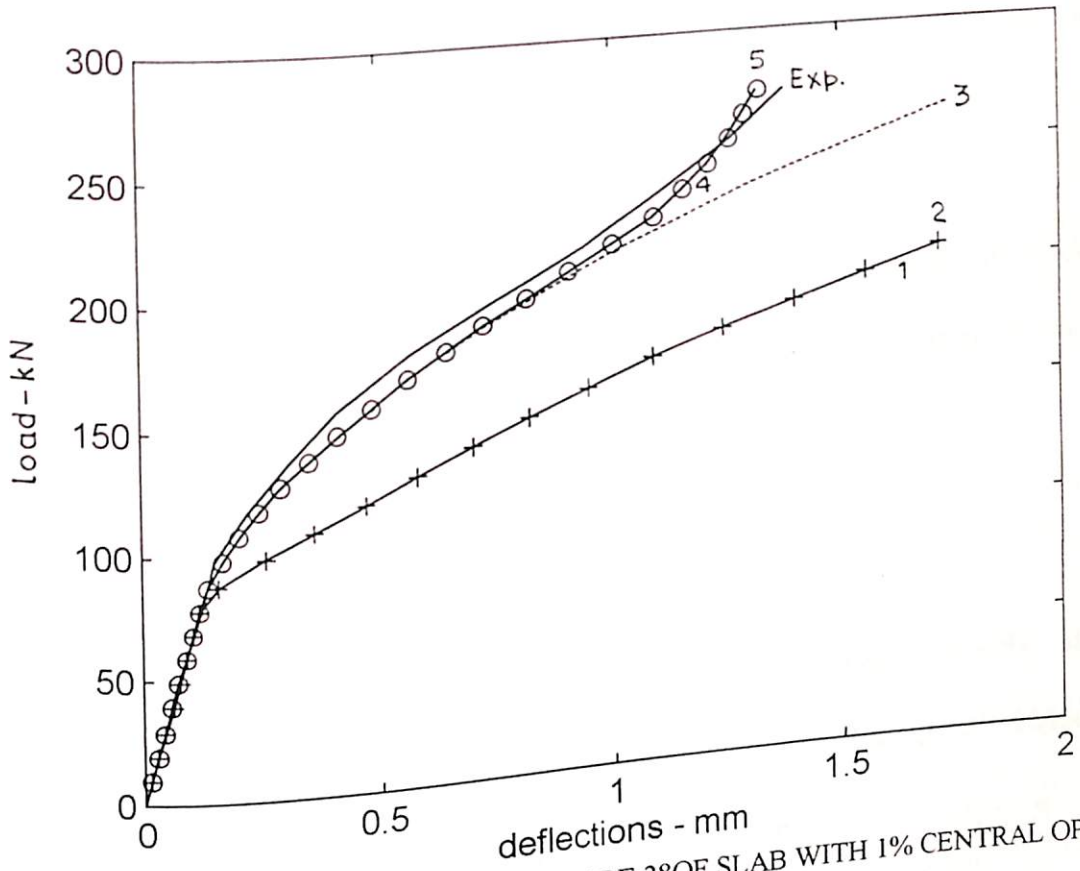


Fig. 8.14 LOAD-DEFLECTION CURVES AT NODE 28 OF SLAB WITH 1% CENTRAL OPENING

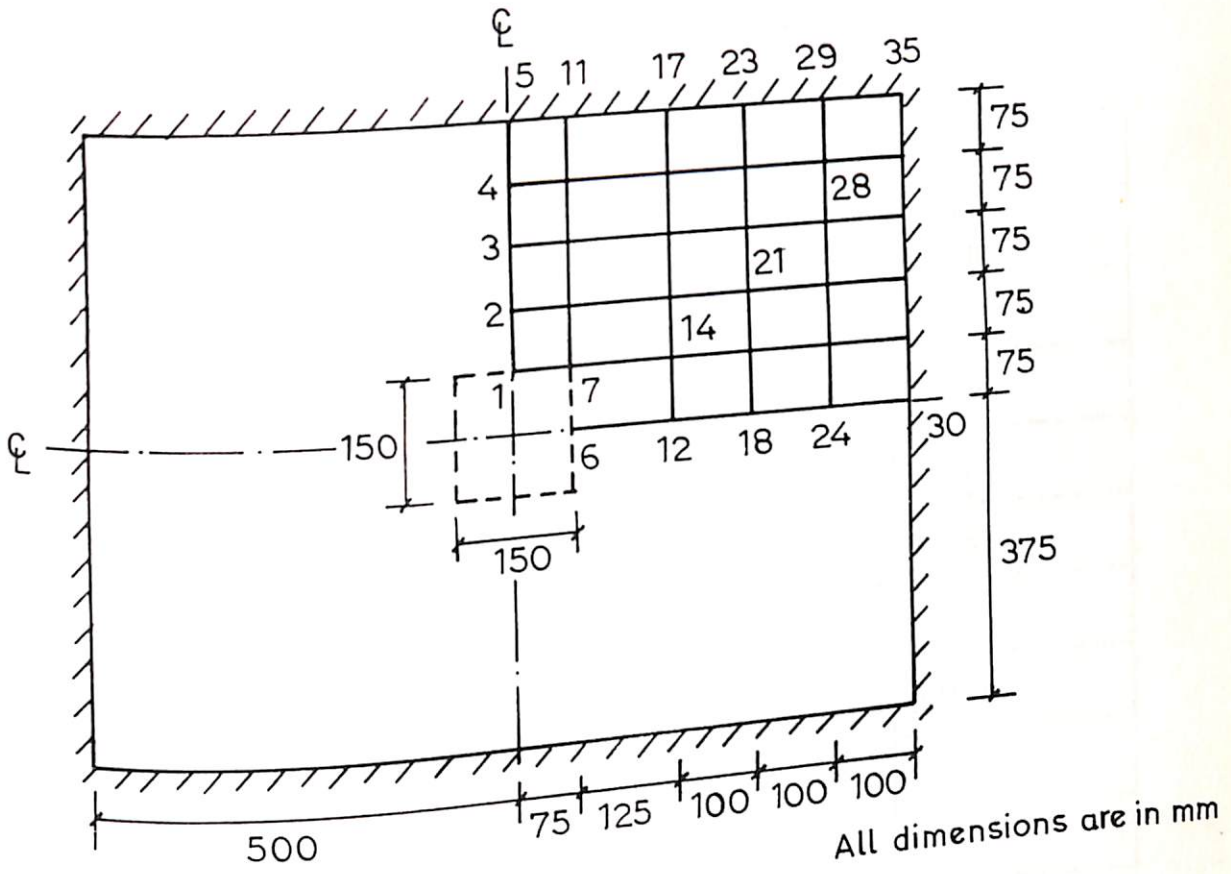
shows the comparison between experimental and analytical load deflection curves. The maximum difference of 8.97% to 19.69% was found between aggregate interlock values of deflections and experimental values of deflections for selected points at 280 kN. Fig. 8.10 1 shows the effect of each model incorporated in the analysis for node 7 of slab model.

The analytical load deflection curves of bond and aggregate interlock are crossing the experimental load deflection curves due to overestimation of the slab stiffness.

Slab 3:

A simple supported rectangular slab with 3% central opening of size 150mm x 150mm tested under uniformly distributed load is investigated. The slab is modeled as shown in Fig. 8.15 with 5x5 finite element mesh.

The recorded experimental initial values of cracked and yielding of steel reinforcement were 60 kN and 140 kN respectively. The slab crushed when the load has reached 270 kN. The initial cracking of concrete and initial yielding of steel reinforcement were observed as 22.22% and 51.85% of ultimate load of slab. The dial gauge points along the predicted yield lines are node numbers 7, 14, 21 and 28 of Fig. 8.15. The deflection values of these points are given in Table 8.5.



$$f_c = 15.91 \text{ N/mm}^2$$

$$E_c = 0.189 \times 10^5 \text{ N/mm}^2$$

$$E_s = 2.5 \times 10^5 \text{ N/mm}^2$$

$$f_{sy} = 495.15 \text{ N/mm}^2$$

$$h = 160 \text{ mm}$$

$$d = 40 \text{ mm}$$

$$\nu = 0.15$$

$$A_{sx} = 0.31 \text{ mm}^2/\text{mm}$$

$$A_{sy} = 0.31 \text{ mm}^2/\text{mm}$$

Fig.8.15 Simple supported slab with 3% central opening

Table 8.5
Experimental Deflections of Slab with 3% Central opening

Load (kN)	Deflections (mm)			
	Node No.7	Node No.14	Node No.21	Node No.28
0	0.00	0.00	0.00	0.00
20	0.21	0.13	0.07	0.018
40	0.39	0.28	0.14	0.036
60	0.59	0.41	0.22	0.068
80	0.85	0.59	0.33	0.09
100	1.21	0.91	0.51	0.15
120	1.75	1.31	0.74	0.21
140	2.55	1.85	1.04	0.24
160	3.64	2.42	1.38	0.39
180	4.85	3.18	1.78	0.52
200	5.99	4.01	2.22	0.66
220	7.01	4.65	2.62	0.78
240	8.29	5.44	2.92	0.87
260	9.23	6.35	3.36	0.98
270	9.64	6.72	3.57	1.03

The predicted load values of initial cracking of concrete, yielding of steel reinforcement and crushing of concrete by proposed analysis are presented in

Table 8.6

Salient Results of Investigation

Method of analysis	Load value of initial crack (kN)	Load value of initial yielding of steel (kN)	Ultimate load (kN)
1	60	100	200
2	60	100	200
3	60	140	250
4	60	140	270
5	60	140	270
Exp.	60	140	270

It is observed that the first two methods of analysis predicted the yielding of steel and crushing of concrete as 71.43% and 74.07% of actual values of experimental investigation. The deflection values are in the range of 97.5% to 112.5% more than the recorded values of deflections at 200 kN. The tension-softening phenomenon of proposed analysis predicted the ultimate load 96% of experimental value. The difference in deflections ranged from 31.13% to 41% for node points 7 and 28 at 250 kN load. Tension-stiffening effect of bond model calculated the deflection values 2.43% and 8.22% less than the measured deflections at node points 7 and 28 respectively.

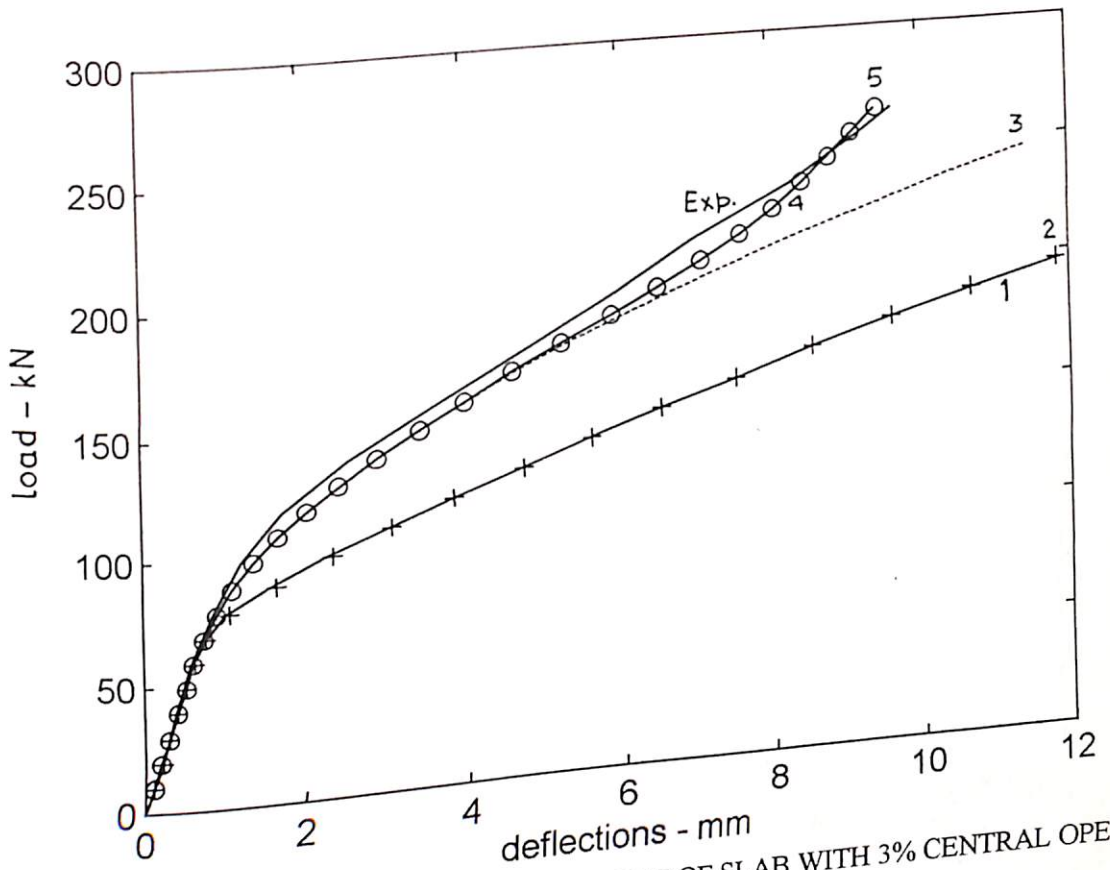


Fig. 8.16 LOAD-DEFLECTION CURVES AT NODE 7 OF SLAB WITH 3% CENTRAL OPENING

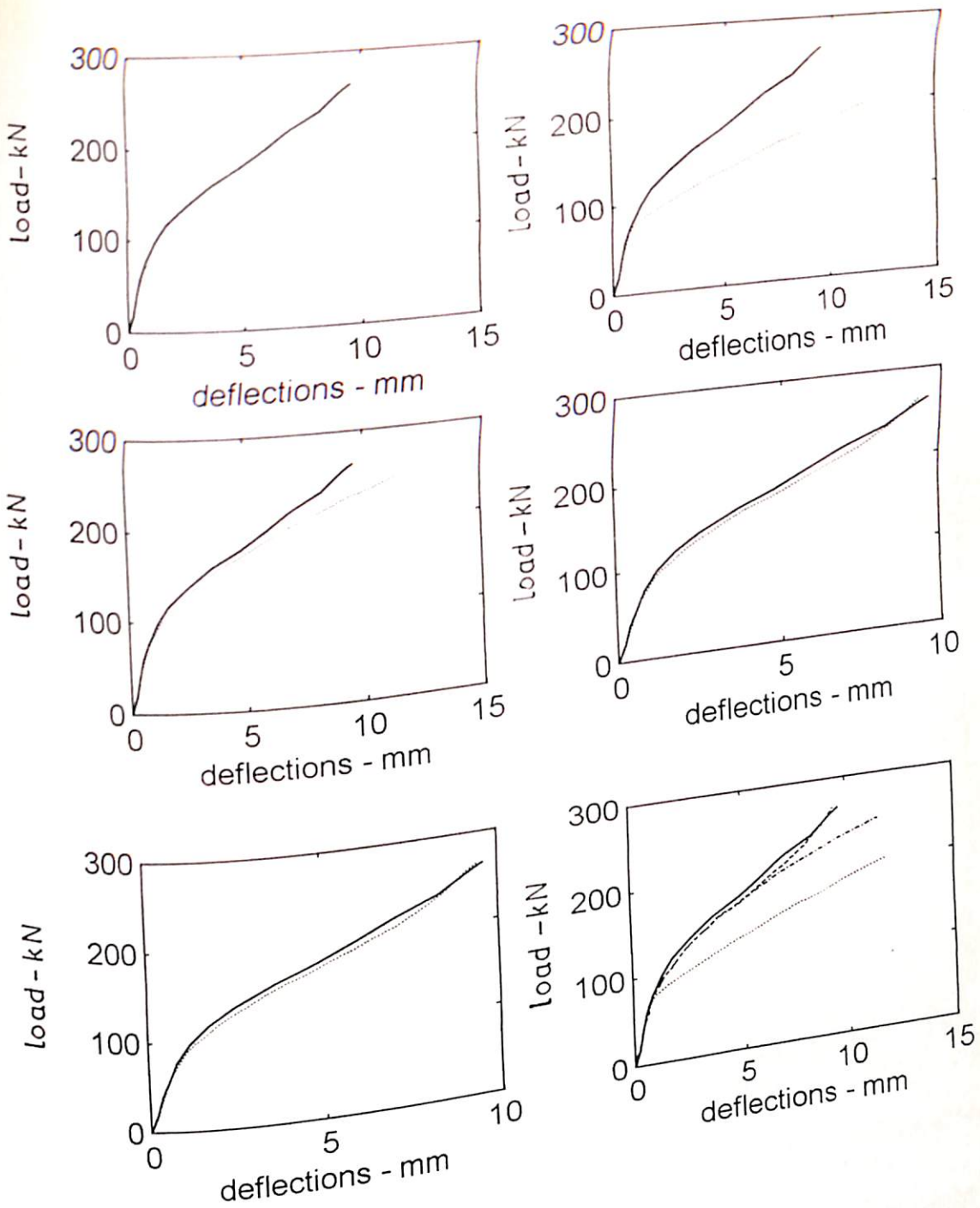


Fig. 8.16.1 LOAD-DEFLECTION CURVES AT NODE 7 OF SLAB WITH DIFFERENT METHODS OF ANALYSIS

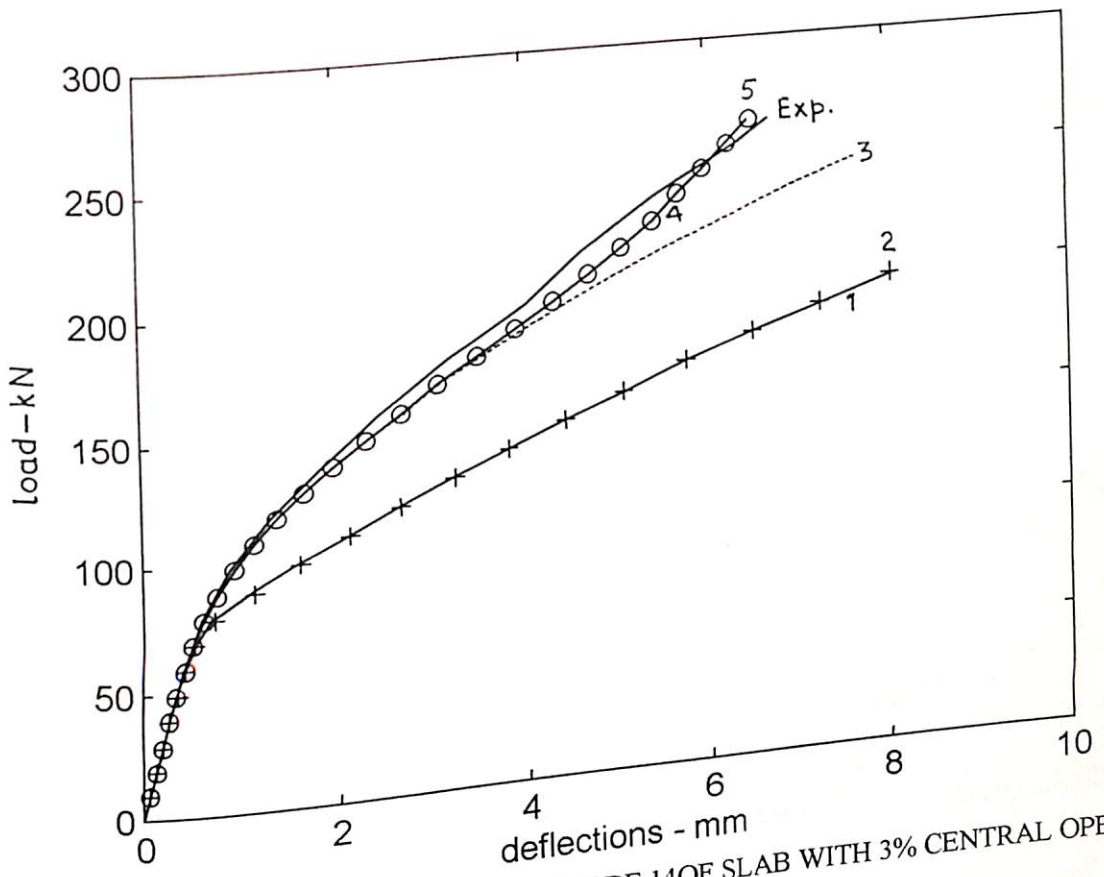


Fig. 8.17 LOAD-DEFLECTION CURVES AT NODE 14 OF SLAB WITH 3% CENTRAL OPENING

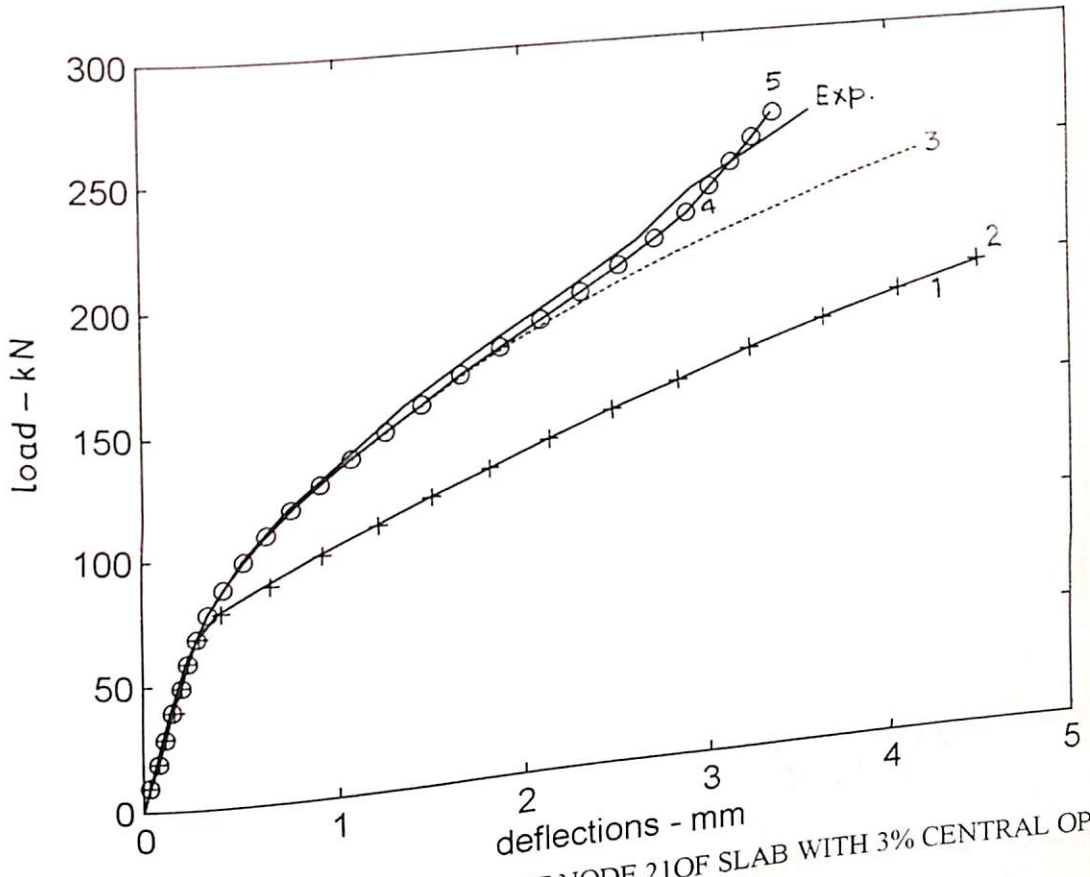


Fig. 8.18 LOAD-DEFLECTION CURVES AT NODE 21 OF SLAB WITH 3% CENTRAL OPENING

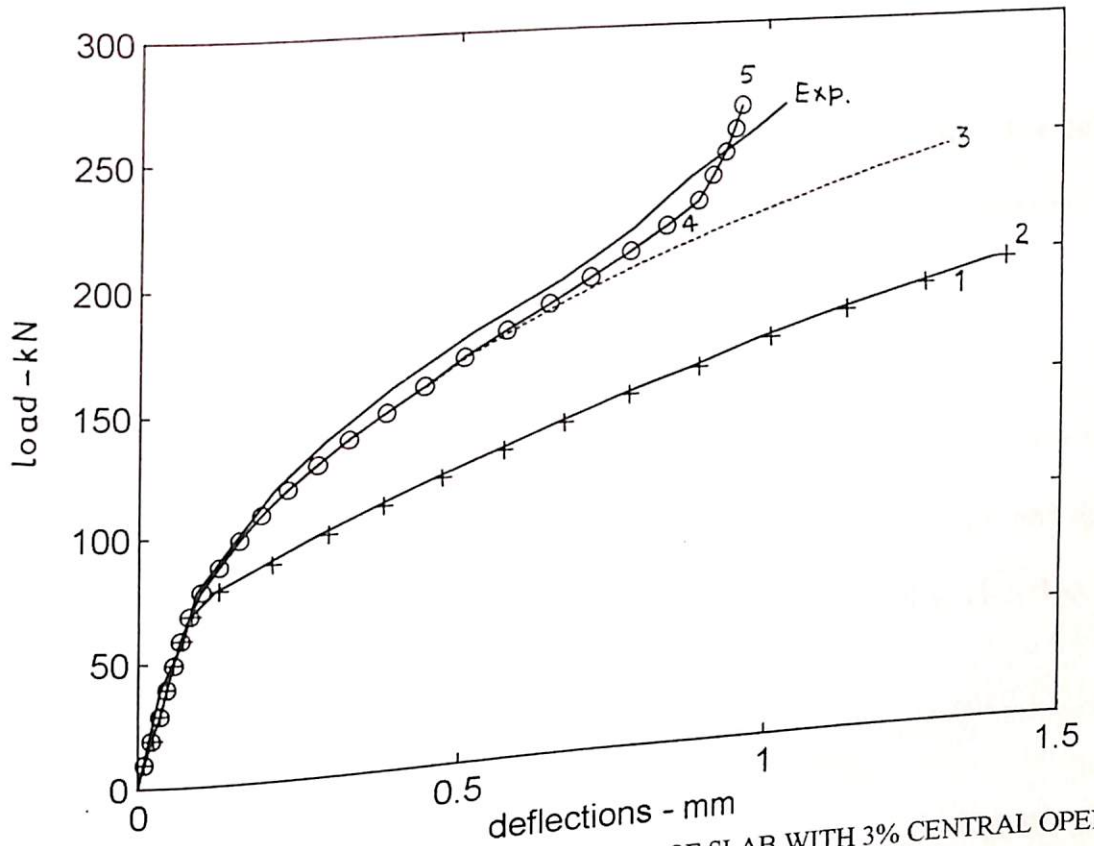


Fig. 8.19 LOAD-DEFLECTION CURVES AT NODE 28 OF SLAB WITH 3% CENTRAL OPENING

Aggregate interlock model predicted these values 2.17% and 8.07% less than the experimental values. Load-deflection curves of 8.16 to 8.19 compares the experimental and analytical investigation of the slab.

Slab 4

A simple supported rectangular slab with central opening of size 250mm x 150mm is studied for both experimental and analytical investigations. The finite element mesh used for the analysis is 5x5 mesh of different size of elements as shown in Fig. 8.20.

Load deflection values of nodes 7, 14, 21 and 28 are presented in Table 8.7. The salient values of proposed analysis are given in Table 8.8. Fig. 8.21 and 8.24 clearly shows the comparison between experimental and analytical load-deflection curves.

The load values of initial cracks in concrete and initial yielding of steel reinforcement were experimentally observed as 50 kN and 130 kN respectively. The slab crushed at load value of 250 kN. The cracking of concrete occurred at 20% of ultimate load. Initial yielding of steel observed at about 52% of ultimate load.

Table 8.7

Experimental Deflection of Slab with 5% central opening

Load (kN)	Deflections (mm)			
	Node No.7	Node No.14	Node No.21	Node No.28
0	0.00	0.00	0.00	0.00
20	0.19	0.13	0.07	0.02
40	0.38	0.26	0.15	0.05
60	0.57	0.39	0.22	0.07
80	0.84	0.61	0.34	0.092
100	1.25	0.98	0.51	0.16
120	1.87	1.41	0.79	0.23
140	2.71	1.92	1.07	0.33
160	3.73	2.62	1.45	0.45
180	4.84	3.28	1.84	0.56
200	5.94	4.04	2.24	0.67
220	6.96	4.95	2.65	0.79
240	8.14	5.84	3.18	0.92
250	8.87	6.27	3.41	0.99

Table: 8.8

Salient results of Investigation

Method of analysis	Load value of initial crack (kN)	Load value of initial yielding of steel (kN)	Ultimate load (kN)
1	50	100	190
2	50	100	190
3	50	130	240
4	50	130	250
5	50	130	250
Exp.	50	130	250

The simple nonlinear analysis of proposed method calculated the deflection values 102% to 123% more than the recorded values of node 7 and 28 at 190 kN load. The second method of analysis predicted these values 101.7% to 122.5% more than the experimental values of node 7 and 28 at 190 kN load. Third method of analysis gave 26.8% to 33.86% more than the measured deflections at 240 kN load. The fourth method of analysis predicted deflection values at ultimate load as 7.79% to 6.49% less than the actual measured values at 250 kN load. The method of analysis with aggregate interlock resulted in 8.87% to 6.46% less than the actual deflection values at ultimate load.

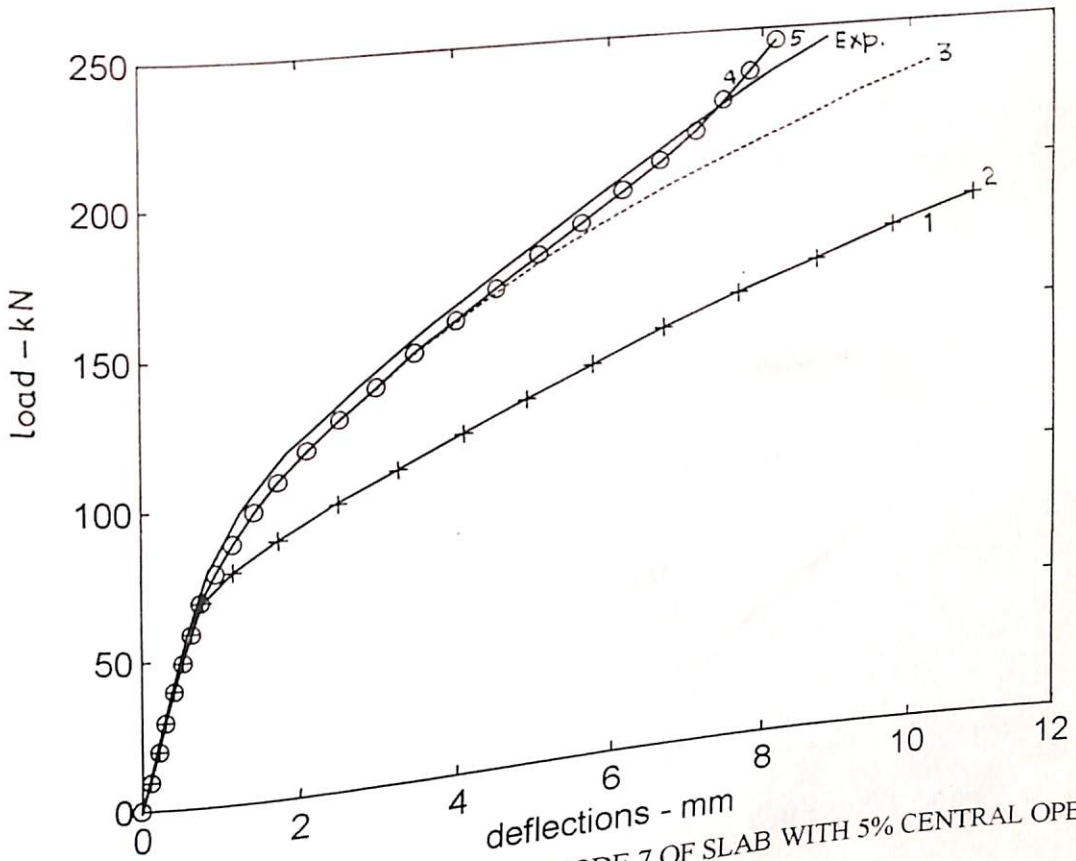


Fig. 8.21 LOAD-DEFLECTION CURVES AT NODE 7 OF SLAB WITH 5% CENTRAL OPENING

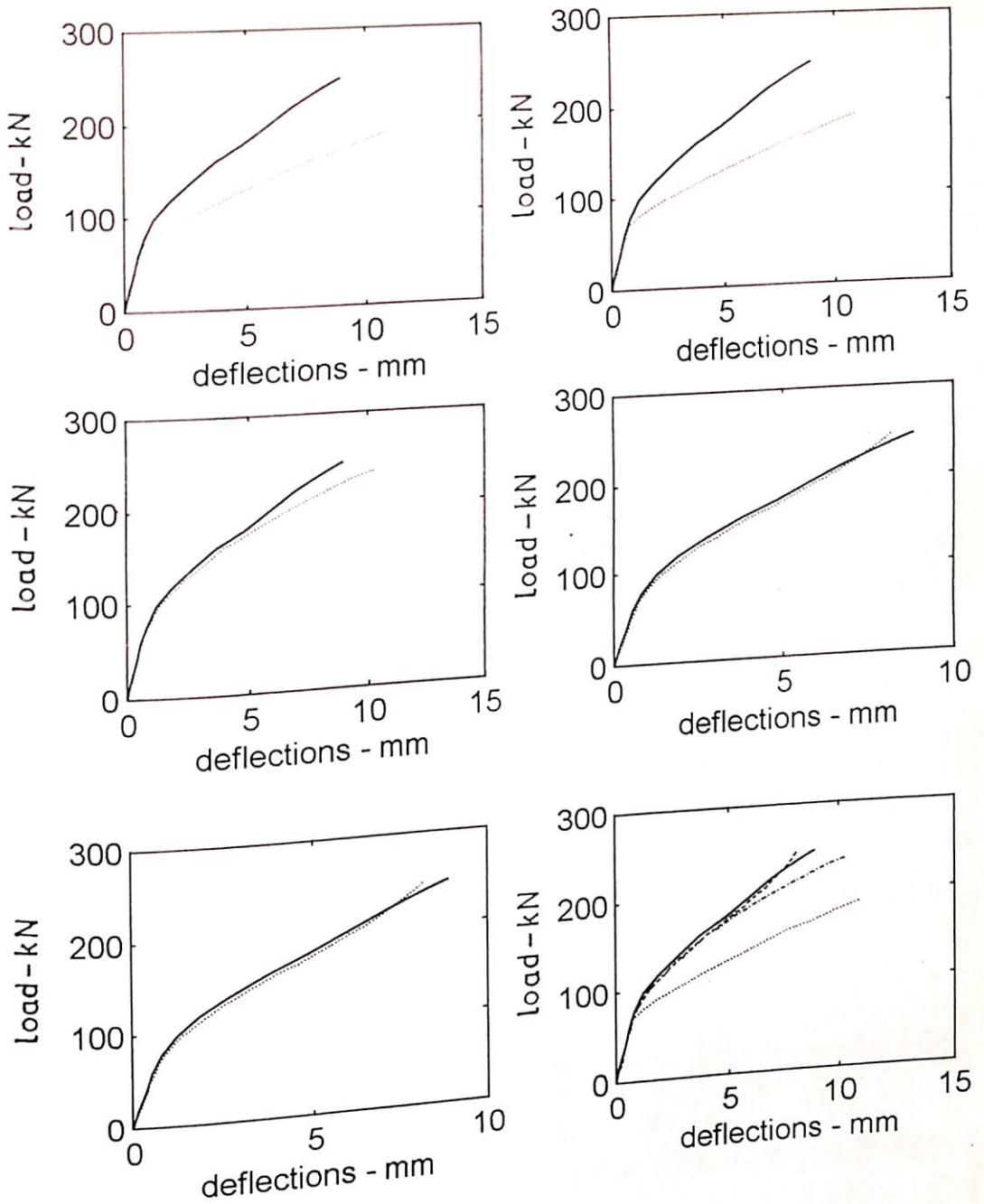


Fig. 8.21.1 LOAD-DEFLECTION CURVES AT NODE 7 OF SLAB WITH DIFFERENT METHODS OF ANALYSIS

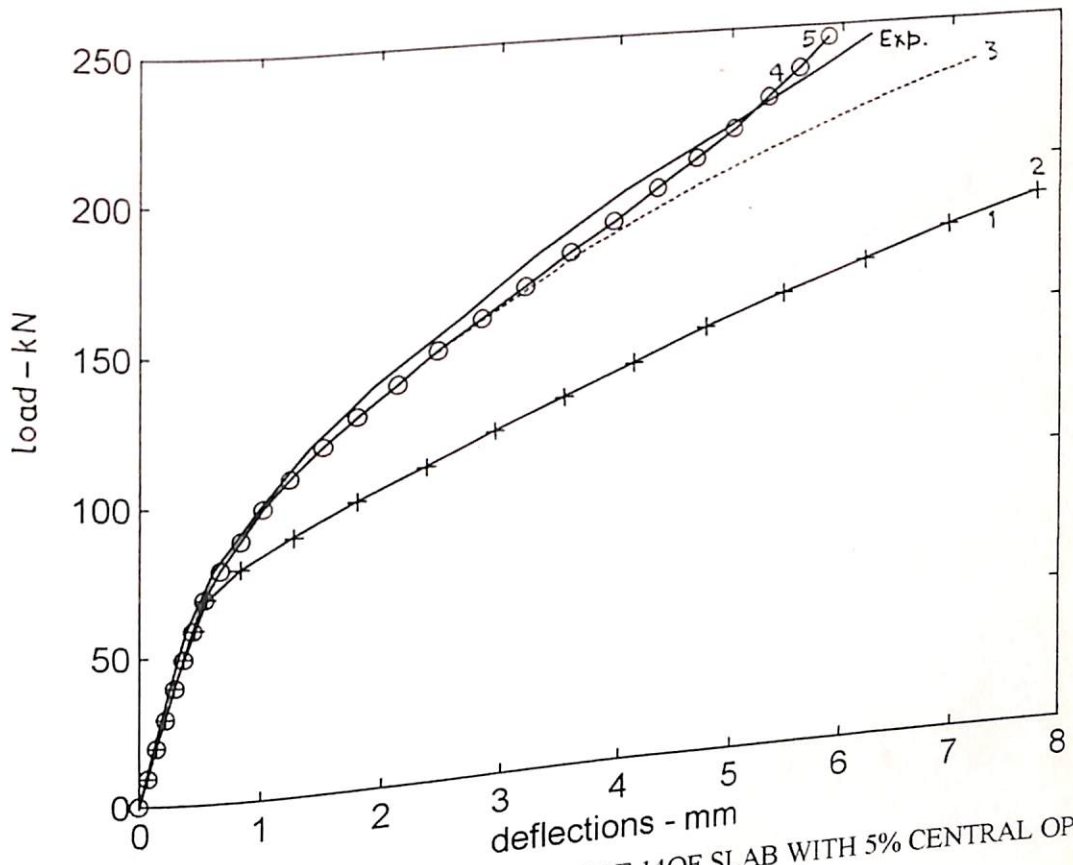


Fig. 8.22 LOAD-DEFLECTION CURVES AT NODE 14 OF SLAB WITH 5% CENTRAL OPENING

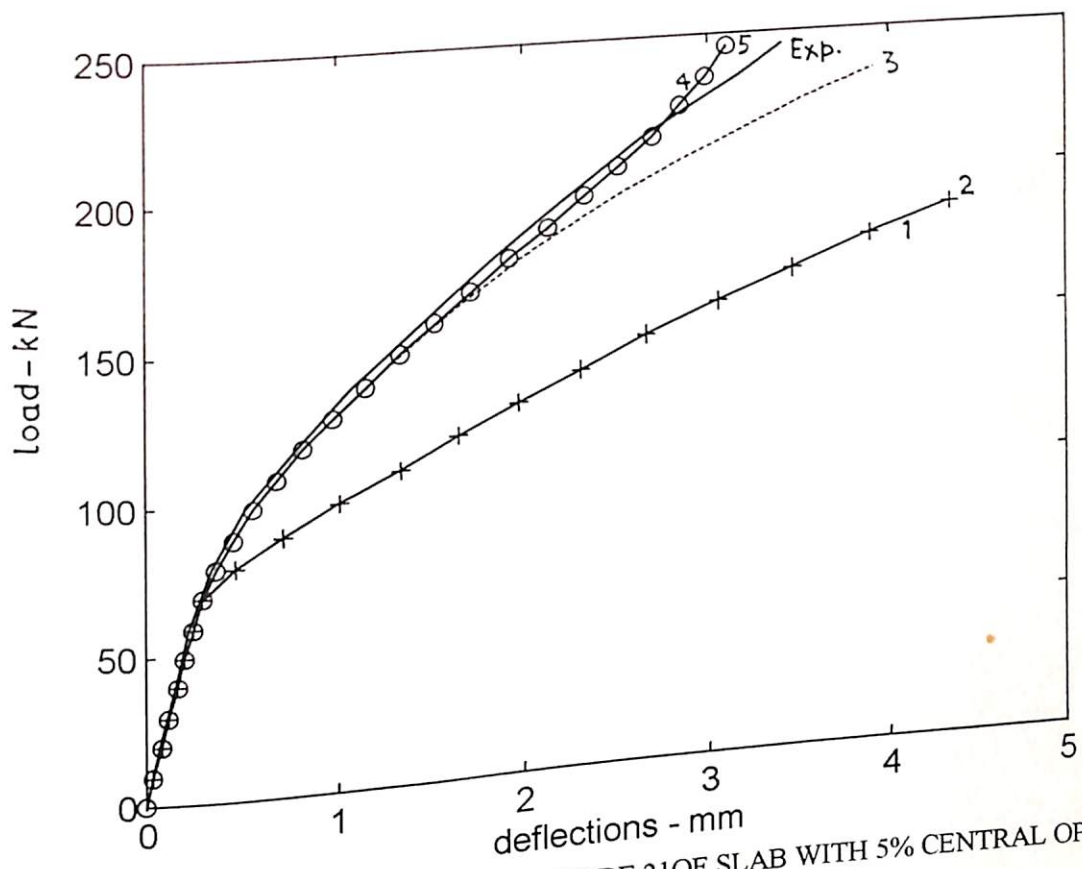


Fig. 8.23 LOAD-DEFLECTION CURVES AT NODE 21 OF SLAB WITH 5% CENTRAL OPENING

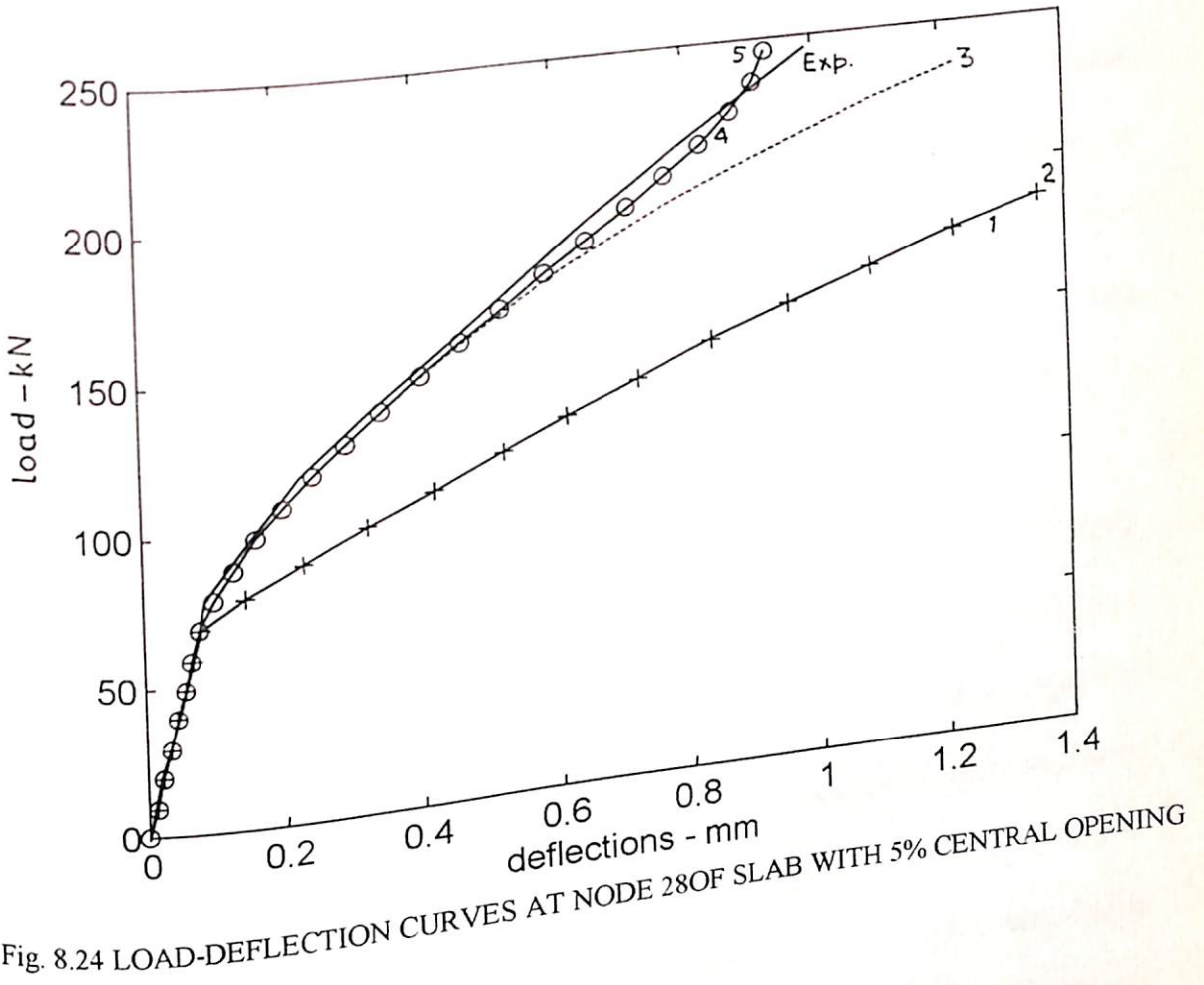


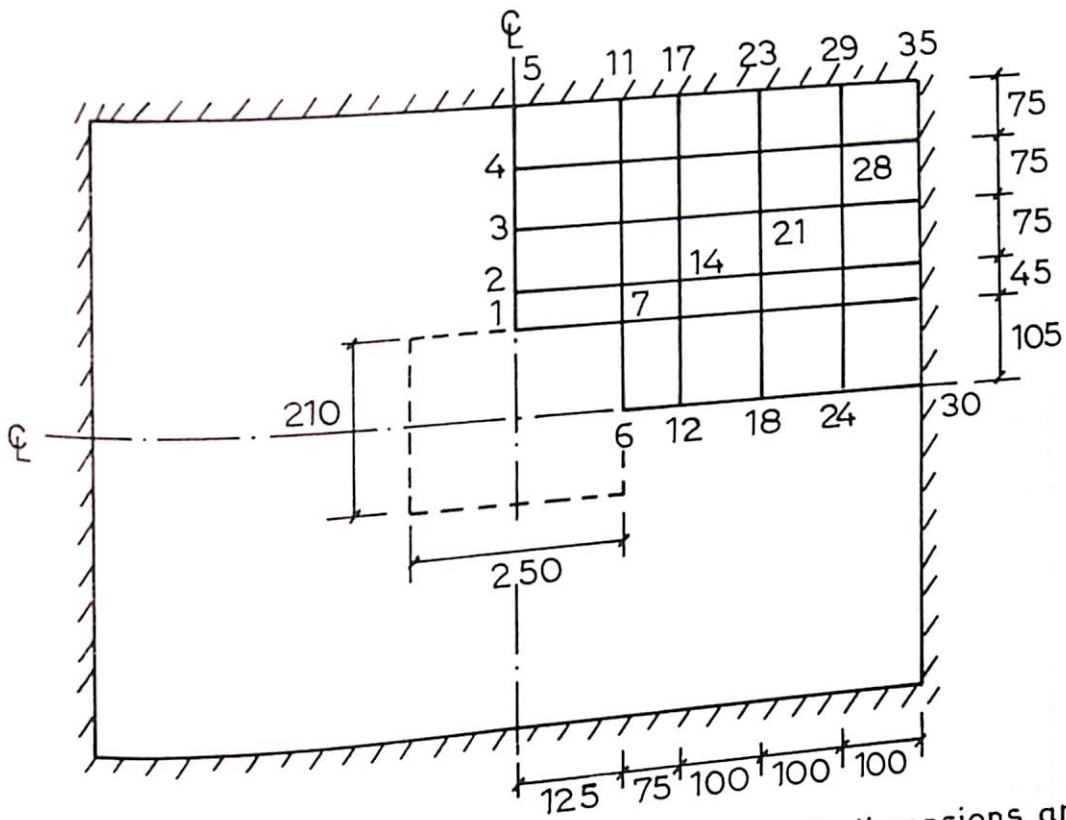
Fig. 8.24 LOAD-DEFLECTION CURVES AT NODE 28 OF SLAB WITH 5% CENTRAL OPENING

Slab 5:

A simple supported two-way slab with 7% central opening of size 250mm x 210mm is studied when subjected to uniformly distributed load. The slab is modeled for finite element analysis as shown in Fig. 8.25.

The initial load values of cracking of concrete and initial yielding of steel were observed as 50 kN and 120 kN respectively. The slab failed due to crushing at about 240 kN. Therefore, the concrete failed in tension at 20.83% of ultimate load and steel yielded initially at about 50% of ultimate load. The recorded load deflection values at node 7, 14, 21 and 28 of Fig. 8.25 are presented in Table 8.9.

The first method of analysis predicting the values 109.5% to 131% more than the recorded values of deflections at 160 kN load. By incorporating steel stiffness before cracking, these values are 108.8% to 124.2% more than the observed values at 160 kN load. The tension softening phenomenon which increases the slab stiffness predicting 25.48% to 30% increase in deflection values of node 7 to node 28 at 210 kN load. The bond effect predicting 3.07% to 7.72% decrease in deflection values of node 7 to node 28 at ultimate load. At ultimate load, aggregate interlock predicting these values 3.31% and 10.6% less than the recorded values at node 7 and node 28 respectively.



All dimensions are in mm

$$f'_c = 16.24 \text{ N/mm}^2$$

$$E_c = 0.19 \text{ N/mm}^2$$

$$E_s = 2.5 \times 10^5 \text{ N/mm}^2$$

$$f_{sy} = 495.15 \text{ N/mm}^2$$

$$h = 60 \text{ mm}$$

$$d = 40 \text{ mm}$$

$$\rho = 0.15$$

$$A_{sx} = 0.31 \text{ mm}^2/\text{mm}$$

$$A_{sy} = 0.31 \text{ mm}^2/\text{mm}$$

Fig.8.25 Simple supported slab with 7% central opening

Table 8.9
Experimental Deflections of Slab with 7% Central opening

Load (kN)	Deflections (mm)			
	Node No.7	Node No.14	Node No.21	Node No.28
0	0.00	0.00	0.00	0.00
20	0.22	0.16	0.08	0.02
40	0.44	0.32	0.16	0.04
60	0.66	0.39	0.25	0.07
80	1.06	0.84	0.43	0.12
100	1.63	1.28	0.65	0.21
120	2.48	1.89	0.95	0.31
140	3.44	2.63	1.32	0.41
160	4.42	3.49	1.73	0.54
180	5.72	4.38	2.21	0.68
200	6.82	5.11	2.73	0.85
220	7.85	6.01	3.23	0.96
240	8.75	6.78	3.69	1.09

The major results of proposed method of analysis are presented in Table 8.10. Fig. 8.26 to 8.29 compares the load deflection curves of recorded and calculated values.

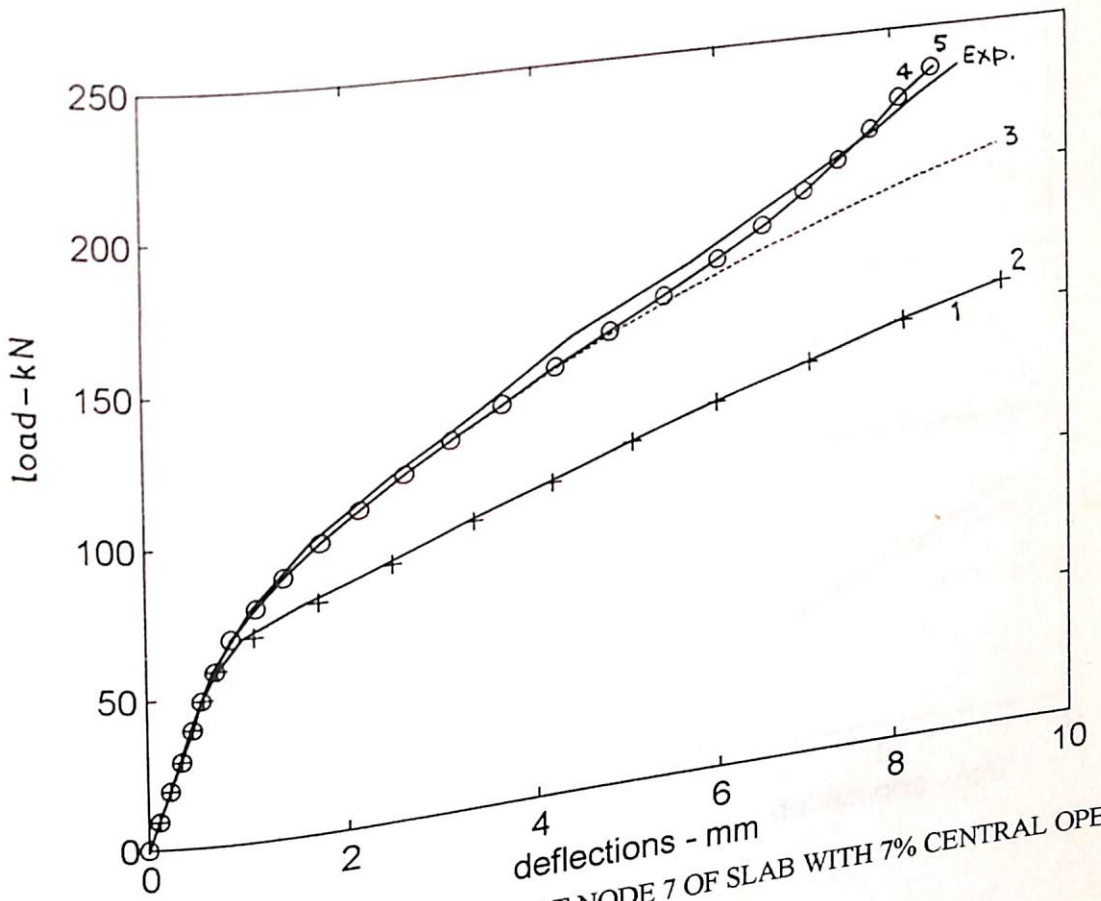


Fig. 8.26 LOAD-DEFLECTION CURVES AT NODE 7 OF SLAB WITH 7% CENTRAL OPENING

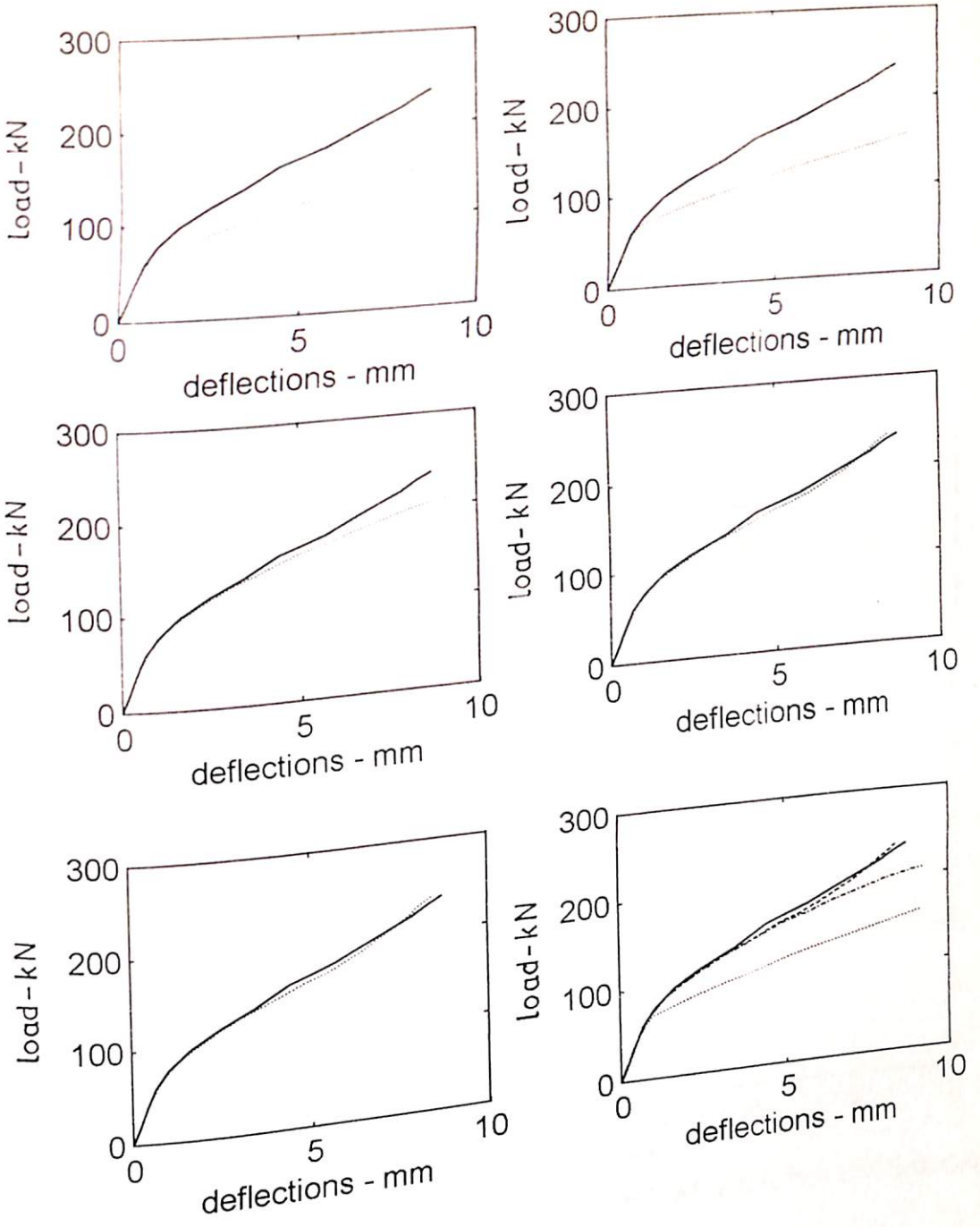


Fig. 8.26.1 LOAD-DEFLECTION CURVES AT NODE 7 OF SLAB WITH DIFFERENT METHODS OF ANALYSIS

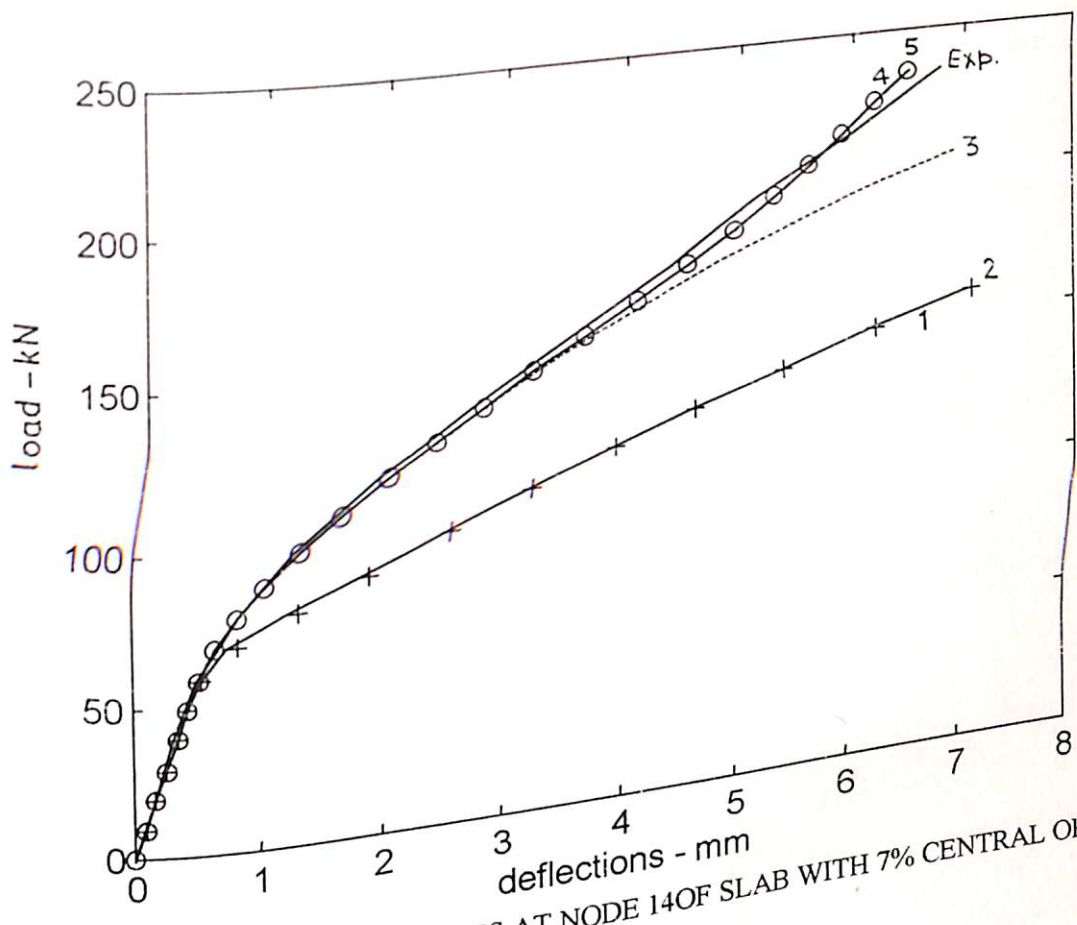


Fig. 8.27 LOAD-DEFLECTION CURVES AT NODE 14 OF SLAB WITH 7% CENTRAL OPENING

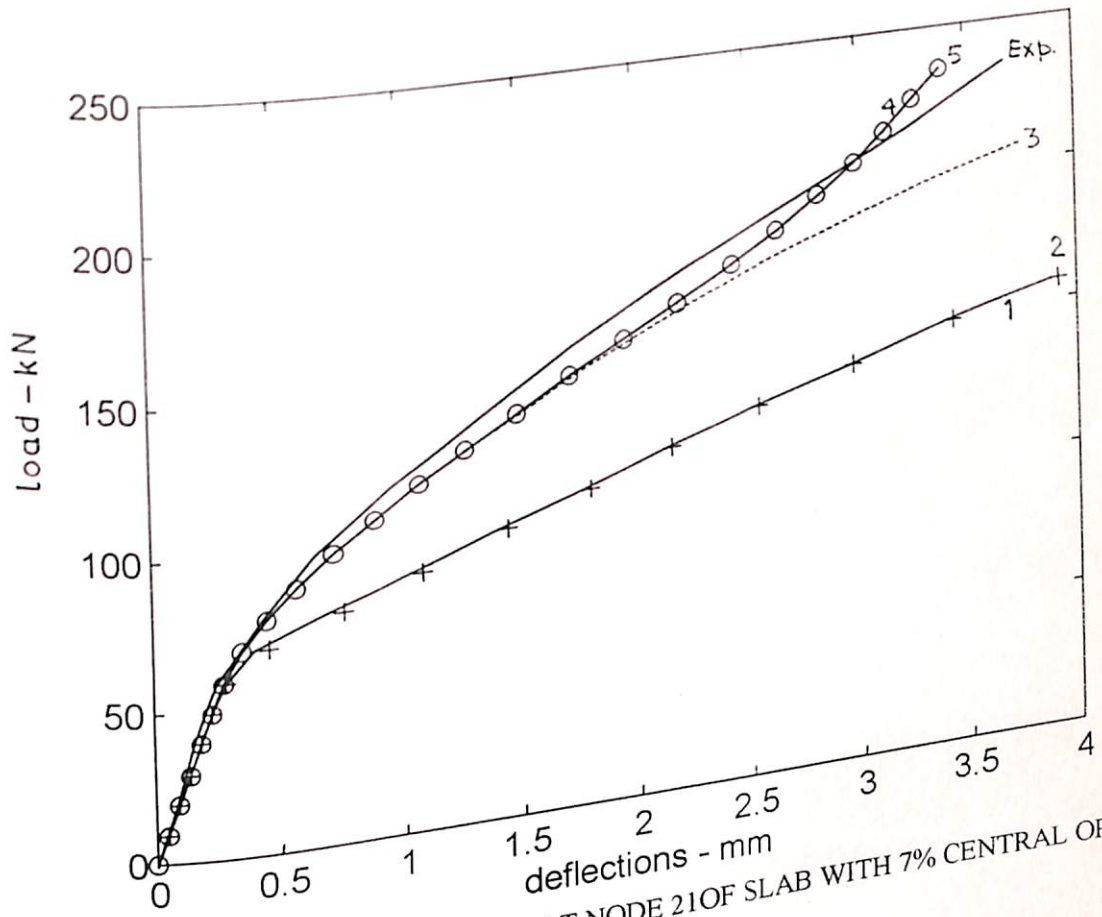


Fig. 8.28 LOAD-DEFLECTION CURVES AT NODE 21 OF SLAB WITH 7% CENTRAL OPENING

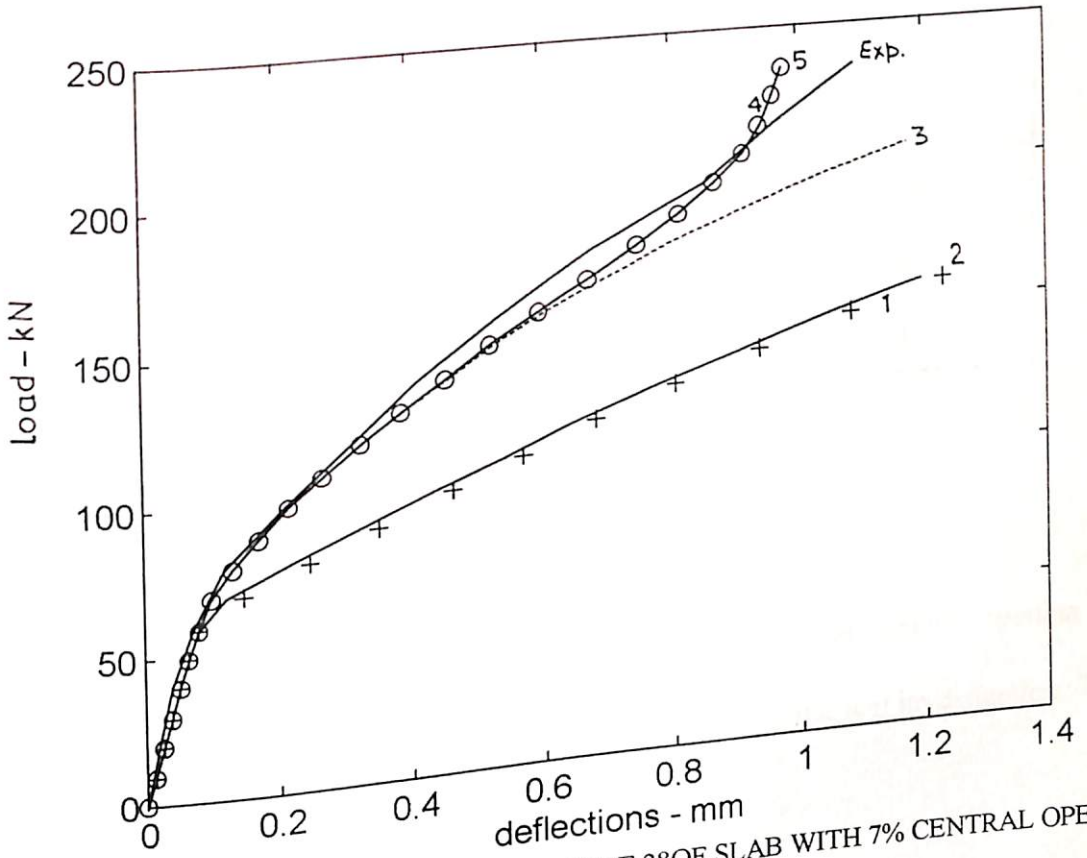


Fig. 8.29 LOAD-DEFLECTION CURVES AT NODE 28 OF SLAB WITH 7% CENTRAL OPENING

Table 8.10

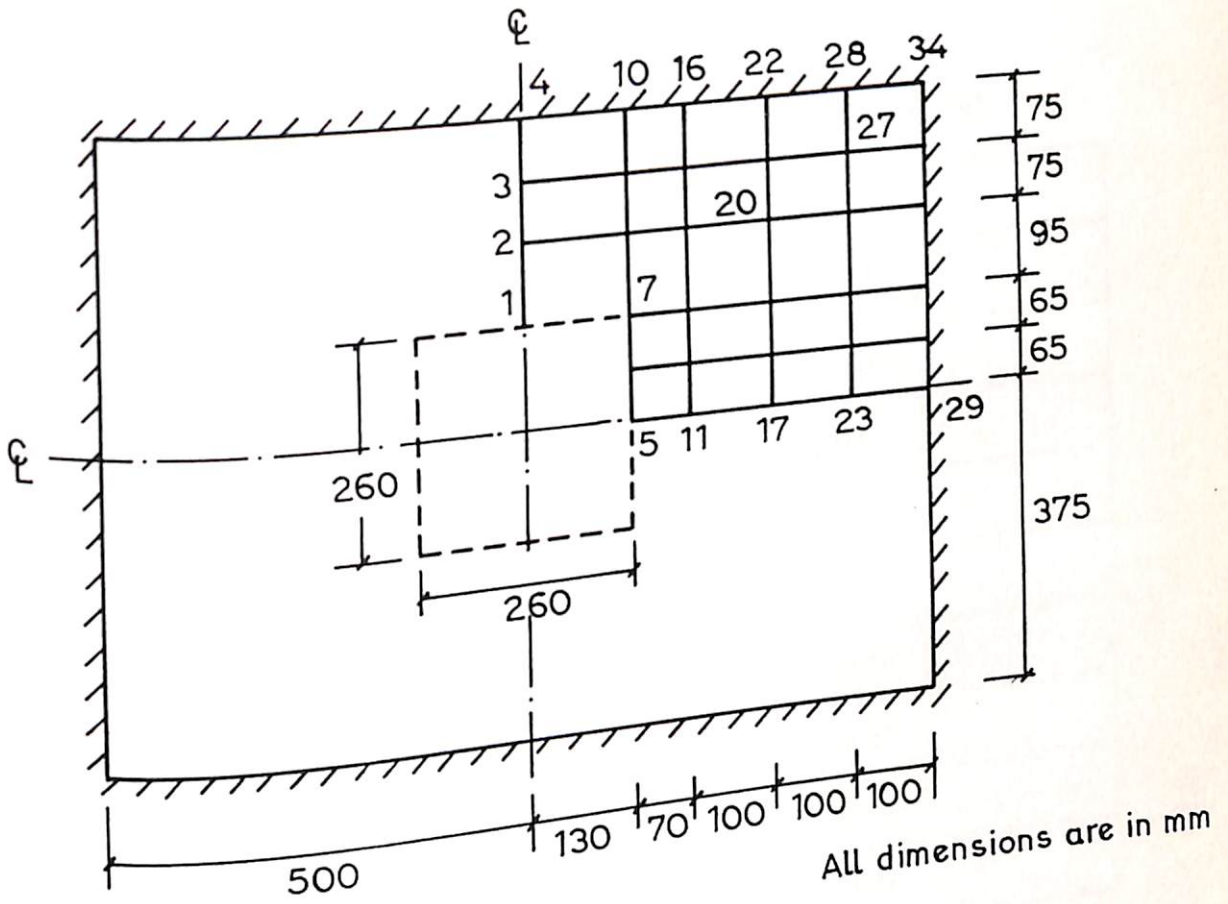
Salient Results of Investigation

Method of analysis	Load value of initial crack (kN)	Load value of initial yielding of steel (kN)	Ultimate load (kN)
1	50	90	160
2	50	90	160
3	50	120	210
4	50	120	240
5	50	120	240
Exp.	50	120	240

Slab 6:

Simple supported rectangular slab with 9% central square opening of 260mm x 260mm is analysed for both experimental and numerical investigation. The slab is modeled as shown in Fig. 8.30.

Initial cracks were observed at load value of 50 kN and initial yielding of steel reinforcement at 110 kN load. The slab failed due to crushing at about 220 kN load. Therefore, the slab failed in tension at 21.72% of ultimate load and steel initially yielded at 50% of ultimate load.



$$f'_c = 16.45 \text{ N/mm}^2$$

$$E_c = 0.192 \times 10^5 \text{ N/mm}^2$$

$$E_s = 2.5 \times 10^5 \text{ N/mm}^2$$

$$f_{sy} = 495.15 \text{ N/mm}^2$$

$$h = 60 \text{ mm}$$

$$d = 40 \text{ mm}$$

$$\nu = 0.15$$

$$A_{sx} = 0.31 \text{ mm}^2/\text{mm}$$

$$A_{sy} = 0.31 \text{ mm}^2/\text{mm}$$

Fig.8.30 Simple supported slab with 9% central opening

The measured dial gauge readings of node number 7, 20 and 27 of Fig. 8.30 are presented in Table 8.11.

Table 8.11
Experimental Deflections of Slab with 9% Central opening

Load (kN)	Deflections (mm)		
	Node No.7	Node No.20	Node No.27
0	0.00	0.00	0.00
20	0.21	0.08	0.03
40	0.42	0.16	0.06
60	0.61	0.27	0.08
80	1.01	0.45	0.14
100	1.66	0.75	0.21
120	2.32	1.11	0.34
140	3.35	1.53	0.48
160	4.68	2.01	0.61
180	5.86	2.59	0.75
200	7.12	3.06	0.91
220	8.02	3.54	1.02

The predicted major values of proposed analysis are presented in Table 8.12. Fig. 8.31 to 8.33 gives the comparison of experimental and analytical load deflection curves.

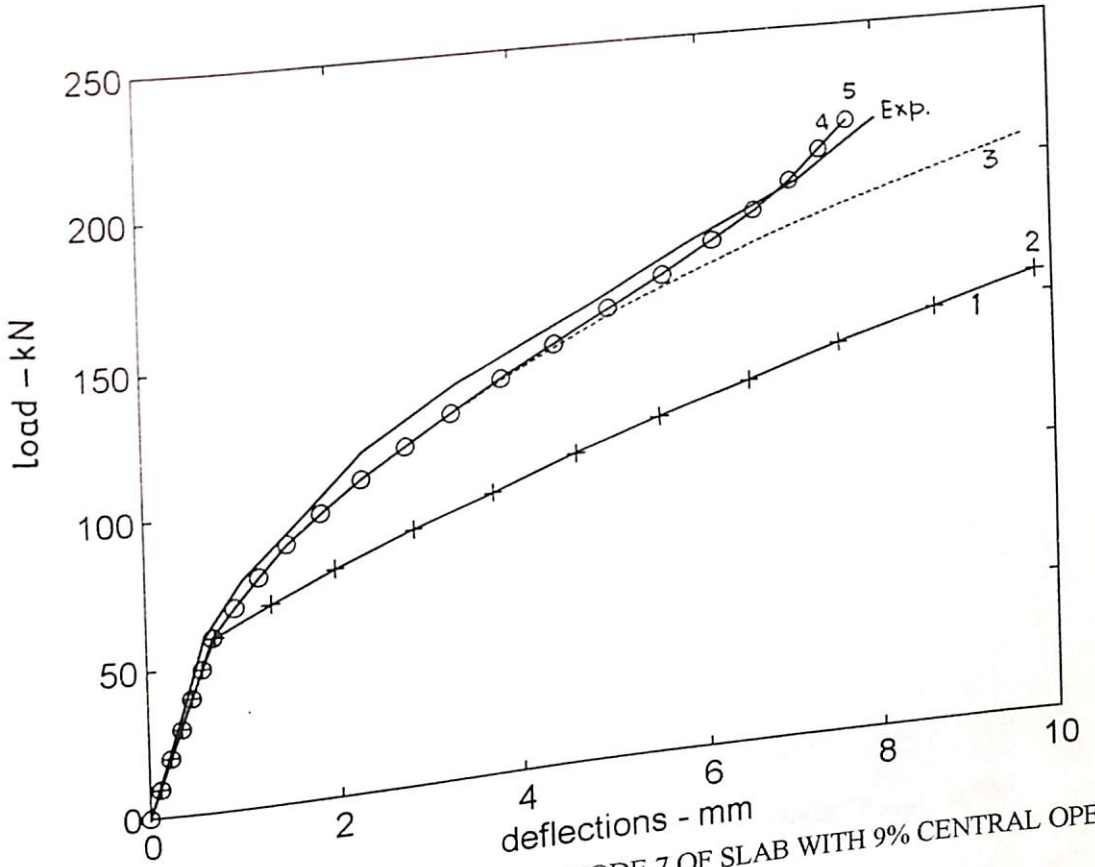


Fig. 8.31 LOAD-DEFLECTION CURVES AT NODE 7 OF SLAB WITH 9% CENTRAL OPENING

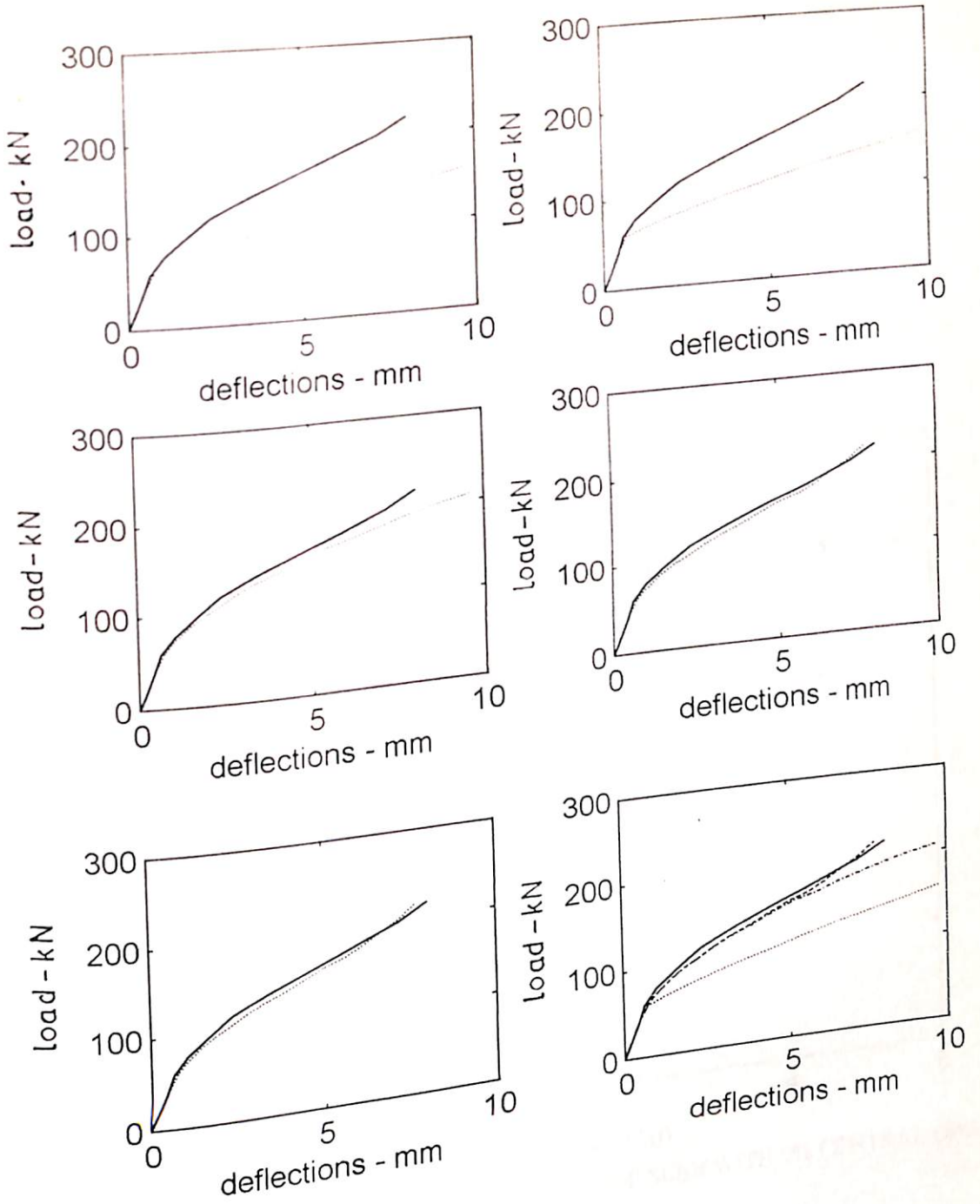


Fig. 8.31.1 LOAD-DEFLECTION CURVES AT NODE 7 OF SLAB WITH DIFFERENT METHODS OF ANALYSIS

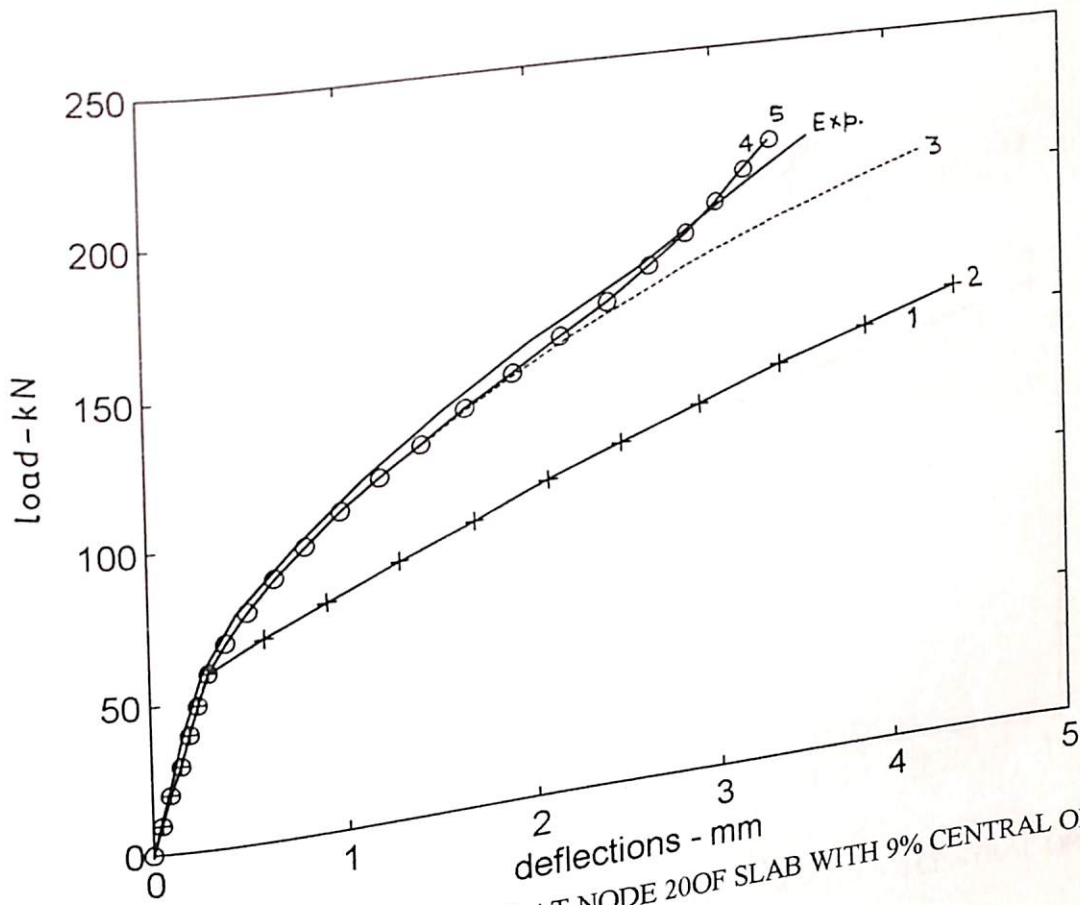


Fig. 8.32 LOAD-DEFLECTION CURVES AT NODE 20 OF SLAB WITH 9% CENTRAL OPENING

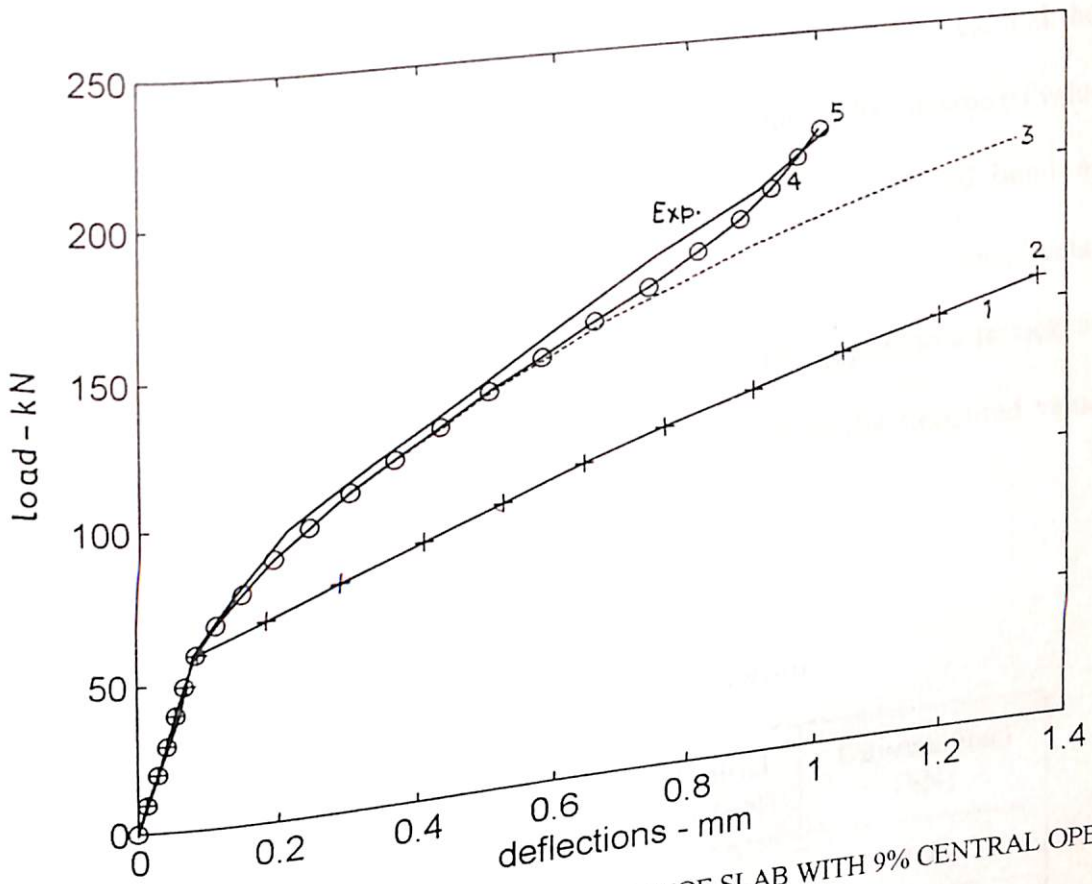


Fig. 8.33 LOAD-DEFLECTION CURVES AT NODE 27 OF SLAB WITH 9% CENTRAL OPENING

Without considering the tension-softening phenomenon in the analysis, the calculated values of deflections at 160 kN found ^{to be} 127% ~~larger than~~ the experimental deflection values. These deflection values reduced in case of second method of analysis which incorporates flexural stiffness of steel in material matrix before cracking. However, the deflection values are still 110% ~~more than~~ the measured values. The effect of tension softening which increases the slab stiffness and thereby reduces the deflection values predicted 28% and 37% more than measured values of node numbers 7 and 27 respectively at 210 kN. The developed bond model predicted deflection values as 4.14% and 1.3% less than the experimental values at 220 kN load for node number 7 and 27. The proposed aggregate interlock model further predicted these values 4.05% and 1.08% less than the measured values of deflections.

Table 8.12

Salient Results of Investigation

Method of analysis	Load value of initial crack (kN)	Load value of initial yielding of steel (kN)	Ultimate load (kN)
1	50	90	160
2	50	90	160
3	50	110	210
4	50	110	220
5	50	110	220
Exp.	50	110	220

Finally it had been observed that ultimate load is reduced as size of the % of opening increases. The analysis without softening phenomenon predicted the loads less than the actual and calculated deflections larger than the measured values. Moreover, the tension-softening phenomenon increases the stiffness of the slab and thereby reduces the difference in deflections. The bond effect further increased the stiffness of the concrete and **calculated** the deflections more close to the observed experimental values. The difference in experimental and analytical deflection at ultimate load found as 3 to 5.5%. However, the maximum difference observed immediately after the yielding of steel reinforcement in the range of 10 to 20%.

CHAPTER 9

CONCLUSIONS

Six rectangular reinforced concrete slabs which were supported on four sides, with and without central openings were tested under transverse loads.

Theoretical and observed yield line patterns are in good agreement. More over, it is observed that the Yield line patterns do not change with the size of central openings. For slabs with central opening, the yield lines proceeds from the four corners of the openings towards the slab corners as shown in Figs. 7.7 to 7.12.

The test results indicate that the ultimate loads are effected by central openings as given in Table 7.4. The reduction in ultimate loads are found as 3.45, 6.9, 13.79, 17.24 and 24.13 per cent with respect to 1, 3, 5, 7 and 9 percent of central openings in comparison with ultimate load of solid slab. The failure of slabs tested under uniformly distributed load is caused by crushing of concrete.

The finite element procedure, based on a 16 degrees of freedom rectangular plate bending element, nearly predicts the nonlinear post-cracking behaviour of rectangular reinforced concrete slabs over the full range of transverse loading.

From the observation of numerical results of finite element analysis, it is found that the proposed constitutive models can represent the essential behaviour of *the cracked reinforced concrete slabs* and agree well with experimental results. The proposed method of analysis appears to be a powerful tool for the nonlinear analysis of rectangular reinforced concrete slabs.

The results of the relatively realistic model used for representing the reinforced concrete slabs are encouraging. Before cracking, the direction of the maximum stress of concrete is that of the maximum principal stress. After cracking, the direction of maximum stress of concrete is along the principal curvature dictated by the compatibility and equilibrium of the crack.

Experimentally observed initial crack loads of slabs are in good agreement with the calculated first crack loads of finite element analysis. It is found that these load values are in the range of 20 to 25% of ultimate load of respective slabs.

The observed test results of initial yielding of slabs are also in good agreement with the calculated first yield loads of finite element analysis. These values are in the range of 50 to 53.5% of ultimate load of respective slabs.

The effect of incorporating flexural rigidity of steel before cracking is found to be almost negligible.

The stiffness of reinforced concrete is significantly increased by the tension softening effect in the concrete between adjacent cracks. If this effect is neglected, the calculated slab deflections are too large in comparison with the experimental values in post-cracking range.

The tension softening effect nearly predicts the cracking of concrete, yielding of reinforcement and ultimate load values with that of experimental values.

The tension stiffening model of uniaxial tension members on the basis of bond slip mechanism between the reinforcing bars and surrounding concrete is developed and extended to the analysis of slabs. It is observed that the results are more interesting.

The tension stiffening effect further increases the stiffness of concrete slabs and thereby predicts the deflections more nearer to the experimental deflections. The behaviour of slabs in the post cracking range is effectively observed by incorporating this effect, i.e. cracking of concrete, yielding of reinforcement and ultimate load of slabs. The bond-slip model is effective from cracking of concrete to the yielding of reinforcement.

The advantage of proposed relations for bond-slip model is that it can be easily implemented in the analysis, requiring no additional inter element ^{linkages} like bond elements.

The aggregate-interlock effect referred to the frictional contact slip model taken into consideration is found to be negligible. Therefore, it appears that significant slip does not occur between the adjacent crack surfaces.

The implemented and developed models of concrete in compression, concrete in tension, bond-slip and aggregate interlock of uniaxial members when extended to the slab analysis predicts deflections more close to the experimental values with in the range of 94 to 97%. The maximum difference between the analytical and experimental curves are observed after the yielding of steel.

The difference between the experimental and analytical load-deflection curves may be due to the following reasons:

Experimental Errors:

1. Non-uniform rating of load to the slab.
2. The loads applied to the slabs is within the limitations of available loading frame and loading arrangement.
3. Improper compaction, placement of reinforcement and finishing of slab surface *during the casting* of slab.
4. Probable slight *eccentricity of loading arrangement*.
5. Slight dislocations of dial gauges under the points of *experimental investigation*.

Analytical Errors:

1. The analysis is restricted to small deformation bending theory, i.e. no geometrical nonlinearity is considered for the analysis.
2. Membrane stresses and strength variation due to biaxial stresses are neglected.
3. Time dependent effects such as creep, shrinkage and temperature, etc. are not included.
4. Kinking of reinforcing bars and dowel forces are neglected.
5. It may be due to round off errors which can be eliminated by using double precision in the software.
6. Finite element is an approximate analysis and it never attains the true solution.
7. Steel is assumed as perfectly elastic-plastic, trilinear stress-strain response of steel may reduce the difference immediately after the yielding of steel.
8. The analysis stops immediately, once the extreme compression fibre reaches the strain value as 0.0035 and above.

Limitations

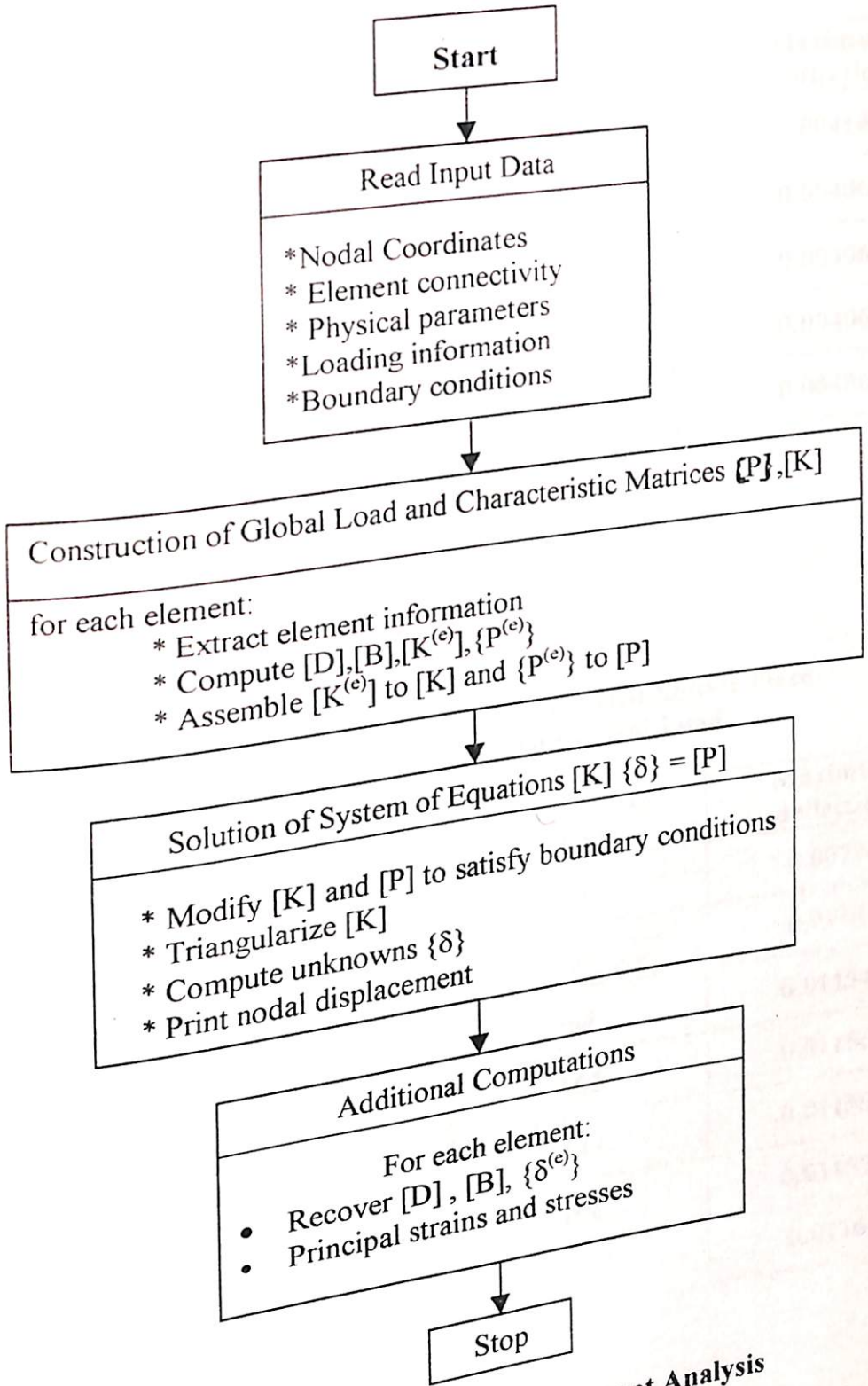
1. Although the plate bending element used here is not suitable for slabs with nonrectangular boundaries, the solution method itself is quite general and can be applied, without added difficulty, to irregular shaped slabs with irregularly placed reinforcement by the use of a more suitable plate bending element such as a quadrilateral plate bending element.

2. The bending of bars at end and openings to provide bond between steel and concrete is difficult to consider in the model. The reinforcement is assumed as rectangular mesh.
3. The analysis is valid only for transverse loading on slabs. No provision has been made for axial loads.

Future Investigation Needed

1. The present analysis can be further extended by taking 20 degree of freedom ($u, v, w, \theta_x, \theta_y$ per node) quadrilateral element or shell element to investigate the slabs subjected to both axial and transverse loading. Also it can be used for analysis of slabs with irregular shapes.
2. The overall effect of both material and geometrical nonlinearity can be further investigated by incorporating higher order terms in strain-displacement relations.
3. The aggregate interlock may be more effective in case of thick slabs, which can be further investigated.
4. Moreover the analysis can be extended to study the thermal effects of slabs by considering thermal load vectors in the analysis.

Appendix - A



Flow Chart for Linear Finite Element Analysis

Table: A1
Central Deflection of a Simple Supported Square Plate,
Subjected to Uniform Distributed Load.

No of elements in a quadrant	Total No of nodes	Total No. of d.o.f	Maximum deflection
1	4	16	0.004147
4 (2x2 mesh)	9	36	0.004065
9 (3x3 mesh)	16	64	0.004063
16 (4x4 mesh)	25	100	0.004062
Exact [70]			0.004062

Table A2
Central Deflection of a Simple Supported Square Plate
Subjected to Concentrated Central Load.

No of elements in a quadrant	Total No of nodes	Total No. of d.o.f	Maximum deflection
1	4	16	0.00774
4 (2x2 mesh)	9	36	0.01147
9 (3x3 mesh)	16	64	0.011543
16 (4x4 mesh)	25	100	0.011568
25 (5x5 mesh)	36	144	0.011584
36 (6x6 mesh)	49	196	0.011595
Exact [70]			0.01160

Table A3
Simple Supported Rectangular Plate Subjected to
Uniformly Distributed Load (4x4 mesh)

b/a	Exact [70]	Calculated
1.1	0.00485	0.00486
1.2	0.00564	0.00565
1.3	0.00638	0.00639
1.4	0.00705	0.00708
1.5	0.00772	0.00772
1.6	0.00830	0.00830
1.7	0.00883	0.00883
1.8	0.00931	0.00931
1.9	0.00974	0.00974
2.0	0.01013	0.01013
3.0	0.01223	0.01223
4.0	0.01282	0.01281
5.0	0.01297	0.01297

Table A4
Simple Supported Rectangular Plate Subjected to
Concentrated Load at Centre (6x6 mesh)

b/a	Exact [70]	Calculated
1.1	0.01265	0.012645
1.2	0.01353	0.01352
1.4	0.01484	0.01483
1.6	0.01570	0.01568
1.8	0.01620	0.01619
2.0	0.01651	0.01650
3.0	0.01690	0.01688

Table A5
Clamped Square Plate Subjected to
Uniform Distributed Load

No of elements in a quadrant	Total No of nodes	Total No. of d.o.f	Maximum deflection
1	4	16	0.00132
4 (2x2 mesh)	9	36	0.001265
9 (3x3 mesh)	16	64	0.001261
16 (4x4 mesh)	25	100	0.00126
Exact [70]			0.00126

Table A6
Clamped Square Plate Subjected to
Concentrated Load at Centre

No of elements in a quadrant	Total No of nodes	Total No. of d.o.f	Maximum deflection
1	4	16	0.00530
4 (2x2 mesh)	9	36	0.00545
9 (3x3 mesh)	16	64	0.00552
16 (4x4 mesh)	25	100	0.00558
25 (5x5 mesh)	36	144	0.00559
36 (6x6 mesh)	49	196	0.00560
Exact [70]			0.00560

Table A7
Clamped Rectangular Plate Subjected to
Concentrated Central Load.

b/a	Exact [70]	Calculated
1.2	0.00647	0.00646
1.4	0.00691	0.00690
1.6	0.00712	0.00711
1.8	0.00720	0.007195
2.0	0.00722	0.00721

Table A8
Clamped Rectangular Plate Subjected to
Uniform Distributed Load

b/a	Exact [70]	Calculated
1.1	0.00150	0.00150
1.2	0.00172	0.00172
1.3	0.00191	0.00191
1.4	0.00207	0.00207
1.5	0.00220	0.002196
1.6	0.00230	0.002299
1.7	0.00238	0.00238
1.8	0.00245	0.00245
1.9	0.00249	0.002495
2.0	0.00254	0.00253

Appendix – B

Slab Design

Dimensions of slab

$$l_x = 0.75\text{m}$$

$$l_y = 1\text{m}$$

concrete: M₁₅

steel: Fe-250

$$\text{Span ratio} = \frac{l_y}{l_x} = \frac{1}{0.75} = 1.33 < 2$$

The span ratio is less than two. Therefore the slab is two way slab.

Minimum depth calculations:

Minimum depth requirement to meet deflection criterion according to I.S.

Code 456:1978.

$$\text{Minimum span/ effective depth} = 35$$

$$\text{effective depth} = \frac{750}{35} = 21.42 \text{ mm}$$

Let the effective depth = 55mm

Therefore overall depth = 55 + 4 + 16 = 75mm.

0.75 kN/m²

Live load on slab = 2.0 kN/m^2

Total load on slab = 3.875 kN/m^2

$$\text{For } \frac{l_y}{l_x} = 1.33$$

the values of $\alpha_x = 0.0949$, $\alpha_y = 0.05368$

Moment in x-direction = $M_x = \alpha_x w_s l_x^2$

$$= 0.0949 \times 3.875 \times 0.75^2 \times 1000 = 206.852 \text{ N-m}$$

Moment in y-direction = $M_y = \alpha_y w_s l_x^2$

$$= 0.05368 \times 3.875 \times 0.75^2 = 117.005 \text{ N-m}$$

Ultimate moment = factor of safety \times maximum bending moment

$$= 1.5 \times 206.852 = 310.278 \text{ N-m}$$

$$\text{effective depth} = \frac{M_u \text{ lim}}{0.148 f_{cl_y}} = \frac{310.278 \times 1000}{0.148 \times 15 \times 1000} = 11.82 \text{ mm}$$

Therefore provided effective depth is within limits.

$$\text{For Fe-250, } \frac{kh}{d} = 0.53$$

$$M_u \text{ lim} = 0.87 f_y A_{sx} (d - 0.42 kh)$$

Area of steel in shorter direction

$$310.278 \times 1000 = 0.87 \times 250 \times A_{st1} \times 55 [1 - (0.42 \times 0.53)]$$

$$A_{st1} = 33.36 \text{ mm}^2$$

Number of 8 mm diameter bars required per meter width

$$= \frac{33.36}{\pi/4 \times 8^2} < 1$$

Area of steel in longer direction

effective depth = $55 - 8 = 47$ mm

$$15 \times 117.005 \times 1000 = 0.87 \times 250 \times A_{st2} \times 47 (1 - 0.42 \times 0.53)$$

$$A_{st2} = 22.08 \text{ mm}^2$$

Therefore, the number of 8 mm diameter bars required per meter width is less than one.

Redesigning slab for reading room in library, the design calculations follows as:

$$\text{Effective span } l_x = 750 - 70 = 680 \text{ mm}$$

$$l_y = 1000 - 65 = 935 \text{ mm}$$

$$\text{Live load} = 4 \text{ kN/m}^2$$

$$\text{Overall depth} = 60 \text{ mm}$$

$$\text{Effective depth} = 60 - 15 - 5 = 40 \text{ mm}$$

Minimum depth according to IS code 456:1978.

$$d = l_x/35$$

$$= \frac{680}{35} = 19.42 \text{ mm}$$

$$\text{Self weight of slab} = 0.06 \times 25 = 1.5 \text{ kN/m}^2$$

$$\text{Live load} = 4.0 \text{ kN/m}^2$$

$$\text{Total load} = 5.5 \text{ kN/m}^2$$

$$\frac{l_y}{l_x} = \frac{935}{680} = 1.375$$

$$\text{For } l_y/l_x = 1.375$$

$$\alpha_x = 0.975 \text{ and } \alpha_y = 0.052$$

$$M_x = \alpha_x w_s l_x^2 = 0.975 \times 5.5 \times 0.68^2 \times 1000$$
$$= 247.962 \text{ N-m}$$

$$M_y = \alpha_y w_s l_x^2 = 0.052 \times 5.5 \times 0.68^2 \times 1000$$
$$= 132.246 \text{ N-m}$$

$$M_u \text{ lim} = 1.5 \times 247.962 = 371.943 \times 10^3 \text{ N-mm}$$

$$d = \frac{M_u \text{ lim}}{0.148 f_{ck} l_y} = \frac{371.943 \times 1000}{0.148 \times 15 \times 1000} = 12.9 \text{ mm}$$

Therefore provided depth is within same limit.

Area of steel in short direction.

$$371.943 \times 1000 = 0.87 \times 250 \times A_{st1} \times 40 \left[1 - \frac{A_{st1} \times 250}{1000 \times 40 \times 15} \right]$$

$$\Rightarrow A_{st1} = 43.5 \text{ mm}^2 \text{ or } (2356.45 \text{ mm}^2)$$

$$\frac{kh}{d} = \frac{0.87 f_y A_{st}}{0.36 f'_c b d} = \frac{0.87 \times 250 \times 43.5}{0.36 \times 15 \times 1000 \times 40} = 0.04386$$

Providing minimum reinforcement = 0.15% $l_y h$

$$= \frac{0.15}{100} \times 1000 \times 60 = 90 \text{ mm}^2$$

Using 6 mm diameter bars,

$$\text{No. of bars required} = \frac{90}{\pi/4 \times 6^2} = 3.18 = 4 \text{ bars}$$

Slab design meeting minimum spacing requirement:

Let the spacing of reinforcement be 100 mm c/c

$$\text{Spacing } s_p = \frac{1000}{A_{st}/\pi/4 d_r^2}$$

Using 6 mm diameter bars and spacing 100 mm c/c

$$A_{st} = 1000 \times \pi/4 \times 6^2/100 = 282.74 \text{ mm}^2$$

$$\frac{kh}{d} = \frac{0.87 \times 250 \times 282.74}{0.36 \times 15 \times 1000 \times 40} = 0.2819$$

$$M_u = 0.87 f_y A_{st} d \left[1 - \frac{A_{st} f_y}{f_c l_y d} \right]$$

$$= 0.87 \times 250 \times 282.74 \times 40 \left[1 - \frac{282.74 \times 250}{15 \times 1000 \times 40} \right]$$

$$= 2151.8 \text{ N-m}$$

$$M_u = 1.5 \alpha_x W_1 l_x^2 \Rightarrow W_1 = \frac{M_u}{1.5 \alpha_x l_x^2} \quad \dots(a)$$

$$W_1 = \frac{2151.8}{1.5 \times 0.0975 \times (0.68)^2} = 31.819 \text{ kN/m}^2$$

$$M_u = 1.5 \alpha_y W_2 l_x^2 \Rightarrow W_2 = \frac{M_u}{1.5 \alpha_y l_x^2} \quad \dots(b)$$

$$W_2 = \frac{2151.8}{1.5 \times 0.052 \times (0.68)^2} = 59.66 \text{ kN/m}^2$$

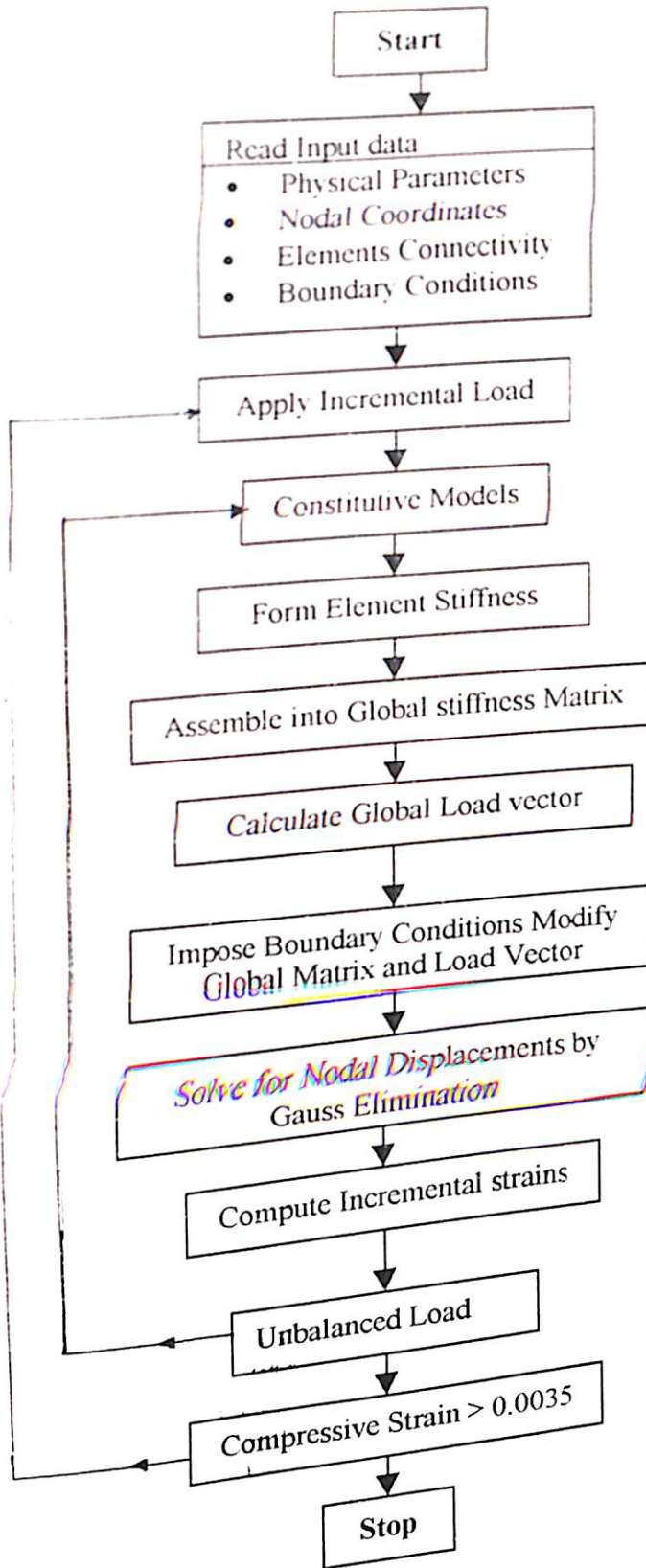
The collapse load is minimum of eq. (a) and eq. (b), that is 31.819 kN/m²

Percentage of steel

$$p = \frac{280}{1000 \times 60} \times 100 = 0.467$$

Therefore provide 11 bars and 8 bars of 6 mm diameter mild steel bars along long and short direction of slab.

Appendix-C



Flow Chart for Nonlinear Analysis of Slabs

REFERENCES

1. Westergaard, H.M. and Slater, W.A. "Moments and Stresses in Slabs", Proceedings ACI, Vol. 17, 1921, pp. 415-538.
2. Di Stasio, T. and Van Buren, M.P. "Slabs Supported on Four Sides", Proceedings ACI, Vol. 32, Jan-Feb. 1936, pp. 350-364.
3. Rogers, P. "Two-way Reinforced Concrete Slabs", J. ACI, Vol. 41, Jan. 1944, pp. 21-36.
4. Huggins, M.D. and Lin, D.L. "Moments in Flat Slabs", Transactions ASCE, Vol. 123, 1958, pp. 824-881.
5. Brotchie, J.F. "General Elastic Analysis of Flat Slabs and Plates", Proceedings ACI, Vol. 56, Aug. 1959, pp. 1127-1152.
6. Gamble, W.L. "Moments in Beam-supported slabs", J. ACI, Vol. 69, March 1972, pp. 149-157.
7. Rice, P.F. "Practical Approach to Two-way Slab Design", J. Str. Div., ASCE, Vol. 99, No. ST1, Jan., 1973, pp. 131-143.
8. Zweig, A. "Design Aids for the Direct Design Method of Flat Slabs", Proceedings ACI, Vol. 70, April, 1973, pp. 285-299.
9. "The Shear strength of Reinforced Concrete Member Slabs", ASCE-ACI Task Committee 426, J. Str. Div., ASCE, Vol. 100, No. ST8, 1974, pp. 1543-1591.

10. Park, R and Gamble, W.L. "Reinforced Concrete Slabs", John Wiley and Sons, New York, 1980
11. Ingerslev, A "The strength of Rectangular slabs", J. Inst. Struct. Engg., London, Vol. 1, Jan, 1923, pp. 3-14.
12. Hognestad, E. "Yield Line Theory for the Ultimate Flexural Strength of Reinforced Concrete Slabs", J. ACI, Vol. 24, July, 1953, pp. 637-656.
13. Jones, L.L. and Wood, R.H. "Yield Line Analysis of Slabs", American Elsevier, New York, 1967.
14. Lenschow, R. and Sozen, M.A. "A Yield Criterion for Reinforced Concrete Slabs", J. ACI, Vol. 64, May, 1967, pp. 267-273.
15. Simmonds, S.H. and Ghali, A. "Yield Line Design of Slabs", J. Str. Div., ASCE, Vol. 102, No. ST1, 1976, pp. 109-123.
16. Demsky, E.C. and Hatcher, D.S. "Yield Line Analysis of Slabs Supported on Three Sides", J. ACI, Vol. 66, Sept., 1969, pp. 741-744.
17. Zaslavsky, A. "Yield Line Analysis of Rectangular Slabs with Central Openings", J. ACI, Vol. 64, Dec., 1967, pp. 838-844.
18. Islam, S. and Park, R. "Yield Line Analysis of Two-way Reinforced Concrete Slabs with Openings", J. Inst. Struct. Engg., Vol. 49, June, 1971, pp. 269-276.
19. Jain, S.C. and Kennedy, "Yield Criterion for Reinforced Concrete Slabs", J. of Str. Div., ASCE, Vol. 100, No. ST3, March, 1984, pp. 631-644.

20. Nilson, A H and Winter, G W "Design of Concrete Structures", McGraw Hill, Eleventh Edition, 1991.
21. Kemp, K O., "Continuity conditions in the strip method of slab design", proc. inst. civ engg., vol. 45, 1970, p. 283.
22. Wood, R.H., and Armer, G.S.T., "The Theory of the strip method for the Design of slabs", proc. inst. civ. engg , vol. 41, 1968, pp. 285-311.
23. Armer, G.S.T., "Ultimate Load Tests of Slabs Designed by the Strip Method", proc. Inst. Civ. Eng., Vol. 41, 1968, pp. 313-331.
24. Vijayarangan, B., "Lower Bound Solutions for Continuous Orthotropic Slabs", J . of Str. Div., ASCE, Vol. 99, No. ST3, Mar., 1973, pp. 443-452.
25. Gergely, P. and Lutz, L.A. "Maximum Crackwidth in Reinforced Flexural Members", Special Publication SP- 20, ACI, 1968, pp. 87-117.
26. Beeby, A.W., "The Prediction and Control of Flexural Cracking in Reinforced Concrete Members", Special Publication SP-30, ACI, 1971, pp. 55-57.
27. ACI Committee 224, "Control of Cracking in Concrete Structures", Proceedings ACI, Vol. 69, Dec., 1972, pp. 715-753.
28. Desai, P. and Kulkarni, A.B. "Determination of maximum crack width in two-way reinforced concrete slabs", Proceedings Institution of Civil Engineers, London, Part 2, Research and Theory, Vol. 61, June 1976, pp. 343-349.

29. Brason, D.E. "Deformation of Concrete Structures", McGraw Hill, New York, 1977.
30. Jofriet, J.C. "Short Term Deflections of Concrete Flat Plates", J. of Str. Div., ASCE, Vol. 99, No. ST1, Jan., 1973, pp. 167-182.
31. Desai, P. and Kulkarni, A.B. "Load Deflection Behaviour of Simply Supported Rectangular Reinforced Concrete Slabs". International Association for Bridge and Structural Engineering, Feb., 1978.
32. Desai, P. and Kulkarni, A.B. "Load Deflection Behaviour of Restrained R.C. Slabs", J. of Str. Div., Vol. 103, No. ST2, Feb. 1977, pp. 405-419.
33. Moy, S.S.J. and Mayfield, B. "Load-Deflection Characteristics of Reinforced Concrete Slabs", Magazine of Concrete Research, Vol. 24, No. 81, Dec. 1972, pp. 209-218.
34. Furr, H.L. "Numerical methods for approximate analysis of building slabs", Proceedings ACI, Vol. 56, Dec., 1959, pp. 511-514.
35. Woodring, R.E. and Sein, C.P. "Influence surfaces for continuous plates", J. of Str. Div., ASCE, Vol. 94, No. ST1, Jan., 1968, pp. 211-226.
36. Melosh, R.J. "A stiffness matrix for the analysis of thin plates in bending", Journal Aero Sciences, Vol. 28, 1961, pp. 34-42.
37. Zienkiewicz, O.C. "The Finite Element Method". Tata McGraw Hill, Third Edition, 1987.

38. Ngo, D., and Scordelis, A.C., "Finite Element Analysis of Reinforced Concrete Beams", American Concrete Institute Journal, Vol. 64, March, 1967, pp. 152-163
39. Rashid, Y.R. "Ultimate Strength Analysis of Prestressed Concrete Pressure Vessels", Nucl. Engg. Design, Vol. 7, April, 1968, pp. 334-344.
40. Nilson, A.H. "Nonlinear Analysis of Reinforced Concrete by the Finite Element Method", ACIJ, Vol. 65, Sept., 1968, pp. 757-766.
41. Cedolin, L. and Dei Poli, S. "Finite Element Studies of Shear Critical Reinforced Concrete Beams", Journal of Engineering Mechanics Division, ASCE, Vol. 103, No. EM3, June, 1977.
42. Valliappan, S. and Doolan, T.F. "Nonlinear Analysis of Reinforced Concrete", Journal of Structural Division, ASCE, Vol. 98, No. ST4, April, 1972.
43. Colville, J. and Abbasi, J. "Plane Stress Reinforced Concrete Finite Elements", Journal of Structural Division, ASCE, Vol. 100, No. ST5, May, 1974.
44. Nam, C.H. and Salmon, C.G. "Finite Element Analysis of Concrete Beams", Journal of Structural Division, ASCE, Vol. 100, No. ST12, December, 1974.
45. Gajer, G. and Dux, P.F. "Crack Band Based Model for FEM Analysis of Concrete Structures", Journal of Structural Engineering, Vol. 116, June, 1990, pp. 1696-1713.
46. Yamaguchi, E. and Chen, W.F. "Cracking Model for Finite Element Analysis of Concrete Materials", J. Engg. Mech. ASCE, Vol. 116, June, 1990, pp. 1242-1260.

47. Jofriet, J.C. and Mc Niece, G.M. "Finite element analysis of reinforced concrete slabs" J. Struct. Div., ASCE, Vol. 97, March, 1971, pp. 785-806.
48. Bell, J.C. and Elms, O.G. "A finite element approach to post elastic slab behaviour" Sp 30-15, ACI, 1971, pp. 325-344.
49. Hand, F.R., Pecknold, D.A. and Schnobrich, W.C. "Nonlinear Layered Analysis of RC Plates and Shells," J. of Str. Div., ASCE, Vol. 99, No. ST7, July, 1973, pp. 1491-1505.
50. Scaloni, A. and Murray, D.W. "Time dependent reinforced concrete slab deflections" J. Struct. Div., ASCE, Vol. 100, Sept., 1974.
51. Wanchoo, M.K. and May, G.W. "Cracking Analysis of reinforced concrete plates" J. Struct. Division, ASCE, Vol. 101, Jan., 1975, pp. 201-215.
52. Lin, C.S. and Scordelis, A.C. "Nonlinear analysis of RC shells of general form" J. Struct. Div., ASCE, Vol. 101, March, 1975, pp. 523-538.
53. Vebo, A. and Ghali, A. "Moment-Curvature Relation of Reinforced Concrete Slabs", J. Struct. Div., ASCE, Vol. 103, March, 1977, pp. 515-531.
54. Bashur, F.K. and Darwin, D. "Nonlinear Model for Reinforced Concrete Slab", J. Struct. Div., ASCE, Vol. 104, Jan., 1978, pp. 157-170.
55. Gilbert, R.I. and Warner, R.F. "Tension Stiffening in Reinforced Concrete Slabs", J. Struct. Div., ASCE, Vol. 104, Dec., 1978, pp. 1885-1900.
56. Cope, R.J. and Rao, P.V. "Nonlinear Finite Element Analysis of Concrete Slab Structures", Proc. Inst. Civ. Engrs., Part 2, 63, 1977, pp. 159-179.

57. Cope, R.J. and Rao, P.V. "A Two-Stage Procedure for the Nonlinear Analysis of Slab Bridges", Proc. Inst. Civ. Engrs., Part 2, 75, 1983, pp. 671-688.
58. Cope, R.J. "Material Modeling of Real, Reinforced Concrete Slabs", Proc. Int. Conf. on Computer-Aided Analysis and Design of Concrete Struct., Split, Yugoslavia, 1984, pp. 85-117.
59. Zarris, P.D. "State of stress in RC plates under service conditions", J. Struct. Engg., ASCE, Vol. 112, Aug., 1986, pp. 1908-1927.
60. Lewinski, P.M. and Wojewodzki, D. "Integrated Finite Element Model for Reinforced Concrete Slabs." J. Str. Div., Vol. 117, April, 1991, pp. 1017-1038.
61. Sathurappan, G., Rajagopalan, N. and Krishnamoorthy, C.S. "Nonlinear Finite Element Analysis of Reinforced and Prestressed Concrete Slabs with Reinforcement (Inclusive of Prestressing Steel) modelled as Discrete Integral Components", Comp. and Struct., Vol. 44, March, 1991, pp. 575-584.
62. Di, S. and Cheung, Y.K. "Nonlinear analysis of RC shell structures using laminate element-II", J. Struct. Div., ASCE, Vol. 119, July, 1993, pp. 2074-2095.
63. Courant, R. "Variational methods for the solution of problems of equilibrium and vibrations". Bulletin of American Mathematical Society, Vol.49, 1943, pp. 1-43.
64. Turner, M.J., Clough, R.W., Martin, H.C. and Toop, L.J. "Stiffness and Deflection Analysis of Complex Structures". Journal of Aeronautical Sciences, Vol.23, 1956, pp.805-823.

65. Clough, R.W. "The Finite Element Method in Plane Stress Analysis", J. Struct. Div., ASCE, Proceed., 1960, pp. 345-379
66. Clough, R.W. and Tocher, J.L. "Finite Element Stiffness matrices for the analysis of plate bending", Proc. 1st Conf. on Matrix Methods in Structural Mech., Ohio, 1965, pp. 515-545.
67. Bogner, F.K., Fox, R.L. and Schmit, L.A. "The generation of interelement compatible stiffness and mass matrices by use of interpolation formulas", Proc. 1st Conf. on Matrix Methods in Structural Mech., Ohio, 1965, pp. 397-443
68. Irons, B.M. and Drooper, K.J. "Inadequacy of nodal connections in a stiffness solution for plate bending", American Inst. Aeronaut. Astronaut J., Vol. 3, May, pp. 61.
69. Harbok, M.M. and Hruday, T.M. "A Review of and Catalogue of plate Bending Finite Elements", Computers and Structures, Vol. 19, March, 1984, pp. 479-495.
70. Timoshenko, S.P. and Krieger, S.W. "Theory of Plates and Shells", Tata McGraw Hill, Second Edition, 1959.
71. Chen, W. F. and Suzuki, A.F. "Constitutive Equations for Engineering Materials", Computers and Structures, Vol. 12, 1980, pp. 23-32.
72. Han, D.J. and Chen, W.F. "Constitutive Modeling in Analysis of Concrete Structures", J. Eng. Mech. Div., ASCE, Vol. 112, 1986.

73. Hsu, T T C , Slate, F O ., Sturman, G M ., and Winter, G "Microcracking of Plain Concrete and the Shape of the Stress-strain Curve", ACIJ, Vol 60, Feb , 1963, pp 209-224
74. Shah, S P and Chandra, S. "Critical Stress, Volume Change and Microcracking of Concrete", ACI Journal, Vol. 65, 1968, pp. 770-781.
75. Krishnaswamy, K.T. "Microcracking of Plain Concrete under Uniaxial Compressive Loading", Indian Concrete Journal, Vol. 66, April, 1969, pp 143-145.
76. Kupfer, H., Hilsdorf, H.K and Rusch, H.. "Behaviour of Concrete under Biaxial Stresses", ACIJ, Vol. 66, Aug. 1969. pp. 656-666.
77. Darwin, D., and Pecknold, D.A. "Analysis of RC Shear Panels under Cyclic Loading", Journal of Str. Div., ASCE, Vol. 102, No. ST2, Proc. Paper 11896, Feb.,1976, pp. 355-369.
78. Aktan, A.E. and Pecknold, D.A. "Response of a Reinforced Concrete Section to Two-Dimensional Curvature Histories", ACIJ, Vol. 71, May 1975, pp. 246-250.
79. Karasan, J.K. and Jirsa, J.O. "Behaviour of Concrete under Compressive Loadings", J. Str. Div., ASCE, Vol. 95, No. ST12, Dec. 1969, pp. 2543-2563.
80. Liu, T.C.Y., Nilson, A.H. and Slate, F.O. "Stress- Strain response and fracture of concrete in uniaxial and biaxial compression", ACIJ, Vol. 69, May, 1972, pp. 291-295.

81. Liu, T C Y , Nilson, A H and Slate, F O "Biaxial stress-strain Relations for Concrete", J Str. Div , ASCE, Vol 98, No ST5, 1972, pp 1025-1034
82. Tasuji, M E , Slate, F O and Nilson, A H "Stress- Strain Response and Fracture of Concrete in Biaxial Loading", ACIJ, Vol. 75, July, 1978, pp. 306-312
83. Kupfer, H B. and Gerstle, K.H. "Behaviour of Concrete under Biaxial Stress". J. Engg. Mech. Div., ASCE, Vol. 99, No. EM4, Aug., 1973, pp. 852-866
84. Romstad, K. M., Taylor, M. A. and Herrman, L. R. "Numerical Biaxial Characterization for Concrete", J. Engg. Mech. Div., ASCE, Vol. 100, No. EM5, Oct. 1974, pp. 935-943.
85. Gerstle, K.H. "Simple Formulation of Biaxial Concrete Behaviour", ACIJ, Vol. 78, Jan., 1981, pp. 62-68.
86. Cedolin, L., Crutzen, Y.R.J. and Dei Poli, S. "Triaxial Stress-strain Relationship for Concrete", J. Engg. Mech. Div., ASCE, Vol. 103, No. EM3, June, 1977, pp. 423-439.
87. Mills, L.L. and Zimmerman, R.M. "Compressive Strength of Plain Concrete under Multiaxial Loading Conditions", ACIJ, Vol. 67, Oct., 1970, pp. 802-807.
88. Kotsovos, M.D. "Effect of Stress Path on the Behaviour of Concrete under Triaxial Stress States", ACIJ, Vol. 76, Feb., 1979, pp. 213-223.

89. Bazant, Z.P. and Tsubaki, T. "Total Strain Theory and Path Dependence of Concrete", *J. Engg. Mech. Div., ASCE*, Vol. 106, No. EM, Dec., 1980, pp. 1151-1173.
90. Ottosen, N.S. "Constitutive Model for Short-Time Loading of Concrete", *J. Engg. Mech. Div., ASCE*, Vol. 105, No. EM1, Feb., 1979, pp. 127-141.
91. Palaniswamy, R. and Shah, S.P. "Fracture and Stress-strain Relation of Concrete under Triaxial Compression", *J. Str. Div., ASCE*, Vol. 100, No. ST5, May, 1974, pp. 901-916.
92. Philips, D.V. and Zeinkiewicz, O.C. "Finite Element Nonlinear Analysis of Concrete Structures", *Proceedings, The Institute of Civil Engineers*, Vol. 61, Part 2, Mar., 1976, pp. 59-88.
93. Elwi, A.A. and Murray, D.W. "A 3D Hypoelastic Concrete Constitutive Relationship", *Journal of Engineering Mechanics Division, ASCE*, Vol. 105, No. EM4, Proc. Paper 14746, Aug., 1979, pp. 623-641.
94. Coon, M.D. and Evans, R.J. "Incremental Constitutive Laws and Their Associated Failure Criteria with Application to Plain Concrete", *International Journal of Solids and Structures*, Aug., 1972, pp. 1169-1183.
95. Buyukozturu, O. "Nonlinear Analysis of Reinforced Concrete Structures", *Computers and Structures*, July, 1977, pp. 149-156.
96. Chen, A.C.T. and Chen, W.F. "Constitutive Relations for Concrete", *J. Engg. Mech. Div., ASCE*, Vol. 101, No. EM4, August, 1975, pp. 465-481.
97. Chen, W.F. and Ting, E.C. "Constitutive Models for Concrete Structures", *J.*

Engg. Mech. Div., ASCE, Vol. 106, No. EM1, Feb., 1980, pp. 1-19

98. Suidan, M. and Schnobrich, W.C. "Finite Element Analysis of Reinforced Concrete", J. Str. Div., ASCE, Vol. 99, No. ST10, Oct., 1973, pp. 2109-2122
99. Dougill, J.W. "Some Remarks on Pair Independence in the Smelt in Plasticity", Quarterly of Applied Mathematics, Vol. 32, 1975, pp. 233-243.
100. Bazant, A.P. and Kim, S. "Plastic-Fracturing Theory for Concrete", J. Engg. Mech. Div., ASCE, Vol. 105, EM3, June, 1979, pp. 407-428.
101. Bazant, Z.P. and Bhat, P.D. "Endochronic Theory of Inelasticity and Failure of Concrete", J. Engg. Mech. Div., ASCE, Vol. 102, EM4, Aug., 1976, pp. 701-722.
102. Saenz, L.P., discussion of "Equation for the stress- strain Curve of Concrete" by Desai and Krishna. ACIJ, Vol. 61, Sept., 1964, pp. 1229-1235.
103. Reinhardt, H.W., Cornelizzen, H.A.W. and Hordijk, D.A. "Tensile Tests and Failure Analysis of Concrete", J. Str. Engg., ASCE, Vol. 112, Nov., 1986, pp. 2462-2477.
104. "Cracking of Concrete members in direct tension", ACIJ, ACI Committee 224, Vol. 82, Jan., 1986, pp. 3-13.
105. Cervenka, V. "Constitute model for cracked reinforced concrete", ACIJ, Vol. 82, Nov., 1985, pp. 877-882.
106. Valliappan, S. and Doolan, T.F. "Nonlinear Stress Analysis of Reinforced

- Concrete," *Jr of Str. Div., ASCE*, Vol 98, No ST4, April, 1972, pp 885-898
107. Suidan, M. and Schnobrich, W.C. "Finite Element Analysis of Reinforced Concrete", *J. of Str. Div., ASCE*, Vol. 99, No. ST10, October, 1973, pp. 2109-2122.
108. Vecchio, F.J. "Nonlinear finite element analysis of reinforced concrete membranes", *ACI Struct. J.*, Vol. 86, Jan., 1989 pp. 26-35.
109. Bresler, B. and Bertero, V.V. "Behaviour of Reinforced Concrete under Repeated Load," *Trans. ASCE, J. Struct. Div.*, Vol. 94, No. ST6, June, 1968, pp. 1567-1590.
110. Bazant, Z.P. and Gambarova, P. "Rough Cracks in reinforced concrete", *J. Struct. Div., ASCE*, Vol. 106, April,, 1980, pp. 819-842.
111. Frantzeskakis, C. and Theillout, J.N. "Nonlinear Finite Element Analysis of Reinforced Concrete structures with a particular strategy following the cracking process", *Comp. & Struct.*, Vol. 31, March, 1989, pp. 395-412.
112. Watstein, D. and Mathey, R.G. "Strains in beam having diagonal cracks", *ACIJ*, Vol. 55, April, 1958.
113. Kani, G.N.J. "The Riddle of Shear failure and its solution", *ACIJ*, Vol. 61, April, 1964.
114. Taylor, R. "A Note on the Mechanism of Diagonal cracking in Reinforcements", *Magazine of Concrete Research*, Vol. 31, Nov., 1959, pp. 151-158.

115. Fenwick, R.C. and Pauley, T. "Mechanism of Shear Resistance of Concrete Beams", J. of Str. Div., ASCE, Vol. 94, Oct., 1968, pp. 2325-2350.
116. White, R.N. and Holley, M.J., J. "Experimental studies of Membrane Shear Transfer", J. Str. Div., ASCE, Vol. 98, No. ST3, August, 1972.
117. Houde, J. and Mirza, M.S. "A Finite Element Analysis of Shear strength of Reinforced Concrete Beams", Shear in Reinforced Concrete, Vol. 1, Sp-42, ACI, 1974.
118. Paulay, T. and Loeber, P.S. "Shear Transfer by Aggregate Interlock, Shear in Reinforced Concrete", Vol. 1, SP-42, ACI, 1974.
119. Gambhir, M.L. "Concrete Manual", Dhanpat Rai & Sons, 1992.
120. IS Code 456-1978. (Third revision) Code of practice for plain and reinforced concrete.